NOTICE

The quality of this microform is heavily dependent upon the quality of the original thesis submitted for microfilming. Every effort has been made to ensure the highest quality of reproduction possible.

If pages are missing, contact the university which granted the degree.

Some pages may have indistinct print especially if the original pages were typed with a poor typewriter ribbon or if the university sent us an inferior photocopy.

Reproduction in full or in part of this microform is governed by the Canadian Copyright Act, R.S.C. 1970, c. C-30, and subsequent amendments.

AVIS

La qualité de cette microforme dépend grandement de la qualité de la thèse soumise au microfilmage. Nous avons tout fait pour assurer une qualité supérieure de reproduction.

S'il manque des pages, veuillez communiquer avec l'université qui a conféré le grade.

La qualité d'impression de certaines pages peut laisser à désirer, surtout si les pages originales ont été dactylographiées à l'aide d'un ruban usé ou si l'université nous a fait parvenir une photocopie de qualité inférieure.

La reproduction, même partielle, de cette microforme est soumise à la Loi canadienne sur le droit d'auteur, SRC 1970, c. C-30, et ses amendements subséquents.

Canada

Preparation and Characterization of Solid Acidic Catalysts for the Hydrocracking of n-Paraffins

Shuyong Xiao

A Thesis

in

The Department

of

Chemistry and Biochemistry

Presented in Partial Fulfilment of the Requirement

for the Degree of Doctor of Philosophy at

Concordia University

Montreal, Quebec, Canada

February, 1995

ISBN 0-612-01258-1

ABSTRACT

Preparation and Characterization of Solid Acidic Catalysts for the Hydrocracking of n-Paraffins

Shuyong XIAO, Ph.D

Concordia University

Novel classes of bi-functional catalysts used in the conversion of n-paraffins, including various zeolites, lanthanum Y zeolites, desilicated zeolites, and sulfate-promoted hybridized zeolites have been prepared and characterized. The mechanisms and kinetic behaviours for n-paraffin(n-octane as a model) conversion over these catalysts have been thoroughly studied. The resulting information can be used for catalyst design and optimizing reaction conditions to favour a desired product distribution.

It has been shown that the cation-exchange capacity and acid density of a zeolite can be significantly improved by selectively removing some of its framework Si atoms with a basic solution under very precise conditions. However, these desilicated zeolites in the acid form are not as thermally stable as the parent zeolites. The presence of La is found to enhance such stability.

It has been confirmed that there exists a temperature window from 770 K to 870 K for optimum activation of sulfate-promoted zirconia used as a co-catalyst in a hybrid catalyst and a tetragonal crystalline structure for zirconia was obtained, without loss of sulfate groups and with subsequent good catalytic performance. Superacidic properties of the sulfate-promoted zirconia were characterized. The synergistic effect of the hybrid catalyst was credited to the transfer of reaction intermediates from the sulfate-promoted zirconia surface to the zeolite pore system.

Conversion of n-paraffins(C_7-C_{16}) over bi-functional catalysts is catalyzed at Bronsted acid sites, whereas Pt is necessary for their catalytic on-stream stabilities. Hydrocracking of n-paraffins proceeds in consecutive steps, and isomerization and cracking reactions have different values of activation energy. The "cage effect" of the zeolite has been proposed, which affects both the adsorption of reactants onto the active sites and the formation of the carbenium ion intermediates.

Large amounts of isobutane and gasoline-grade isoparaffins are obtained over Pt-containing Y zeolite and hybridized catalysts at low reaction temperatures (< 500 K) and long contact times. The moderately acidic Pt/LaNaY catalyst is favourable to the production of the multi-branched isomers even at temperatures above 550 K.

Acknowledgements

I would like to thank Dr. Raymond Le Van Mao for his precious guidance and continuous encouragement throughout my Ph.D program.

I would like to thank the members of my research committee, Dr. O.S. Tee and Dr. S.R. Mikkelsen for their time and helpful suggestions.

I wish to give my special thanks to Dr. A. Lavigne and Miss. A. Ramasaran for their patience and interest in reading this manuscript.

I wish to thank Dr. R. Patterson and Dr. N. Kapoor for their assistance in determining the sulfur content and in performing SEM experiments. I also wish to thank Dr. G. Denes, Dr. M.F. Lawrence, and my friends in this department, especially, Mr. S.T. Le and Mr. D. Kolokotronis for their helpful discussion.

I am grateful to Concordia University for awarding me the International Fee Remissions.

Finally, I dedicate this thesis to my wife and my daughter for their understanding and believing in me.

Table of Contents

List of Figures

List of Tables

CHAPTER I

INTRODUCTION

AND

CRITICAL REVIEW OF LITERATURE

1.1 Petroleum and Petroleum Refinery

Petroleum, more commonly called "crude oil", can be regarded broadly as a mixture of hydrocarbons and hydrocarbon derivatives that occur naturally in the earth. On a molecular basis, it is a complex mixture of hydrocarbons plus organic compounds of sulphur, oxygen, and nitrogen, as well as compounds containing metallic constituents, particularly, vanadium, nickel, iron and copper. Hydrocarbons can account for more than 75% of the constituents of many petroleums, and are of three classes of compounds: the alkanes (or paraffins), the cycloalkanes (or naphthenes), and aromatic compounds[1].

Petroleum products derived from crude oil are convenient source of energy(90%) and raw chemicals(10%). The separation of petroleum into fractions and subsequent treating of these fractions to make them into petroleum products is called petroleum refining[2]. The gasoline produced from the distillation of crude oil, without any other chemical treatments, is called "straight run gasoline". The problems associated with straight run gasoline are that its total yield is not adequate and the lower quality (low octane number) to meet the demands for gasoline[3]. Cracking heavier molecules is a method to increase the yield of products in the gasoline range at the expense of other less desirable petroleum fractions.

1.2 Cracking

1.2.1 Terminology and Technology

(1). Cracking: Cracking in petroleum chemistry refers to the breakdown of high-molecular weight hydrocarbons to light-molecular weight ones, which involves chemical cleavage of C-C bonds[4]. Figure 1.1 shows the reactions[4] involved in cracking of a paraffin. Reaction I, in which a saturated aliphatic hydrocarbon molecule splits into one paraffinic and one olefinic molecule, is the primary reaction. The primary products may crack again and yield a variety of hydrocarbons. In principle, the chemistry of paraffin cracking is simple, but the actual course of the reaction is much more complex, since many extraneous reactions occur at the same time. In practice, industrial cracking processes are of two general types: thermal cracking and catalytic cracking.

(2). Thermal Cracking: Thermal cracking is the process of heating the high boiling material in the absence of a catalyst. Under high temperature, large molecules are cracked or broken into smaller fragments. This process was developed shortly before World War I, and was used to meet increased gasoline demand in the following decades.

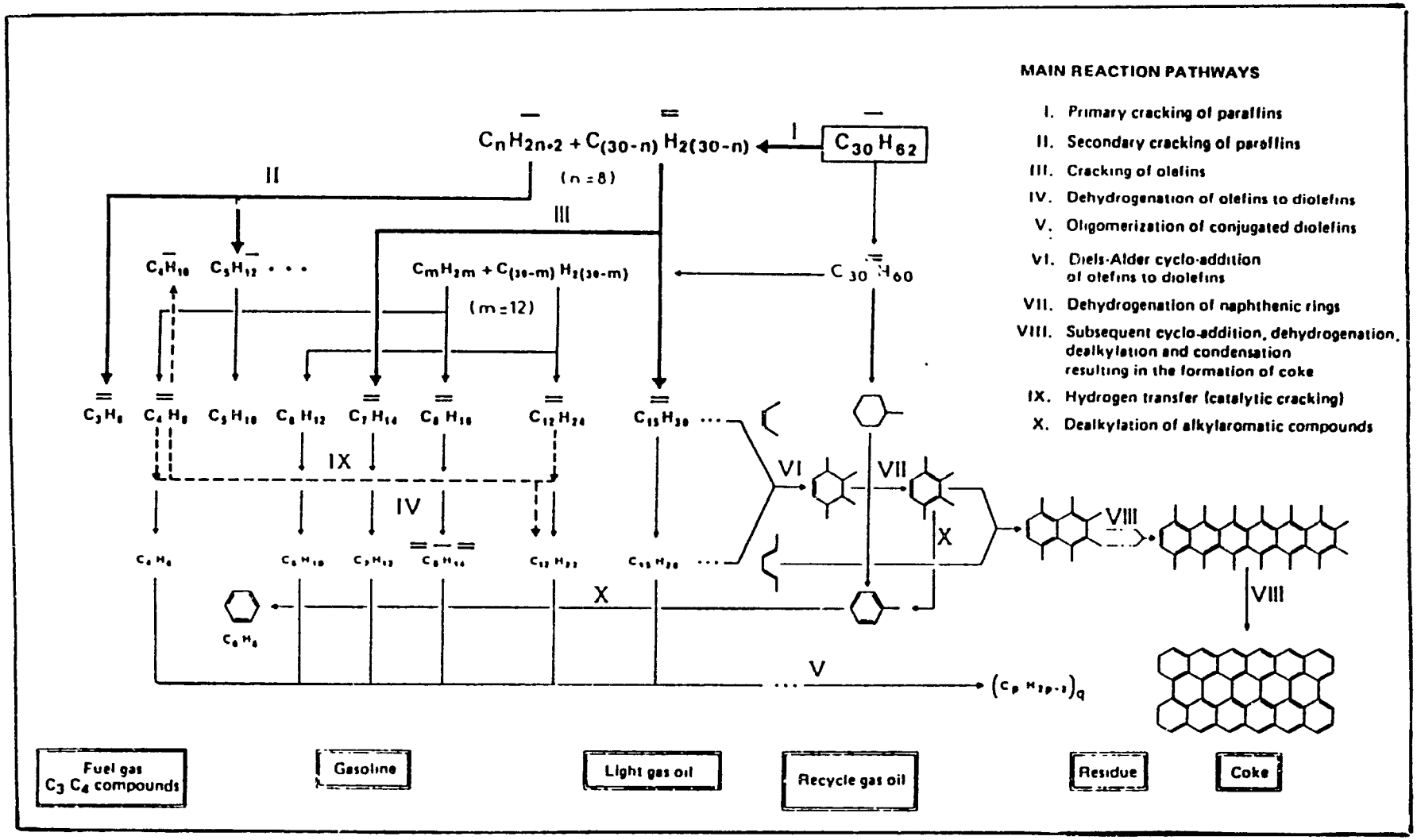

Figure 1.1 Reactions Involved in Cracking of paraffins

Steam cracking is thermal cracking of light hydrocarbons in the presence of steam which is used as the "inert" diluent. It also has some other beneficial effects: removal of coke via the water gas shift ($C + H_2O \rightleftarrows CO + H_2$), and improvement of heat transfer. The primary objective of steam cracking is to maximise the yield of ethylene.

(3). Catalytic cracking: Catalytic cracking is the process of heating the high-boiling material under pressure in the presence of a catalyst. Under these conditions large molecules are cracked or broken into smaller fragments. Fixed-bed catalytic cracking was first introduced commercially in 1936 as a result of work done by Eugene Houdry in the 1920's[5]. The ever greater demand for aviation fuels during World War II prompted the foundation of today's Fluid Catalytic Cracking (FCC) process in which small particles of catalyst (eg. 20-200 μm in diameter) are suspended in upflowing hot vapours of the cracking stock (crude oil or distillation cut), to be handled like a single phase fluid and circulated through pipes and valves between reaction and regeneration vessels. This fluidization process ensures intimate contact of the vapour with the catalyst particles. It not only allows a continuous process but also transfers heat from the regenerator to the reactor where it is needed. A typical catalytic cracking catalyst employed in a modern FCC unit contains up to 25% zeolite material (Rare Earth ion exchanged Y zeolite, REHY, about 21%wt in degree of ion-exchange). The introduction of zeolitic cracking catalysts revolutionized

the petroleum refining industry. It was, indeed, the most important breakthrough in cracking technology in the last few decades.

Hydrocracking is a catalytic cracking process which proceeds in the presence of hydrogen. A dual-functional catalyst comprised of a hydrogenation/dehydrogenation component and an acidic component is usually employed in this process. In theory, any desired petroleum fraction can be produced by hydrocracking.

1.2.2 Theories of Cracking Processes

1). Free radical chemistry

Thermal cracking including steam cracking proceeds via a conventional free radical chain pathway which consists of three main steps(Scheme I). The primary initiation is homolysis of C-C bonds. It has a high (composite) activation energy, ca. 220 $kJ.mol^{-1}$. Overall, the initiation and propagation reactions serve to reduce the molecular weight of the product. The termination reactions have zero activation energy and being bimolecular, are favoured at high radical concentrations. In addition to these "primary reactions" some secondary reactions take place. These become more important as the reaction proceeds at high conversion. They include olefin polymerization, alkylation, and condensation of aromatics leading to the production of coke.

(a) *Initiation*: $C_{10}H_{22} \rightarrow C_2H_5\bullet + \bullet C_8H_{17}$

(b) *Propagation*: $C_2H_5\bullet \rightarrow C_2H_4 + H\bullet$

or: $C_2H_5\bullet + C_{10}H_{22} \rightarrow C_2H_6 + \bullet C_{10}H_{21}$

or: $\bullet C_8H_{17} \rightarrow C_2H_4 + \bullet C_6H_{13}$

or: $\bullet C_8H_{17} \rightarrow C_2H_5\bullet + C_6H_{12}$

and: $\bullet\bullet\bullet\bullet\bullet$

(c) *Termination*: $H\bullet + \bullet C_2H_5 \rightarrow C_2H_6$

Scheme I: Free Radical Pathway for Thermal Cracking

The above process to cleave C-C bonds without any assistance other than heating from the surroundings is called pyrolysis. If cleavage of C-C bonds is accompanied by hydrogen saturation of the fragments, it is then characterized as hydrogenolysis[1]. An essential difference between pyrolysis and hydrogenolysis is that in pyrolysis a certain amount of polymerized heavier products, such as tar or coke, are always formed along with the light products, but during hydrogenolysis polymerization may be partly, or even entirely, prevented so that only light products are formed.

2). Carbocation chemistry

Catalytic cracking including hydrocracking proceeds via the general carbocation intermediates. Two classes of carbocations, alkylcarbenium ions and alkylcarbonium ions[6], have been distinguished according to the coordination number of the positively charged carbon atom. Whereas, alkylcarbenium ions can be generally represented by the formula CR_3^+, the general chemical formula for alkylcarbonium ions is CR_5^+, in which R stands for a hydrogen atom or an alkyl group. The stability of either alkylcarbonium ions or alkylcarbenium ions increases along the following sequence:

primary < secondary < tertiary < quaternary

Alkylcarbonium ions are not essentially involved in catalytic cracking reactions, but they are potential intermediates in the isomerization mechanism of acyclic alkylcarboniums as substituted protonated cycloalkanes[7]. Among these substituted protonated cycloalkanes, substituted protonated cyclopropane(PCP) is the most interesting one in the mechanism of isomerization. It contains the smallest possible ring among these structures and exists in three different forms, as shown in Figure 1.2.

Isomerization of alkylcarbenium ions over acid catalysts is of two types (Type A and Type B), depending on whether the degree of branching of the carbon skeleton is changed or not[6]. Both types of isomerizations or

rearrangements involve the formation of an intermediate substituted corner protonated cyclopropanes(CPCP).

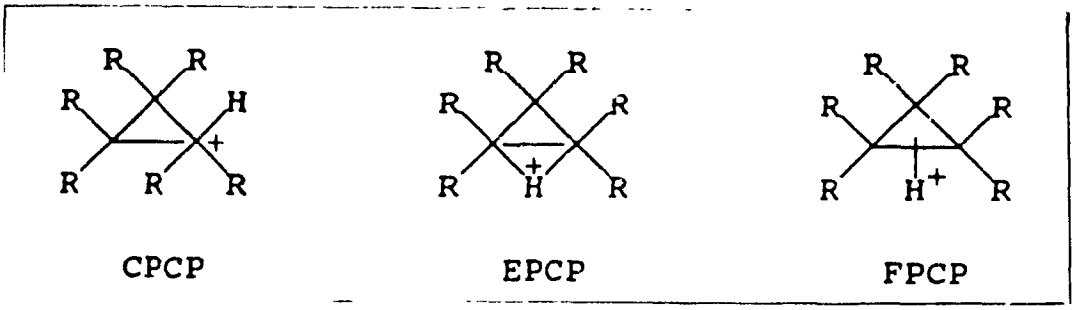

Figure 1.2 Representation of substituted corner(CPCP), and edge(EPCP) and face(FPCP) protonated cyclopropanes. R stands for a hydrogen or an alkyl group

Cracking of alkylcarbenium ions proceeds via β-scission. Depending on the branching configuration of the original carbenium ion, there are five modes of β-scission reactions of secondary and tertiary alkylcarbenium ions possible as described in Figure 1.3[6].

Kinetics studies (Table 1.1) show that type A β-scission is much faster

than isomerization via 1,2-methyl shifts, which in its turn is substantially faster than types B_1, B_2, and C β-scission. Accordingly, the conversion pathway of octyl cations, for example, can be represented by Figure 1.4[8-9].

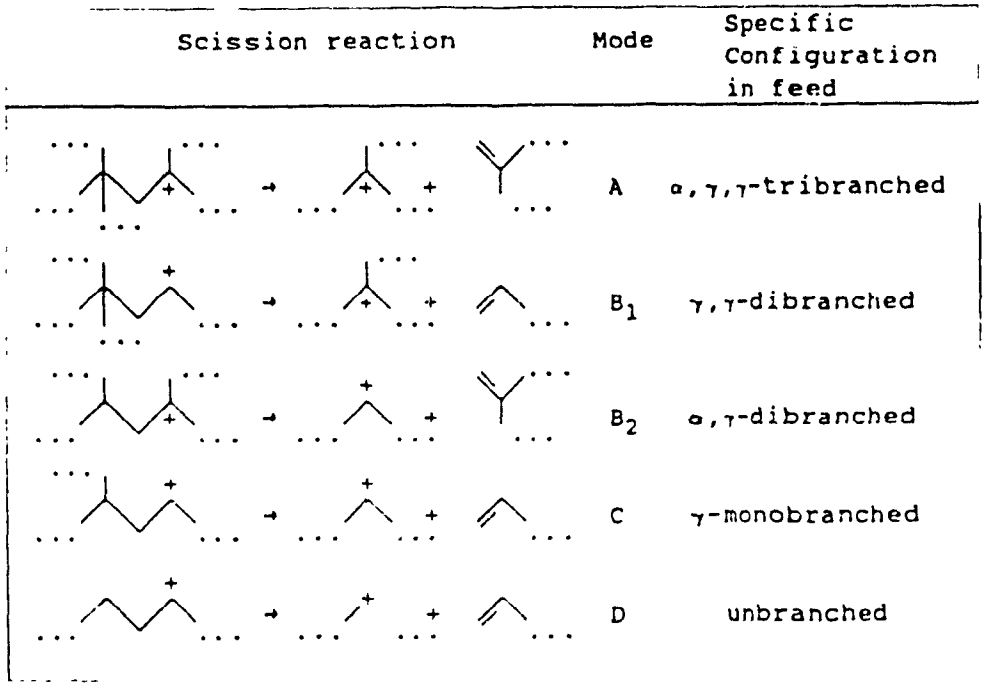

Figure 1.3 Specific branching configurations and β-scission modes of acyclic alkylcarbenium ions(the dashed lines stand for n-alkyl groups)

Table 1.1 Relative apparent rate constants of types A, B_1, B_2 and C hydrocracking, 1,2-methyl shift, and branching of iso-octanes, iso-nonanes, and iso-decanes with B_2 as standard over the Pt/USY catalyst [6]

	Temperature (K)			
	469	439	434	405
	Isooctanes	Isononanes	Isodecanes	
Hydrocracking				
B_1	0.34	1.5	2.8	
B_2	1.0	1.0	1.0	
C	0.34	0.77	0.40	
A				1050
B isomerization				
mono-> dibranched	0.34	0.85	0.80	0.80[a]
di-> tribranched	0.28	0.77	0.80	
A isomerization				
1,2-methyl shift				56

[a] taken as standard = 0.80

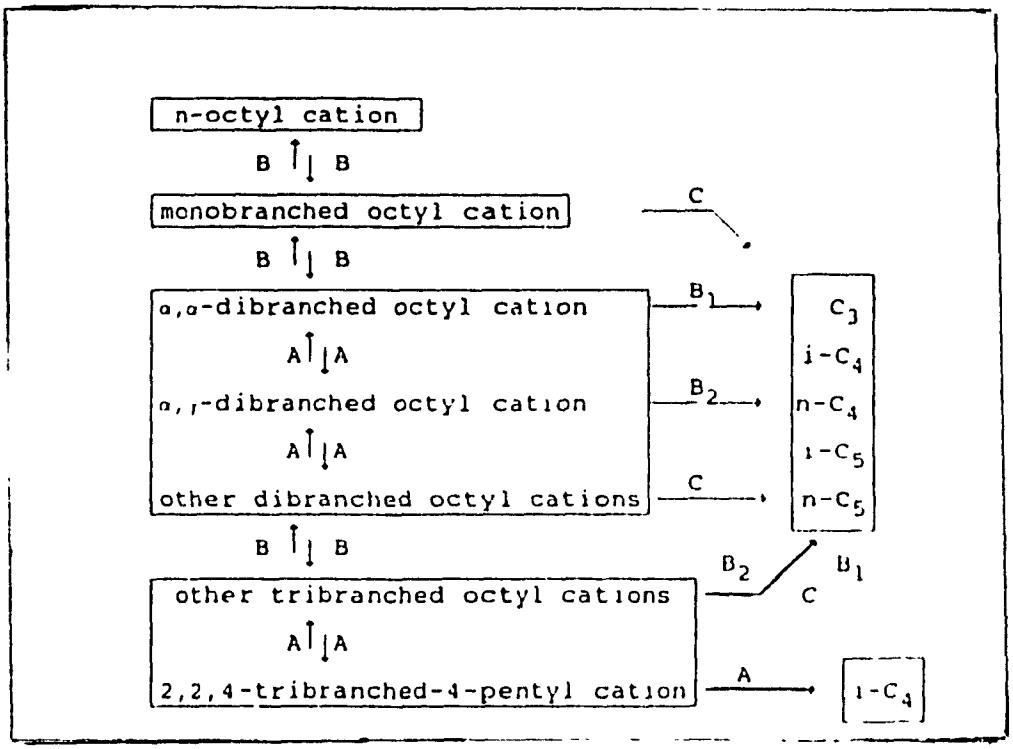

Figure 1.4 Conversion pathways of octyl cation at 469 K in Pt/USY zeolite (from Ref.6)

Thus, according to the above classical carbocation chemistry, hydrocracking proceeds via β-scission as represented in Scheme II, whereas, hydroisomerization proceeds via protonated cyclopropane intermediates as described in Scheme III. These two processes have approximately the same activation energy[10] and compete with each other over acidic catalyst; the product spectrum thus obtained from the conversion of a long-chain n-alkane depends on the degree of conversion[8-9] as shown in Figure 1.5[6] with the following typical features[8]:

- high selectivity for feed isomers at low to medium conversion;
- pure primary cracking of the feed isomers, resulting in a symmetric molar distribution of the cracked products among their carbon numbers;
- no formation of methane nor ethane and formation of only relatively low amounts of propane;
- high yields of monobranched cracked products, especially in the carbon number fraction obtained by propane abstraction.

Although the above theory of hydrocracking has found widespread acceptance and is still being quoted in most literature, it has been seriously questioned by Sie[11-13], recently. He proposed a protonated cyclopropane as a reaction intermediate, just as in the mechanism of isomerization of paraffins. According to this new mechanism, as shown in Scheme IV, the cleavage of C-C bonds proceeds through a 1,3-hydride shift following by a hydride shift

scission (a combination a 1,2-hydride shift and bond scission) instead of a β-scission in the classical hydrocracking mechanism. The mechanism not only casts fresh light on the relation between hydroisomerization and hydrocracking, but it is also capable of providing a logical explanation for many experimental observations. However, since there is no direct proof for the existence of the protonated dialkylcyclopropane ion under catalytic cracking or hydrocracking conditions, this mechanism is still considered as a speculation[13].

Another questionable consideration is that both the "old" and the "new" mechanisms for hydrocracking are mostly concerned with the structure of the reaction intermediates regardless of the structure of the catalyst used. Thus, it is not surprising for them to induce the conclusion that the product spectrum depends mainly on the conversion level as shown in Figure 1.5[6], and is independent of reaction temperature, pressure and even the structure of the catalyst[8]. This is probably due to the fact that most catalysts previously investigated are either amorphous or open pore molecular sieves, and they impose no shape selective restrictions on any of the reactions involved. However, this is not the case with medium or small pore zeolites. Obviously, these mechanisms have to be reconsidered when dealing with reactions over these zeolite catalysts.

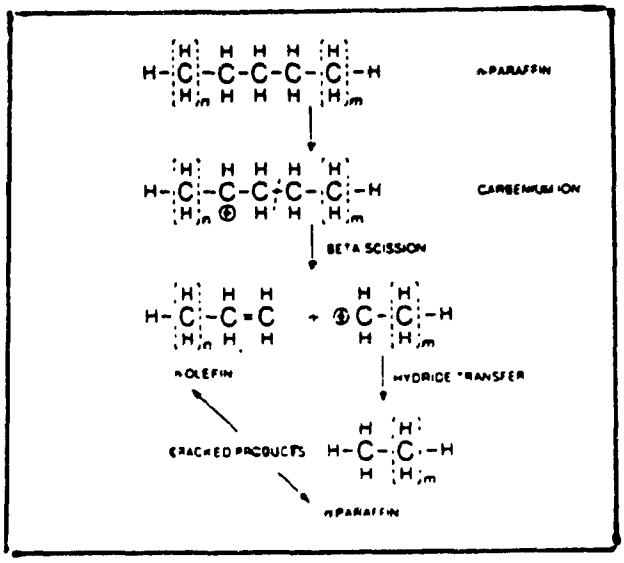

Scheme II Cracking of a n-Paraffin by the Classical Carbenium Ion Mechanism

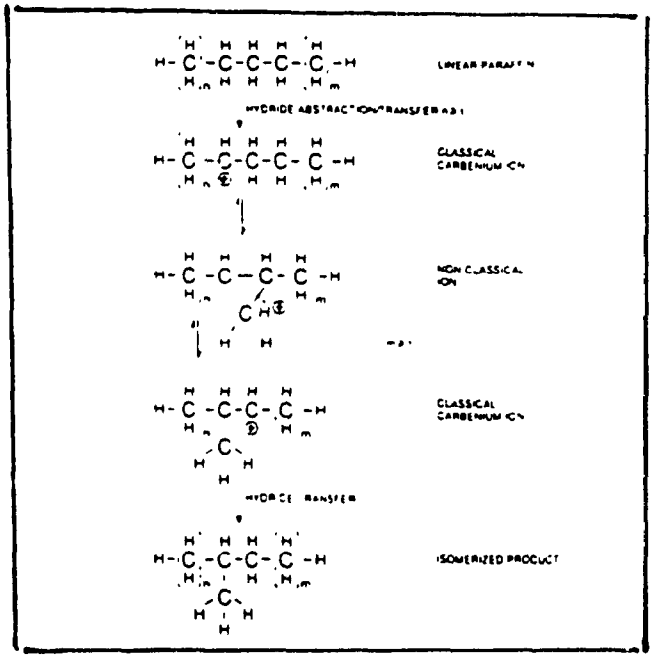

Scheme III Mechanism of Acid-Catalyzed Isomerization of a n-Paraffin

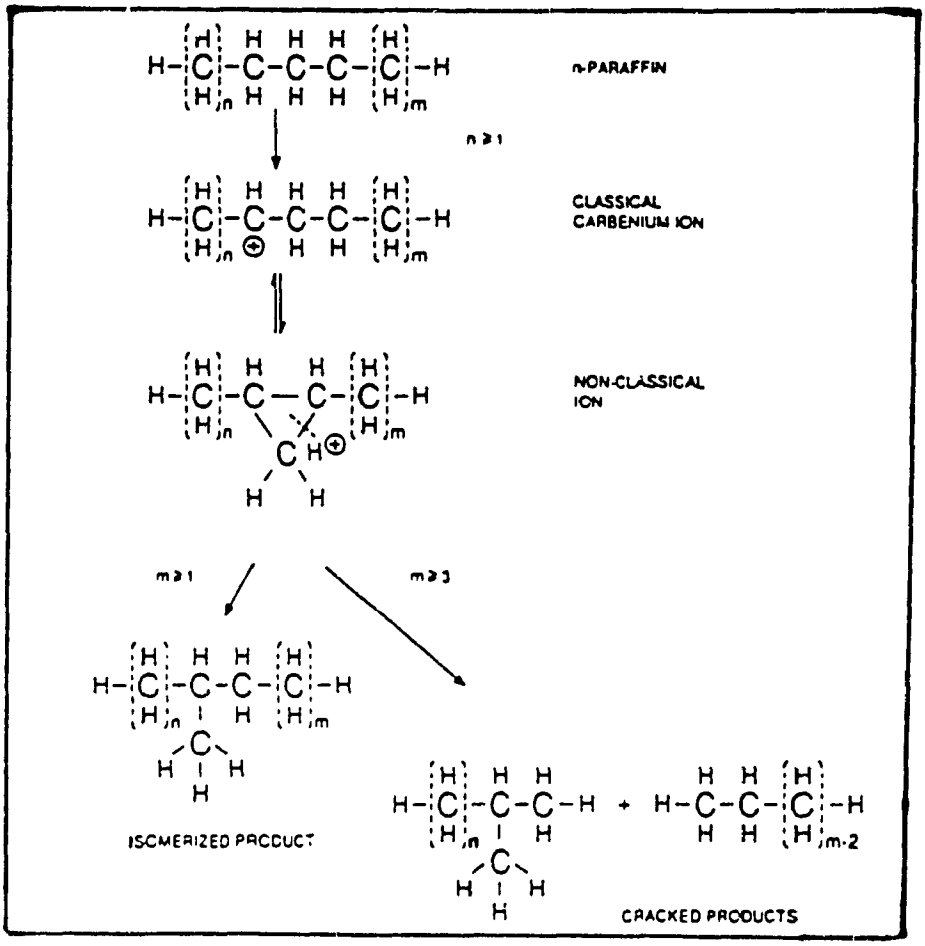

Scheme IV. Simplified Reaction Scheme for Hydroisomerization and Hydrocracking of a Normal Paraffin by the Protonated Cyclopropane Mechanism

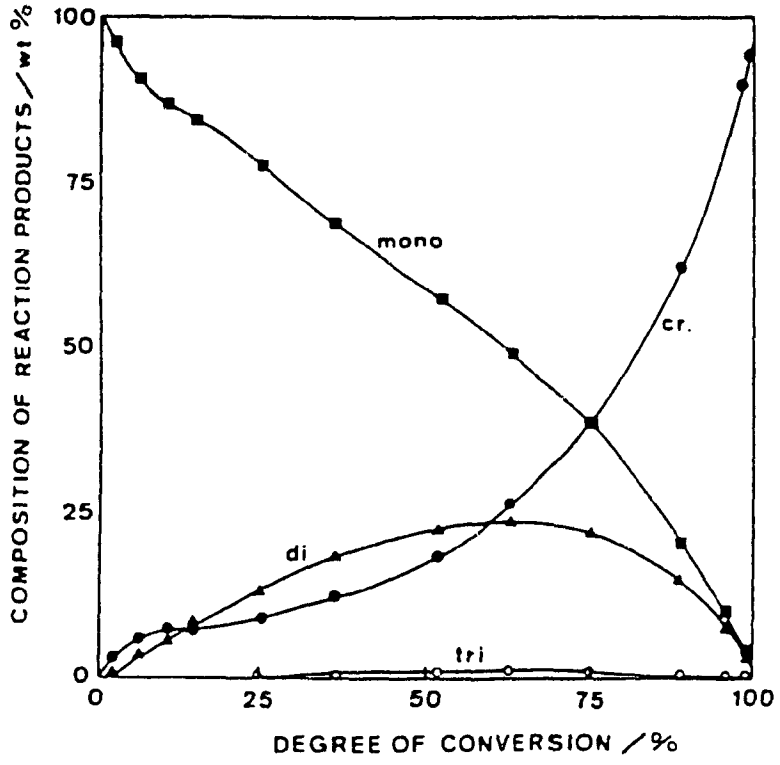

Figure 1.5. Distribution of mono-, di- and tribranched isomers and cracked products(in weight%) from decane against its degree of conversion(%) using a Pt/HY catalyst.

(Where, the total reaction pressure was 0.35 MPa, the H_2/decane molar ratio was 100, the molar flow rate at the reaction inlet (F_o/W) was 0.4 mmol $kg^{-1}s^{-1}$. The conversion was changed by increasing the reaction temperature from 400 to 500 K [6]

3). Comparison of thermal process and catalytic process

In summary, pyrolysis and hydrogenolysis are thermal processes which proceed via free radical chain pathways. Catalytic cracking and hydrocracking are catalyzed by acid (mostly Brønsted acid) which proceed via carbocation intermediate. As isomerization is also accompanied with carbocation intermediates, these catalytic processes may have high yields of branched alkanes in the products. Another essential difference is that pyrolysis and hydrogenolysis produce a large amount of light alkenes or alkanes such as methane, ethane, and ethylene, because of the shorter life of the smaller radicals; but these light alkanes or alkenes are normally absent in catalytic cracking and hydrocracking due to the difference in stability of different carbocation intermediates.

Some typical characteristics of these cracking technologies are presented in table 1.2. Table 1.3 is a list of key developments in cracking technology[14]. It can be seen that innovations of catalysts has played an important role in the development of cracking technology.

Table 1.2 Typical characters of cracking technologies

cracking:	Thermal cracking	Steam cracking	Catalytic cracking	Hydro cracking
Feed:	kerosene gas oil naphtha	ethane propane naphtha	gas oil heavy naphtha	gas oil
Products	gasoline (low,RON) alkene	ethylene	gasoline	gasoline (high RON) chemicals
Catalyst:	no	no	RE-HY	NiMo/ $SiO_2Al_2O_3$ Pd/Y
Operating:	750-900°C	750-1100°C	465-544°C ~0.3 MPa	380-420°C 5.4-10 MPa
Mechanism	Free Radicals	Free Radicals	Carbon Cation	Carbon Cation

Table 1.3 Key Development Related to Cracking Technology

Year	Event
1913	Thermal cracking (W.M. Burton)
1915	Aluminum chloride catalyst (A.M. McAfee)
1922	TEL additive to gasoline (Standard Oil Co. of N.J.)
1928	Acid activated clays as catalyst (E.Houdry)
1936	1st 2000b/d cracking unit (Socony Vacuum Oil Co.)
1940	Synthetic silica-alumina (Houdry & Socony Vacuum Oil)
1942	1st FCC unit (Model I, Standard Oil Co. of N.J.)
1943	1st TCC unit (Magnolia Iol Co.)
1948	Microspheroidal FCC (Davison Chemical Co.)
1954	Synthesis of zeolite X (Union Carbide Co.)
1956	Riser cracking (Shell Oil Co.)
1959	Synthesis of zeolite Y (Union Carbide Co.)
1962	Zeolite cracking catalysts (Mobil Oil Co.)
1964	USY and REY FCC catalysts (Davison Chemical Co.)
1971	Riser FCC (Kellogg Co.)
1974	Platinum CO combustion promoter (Mobil Oil Co.)
1974	SO_x reduction catalyst (Amoco)
1975	Ni passivation (Sb, Phillips Petroleum Co.)
1978	V passivation (Sn, Gulf Oil Co.)
1983	High-Silica Y from $(NH_4)_2SiF_6$ (Union Carbide Co.)
1986	ZSM-5 octane additive (Mobil Oil Co.)

TEL = Tetraethyl lead; FCC = Fluidized Catalytic Cracking
TCC = Therofor Catalytic Cracking.

The reactions of interest in catalytic cracking take place on the surface of heterogeneous catalysts. For any industrial heterogeneous catalyst, three important criterias must be fulfilled. The first criterion is activity. The catalyst must actually catalyze the reaction and have a rate of reaction that is high enough to achieve the desirable conversion rate in commercial-scale reactors. The second criterion is selectivity. The catalyst must induce the formation of the desired products and suppress, or at least not enhance, the formation of those which are not desired. The third criterion is stability; it must have sufficient physical stability to withstand the high temperatures and pressures at which it is likely to be employed. In the following section, I will introduce the zeolite catalysts and show how they meet these three criteria.

1.3 Zeolites and Their New Developments

Zeolites employed as cracking catalysts is one example of their wide variety of applications. Table 1.4 lists several innovations in applied catalysis developed since 1980[15]. A substantial number of them are based on zeolites and related solids. The properties and uses of zeolites are being explored in many scientific disciplines: inorganic and organic chemistry, physical chemistry, biochemistry, mineralogy, geology, crystallography, catalysis, and in all types of chemical engineering process technology. Indeed, some breakthroughs have gone beyond the "old" definition of zeolites.

Table 1.4 Innovations in Applied Catalysis since 1980

Process	Catalyst
conversion of ethane and benzene to ethyl benzene	H-ZSM-5
methanol to gasoline(petrol)	H-ZSM-5
conversion of ethane and acetic acid to vinyl acetate	Pd
oxidation of tert-butyl alcohol to methylmethacrylate	Mo oxide
improved means of liquefying coal	Co, Ni sulfides
production of diesel fuel from CO + H_2 (syngas)	Co
hydrotreating of hydrocarbons	Pt or Ni/Zeolite,
catalytic distillation(in MTBE production)	acidic resins
vitamin K_4 production	Pd membrane
dehydrocyclization(Cyclar process) of LPG to aromatics	Ga-ZSM-5
oxidation of methacrolein, hydration of isobutene	Mo-V-P heteropolyacid
polymerization of tetrahydrofuran	phase-tran.catalyst
1990-1993	
production of dimethyl carbonate from acetone	CuCl
conversion of phenol to hydroquinone and catechol	Ti-silicate
isomerization of but-1-ene to 2-methylpropene	H-ferrierite
isomerization of oxime of cyclohexanone to ε-caprolactam	SAPO-11
ammoxidation of cyclohexanone to its oxime using H_2O_2	Ti-silicalite
production of acrylamide from vinyl cyanide	nitrile hydratase
complete combustion of natural gas (at ca. 1300 °C)	nobel metal oxides
sweetening of natural gas by oxidation of H_2S to S	mixed oxides
oxidation of benzene to phenol via cyclohexene	zeolites
methanol to light alkenes	SAPO
olefin oligomerization("Shell" process)	zeolite
L-aspartic acid and L-alanine from NH_4 fumarate	micro-organisms
from toluene to toluene cis-1,2-dihydroxy-3 methylbenzene	Pseudomonas putida
production of 2,6-diisopropylnaphthalene using propene	mordenite
decomposition of hypochlorite	NiO
dehydration of alkanols	heteropolyacid salt

Zeolites have always been defined as a group of aluminosilicate minerals with the general formula[16]:

$$M_{x/n}[(AlO_2)_x(SiO_2)_y].wH_2O.$$

where M is an n-valent cation, w is the number of water molecules and the ratio y/x is called silicon-aluminum ratio with values that depend upon the structure. However, this definition can no longer comprise all kinds of materials. First, zeolite frameworks are no longer constructed solely of the AlO_4 and SiO_4 tetrahedra combinations. They can also contain other metals. About a quarter of the elements of the periodic table can now be incorporated into the framework structure of this kind of solid. In other kinds of zeolites like the large family of microporous aluminium phosphates (AlPOs, MAPOs)[17], there are no SiO_4 tetrahedra in the framework, whereas, in some kinds of zeolites like titanium silicates (TS-1)[18], aluminum tetrahedra are absent. Secondly, zeolite frameworks are no longer exclusively made of inorganic oxides. It has been reported that an organic solid with wide channels based on hydrogen bonding between macrocyclics has been successfully synthesized[19]. It could also be very interesting to construct these structures from C_{60} blocks. Although these organic zeolite-like structures would be fragile compared to inorganic materials, they may be suitable as low-temperature molecular sieves and in specialized catalyst applications. Thirdly, zeolite frameworks might possess positive charges in nature. It has been recently reported that a novel microporous boron-aluminium chloride with a cationic framework has been successfully

synthesized[20-21]. Although it appears difficult by conventional thermal-crystallization methods to make a positively charged zeolite framework, this could be approached by modification of existing zeolites through insertion or removal of some elements from the zeolite frameworks. These methods have been well developed. Combinations of these separate techniques could provide a path towards the desired framework (such as $ZrPO_4$, $SiPO_4$). Applications for such materials would make use of their basicity and ion-exchange capacity. Of particularly interest is to have the positively charged frameworks arising from $[ZrO_4]$ tetrahedra to provide another material from which to prepare superacidic crystalline solids by sulfate-promotion. In conclusion, zeolites represent only one type of material which has molecular sieving ability. Zeolites are molecular sieves, but molecular sieves are not necessary zeolites unless the definition of zeolites is changed. Since only aluminosilicate type zeolites are involved in this thesis, attention will be given to why and how this family of materials can be used as catalysts with respect to the three criteria.

The important structural feature of zeolites is the network of linked cavities or pores which form a system of channels throughout the structure. Windows to these channels(or pores) thus form a three-dimensional sieve, hence the well-known name molecular sieve. These windows range from 4 Å to 13 Å (pore sizes) as illustrated in Figure 1.6[22-23]. In addition to zeolites, there are now many non-aluminosilicate molecular sieves with pore sizes up to

50 Å [23]. The dimensions of these windows govern the size and shape of the reactant molecules that may enter it, the product molecules that may exit it, and the nature of the reaction intermediates that can form within it. These factors define the selectivity of zeolite catalysts.

The catalytic activity of zeolites is attributed to the presence of acidic sites arising from the [AlO_4] tetrahedral units in the framework. These acid sites may be Brønsted or Lewis in character. Zeolites usually are in sodium-form due to the nature of their synthesis. Brønsted acid sites are formed by ion-exchange of sodium ions by protons, or by ammonium ions followed by heating. Brønsted sites are converted into Lewis sites as the temperature is increased above 600 °C. It is also common to exchange the sodium ions with lanthanide ions such as La^{3+} or Ce^{3+}. These ions can better neutralize the three separate negative charges on the tetrahedral Al framework(Figure 1.7). The separation of such charges causes high electrostatic field gradients in the cavities which are sufficiently large to polarize C-H bonds or even to ionize them, enabling reactions to take place. In fact, it was a rare-earth substituted form of zeolite-X that became the first commercial zeolite catalyst for the cracking of petroleum in the 1960s. Since then, a rare-earth substituted form of zeolite-Y, that has proved more stable at high temperature is now used.

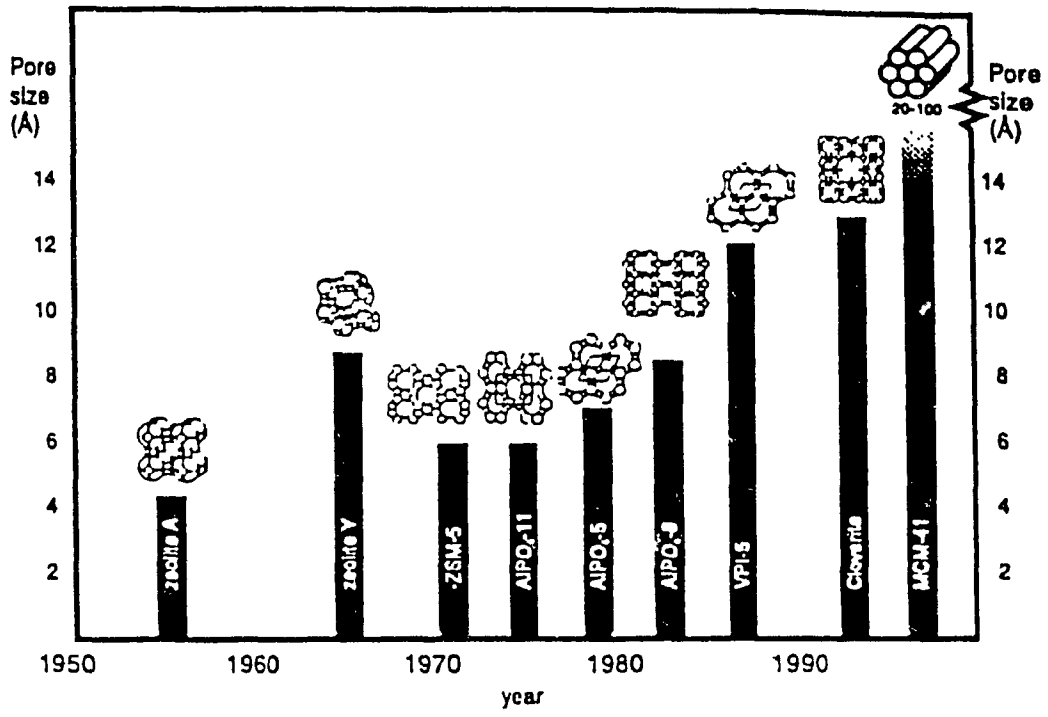

Figure 1.6 Evolution in zeolite/molecular sieve materials

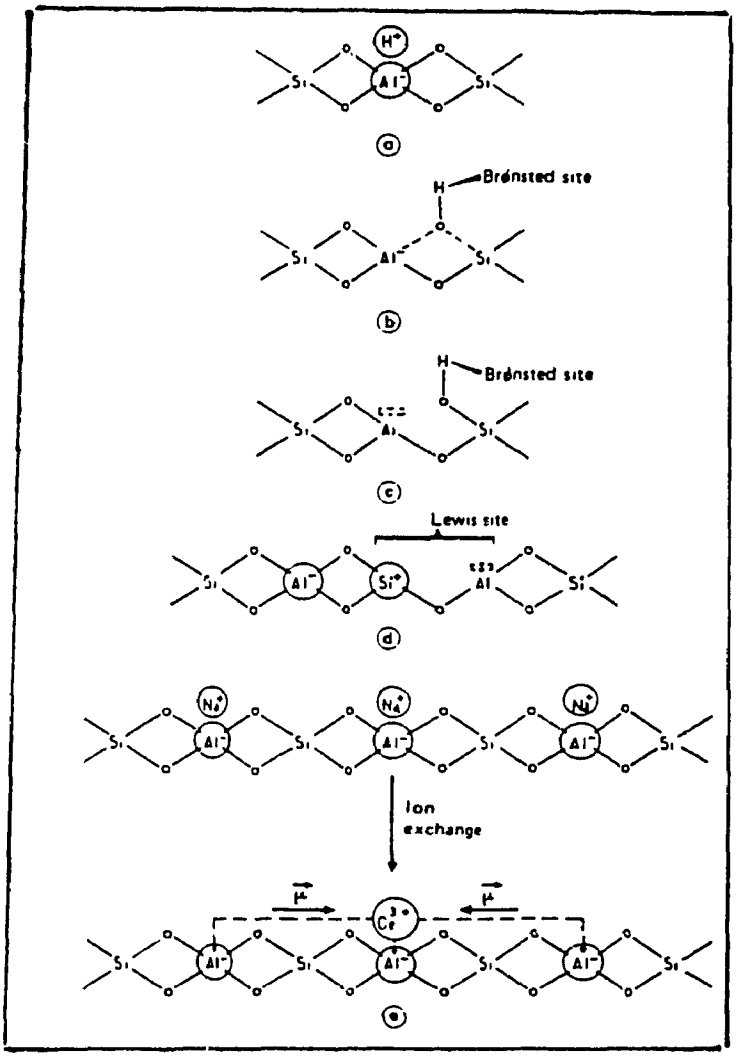

Figure 1.7 The acid sites on the zeolite surface[16]

As discussed earlier, besides activity and selectivity, an industrial catalyst has to meet another criteria: stability. The primary building units of zeolites are $[SiO_4]^{4-}$ and $[AlO_4]^{5-}$ tetrahedra linked together by corner-sharing, forming bent oxygen bridges as in quartz. In some respects, they behave like ceramics and as such high thermal stability is also one of their characteristics. For example, the crystal structure of Y zeolite may remain unchanged at temperatures as high as 700 °C. Various stabilizing treatments have also been developed[24], with some modified zeolites becoming thermally stable to over 1000 °C.

The use of a zeolite catalyst affords a high yield of gasoline with less coke formation due to its high activity, selectivity and stability. However, it gives gasolines with lower octane numbers, due to its lower olefinicity(Table 1.5)[14]. The diminished octane number was partially compensated for by adding octane-boosting tetraethyl or tetramethyl lead (TEL, TML). Unfortunately, lead compounds such as TEL and TML not only are dangerous to human health by causing hyperactivity and reducing learning ability in children but they also poison catalytic converters. The phaseout of lead additives mandated by the EPA(Environmental Protection Agency) is forcing the refining industry to look for alternatives for meeting octane blending requirements. This has also stimulated the development of new techniques including our work being presented in this thesis, all of which must be economically and environmentally promising.

Table 1.5 Comparison of Product Yields at Constant Coke Obtained over Amorphous and Zeolite Catalyst[14]

Catalyst	Amorphous SiO_2-Al_2O_3	Zeolite Catalyst	Difference
Coke, wt%	5.0	5.0	0
Conversion, vol%	77.0	86.0	+ 9
H_2, wt%	0.07	0.04	- 0.03
$C_1 + C_2$, wt%	3.1	2.7	- 0.4
C3, vol%	1.4	1.6	+ 0.2
C_3^-,vol%	14.2	14.0	- 0.2
i-C_4, vol%	6.8	8.9	+ 2.1
n-C_4, vol%	0.6	0.8	+ 0.2
C_4^-,vol%	9.9	8.5	- 1.4
C_5^+ gasoline ,vol%	55.5	65.5	+10.0
Paraffins, %	13	23	+10
Olefins, %	17	5	-12
Napthenes, %	41	23	-18
Aromatics, %	29	49	+20
Gasoline RON	94	91	- 3
LCO, vol%	5.0	4.3	- 0.7
HCO, vol%	18.0	9.7	- 8.3

1.4 Economic and Environmental Considerations

Today, energy consumption is an economic indicator. Significant world-wide growth is expected to continue in terms of energy consumption and fossil fuels are expected to remain very important well into the foreseeable future[25,26]. The aim of the petroleum industry is to find techniques to use these natural energy resources more efficiently. Of these techniques, one is catalytic cracking. The catalytic cracking of gas oil into gasoline, jet fuel, heating oil, and other lower molecular weight hydrocarbons is the largest volume commercial catalytic process[27]. The total current production capacity in the United States alone is about 15 million barrels per day. Over 500 tons of catalyst are required daily[28]. The annual worldwide sales of catalysts are expected to exceed 5 billion dollars by the end of this century[29]. Therefore, with such a tremendous operation, even very small modifications are of major economic significance.

One of the most dramatic changes caused by environmental legislation has been the removal of lead from gasoline. It was initially driven by concerns related to the toxicity of the lead emissions from motor vehicles and then later reinforced by the fact that lead poisons the autoexhaust catalyst system. Legislation related to unleaded gasoline emission controls and clean fuels has

now penetrated to a global scene. In addition, the advent of lead-free gasoline requiring a hydrocarbon based octane replacement stimulated research on development of novel catalytic processes such as the aromatization of LPG (Liquified Petroleum Gas)[30-32].

However, the implementation of the full RFG (Reformulated Gasoline) specification (The CAA: The 1990 Clean Air Act Amendments)[33], which is reflected by the requirement of lower aromatic content in diesel fuels and incorporation of oxygenates into gasoline, has again dramatically changed the way petroleum refiners think. Concerns that aromatics are toxic and related to CO emissions is again forcing the refiners to look for alternatives. One of these could be the MTBE (Methyl tertiary-Butyl Ether).

1.5 MTBE and Its Production

Presently, MTBE is the only oxygenate additive approved by EPA. The driving forces for using this octane enhancer are both emissions control and attractive octane properties. When compared to aromatic hydrocarbons which can be used for upgrading gasoline, MTBE evolves no toxic products from incomplete combustion in engines. When compared with methanol, MTBE does not provoke demixing when blended with gasoline. Furthermore, MTBE, which is characterized with specifications close to those of gasoline, does not require

dramatic modifications in engine technology. MTBE, being an oxygenate and having a fairly high octane number (RON = 110 - 130), accordingly favours the "clean" combustion of gasoline and other fuels. The size of the global gasoline pool is so large that the incorporation of even 10-15% of an ether has a huge impact in terms of demand. As demonstrated in Figure 1.8, its annual capacity amounted to nearly 14,000 million metric tons (14 MM mt) in 1992 and is projected to increase to over 24 MMmt by 1997[34]. Consequently, a shortage of the precursor, iso-butene, for the production of MTBE[35] via reaction with methanol is unavoidable. The refineries are required to find some way to make up for this shortage of iso-butene.

One route to increasing iso-butene production is by the isomerization of n-butene available from steam cracker, catalytic crackers. However, until recently this route to iso-butene has not been workable due to the lack of a selective catalyst to affect the desired alkene isomerization rather than the undesired dimerization. Medium pore sized zeolites have been found to have significant performance advantages over other catalysts with respect to this selectivity. Mechanistic studies indicate this reaction to go through a dimerization step to form a C_8 intermediate, and the relatively high diffusional resistance to this C_8 intermediate is an important characteristic for optimal shape selective control for this reaction (Figure 1.9)[36].

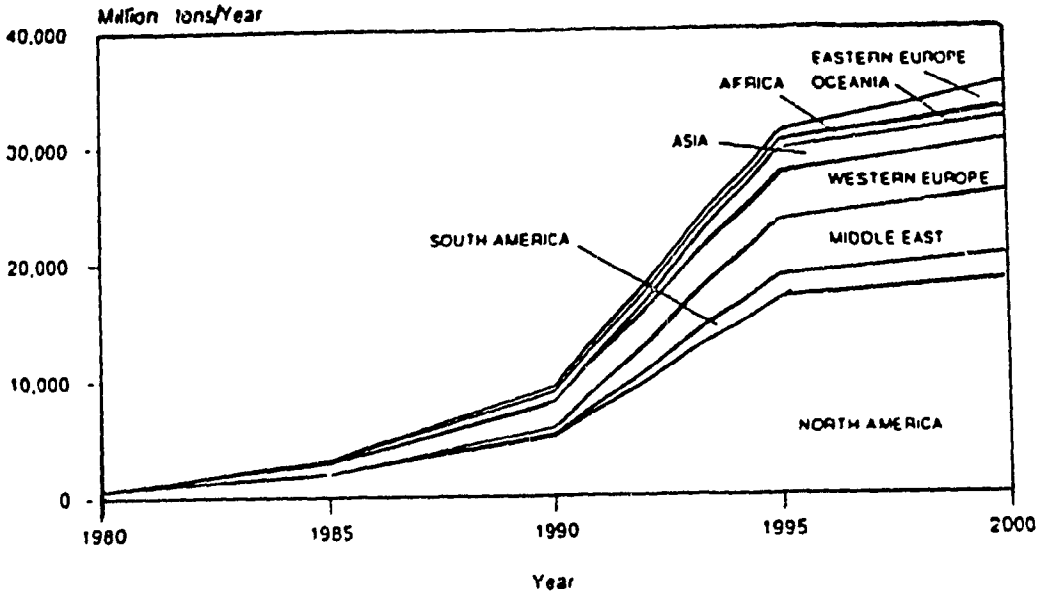

Figure 1.8 World growth in MTBE production

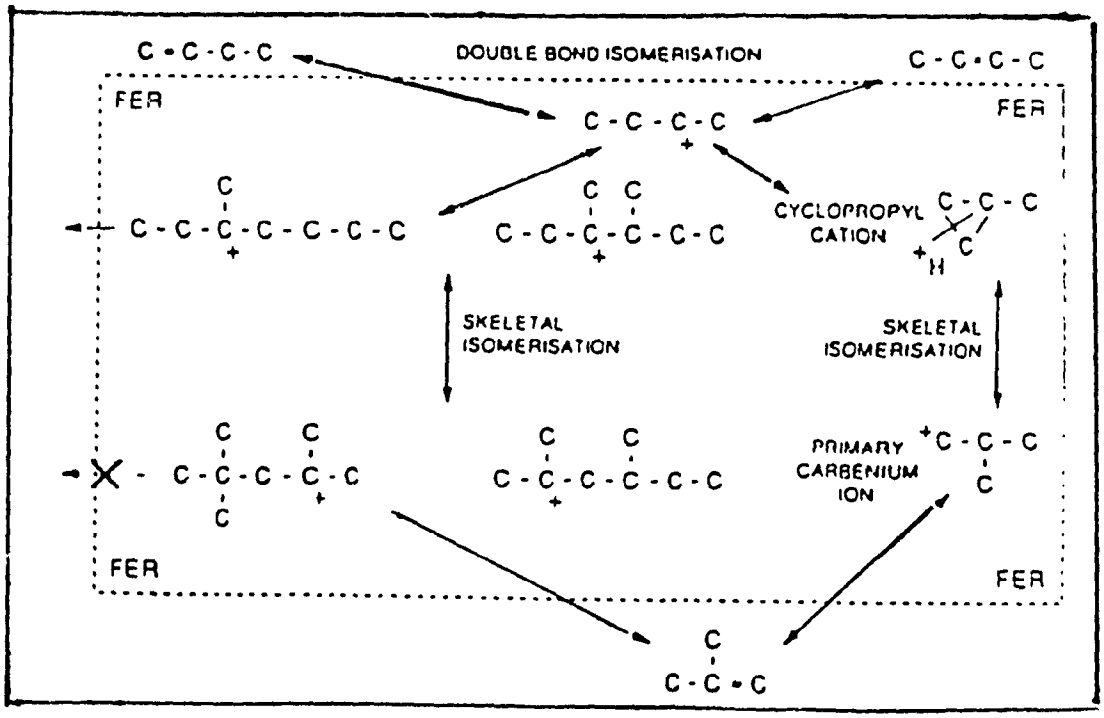

Figure 1.9 Proposed mechanism for butene skeletal isomerization

Another route for iso-butene production is by dehydrogenation of iso-butane. The U.O.P I-Forming[33] process which selectively cracks naphtha, kerosene, or both to generate high yields of isobutane demonstrates the source of this route. It is worth mentioning that while dehydrogenation of isobutane is a relatively easy reaction, skeletal isomerization of n-butane is however a rather demanding reaction[37].

At Concordia University, Le Van Mao and collaborators have set up a program similar to the I-forming program of U.O.P has been set up in order to produce isobutane and gasoline-range isoparaffins from two sources: heavy hydrocarbon mixtures and light alkanes (LPG or liquefied petroleum gas, propane, n-butane). Figure 1.10 is a scheme of this program.

"Truncated aromatization" reactions (TAR) or oligomerization of light paraffins might lead to a high production of the C_8-C_{12} hydrocarbons, with a product spectrum strongly dependent on the zeolite structure. It is obvious that the TAR conditions are significantly different from those of normal aromatization of light alkanes[38-42]. The previous research conducted by Le Van Mao implied that this reaction might be carried out with catalysts which are prepared according to a procedure similar to that of the hybrid catalyst used in aromatization of light alkanes[43].

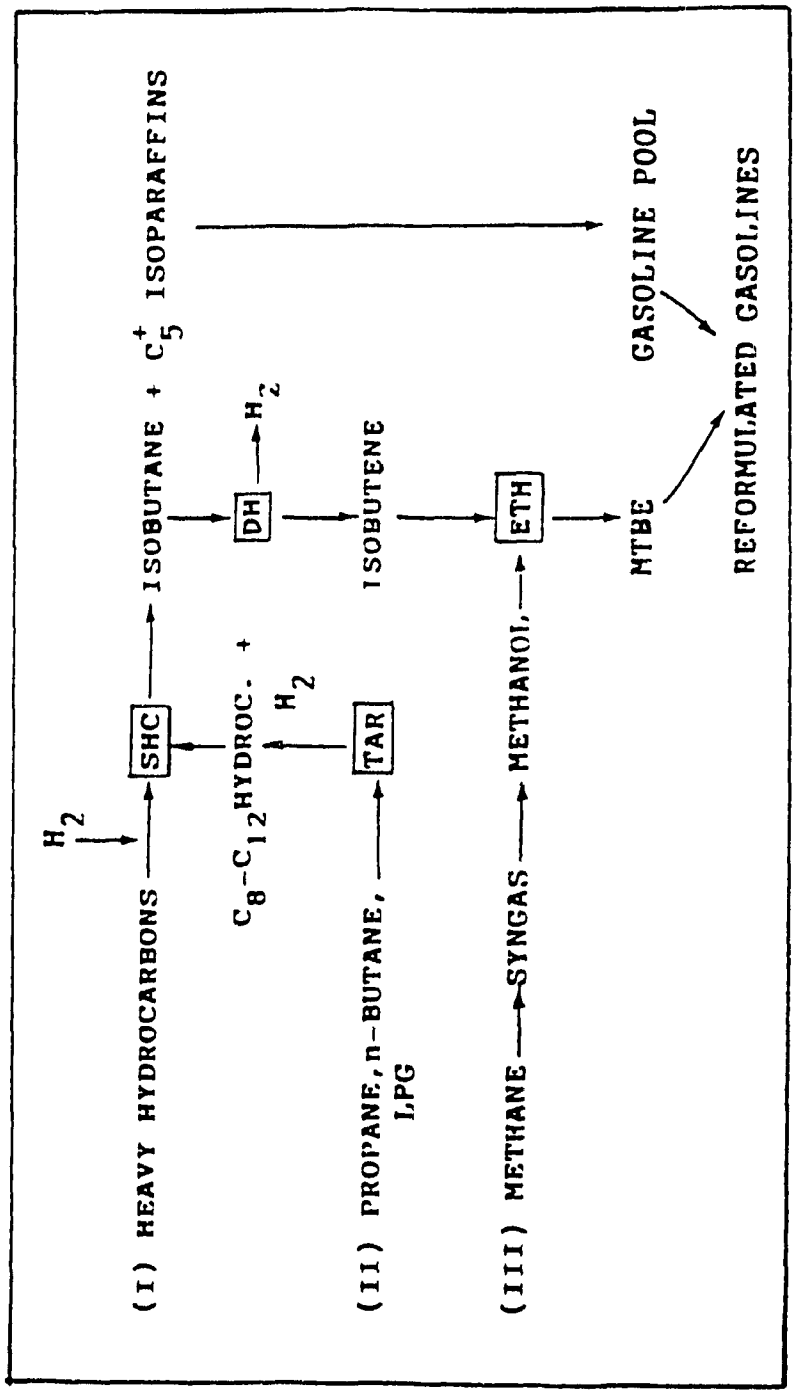

Figure 1.10 Various routes to reformulated gasolines

Etherification (ETH) of isobutene with methanol is commercially carried out over the acidic ion-exchange resin Amberlyst 15. Drawbacks to this process include low thermal stability, acid leaching from resin surface, and a high methanol/isobutene ratio. The ZSM-5 zeolite from Mobil Oil avoids such inconveniences. However, this zeolite is not as strong an acid catalyst as is the Amberlyst type resin[44]. The ETH has also been studied in our laboratories, and it has been shown that the triflic acid (Trifluorosulfonic Acid) modified Y-zeolite catalyst provided the best performance at a temperature of 85-90 °C and for a contact time of about 2.5 hours[34].

Selective hydrocracking (SHC) of C_8-C_{12} linear paraffins for the production of isobutane and other gasoline-range isoparaffins is the practical objective of this thesis.

1.6 Thesis Presentation

In this chapter, the general background and basic theories associated with this project have been reviewed. The more specific principles and developments with the relating problems are be individually introduced in each chapter.

In chapter 2, using the original Y zeolite and n-octane, one of the model

molecules, the effect of reaction parameters including reaction temperature, hydrogen partial pressure, and contact time are investigated. The reaction conditions for catalyst evaluation are chosen by optimising the above parameters.

Chapter 3 deals with the modification of zeolite with sodium carbonate followed by lanthanide ion-exchange.

Chapter 4 is another attempt in this project to improve Y zeolites's catalytic performance by hybridization with a super-acid component, sulfate-promoted zirconia. The " super acidic " behaviour of sulfate-promoted zirconia will be reviewed. The synergic interaction toward hydrocracking of n-octane between HY zeolite and sulfate zirconia is discussed.

In chapter 5, the different types of zeolites with respect to pore size configuration are compared. Also n-alkane reactants with different chain lengths are tested. To explain product distributions, a mechanism based on intermediate selectivity, consistent with the " Cage Effect", is proposed.

The kinetic studies used to compare the intrinsic catalytic properties of different types of catalyst are reported in Chapter 6. The apparent activation energies and pre-exponential factors are estimated from the proposed kinetic

model.

The conclusion of this project is given in Chapter 7 in which I have outlined the technology and proposed the reaction pathway.

CHAPTER II

HYDROCRACKING OF N-OCTANE

Reaction System Set-up

and Reaction Condition Optimizing

2.1 Introduction

Hydrocracking has been generally described as the conversion of hydrocarbons to lower molecular weight compounds under high hydrogen pressure. Hydrogen in the catalytic cracking system can hydrogenate the adsorbed olefinic hydrocarbons produced by the primary cracking reaction as in Figure 1.1, and thus reduce coke formation and eventual catalyst deactivation. It also allows catalytic cracking to occur at lower operating temperatures and considerably enhances selectivity towards branched isomers[45].

The catalysts employed in earlier hydrocracking processes as developed and practised in Germany during World War II were essentially non-acidic hydrogenating agents such as molybdenum or tungsten disulphate[46]. These catalysts were not efficient enough although their commercialization was supported by the government[47]. The development and widespread adoption of catalytic cracking processes around 1940 still further reduced interest in hydrocracking. However, with increased demand for higher octane gasolines and the adoption of catalytic reforming(which provides a large amount of hydrogen as a by-product) near 1950, new incentives for hydrocracking emerged. A large number of patents and publications were contributed to this technology[48,49]. The dual-functional catalysts comprised of a hydrogenating

agent such as tungsten or molybdenum (as oxides or sulfides), nickel, cobalt, or iron and an acidic cracking agent such as an active clay treated with hydrofluoric acid had been thoroughly studied. In the early 1960s, these dual-functional catalysts expanded to some noble metals such as platinum, and/or ruthenium impregnated on silica-alumina[50]. In the late 1960s, emphasis shifted from amorphous acidic materials to zeolites as the acidic component[51-53]. The high acidity of zeolites both in density and strength allowed reactions to occur at even lower temperatures[51,54].

From extensive research work[8,9, 11-13, 55] emerged a number of techniques like "Shell 's Hydro-Isomerization Process"[56]. However, the primary goal of these industrial and academic research efforts was to maximize the yield of gasoline (C_5-C_{12}). Not only was the yield of dry gas (C_1-C_3 hydrocarbons) minimized, but the yield of butanes and pentanes was also limited in favour of C_7^+ hydrocarbons. As well, there was more concern focused on hydroisomerization than the hydrocracking reaction.

My research program objective is to find a way of enhancing production of the MTBE precursor, isobutene, for which there is a growing market demand. The technique should be significantly different from those used in normal hydrocracking and hydroisomerization, which are focused on gasoline-range hydrocarbon products.

2.2 Experimental

2.2.1 Zeolite Materials.

Zeolite (LZY-82), in a powder and 1/16" pellet forms, was purchased from Universal Oil Products (UOP). They are referred to as Y and Yb, respectively. Both are calcined in air at 673 K for 12 h in order to convert the ammonium forms into the proton ones used to prepare the "acidic" catalysts.

2.2.2 Pt-loading and Catalyst Formation

1). Dry impregnation.

In this method, Pt-loading is done simultaneously with catalyst formation[57-58]. After the Y zeolite powder was throughly mixed with 20 wt.-% bentonite clay (Anachemia, laboratory grade), an aqueous solution of tetraamine platinum(II) chloride (Aldrich, 98%) was added in drops to obtain a malleable paste. The resulting malleable paste was extruded with a syringe to a spaghetti-like piece. These extrusions were dried at 393 K and followed by activation in air at 673 K for 12 h. The activated "spaghetti" of 1 mm diameter were broken down to smaller lengths (ca.2 mm). This final form of the catalyst called "Pt/Y" was used for catalytic testing. The amount of Pt incorporated in

this catalyst was 0.5 wt.-%.

2). Wet impregnation

Using the conventional "incipient wetness" impregnation method, Pt was first incorporated into the Y zeolite. Then the Pt-containing zeolite was extruded with bentonite using distilled water as wetting agent. The impregnation process was as follows. In a rotavapor flask, the zeolite powder was slowly added to an aqueous solution of tetraamine platinum (II) chloride solution. The flask containing the above suspension was connected to a vacuum pump and water was gradually removed at a temperature of about 350 K. The solid thus obtained was dried at 393 K and calcined in air at 673 K for 12 h. The resulting Pt-zeolite material was extruded into "spaghettis" according to the dry impregnation method, however using pure water to prepare the malleable paste. The catalyst made by this method is thereafter referred to as "Pt-Y". The Pt content of this catalyst was also 0.5 wt.-%.

3). Coating preparation.

A method similar to a coating process was used to make Pt-loaded catalyst with Y zeolite pellets(Yb). The (Yb) zeolites were slowly added to a vacuum flask containing a predetermined amount of tetraamine platinum (II) chloride solution in water. The flask connected to the Rotavapor system was rotated gently and the solution evaporated under vacuum at ca. 350 K. The Pt-

coated extrusions were dried at 393 K and calcined in air 673 K for 12 h. A series of catalysts with different Pt content were obtained by carefully controlling the amount of tetramine platinum (II) chloride used; they are referred hereafter to as Pt(x)/Yb, where x represents the Pt content in wt.-% in the final catalyst.

2.2.3 Characterization

1) Chemical analysis

Two methods were used to decompose the zeolite samples: fusion melting and acid leaching.

In the fusion melting method, about 0.1 g of sample previously dried in a platinum crucible (1070K, 1h) was throughly mixed with 0.8 g of the fusion mixture (potassium carbonate, 99.99% and lithium tetraborate, 99.9%, in a 2:1 ratio), and heated to 1070 K for one hour. The melt was cooled and dissolved in two acids; 4 ml of concentrated HCl and 10 ml of 10 -%(v/v) H_2SO_4. After appropriate dilutions, the contents of aluminum, sodium, and platinum (if applicable) in a sample were determined by atomic absorption (Perkin Elmer Model 503) spectroscopy. The contents of aluminum, sodium and platinum in their metal oxides were determined using external standard references. The silicon oxide(SiO_2) was obtained by subtraction from 100%

of the sum of aluminum oxide (Al_2O_3), sodium oxide (Na_2O) and platinum oxide(PtO).

In the acid leaching method, 0.5 ml of 2 M H_2SO_4 and 20 ml of concentrated HCl were added to about 0.4 g of dried (1073 K, 1h) zeolite sample in a 100 ml beaker and then evaporated at a temperature of ca. 353 K to dryness. The same mixture of these two acids was added to this dried sample and the drying process was repeated. The dried zeolite was then suspended in 20 ml of concentrated HCl and allowed to precipate overnight at room temperature. The precipitate was filtered with ashless filter paper, washed thoroughly with deionized water, and calcined in air at 1070 K to a constant weight. The precipitate thus obtained were assumed to be pure silica (SiO_2). The filtrate was used for atomic absorption spectroscopy analysis. The contents of aluminum oxide (Al_2O_3) and sodium oxide (Na_2O) were determined by the procedure used in the fusion melting method.

2) Chemical adsorption of CO

Since the carbon monoxide molecules interact chemically only with the metallic component of a bifunctional catalyst, it is possible to calculate the specific surface area of metallic particles, estimate their dispersion and sizes from catalyst's adsorption properties. Carbon monoxide adsorption on catalyst was performed by using the ASAP 2000 Chemical Adsorption System at a

temperature of 308 K. Prior to chemical analysis, the catalyst was processed through several steps outlined in Table 2.1.

Table 2.1 Procedure for carbon monoxide adsorption test

Step	Action	Temp. (K)	Time (min.)
1	Outgas sample	623	60
2	Air flow (30 cm^3min^{-1})	100	30
3	Air flow (30 cm^3min^{-1})	623	30
4	Evacuate (to 0.5 Pa)	623	30
5	Evacuate (to 0.5 Pa)	373	10
6	Flow hydrogen	373	10
7	Flow hydrogen	623	120
8	Evacuate (to 0.5 Pa)	623	60
9	Evacuate (to 0.5 Pa)	308	10
10	Begin analysis	308	

By using a sequential sorption/vacuum procedure which allows the elimination of weak CO physisorption phenomena, the Pt specific surface areas can be related only to the CO chemisorption sites.

3) GC-MSD (Gaschromatography-mass selective detector)

This technique was used to identify the carbonaceous species (known as coke) deposited on the surface of the spent catalyst. The deposited

carbonaceous species were extracted with an organic solvent (heptane or methanol) from the spent catalyst and analyzed by GC-MSD (HP 5890 GC equipped with the HP 5970 MSD). A 50-m PONA tpye capillary column was used. The carrier gas was helium with flow rate of 1 cm^3min^{-1}.

4) Thermal analysis

Thermal analysis, including thermogravimetric (TGA) and differential thermal analysis (DTA), was performed using a PL Thermal Science STA 1500 instrument interfaced to an IBM PS/2 computer. The flow rate of the carrier gas was 30 cm^3min^{-1}, and about 15 mg of sample was used in each run. The temperature of the system was linearly increased at a rate of 15 $Kmin^{-1}$. The ceramic crucibles were used for both the sample pan and the reference pan. In the reference pan, 15 mg of calcined alumina was loaded as the reference material.

5) Ammonia temperature program desorption.

The sample's acidity was profiled using the Ammonia Temperature Program Desorption (NH_3-TPD) technique. 600 mg of the 20-40 mesh (by self-pressing, crushing and sieving) sample was loaded into an U-type quartz reactor with helium (30 $mL.min^{-1}$) as carrier gas during the run. The sample was activated at 723 K for 2 hours, followed by cooling to 380 K. A mixture of ammonia (30 $mLmin^{-1}$) and helium was passsed on the sample for 20

minutes. The physical adsorption of ammonia was completely eliminated by maintaining this temperature(380 K) for another 2 hours. The desorption of chemically adsorbed ammonia was studied by increasing the temperature of the sample at a constant rate (10 $K.min^{-1}$) with the effluent gas being analyzed with an on-line gas chromatograph equipped with a Thermal Conductivity Detector (TCD). The total ammonia desorbed was collected in aqueous hydrochloric acid and determined by back titration with aqueous sodium hydroxide solution.

A multi-step desorption program was also used in this work to de-convolute the peaks[59]. During the desorption process, several heating steps were applied and the corresponding desorbed ammonia was collected separately and titrated. The desorption was first done by heating the sample from 380 K to 510 K and maintained that temperature for 20 minutes. In the second step, the temperature was increased to 570 K and maintained at that level for 20 minutes. The sample was then heated to 670 K, maintained at this temperature for another 20 minutes, and finally, heated to 970 K. Four separate desorption peaks were obtained in this method. The total amount of desorbed ammonia in this multi-step process was compared with that obtained with the continous program.

2.2.4 Catalytic Testing

1) Micro-reactor system

Figure 2.1 shows a schematic diagram of the experimental set-up.

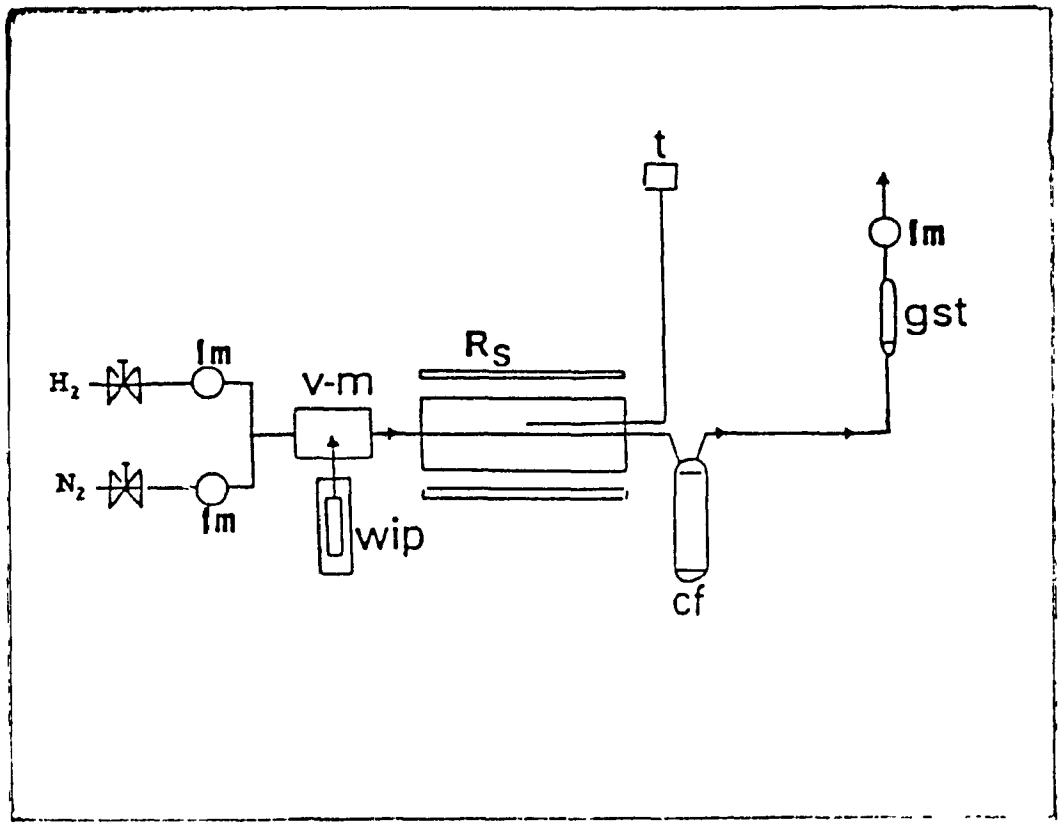

Figure 2.1. Micro-reactor apparatus

fm: flow meter; **v-m**: vaporizer-mixer; **wip**: water infusion pump; R_s Reactor system(quartz tabular tube); **t**: thermocouple(chromel-alumel); **cf**: collecting flask; **gst**: gas sampling tube

2) Catalytic testing procedure

1.25 g of catalyst was loaded into the tubular reactor of 1 cm diameter, which was heated by a digitally controlled electrical furnace. A chromel-alumel thermocouple was placed at the center of the catalyst bed and connected to a digital thermometer unit to monitor the temperature of the catalyst bed. The reaction temperature was set within the 437K-573K temperature range. Before the reaction, the catalyst was activated in situ under N_2 (16 cm^3min^{-1}) and H_2(12 cm^3min^{-1}) at 623 K for 2h (or as specified).

Pure n-octane was fed into the reactor as a gaseous mixture with nitrogen or with nitrogen and hydrogen at a weight hourly space velocity (WHSV) of 0.1-1.0 h^{-1}. For most runs, the partial pressure of n-octane in the inlet stream was maintained at a very low constant rate of 1.6 kPa. All products in the gaseous phase passed through a glass cylinder from which gas samples were taken at 1 hour intervals. The samples were analyzed using a Hewlett-Parkard GC (Model 5790A FID) containing with a 3-m long column packed with chromosorb P coated with 20 wt% squalane. In some runs, in which high partial pressures of n-octane were used, the liquid hydrocarbons in the out-stream were collected in a condensing flask kept at 263 K. The tail-pipe gaseous stream was passed through the cylinder from which the gas samples were done as above. The collected liquid phase was subsequently analyzed with a Hewlett Packard GC(Model 5790, FID) equipped with a 50-m PONA type capillary column. All

chromatographic data were expressed on a carbon atom basis using 2,2-dimethylbutane(2,2-DMB) as internal standard for the gaseous effluent and taking into account the correction factors for the FID detector. Data corresponding to the gas and liquid phases were then combined to provide the complete product composition.

3). Product calculations

The conversion of n-octane is defined as follows:

$$C_t = 100 * [(NC)_t - (NC)_o] / (NC)_t$$

and the selectivity in product hydrocarbons is defined as follows:

$$S_i = 100 * (NC)_i / [(NC)_t-(NC)_o]$$

where $(NC)_i$, $(NC)_t$ and $(NC)_o$ are, the numbers of carbon atoms of hydrocarbon(i), all the hydrocarbons and unconverted n-octane in the reactor outstream, respectively. For comparison, the conversion and product selectivities were obtained as average values of two runs with data collected for up to 6 hours per run. The yield in product (i) is defined as the product of S_i and C_t. Satisfactory mass balances of over 90% were obtained for all data. Satisfactory reproducibilities with respect to reaction runs over the same catalyst under similar conditions were within 2%.

2.3 Results and Discussion

2.3.1 Establishing the Chemical Analysis Method.

Chemical composition is a macroscopic property of a catalyst. Various techniques are known, however, three of them predominate in practical catalyst characterization; atomic absorption spectroscopy (AAS), inductively coupled plasma spectroscopy (ICP) and x-ray fluorescence spectroscopy (XRF). Each technique has its own particular merits and all these techniques are actually complementary. The preferred methods for bulk composition determination are elemental analysis by the AAS and ICP methods. However, they both require the dissolution of the catalyst. Getting a solid state catalyst into an aqueous solution is a problem which has to be solved first.

A fusion melting method to dissolve high silica zeolites is well developed[39]. A new method introduced in this work is the acid leaching method. Table 2.2 shows the comparison of the results obtained with these two methods. It can be seen that the acid leaching method is more reproducible. Since a large amount of the fusion mixture is used in the fusion melting method, small amounts of impurities in the fusion mixture can cause large errors in elements determined, especially sodium, since it is difficult to get rid of it entirely from the potassium carbonate used in this method. Comparison of these two methods shows other advantages. The acid leaching method does not require a special Pt crucible, and thus avoids the introduction of extraneous Pt species possibly leached out from the Pt crucible by the strongly basic fusion mixture (this is important, when the Pt content in the

sample is a concern). The silica content can be directly obtained by weighing the precipitate instead of by subtraction from unity of the other metal oxides. This eliminates errors from elements not determined (impurities in the catalyst) and errors transferred from the analysis of metal oxides. Acid leaching provides a method to estimate elemental content otherwise difficult to detect by AAS, such as La ions by means of subtraction of metal oxides.

However, the acid leaching method is based on the assumption that the zeolite is completely dissolved in hot concentrated hydrochloric acid. This is not the case with the high silica content zeolites such as ZSM-5. Table 2.3 is a summary of the chemical compositions of the zeolites and catalysts investigated.

2.3.2 Introducing Pt onto Zeolites

1). Parent Yb zeolite.

Figure 2-2 is a plot of total n-octane conversion versus the time on stream over the parent Yb zeolite. Total conversion rapidly decreased with time on stream, and, the higher the WHSV, the greater the speed of this decrease in catalytic activity.

Table 2.2 Comparison of Chemical Analysis Methods*

Analysis method	Fusion melting			Acid leaching		
Trials	A	B	Ave.	A	B	Ave.
Al_2O_3	18.9	20.6	20.0	20.6	20.6	20.6
Na_2O	14.5	15.4	15.0	13.7	13.8	13.8
SiO_2	66.6	64.0	65.3	65.3	66.6	66.0
Si/Al			2.7			2.7
Na/Al			1.2			1.1

* sample ID# NaY(LZY52, powder, from Aldrich)

Data were reported in wt.% based on dried(1023 K) sample.

Table 2.3 Typical Chemical Properties of Catalysts[a]

Sample/Catalyst	SiO_2	Al_2O_3	Na_2O	PtO_2
Y(powder)	74.9	24.9	0.1	0.0
Yb(pellets)	65.6	33.6	0.2	0.0
Pt(0.3)/Yb	62.3'	36.6	0.5	0.3
Pt(0.5)/Yb	62.7	36.3	0.3	0.6
Pt(0.9)/Yb	63.0	35.8	0.2	1.0
Pt(1.2)/Yb	62.6	35.4	0.5	1.4

[a] : in wt.%

It is generally believed that coke formation is the main reason for the deactivation of the zeolite used in cracking processes, usually occurring through dehydrogenation and cyclo-addition of the olefinic products (see Figure 1.1). These olefinic products such as ethylene, propylene, butenes etc., are thus called the "precursors" of coke[4].

Table 2.4 lists the product selectivities for hydrocracking of n-octane over the parent zeolite Yb, where there are some so-called coke precursors observed in the outstream. However, we do not consider coke formation from these light olefinic products to be the only reason for catalyst deactivation at these low reaction temperatures. It is possible that catalytic decay results from chemisorption of these olefins onto the active sites, thus preventing the access of the reactant molecules and/or the reaction intermediates to these active sites. Two phenomena, coke formation and chemisorption, probably coexist and their contribution depends on the reaction temperature and other reaction parameters such as hydrogen partial pressure and contact time. Regardless of their roles, these olefinic products were the essential source of deactivation. A good catalyst is needed to either prevent formation of these species, or immediately remove and/or hydrogenate them on their formation.

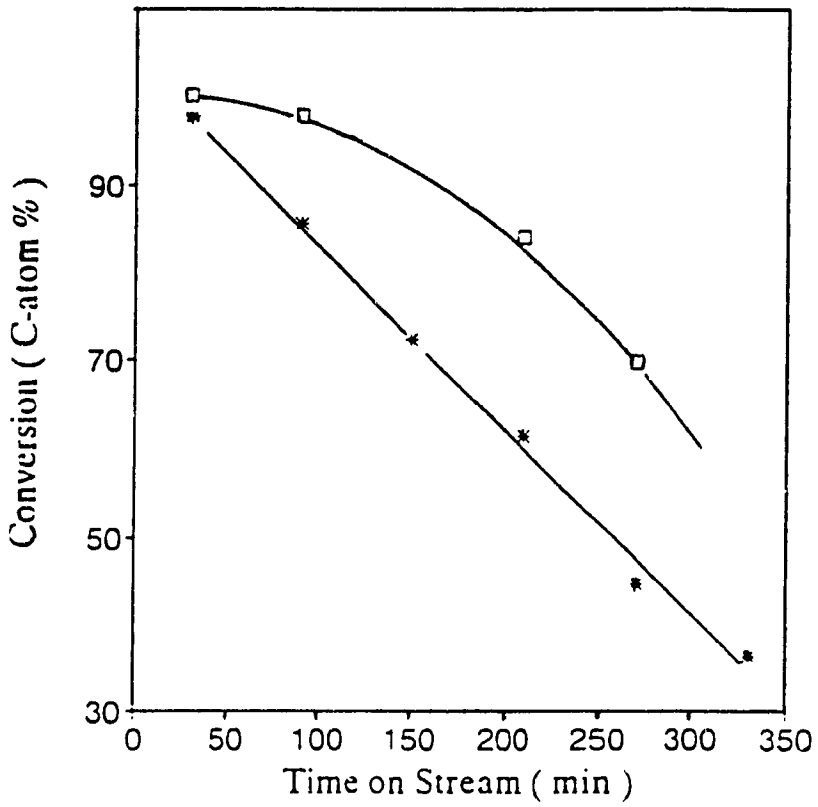

Figure 2.2 On-stream stability of Yb zeolite at different WHSV

(▫) = 0.067 h^{-1}; (*) = 0.125 h^{-1}

T = 475 K

Table 2.4 N-octane conversion and product selectivity over Yb zeolite and Pt(0.5)/Yb catalyst

Catalyst	Yb	Pt(0.5)/Yb
Conversion	59.6	98.7
Product Selectivity		
Methane	0 0	0.3
Ethene	0.1	0.0
Ethane	0.2	0.9
Propene	0.5	0.0
Propane	13.4	16.8
n-Butane	12.1	19.9
iso-Butane	47.3	33.9
Butenes	0.3	0.0
n-pentane	2.4	4.8
iso-pentanes	20.0	11.8
n-Hexane	0.2	0.2
iso-hexanes	2.2	1.2
n-Heptane	0.0	0.0
iso-Heptanes	0.1	2.6
branched-Octanes	0.7	2.5
BTX and C_9^+	0.6	5.2
unsaturated C_2-C_4	0.9	0.0

Reaction conditions: T = 573 K, WHSV = 0.1 h^{-1}

A bifunctional catalyst, in which the metal is the dehydrogenation-/hydrogenation agent and the acidic support is the cracking/isomerization agent was therefore developed. Using a coating preparation method, either nickel, gallium or platinum was loaded onto the Yb zeolite. Figure 2.3 is a plot of the total conversion of n-octane versus time on-stream over these different metal-containing zeolites. This figure shows that platinum is the best metal used for the stabilization of the catalytic activity. In fact, after incorporation of Pt into the HY zeolite, there was no significant amount of olefinic species detectable in the outstream (Table 2.4), and the catalyst exhibited satisfactory on-stream stability (Figure 2.3).

In order to explain the function of Pt, one must consider the general cracking mechanism(Scheme V). Cracking of n-alkanes over Brønsted acid sites in the zeolite framework is probably initiated by olefin impurities (reaction a) in the feed[60], although a hydride abstraction from the reactant molecule(reaction a') is not to be ignored[61]. The intermediates are carbenium ions. The subsequent chain reaction provides relatively stable carbenium ions[60] by reacting with paraffin or provides an olefinic molecule and another carbenium ion through beta-scission (reaction b'). Those carbenium ions which result from a skeletal isomerization of the reaction intermediates might undergo further cracking, disproportionation, and conversion to high molecular weight hydrocarbons[62,63]. The possibility of secondary reactions occurring on the

Initiation:

a) $R_1\text{-}C{=}C + Z\text{-}H^+ \rightarrow Z\text{-}R_1\text{-}C^+\text{-}C$

or a') $R_2\text{-}C\text{-}C + Z\text{-}H^+ \rightarrow Z\text{-}R_2\text{-}C^+\text{-}C + H_2$

where $Z\text{-}H^+$ = zeolite protonic site

Normal chain propagation:

b) $Z\text{-}R_1\text{-}C^+\text{-}C + R_2\text{-}C\text{-}C \rightarrow i\text{-}R_1\text{-}C\text{-}C + Z\text{-}R_2\text{-}C^+\text{-}C$

b') $Z\text{-}R_2\text{-}C^+\text{-}C \rightarrow R_3\text{-}C{=}C + Z\text{-}R_4\text{-}C^+\text{-}C$

Interception process by reaction with hydrogen:

c) $Z\text{-}R_2\text{-}C^+\text{-}C + H_2$ (adsorbed) $\rightarrow R_3\text{-}C\text{-}C + i\text{-}R_4\text{-}C\text{-}C + Z\text{-}H^+$

c') $Z\text{-}R_2\text{-}C^+\text{-}C + H_2 \rightarrow i\text{-}R_2C + Z\text{-}H^+$

Scheme V Interception of Hydrocracking of n-Paraffins by Reaction with Hydrogen

carbenium ions is in agreement with recent results reported by Wojciechowski et al[64,65], who proposed that adsorption equilibria play a major role in the HY catalyst's activity and selectivity. When there is a significant amount of hydrogen co-fed along with the n-octane, the hydrogen molecules may react with the carbenium ions in the same way as any other gaseous molecules (reaction c and c'). Thus, such a chain reaction is prematurely stopped, and the hydrocarbons desorbed will include a high amount of isoparaffins. The presence of some Pt sites in the HY zeolite enhances this desorption process because the hydrogen species pre-adsorbed on the Pt sites are immediately accessible and react rapidly with carbenium ions (reaction c). It is well-known that Pt is more efficient than either nickel or gallium to dissociatively adsorb hydrogen due to its specific d-character. The result of such a more efficient intercepting action by the Pt-loaded zeolite, when compared with the parent zeolite, is a higher on-stream stability owing to the absence of coke precursors in the products formed.

2). Amount of Pt

Figure 2.4 shows the total conversion of n-octane at 475 K over different catalysts versus reaction time. Product selectivities are presented in Table 2.5.

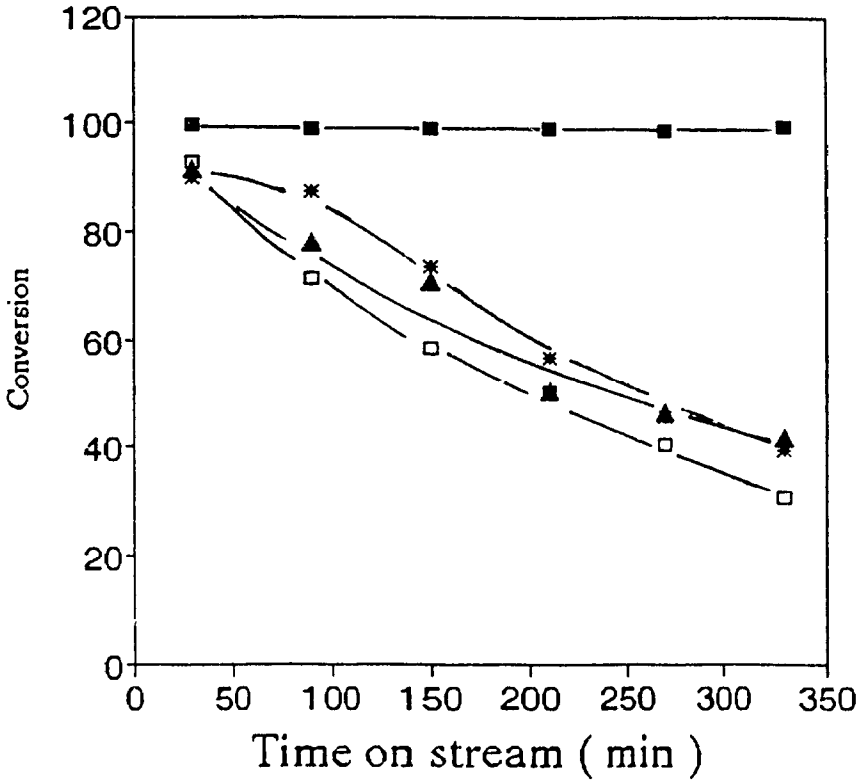

Figure 2.3 On-stream stability of n-octane conversion on different metal-containing Yb catalyst(□) = Yb; (■) = Pt/Yb; (*) = Ni/Yb; (▲) = Ga/Yb

Table 2.5 Conversion and product selectivity of n-octane conversion over Pt/Yb catalyst with different Pt content

Catalyst	Pt(0.3)/ Yb	Pt(0.5)/ Yb	Pt(0.9)/ Yb	Pt(1.2)/ Yb
Conversion	84.6	93.7	96.0	90.2
C_1-C_2	0.1	0.1	0.1	0.1
Propane	10.5	11.5	11.9	12.3
n-Butane	9.5	10.6	11.1	11.4
iso-Butane	44.1	45.4	44.2	44.9
n-Pentane	1.6	1.4	1.9	2.5
iso-Pentanes	17.9	19.2	18.7	18.7
n-Hexane	0.5	0.3	0.2	0.2
iso-Hexanes	4.6	2.9	2.5	1.8
Heptanes	0.0	2.1	0.9	0.0
branching-octanes	11.2	6.7	8.7	8.1
Yield of isobutane	37.3	42.5	42.4	40.5
ratio of iso/n(C_4)	4.7	4.3	4.0	3.9

T = 475 K, WHSV = 0.13 h^{-1}

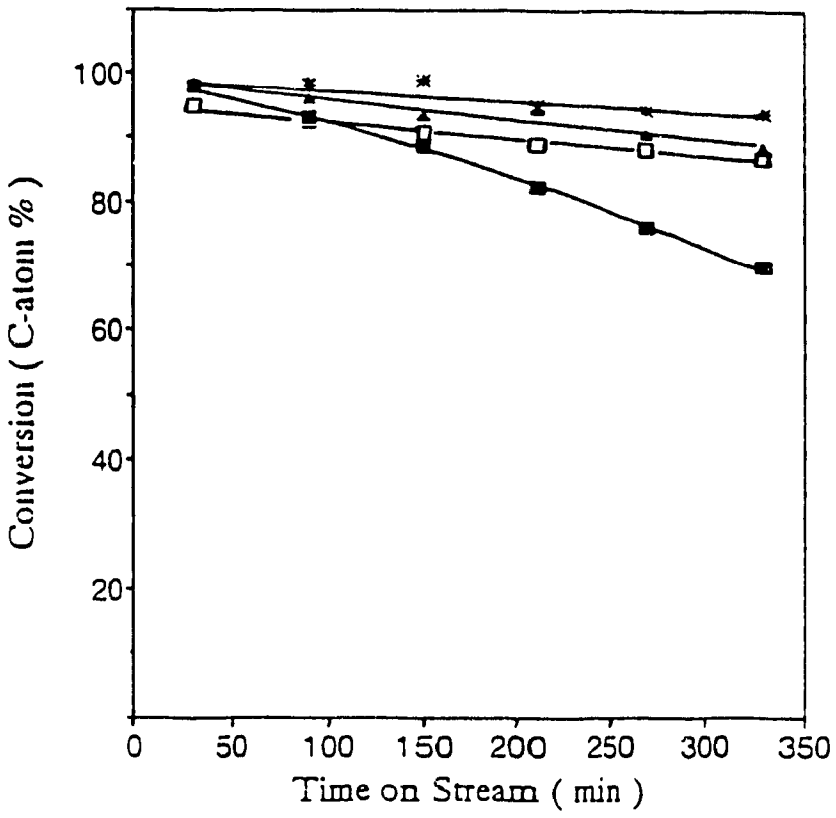

Figure 2.4 On-stream stability of n-octane conversion over different catalysts: (■) = Pt(0.3)/Yb; (▲) = Pt(0.5)/Yb; (✡) = Pt(0.9)/Yb; (□) = Pt(1.2)/Yb

It can be seen that: i) a high on-stream stability with less than 10% variation (for 6 hours) in total octane conversion with Pt loadings greater than 0.5 wt.% and less than 1.2 wt%;

ii) the iso/n-butane molar ratio decreased from 4.6 to 3.9 when the Pt loading increased from 0.3 wt% to 1.2 wt%;

iii) at 475 K, all of the Pt(x)/Yb catalysts did not produce any significant amounts of aromatics or hydrocarbons heavier than C_8.

The best Pt loading was between 0.5% and 0.9 wt% in all respects (high on-stream stability, high activity and the selectivity towards isobutane and other isoparaffins). The high performance of these catalysts stemmed from the relatively high metal surface areas and high metal dispersions. Table 2.6 summarises the Pt dispersions over these catalysts as measured by CO chemisorption. It was noticed that the Pt dispersion on zeolite Yb decreased with an increase of Pt loading. From their catalytic behaviours (Figure 2.4), it was seen that Pt incorporation lower than 0.5 wt% was not efficient in stabilizing the catalytic activity, and neither was it satisfactory when greater than 1.0 wt%. The latter case was due to the fact that the Pt dispersion decreased with an increase in the Pt loading, and that a high amount of loaded Pt species could hinder the zeolite's acidic sites and/or block the pore apertures. It may be concluded that there must be a balance between metallic sites and acidic sites in order to achieve the higher performances.

Table 2.6 Chemisorption results obtained with the Pt loaded zeolites

Catalyst	Pt content (wt%)	[a]Metal surface m^2g^{-1}	[b]Pt disper-sion(%)	Pt_s atom.g^{-1} $*10^{18}$	(c) H^+/Pt_s
Pt(0.3)/Yb	0.28	0.65	92	8.13	400
Pt(0.5)/Yb	0.53	0.35	27	3.38	740
Pt(0.9)/Yb	0.89	0.22	10	2.75	1180
Pt(1.2)/Yb	1.23	0.20	7	2.50	1300

(a): stoichiometry factor for CO chemisorption = 1.0; atomic cross section area of Pt = 0.08 nm^2

(b): number of Pt surface atoms(Pt_s) / total number of Pt atoms

(c): $H^+ = 3.3 * 10^{21}$ atom.g^{-1}; assuming that to each of the tetrahedral Al sites corresponds one protonic site

3). Methods of Pt-loading

Three methods were employed to incorporate Pt into HY zeolite. Table 2.7 lists the catalytic performances of the resulting Pt catalysts and shows that no significant differences exist between them, especially with respect to the total conversion of n-octane and the selectivity to iso-butane. This implies that it is unnecessary for the Pt species to be in close proximity to acid sites in order to have an efficient catalyst. The role of platinum in this bifunctional catalyst is probably to adsorb and activate hydrogen (Scheme V) to a predominantly atomic form thus eliminating the formation of olefinic products. Platinum could play this role according to a well established concept, hydrogen spillover[66]. It has been shown that such a hydrogen spillover can transfer hydrogen species over relatively long distances from one solid phase such as a supported metal where it is easily adsorbed and dissociated onto another solid phase, such as an oxide or a zeolite in contact with the first, where it does not directly adsorb[67]. The efficiency of transferring hydrogen species over long distances between Pt sites and acidic sites provides the advantage of being relatively independent of the location of the platinum particles and the loading method used. Also, the platinum dispersion was found, by carbon monoxide chemisorption tests, to be independent of the preparation method. The fact that no acidity was introduced upon their reduction with hydrogen from NH_3-TPD tests implies that all Pt species existed in the oxide form (PtO, PtO_2) in the three catalysts before their reduction.

Table 2.7 Hydrocracking of n-octane over three Pt-loaded catalysts prepared by different methods[a]

Catalyst	Pt(0.5)/Yb	Pt/Y	Pt-Y
parent zeolite form	pellets	powder	powder
Pt introduced method	coating	dry imp[b]	wet imp.
Conversion	99.1	97.7	98.9
Propane	15.5	15.2	15.6
n-Butane	12.6	13.0	13.2
iso-Butane	54.8	54.6	54.2
n-Pentane	1.9	1.1	1.4
iso-Pentane	13.2	14.8	14.7
C_{6-7} Alkanes	1.2	0.8	0.8
mono-branched Octane	1.8	0.8	0.6
di + tri-branched Octane	0.6	0.2	0.4

(a): T = 495 K, WHSV = 0.1 h^{-1}

(b): imp = impregnation

2.3.3 Optimum Reaction Conditions

1) Hydrogen partial pressure

Figure 2.5 and Table 2.8 show the influence of the hydrogen partial pressure on the catalyst on-stream stability, the average conversion of n-octane and the product distribution. The total pressure in the reaction system and the n-octane partial pressure in the inlet stream were kept constant (103 KPa and 1.6 KPa, respectively). The different hydrogen partial pressures were obtained by adjusting the flow rates of both hydrogen and nitrogen.

A hydrogen partial pressure of at least 40 kPa ensured optimum performance for the catalyst in terms of the on-stream stability and isobutane yield. In the absence of hydrogen or at lower hydrogen partial pressures, conversions and carbon balances were much lower. This was because reactions c and c' in Scheme V could not proceed without hydrogen, and the resulting olefinic species from reaction b' would competitively adsorb onto active sites with reactant molecules and/or reaction intermediates. Moreover, due to the absence of this desorption reaction (reaction c in Scheme V), the reaction intermediates would have longer lifetimes and have longer ... undergo secondary reactions such as dehydrogenation and cyclo-addition to form "coke". This not only results in the deactivation of the catalyst, but also lowers the carbon balance since the "coke" deposited on the catalyst is not accounted

for in the outlet stream carbon-balance. Therefore, in order to make reaction c or c' occur, both the platinum particles and hydrogen have to be present.

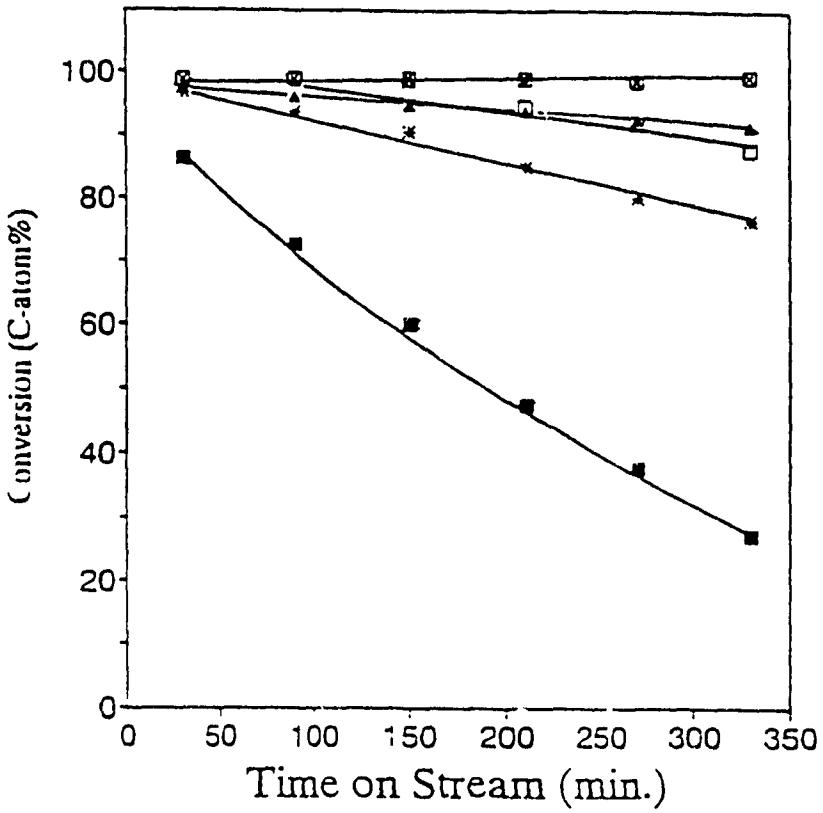

Figure 2.5 On-stream stability of n-octane conversion over Pt(0.5)/Yb at different hydrogen/n-octane molar ratios (■) = 0.0; (*) = 3.6; (□) = 9.1; (▲) = 13.6; (⊠) = 27.1

Table 2.8 Conversion of n-octane and product selectivities according to different hydrogen/n-octane(H/O) molar ratios

$P(H_2)$ KPa	0.0	5.8	14.5	21.7	43.4
(H/O) molar ratio	0.0	3.6	9.1	13.6	27.1
Conversion	55.3	87.1	93.9	94.4	99.0
Carbon Balance(%)	67.7	86.0	85.8	88.7	96.7
C_1-C_2	0.2	0.3	0.1	0.0	0.0
Propane	13.5	15.3	15.3	15.4	15.7
n-Butane	8.0	11.9	12.1	12.5	12.6
iso-Butane	53.8	55.0	55.2	54.1	53.8
n-Pentane	0.6	2.4	2.8	2.8	1.9
iso-Pentanes	11.8	11.5	11.3	11.9	13.2
n-Hexanes	0.1	0.3	0.4	0.2	0.0
iso-Hexanes	3.2	1.4	1.2	0.8	0.4
cyclo-Hexane	1.1	0.2	0.2	0.2	0.0
Heptanes	0.2	0.7	0.8	0.8	0.8
mono-branched Octane	5.4	0.7	0.5	0.9	1.1
di + tri-branched Octane	2.1	0.2	0.2	0.3	0.4
Yield of isobutane	29.7	47.9	51.9	51.1	53.3
iso/n ratio(C_4)	6.7	4.6	4.6	4.3	4.2

T = 495 K

However, hydrogen partial pressure variation did not significantly influence the product distribution (Table 2.8). This indicates that hydrogen does not intervene directly in the beta-scission process of n-octane, even though it has a strong influence on the overall reaction rate. These results are in agreement with those of Sinfelt and Rohrer[68,69], who showed that hydrogen increased the rate of desorption of products via hydrogenation. They observed that, generally, any hydrogenation process requires the presence of metal sites such as those of Pt, and that saturated hydrocarbons presumably undergo hydrocracking over the bifunctional catalysts by two different routes, one involving only the acidic sites of the carrier[68,69] and the other involving a cooperative action[47,50] of these sites with metallic sites. The former route involves the adsorbed hydrogen species which increase the rate of desorption of the hydrogenated products of beta-scission of n-octane. In this case, there is no need for the formation of metal/acid site couples which would require high metal dispersions within the zeolite pore system, as is the case with the cooperative action route. Obviously, our results support this reaction route. This was also why the most efficient catalyst Pt(0.5)/Yb has a ratio of the total number of protonic sites to the number of surface Pt atoms of about 1,000 (Table 2.7) which does not correspond to that expected for the conventional dual site configuration with bifunctional catalysis, and why the catalytic performance was independent of the preparation method.

2) Reaction Temperature.

HY zeolite is not a homogeneous material with respect to its acidic sites. A broad acid distribution is found with NH_3-TPD profiles shown in Figure 2.6. The specific temperature for the NH_3 desorption from the different acid sites correlates their different acidic strengths. In general, the higher the desorption temperature, the stronger the acidity of the corresponding acidic site. The activity of these different acidic sites with different acidic strengths depends on the reaction temperature, which will also affect the activity of platinum and the adsorption/desorption equilibria of the reactants, the reaction intermediates and the products, and consequently the product distribution.

The overall influence of the reaction temperature on the conversion and product selectivities is reported in Figure 2.7 and Table 2.9. It can be seen that:

i) the isobutane yield achieved a maximum at 495 K;

ii) at lower temperature (448 K), the total conversion and the isobutane yield were much lower, but the selectivities to n-octane isomers were much higher.

iii). at low temperatures (< 473 K) , the catalyst activity was unstable and the C-balance was low.

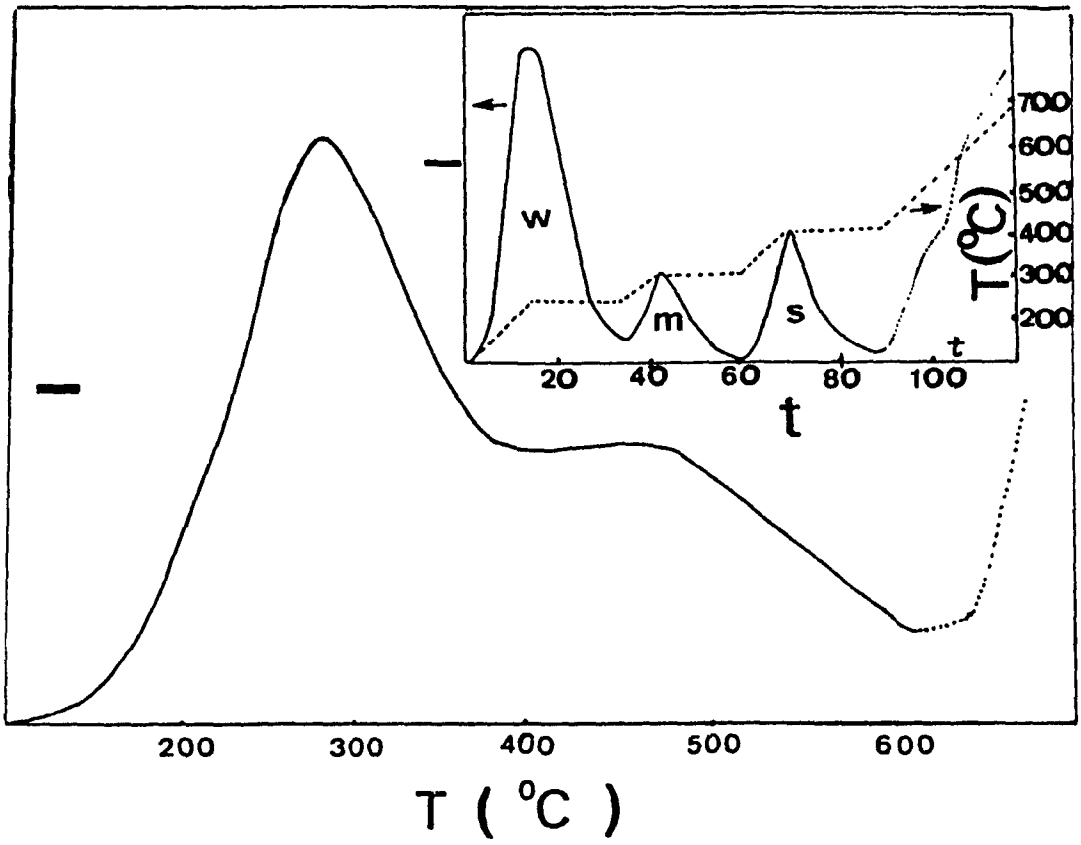

Figure 2.6 NH_3-TPD profile and multi-step desorption profile (inserted figure) of parent zeolite Yb. I = Intensity of response(arb.unit); T = Temperature(°C); t = time (minute). w = weak acid sites; m = medium strong acid sites; s = strong acid sites. The dot lines = desorption of water due to dehydroxylation of zeolite.

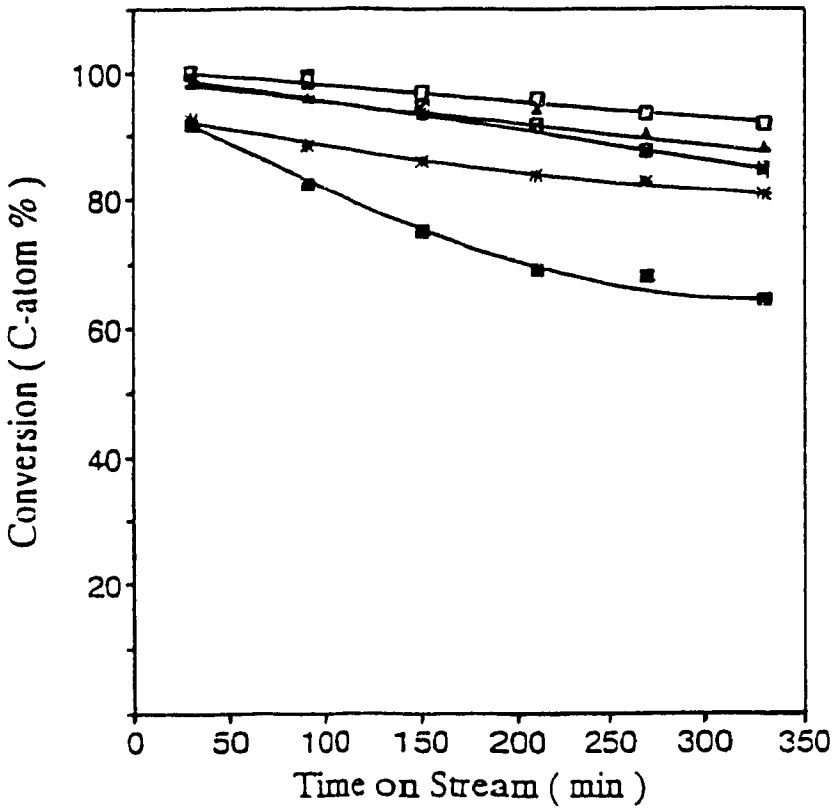

Figure 2.7 On-stream stability of n-octane conversion over Pt(0.5)/Yb at different reaction temperature: (■) = 445 K; (▲) = 475 K; (⊠) = 495 K; (✱) = 525 K; (□) = 577

Table 2.9 Conversion of n-octane and product selectivities according to five different temperatures

Reaction Temperature(K)	445	475	495	525	577
Conversion	75.1	93.7	99.1	85.7	96.3
Carbon balance	81.2	89.9	96.6	94.9	96.0
C_1-C_2	0.2	0.1	0.1	0.2	0.9
Propane	6.7	11.5	15.5	13.2	15.4
n-Butane	6.0	10.6	12.6	14.0	17.5
iso-Butane	33.7	45.4	53.8	39.8	32.5
n-Pentane	0.5	1.4	1.9	4.5	4.5
iso-Pentanes	14.7	19.2	13.2	15.1	13.2
n-Hexane	0.2	0.3	0.2	0.3	0.3
iso-Hexanes	6.0	2.9	0.7	1.9	1.7
Heptanes	0.0	2.1	0.9	0.1	3.9
mono-branched Octanes	8.1	1.6	0.6	2.7	1.6
di + tri-branched Octanes	23.7	4.8	1.8	8.1	4.6
Aromatics	0.0	0.0	0.0	0.3	6.5
Yield of isobutane	25.3	42.5	53.3	34.1	31.3
Ratio of iso/n(C_4)	5.6	4.3	4.3	2.9	1.9

Catalyst: Pt(0.5)/Yb; WHSV = 0.1 h^{-1}.

If we consider the problem of catalytic deactivation, we see that at lower temperatures such as 448 K, the absence of ethylene, propylene and other unsaturated hydrocarbons (Table 2.9) as products in the outlet stream rules out the occurrence of severe coke deposition within the catalyst's pores. However, the low carbon balance obviously indicates that something must have been left on the catalyst after the n-octane passage over the catalyst bed. TG-DTA investigations (Figure 2.8) indeed showed that there were some substances which could desorb from the used catalyst at temperatures ranging from 500 to 1000 K, even under an inert N_2 atmosphere.

GC-MSD was used to identify substances left on the catalyst after n-octane passage. After 6 hours of the reaction, the catalyst, now called the used catalyst, was purged with the carrier gas (the mixture of N_2 and H_2) at the original reaction temperature for another hour, then cooled to room temperature. The used catalyst thus obtained was immersed in the solvent (heptane or methanol) at room temperature for 24 hours in order to extract any adsorbed substances. Subsequently, the extracted solution was subjected to a GC-MSD analysis. Figure 2.9 is a profile of a GC-MSD result obtained from the heptane-extracted solution. It is seen that the substances extracted from the used catalyst were n-octane itself and its branched isomers. That is to say, the catalytic decay at very low reaction temperature was a result of th· ɔw diffusion efficiencies of n-octane and its isomerized products through the zeolite

pore system. The relatively low diffusion coefficient of n-octane in zeolite systems was experimentally proven by Gorring[70] in the early 1970s (Figure 2.10), supporting this argument.

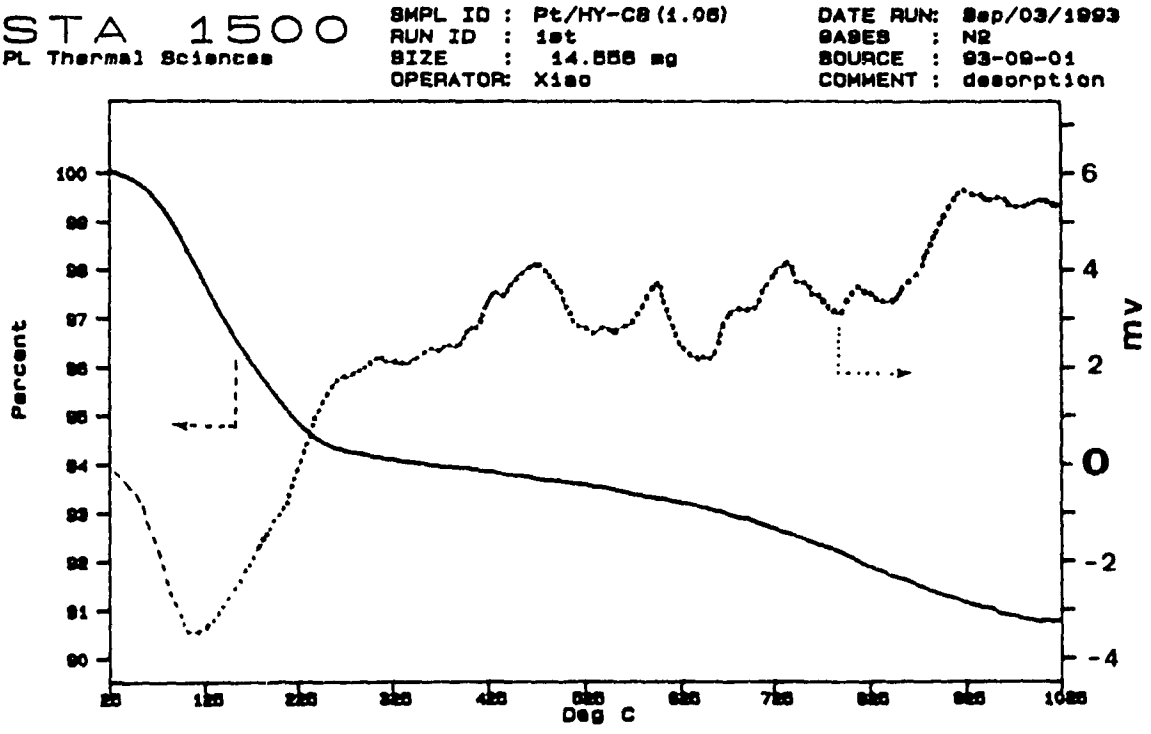

Figure 2.8 TGA/DTA profile of the used catalyst

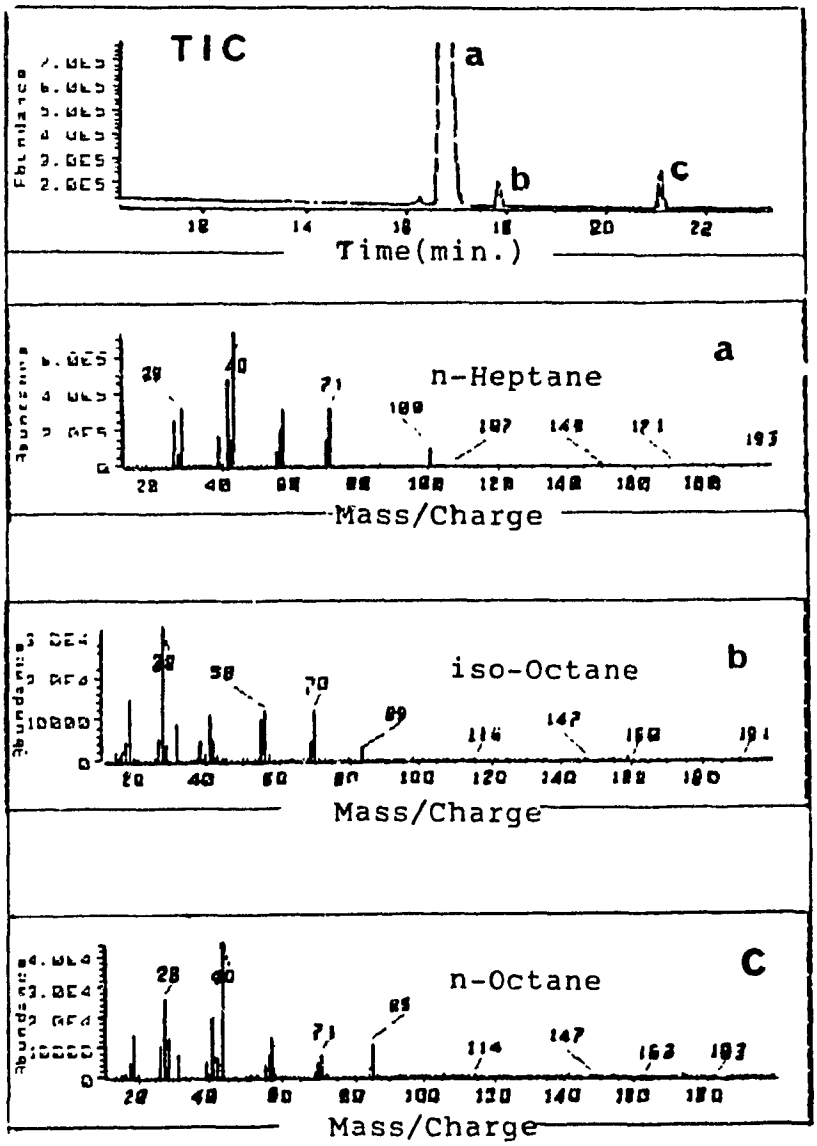

Figure 2.9 GC-MSD analysis of the heptane-extracted solution obtained from the used catalyst Pt(0.5)/Yb.

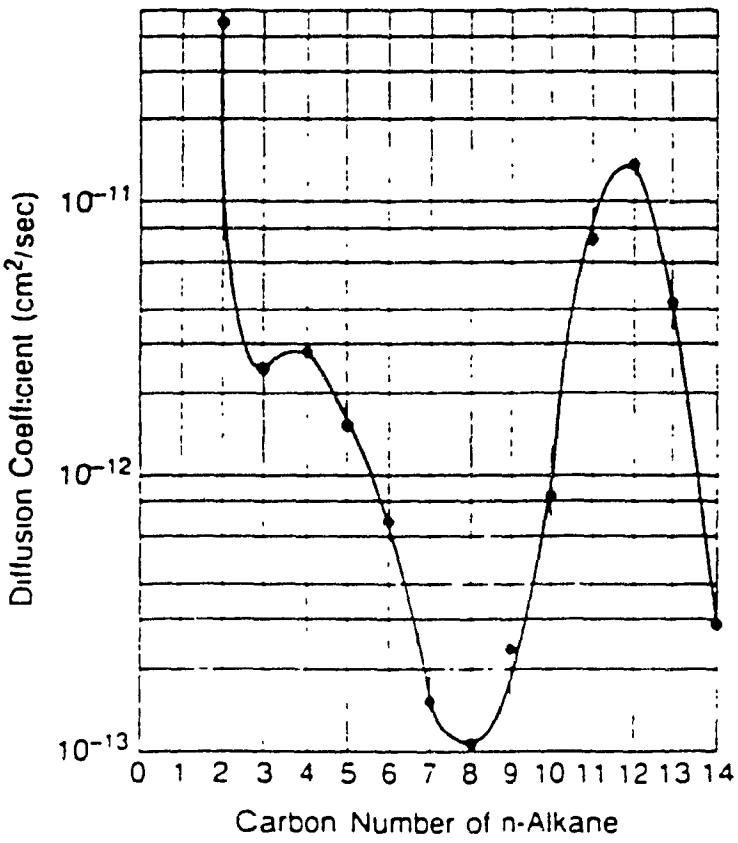

Figure 2.10 Diffusion coefficient of n-paraffins in potassium T zeolites at 573 K (from ref. 70)

The higher selectivities to n-octane isomers and the lower selectivities to lighter products such as propane, butanes, and pentanes at lower reaction temperatures might be explained by a change in the isomerization/cracking competition profile. At lower reaction temperatures, the rate of isomerization is much favoured, such that most of the branched feed isomers remain uncracked and thus trapped (or diffusing slowly) inside the zeolite pores, resulting in a significant activity loss as discussed above. This result also implies that the isomerization step of n-octane is followed by the cracking step which requires more energy than does the isomerization step.

It is worth mentioning that in the above result the product distribution depended closely on the reaction temperature which was inconsistent with that expected from classic hydrocracking mechanisms[6]. In fact, product distribution from an octane feed was found, by Martens et al[6,8-10], to be a unique function of the conversion over Pt/USY, and independent of the reaction temperature. Obviously, that is not the case here. For example, the total conversions of n-octane at 495 K and at 577 K were essentially equal to each other. However, the selectivity to isobutane and the ratio of iso/n for butanes obtained at 495 K were almost twice the values obtained at 577 K (Table 2.9).

3) Contact time.

Catalyst Contact Time (CCT) and Weight Hourly Specific Velocity (WHSV)

are used as measures of the time of the reactant/catalyst contact and the velocity of the reactant flow during the reaction. WHSV is generally expressed as the reactant feed rate (in $g.hr^{-1}$) over the catalyst weight (in g.), and CCT is the reciprocal of WHSV.

Table 2.10 lists the results of the hydrocracking of n-octane over Pt(0.5)/Yb at different catalyst contact times. It can be seen that, the longer the catalyst contact time the higher the total conversion of n-octane; and the longer the catalyst contact time the higher the yield of isobutane. At low catalyst contact times, the n-octane conversion was lower, and a great quantity of branched octane isomers was formed. The loss of activity and the lack of selectivity towards isobutane at shorter catalyst contact times is probably indicative of an enhancement of reactions occurring on the external surface of the zeolite. On the other hand, the higher n-octane conversion and the higher isobutane yield at longer contact times implies that there must be some kind of reaction locus inside the zeolite crystallites which could favour the formation of isobutane. When n-octane had enough time to diffuse inside the zeolite micropores and adsorbed onto these reaction loci, the reaction pathway which leads to the formation of isobutane would dominate. This result also implies that the structure of the zeolite might play an important role in the cracking of n-octane and in the formation of isobutane.

Table 2.10: Conversion and product selectivity of n-octane at different contact times

Contact Time (h)	10.0	4.5	1.9	1.3	1.0
WHSV(nC_8,h^{-1})	0.10	0.22	0.53	0.75	1.00
N_2(ml/min)	16.0	36.0	68.0	120	160
H_2(ml/min)	12.0	28.0	56.0	90.0	120
Conversion	99.1	78.0	74.5	47.5	19.1
Methane	0.0	0.0	0.0	1.6	1.5
Ethane	0.0	0.0	0.2	8.8	8.8
Propane	15.9	15.1	14.1	14.6	10.0
n-C_4	12.9	12.1	11.3	10.0	5.9
iso-C_4	54.5	51.8	47.6	32.1	15.0
n-C_5	1.9	1.9	1.5	1.5	2.8
iso-C_5	13.3	13.0	12.7	12.0	11.6
n-C_6	0.0	0.2	0.3	0.9	1.3
iso-C_6	0.4	0.7	1.8	1.8	4.1
n-C_7	0.0	0.2	0.0	0.5	0.8
iso-C_7	0.2	0.6	0.5	0.4	2.0
mono-B-C_8	0.7	3.2	8.3	11.9	27.1
di + tri-B-C_8	0.2	1.1	2.3	4.0	9.2

T = 495 K

2.4 Conclusions

It was shown that for atmospheric pressure conversion of n-octane over the Pt/Y zeolites, high catalyst stability and high isobutane yield could be obtained when the following conditions were fulfilled:

i) an isomerization/cracking balance to ensure rapid cracking of the reaction intermediates of the multi-branched feed isomer type;

ii) a saturated hydrogen atmosphere and the presence of sufficient Pt sites to ensure hydrogenation/desorption of the products of the central primary cracking(beta-scission mode), and also to prevent the formation of coke "precursors".

In practice, this means that:

a) the preferred reaction temperature is 495 K;

b) the hydrogen partial pressure must be higher than 40 kPa and the Pt content must be at least 0.5 wt% but not exceeding 1.2 wt%.

And c), the higher the contact time (or the lower the flow rate of n-octane), the higher the isobutane yield.

Finally, it is worth stressing that the above reaction conditions were optimized to maximize the production of isobutane. As the objective of this

technology is different from that of conventional hydrocracking, a new technique has been developed (Table 2.11).

Table 2.11 A comparison between the traditional Hydrocracking Technique and the one presented in this thesis

Technique	Traditional	This thesis
Feed	gas oil	paraffin
Product	gasoline	isobutane isopentane
Catalyst	NiS/SiO_2-Al_2O_3 Pd/Y	Pt/Y (0.5 wt% Pt)
Conditions	673 K 100*100 kPa	495 K 100 kPa

CHAPTER III

DESILICATED ZEOLITES AND LANTHANUM ION INCORPORATION

3.1 Introduction

Zeolites are crystalline silicates of aluminum. The ratio between silicon and aluminum (Si/Al in atom), or between silica and alumina (SiO_2/Al_2O_3 in molar) is an important parameter of these materials. It is closely related to their structures, and affects their cation-exchange capacity(CEC), stability, pore shape and size, and thus ultimately their sieving efficiency and catalytic activity.

Each tetrahedrally coordinated aluminum atom in the framework carries a negative charge. These negative charges in the framework must be compensated for by cations located in specific non-framework positions. These cations can be exchanged with others via an ion-exchange process, which defines the cation-exchange capacity of a zeolite. As the number of exchange sites in the zeolite is equivalent to the number of framework aluminum atoms, its cation-exchange capacity should increase with decreasing Si/Al ratio.

When protons are used as cations to compensate for the negative charges arising from the tetrahedrally coordinated aluminum atoms in the framework, Brønsted acidic sites are formed. Although these protons occupy certain preferred positions in the zeolite, they still have considerable freedom

of movement, especially in the hydrated form or at high temperature. From this point of view, the framework of a zeolite behaves like a medium or solvent for a solution. The general principles for solutions should therefore be applied to these zeolite systems. Thus, the density of Brønsted acidic sites or protons should decrease with increasing Si/Al ratio, but the acidic strength of these protonic sites would increase with increasing Si/Al ratio, as the more dilute this pseudo-solution is, the larger is the activity coefficient of the protons.

Increased stability with increased Si/Al ratio is well established and appears to be general whenever isostructural zeolites with different Si/Al ratios occur[71]. The Y zeolites with high Si/Al ratios can maintain their structural integrity up to about 1300 K[72], and are therefore called ultrastable Y(USY).

Since the length of Al-O bonds is somewhat greater than that of Si-O bonds, the exact configuration of the various ring structures depends on aluminum content. A result of this was seen in the decrease in unit cell size with Si/Al ratio for Y zeolites[73] upon dealumination. But, it is still too early to say that this is a general rule which applies over the entire range of Si/Al ratios, because little or no evidence from zeolites with Si/Al ratios lower than the primary synthesized zeolites is available.

A wide range of Si/Al ratios of zeolites with isostructure can be achieved

by precisely controlling the primary synthesis recipe and hydrothermal crystallization conditions[74]. But, it can also be achieved by various post-synthesis modifications.

Most of these post-synthesis modifications for siliceous zeolites are developed with the objective of increasing the Si/Al ratio in order to enhance their thermal/hydrothermal stability. The typical post-synthesis techniques include hydrothermal treatment[75] or chemical modification. In chemical modification, dealumination is accomplished by reacting the zeolite with a suitable reagent in solution or by passing the reagent in vapour phase over the zeolite at high temperatures. Depending upon the reagent used, dealumination can be carried out with or without silicon enrichment of the dealuminated zeolites. In the former case, such as the reaction of zeolites with $SiCl_4$[76] in gas/solid phases and with aqueous $(NH_4)_2SiF_6$[77] in solid/solution phases, silicon atoms from an external source are inserted into the framework vacancies left by dealumination. In the latter case, for example reaction of zeolites with complexing agents such as EDTA[78], no such insertion of silicon occurs. Since the former case may involve the framework "healing" process, it is also called the "secondary synthesis"[79].

Compared to the modification techniques for increasing Si/Al ratio, very little information on decreasing this ratio is available in the literature. Reports

on this subject mostly deals with insertion of aluminum species into the zeolite framework using volatile aluminum halides or solutions of complex aluminates [80-82]. There is even less work on removing silicon from the zeolite framework [83-85]. Ankica, et al [83] investigated the dissolution of ZSM-5 zeolite in hot alkaline (NaOH) solutions and found that the dissolution process is auto-catalyzed by silicate anions. Dessau, et al [84-85] recently reported that the treatment of ZSM-5 crystals with aqueous base (0.5 M Na_2CO_3) at the reflux temperature resulted in partial dissolution of the sample with preferential removal of silica. The resulting zeolites had lower Si/Al ratios and higher cation-exchange capacities, but underwent severe structural collapse. Unfortunately, no successful method for silicon leaching from low silicon containing zeolites, such as faujasite type zeolites, has yet been reported.

The objectives of my work in this aspect of the project were i) to develop an efficient technique for the selective removal of silicon from various types of zeolites; ii) to characterize the resulting materials; and iii) to explore their applications in cation-exchange and in catalytic reactions.

3.2 Experimental

3.2.1 Sample and Treatment Procedure

1). Raw material

Parent zeolites in powder form, NaA (4A), NaY (LZY52) and NaX (13X) were purchased from UOP. The silicalite (ZSM-5 zeolite with Si/Al = 115), in powder form, was purchased from Union Carbide. The ZSM-5 zeolite (Na form, powder) was provided by Chemie Uetikon.

2). Treatment procedure [86-87]

The standard procedure for base-treatment was as follows: 15.0 g of zeolite was placed in a beaker containing 0.450 dm^3 of a base solution in water(Distilled). The base solution was made up of sodium carbonate (Fisher, analytic grade, 0.8 mol dm^3, otherwise as specified) and sodium hydroxide (Aldrich, analytic grade, 0.0 to 0.5 mol dm^3 as specified). The suspension, under moderate stirring, was heated to 353 K for 4 h. The suspension was allowed to settle, and the supernatant was rapidly removed. A fresh volume of the base solution was added, and the suspension was again very mildly stirred at 353 K for a further 4 h. The treatment was repeated the third time and the entire operation lasted 12 h. The suspension was filtered, and the solid was washed on the filter several times. The product was dried in an oven at 393 K overnight. Subsequently, the resulting solids were carefully washed with distilled water and treated the same ways as the base-treatment but using distilled water instead of the base solution. The final resulting samples were called Na(m)Y, Na(m)X, Na(m)ZSM-5 and Na(m)Silicalite.

3) Ion-exchange procedure [89]

Ion-exchange with ammonium and lanthanum followed the basic procedure, except for the aqueous solution used (5 wt. % ammonium chloride and 5 wt. % lanthanum nitrate, respectively). The suspension containing the solid and the corresponding aqueous solution(1 g of solid / 10 cm^3 of solution) was heated at 353 K under moderate stirring for 2 h, and then filtered. This procedure was repeated five times. After filtration and washing, the resulting solid was dried at 393 K for 12 h.

The HY, H(m)Y and HX were prepared by heating the corresponding ammonium forms in air at 623 K for 24 h.

The LaNaY, LaNa(m)Y and LaNaX were obtained by ion-exchanging the corresponding sodium forms with La ions, and then activating in air at 623 K for 24 h. The LaHY, LaH(m)Y and LaHX were obtained by first ion-exchanging the corresponding sodium forms with ammonium ions, then with La ions, and finally activating in air at 623 K for 24 h.

3.2.2 Characterization of the Zeolites

Characterization techniques, as outlined in 2.2.3, include the determination of (i) the chemical composition by atomic absorption

spectrometry; (ii) the limit of the thermal stability by DTA/TGA; and (iii) the surface acidity by ammonia adsorption and temperature-programmed desorption.

The La_2O_3 content was calculated according to equation:

$$\%La_2O_3 = 100 - \%[SiO_2 + Al_2O_3 + Na_2O]$$

where, $\%SiO_2$ was determined by the precipitation method, and $\%Al_2O_3$ and $\%Na_2O$ were determined by the atomic absorption method. The extent of lanthanum incorporation (approximate value) was calculated using the following formula:

$$La_{ex} = (Al^{\cdot} - Na^{+} - H^{+})/Al^{\cdot} \text{ molar ratio} * 100\%$$

Characterization techniques, which were not mentioned in 2.2.3, include the determination of (i) the structure and degree of crystallinity by X-ray powder diffraction (XRD); (ii) the surface area and mesopore size distribution by adsorption-desorption of nitrogen; (iii) the micropore size distribution by adsorption of argon; and (iv) the framework structure by FTIR and NMR.

1) XRD

X-ray powder diffraction patterns were recorded using an X-ray diffraction apparatus equipped with a CuKα radiation source (λ = 1.5418 Å, Ni filter) operated at 40 kV and 20 mA. The solid sample was ground and

pressed in a plexiglass sample holder for X-ray diffraction recording. The X-ray diffraction pattern was compared with the standard pattern[55] to check the structure of the material, and peak intensities were integrated to calculate the degree of crystallinity of each sample investigated.

2) Physical adsorption of N_2 and Ar

According to the classification proposed by IUPAC [56], three types of pores are distinguished based on their pore sizes. Pores of < 2 nm diameter are called "micropores"; those in the range 2-50 nm diameter are " mesopores"; and pores > 50 nm diameter are "macropores". The nitrogen adsorption /desorption isotherms do not give information about micropores, while the Ar adsorption isotherms do.

The nitrogen adsorption/desorption isotherms were recorded at the temperature of liquid nitrogen, 77 K, using the Micromeretics Model ASAP 2000 after outgassing the sampie at 623 K under a pressure less than 1 Pa. The B.E.T. surface area [57], the Langmuir surface area [58], the BJH mesopore size distribution [59] and the average pore diameter were obtained from these isotherms.

The argon adsorption isotherms were recorded at the temperature of liquid argon, 87 K, using the Micromeretics Model 2000M after outgassing the

sample at 623 K under a pressure lower than 1 Pa. The micropore size distributions and the micropore volumes were interpreted by means of the Horvath and Kawazoe (HK) method[60]. The BET and Langmuir surface areas were also determined from argon adsorption isotherms.

3) FTIR

Fourier-Transform Infrared Spectra (FT-IR) were recorded in the 400 cm^{-1} - 1500 cm^{-1} range using an FT-IR (Nicolet 205 model) apparatus which allows a resolution of 2 cm^{-1}. Potassium bromide(KBr) was used as a matrix to make pellets [88].

4) Solid state - NMR

The nuclear magnetic resonance(NMR) spectra of zeolites were obtained on a Varian VXR 300 FT-NMR spectrometer operating at 59.592 MHz (78.159 MHz for ^{27}Al) using superconducting solenoid magnets and amplifiers for final radio frequency pulse generation. A VXR 4000 computer system was used for data acquisition and processing. ^{29}Si magic angle spinning(MAS)-NMR spectra were obtained using probes with a spinning rate of 26 Hz(10 Hz for ^{27}Al)[86]. All ^{29}Si and ^{27}Al chemical shifts were referred to tetramethylsiliane (TMS) and $[Al(H_2O)_6]^{3+}$, respectively.

3.2.3 Cation-Exchange Capacity Testing[87]

Prior to ion-exchange testing, the zeolites were dehydrated overnight at 393 K. The ion-exchange tests were performed in the apparatus shown in Figure 3.1. With such an experimental set-up, the working conditions for detergent powders in washing machines were mimicked. The simulated hard water was placed in a flask containing a strong magnetic stirring bar. The flask was placed in a water bath which was heated at a constant temperature by a hot-plate equipped with a magnetic stirrer which ensured a strong and constant stirring action throughout the experiment. When the solution reached the desired temperature, 1.0 g of the zeolite sample was rapidly poured into the flask. At that moment, the time was taken as zero. A solution sample (2 cm^3) was taken from the flask at one minute intervals using a fraction collector, while a reservoir kept adding water to compensate for the volume lost. The experiment was stopped after 16 min, which corresponds approximately to the residence time of the detergent in the washing machine. A blank test which was carried out according to the same procedure as above but without zeolite addition was used to calibrate the concentration of Ca and Mg ions in each sample.

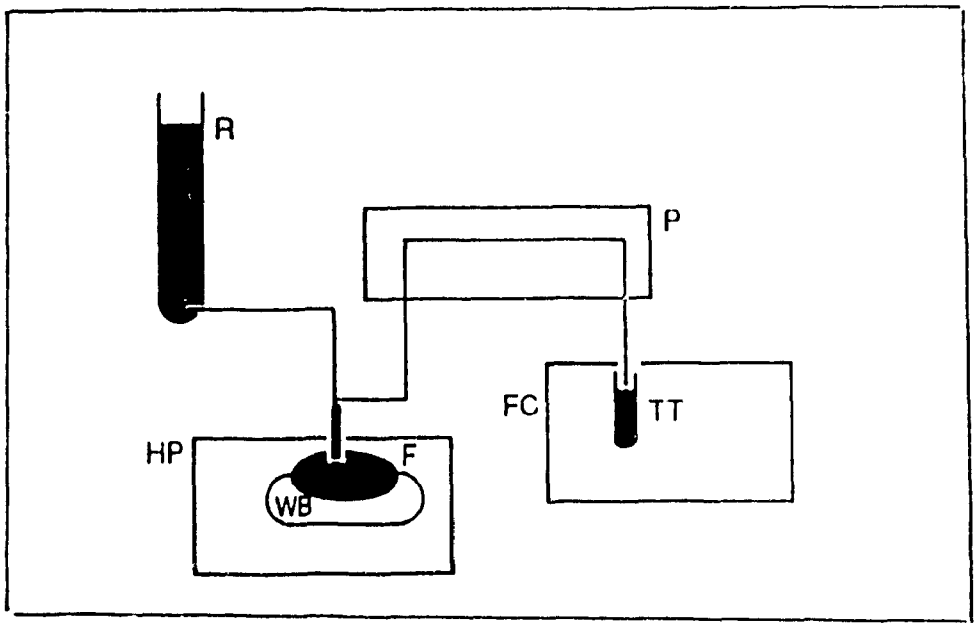

Figure 3.1 Experimental set up for the Ca and Mg ion removal from hard water using zeolite powders

R = distilled water reservoir; P = peristaltic pump; FC = fraction collector; TT = test-tube; F = ion-exchange flask; WB = water bath and HP = hot-plate

The concentrations of Ca and Mg ions remaining in each sample were determined by atomic absorption spectroscopy and expressed in ppm. The concentrations, C_{Ca}, of Ca^{2+} and C_{Mg}, of Mg^{2+} were then plotted against time. A polynomial function (limited to the second degree, for physically meaningful purposes) was used for curve fitting:

$$y = C_{Ca} = a + bt + ct^2$$

The calcium ion removal was expressed as :

$$IR_{Ca}(\%) = [\ C'_{Ca} - C^{f}_{Ca}\ ]/C'_{Ca} * 100$$

where C'_{Ca} and C^{f}_{Ca} were the initial and final concentrations (in ppm) of Ca^{2+}. C^{f}_{Ca} was calculated from the curve by replacing t in the previous equation by ,6 (min). Magnesium ion removal(IR_{Mg}) was determined in the same way. The total ion removal was expressed as:

$$IR_{tot}(\text{equiv. base } \%) = [1-(C^{f}_{Ca} + C^{f}_{Mg})/(C'_{Ca} + C^{i}_{Mg})] * 100$$

where all the concentrations are expressed in ion equivalents.

The rate of calcium removal(in ppm min^{-1}) is equal to the first negative derivative of the function y:

$$r_{Ca} = - dy/dt = - b - 2ct$$

The initial rate of calcium removal was determined by taking t = 0. So, $[r_{Ca}]^{\circ}$ = - b (in ppm min^{-1}). The rate and the initial rate of magnesium removal (r_{Mg} and $[r_{Mg}]^{\circ}$) were determined in the same way.

3.2.4 Catalytic Testing

The final catalysts were prepared by the technique of "dry impregnation" as described in Chapter 2. The experimental set-up, procedure and product analysis for catalytic testing were also identical to those described in Chapter 2. The reaction parameters were chosen as follows: WHSV (weight hourly space velocity of n-octane = 0.1 h^{-1}; temperature = 495 K; flow-rate of nitrogen (used as carrier gas) = 16.0 cm^3min^{-1}; flow-rate of hydrogen = 12.0 cm^3min^{-1}; and weight of catalyst = 1.25 g. Prior to testing, the catalyst was reduced in situ at 573 K for 2 h in the presence of the same H_2/N_2 gaseous mixture used for the reaction.

3.3 Results and Discussion

3.3.1 Desilication Technique

Table 3.1 reports the chemical compositions of NaZSM-5, NaY, and NaX zeolites and the corresponding samples modified by sodium carbonate aqueous solutions under the same treatment conditions. It is seen that the chemical treatment decreased the Si/Al ratio much more with more siliceous zeolites as follows:

Silicalite > ZSM-5 > NaY > NaX

It is easier to remove Si from silicalite and ZSM-5 than from faujasite zeolites. This is probably the reason that base-treatment of ZSM-5 zeolite has been reported previously[83-85], but not of NaY and NaX zeolites. I also found that when Y and X zeolites were to be treated, the use of aqueous solutions of sodium carbonate alone resulted in data which were not very reproducible[88]. Therefore, to improve the efficiency and the reproducibility of the desilication process, some NaOH was added to the sodium carbonate solution.

Table 3.1 Chemical composition of zeolite samples
(a comparison among various types of zeolite)

Zeolite	SiO_2	Al_2O_3	Na_2O	Si/Al	%[a]
NaSilicalite	98.9	0.67	0.3	125	
Na(m)Silicalite	95.8	2.7	1.5	30	76
NaZSM-5	92.2	5.0	2.8	15.7	
Na(m)ZSM-5	86.0	8.6	5.4	8.5	46
NaY	63.7	22.7	13.6	2.39	
$Na(m)Y_{1.8}$	56.1	26.1	17.0	1.83	23
NaX	47.7	32.7	19.6	1.24	
Na(m)X	43.0	36.5	20.5	1.00	19

(a) % change of Si/Al upon treatment

Table 3.2 Influence of NaOH addition
on desilication of Y zeolite

Na_2CO_3	0 M	0.8 M					
NaOH	0 M	0.1 M		0.2 M		0.5 M	
$pH_{suspension}$	9.0	12.5		12.9		13.1	
Times * h[a]	0*0	3*4	6*4	3*4	6*4	3*4	6*4
Recovery(%)	100	67	52	67	34	52	29
D.C[b]	100	93	87	91	87	90	87
Si/Al	2.5	2.2	1.8	2.0	1.7	1.6	1.4

(a) : repetitions * exposure time (h)

(b): degree of crystallinity, DC = 100 for parent NaY

Table 3.2 reports the influence of addition of NaOH to the sodium carbonate solution on the desilication of Y zeolite. The more NaOH added, the more basic the solution which was reflected by a higher pH of the initial suspension. The Si/Al ratio of the final modified zeolites depended on the pH of the initial suspension and the treatment conditions. The efficiency of the desilication process increased with increasing pH of the initial suspension. By

carefully controlling pH of the initial suspension by addition of NaOH, it was possible to effectively remove Si from Y and X zeolites without incurring problems of data reproducibility [88].

Figure 3.2 shows the X-ray diffraction patterns of parent NaY (NaY, Si/Al = 2.4) and modified NaY ($Na(m)Y_{1.3}$, Si/Al = 1.3) zeolites. No dramatic change in the structure upon base-treatment is observed. The degrees of crystallinity of the modified samples are slightly lower than that of parent zeolite NaY, and depend on the pH of the base-solution used(Table 3.2). Therefore, a lower or a milder concentration of NaOH, ie. a lower pH of the initial suspension, is recommended in order to avoid serious damage to the zeolite structure.

^{27}Al-NMR spectra (Figure 3.3) confirm the results of XRD. Although the Si/Al ratio decreases practically by half(from 2.4 in NaY to 1.3 in $Na(m)Y_{1.3}$), all the Al component remains in the tetrahedral configuration[96-97]. On the other hand, the ^{29}Si-NMR peak(IV) corresponding to the [Si4Al] situation increases dramatically obviously at the expense of the other situations ([Si3Al], [Si2Al], and [Si1Al] which are associated with peaks III, II, and I, respectively [96-97]). This indicates that the number of framework Si atoms which have the richest framework Al environment increases steadily when Si atoms are selectively removed.

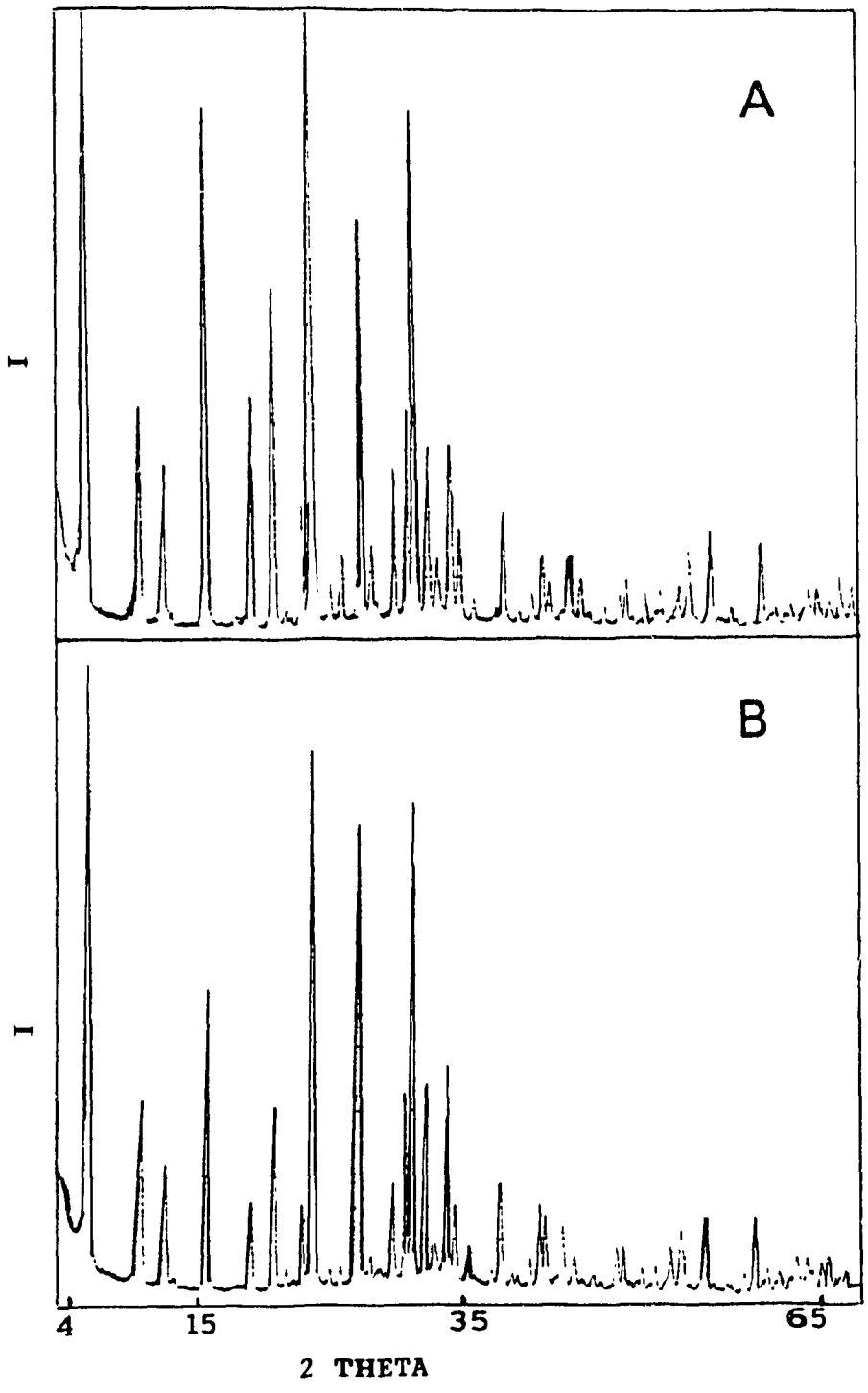

Figure 3.2 X-ray diffraction pattern of NaY(A) and Na(m)$Y_{1.3}$(B)

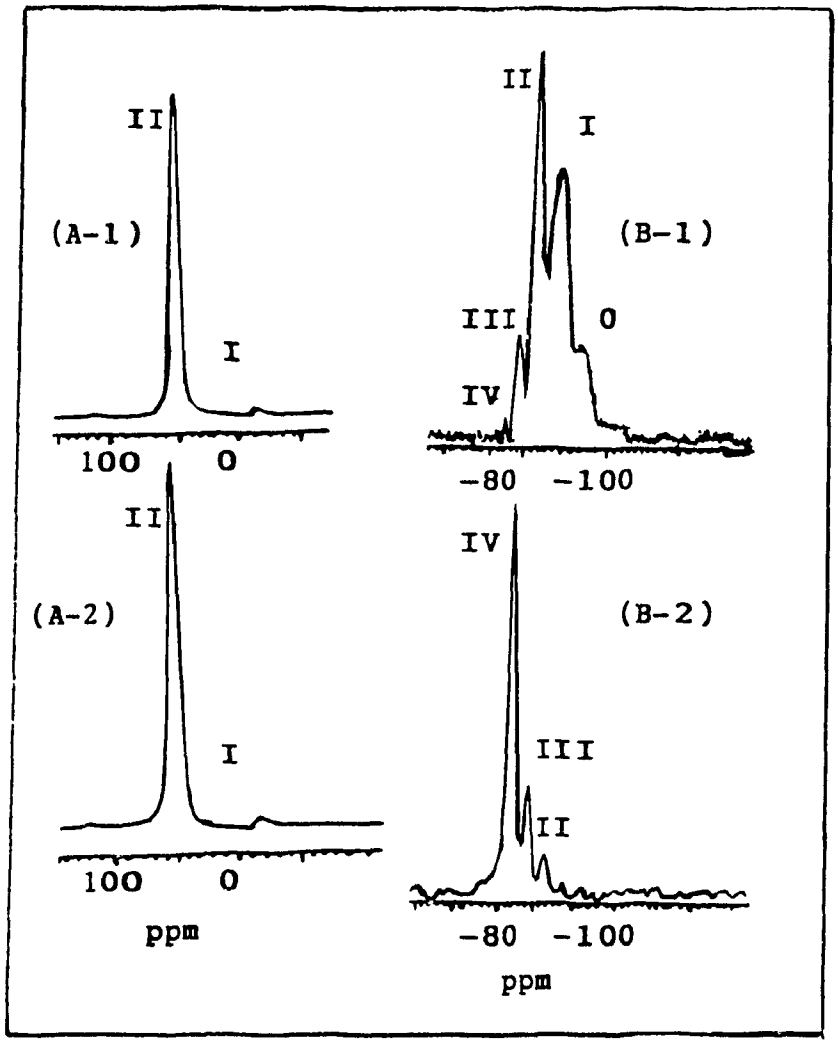

Figure 3.3 MAS-NMR spectra of ^{27}Al(A) and ^{29}Si(B) of sample NaY(1) and $Na(m)Y_{1.3}$(2)

FT-IR spectra provide further evidence supporting the conclusion that all the Al component remained in the framework after Si atoms are removed. FT-IR spectra recorded with the parent Y zeolite and the desilicated Y zeolites (Table 3.3) show two bands (970-1,100 cm^{-1} and 750-820 cm^{-1}) which were assigned by Flanigen et al[98] as corresponding to the asymmetric stretching and symmetric stretching vibrations of the principal T-O bond, respectively (where, T stands for Si or Al). It was also assumed that these two bands were sensitive to the variations in the density of the framework Al sites. In particular, the asymmetric stretching band of the T-O bond shifts to a lower frequency when the content of the tetrahedral Al sites increases. The linear dependence of the frequency of this band on the atomic fraction of Al in the framework is also reported[98]. Therefore, a parallel relationship between the frequency of these bands and the Si/Al ratio of the desilicated Y zeolites as obtained from our FT-IR results (Table 3.3) confirms that all Al atoms remained in the framework after the base-treatment.

Moreover, DTA/TGA studies show that the treated Y zeolite exhibits a thermal stability as high as that of the parent zeolite. Two DTA exothermal peaks at circa 1120 K and 1270 K were observed for both the parent and the treated NaY as shown in Figure 3.4.

Table 3.3 Frequency shift of the FT-IR stretching bands(T-O bond) in the desilicated Y zeolites[a]

Sample	Si/Al	Asymmetric stretch		Symmetric stretch	
		Frequency	ΔF[b]	Frequency	ΔF
NaY	2.5	1011	0	792	0
$Na(m)Y_{1.9}$	1.9	1004	- 7	787	- 5
$Na(m)Y_{1.6}$	1.6	1000	-11	784	- 8
$Na(m)Y_{1.3}$	1.3	989	-22	757	-35
NaX	1.2	985	-26	756	[illegible]

(a): the frequency values of this table are averaged values obtained with at least two analyses(exhibiting differences not exceeding 2 cm^{-1}) carried out with different pellets

(b): frequency given in cm^{-1}. ΔF = variation of frequency with respect to that of the parent Y zeolite.

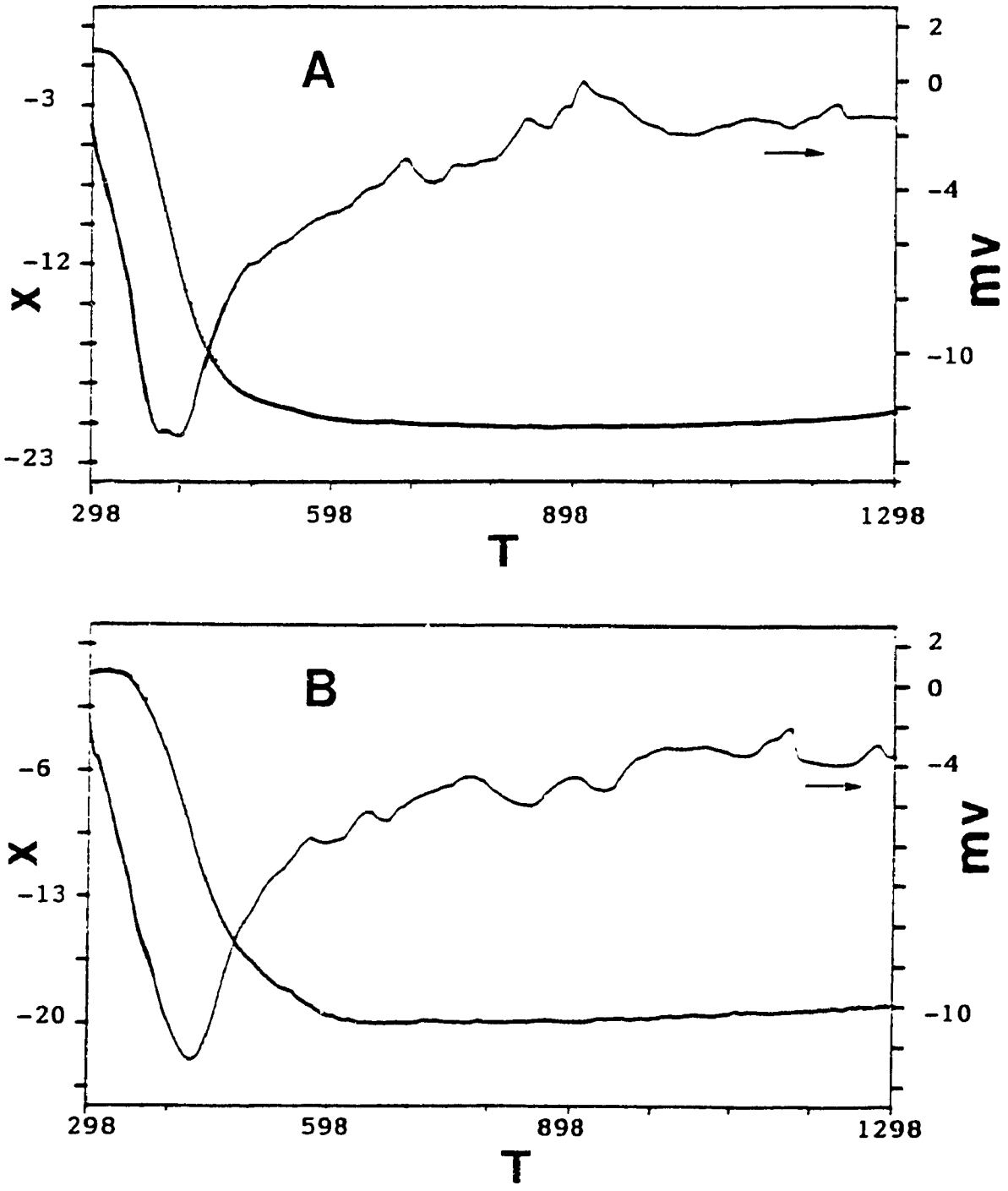

Figure 3.4 TGA and DTA curves of sample NaY(A) and Na(m)$Y_{1.3}$(B)

T = Temperature (K); X = Weight loss (%);

Table 3.4 reports the adsorption and textural properties of the parent zeolites and the desilicated materials. It can be seen that the textural properties of the zeolite do not noticeably change with the treatment. From the BET surface areas and pore volumes, it is found that the micropores still dominate in all the modified zeolites with pore sizes slightly smaller than that of the parent NaY zeolite. The result that the micropore system is fairly well preserved while Si atoms are removed upon the base-treatment, is also proved by nitrogen adsorption and desorption isotherms and by the micropore size distribution. The isotherms (Figure 3.5) obtained with NaY and modified NaY zeolites exhibit the Langmuir isothermal shape and are practically coincident(absence of any hysteresis loop). Both micropore size distributions (Figure 3.6) exhibit a reasonable sharpness.

Table 3.4 Textural properties of the desilicated Y zeolites

Sample	volume of N_2 adsorbed(cm^3g^{-1})		S_{BET} (m^2g^{-1})		pore size(nm)	
	total	m-p[a]	total	m-p	HK(m-p)	BJH
$NaY_{2.5}$	0.365	0.309	742	700	0.74	4.4
$Na(m)Y_{1.9}$	0.414	0.339	765	716	0.73	9.2
$Na(m)Y_{1.6}$	0.347	0.257	684	678	0.73	6.5
$NaY(m)_{1.4}$	0.395	0.327	755	731	0.72	8.0
$NaX_{1.2}$	0.274	0.247	571	531	0.74	4.5

(a) : m-p = micropores

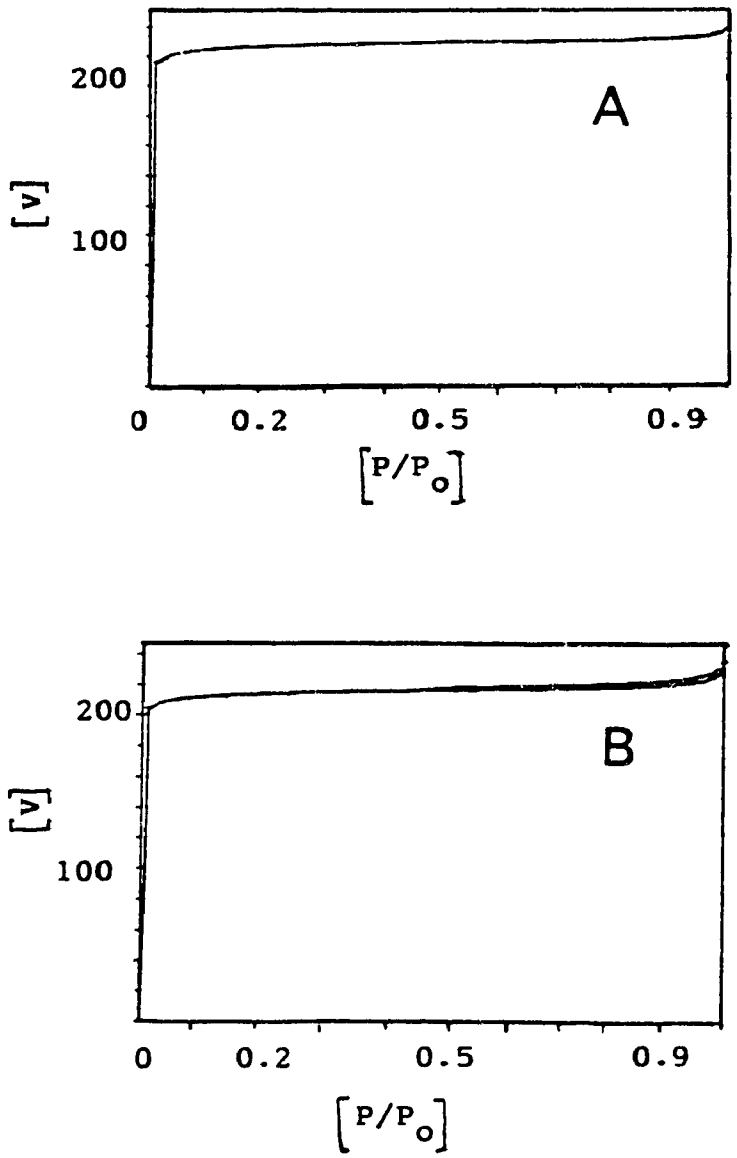

Figure 3.5 N_2 adsorption/desorption isotherm

NaY(A) and Na(m)$Y_{1.3}$(B)

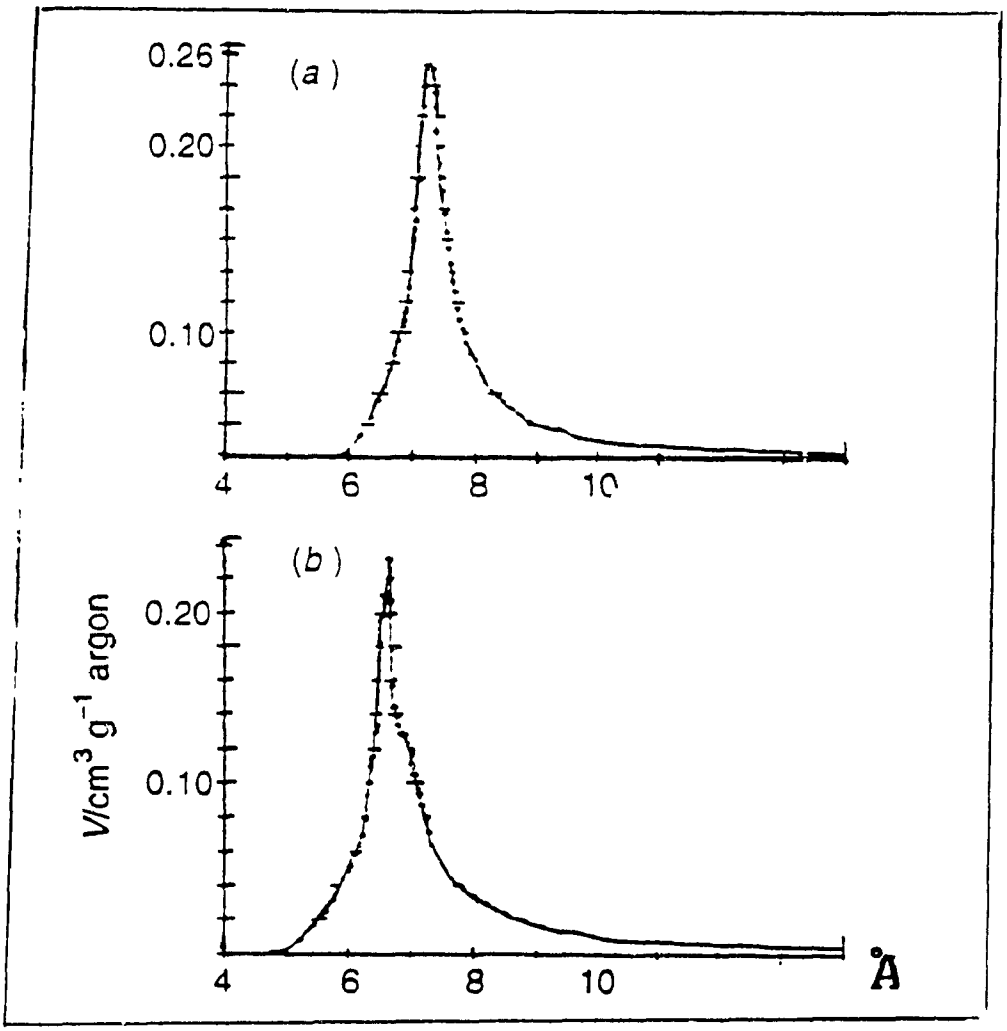

Figure 3.6 Micropore size distribution of

NaY(a) and $Na(m)Y_{1.3}$(b)

Thus, by treatment with the basic solution under very precise conditions, it is possible to significantly increase the Al content of a zeolite by selectively removing some of its framework Si atoms, without drastically changing its structure, thermal stability and texture. Since a tetrahedral Al site corresponds to a cationic site, it should therefore be possible to increase the cation-exchange capacity or the (protonic) acid density of a zeolite.

3.3.2 Cation-exchange Capacity [87]

Table 3.5 summarizes the cation-exchange behaviours of the zeolites. It is seen that ion removal and the initial rate of ion removal, practically Ca^{2+} removal, depend on the operating temperature, Si/Al ratio and micropore size of the zeolite used.

For a given zeolite, the total ion removal increases with rising temperature. So does the Mg^{2+} removal and its initial rate of removal. But, they increase in different ways for different zeolites. The initial rate of removal of Mg^{2+} changes slightly with temperature when the X and Y zeolites are used, but changes dramatically when A-type zeolite is used. This suggests that the ion-exchange rate with Mg^{2+} is strongly dependent on the diffusion rate of these ions through the narrow pores of the NaA zeolite. Such diffusion limitations for the NaA zeolite, especially at lower temperatures, are due to the

strong solvation tendency of Mg^{2+}, which can form bulky complex ions with water molecules [99].

Table 3.5 Ion-removal and some physical properties of zeolites

Zeolites		NaA	Na(m)X	NaX	Na(m)Y	NaY
Si/Al		1.00	1.00	1.24	1.30	2.39
CEC[a]		7.16	7.16	6.41	6.43	4.45
pore size(nm)		0.42	0.72	0.74	0.68	0.74
$IR_{tot.}$	25 °C	69.8	71.5	65.0	65.0	61.7
	45 °C	69.7		73.2		67.7
	65 °C	81.2		80.7		66.3
IR_{Ca}	25 °C	92.5	85.7	71.8	80.4	69.6
	45 °C	74.9		75.0		68.2
	65 °C	80.2		81.0		68.0
IR_{Mg}	25 °C	24.3	43.1	52.5	34.1	46.0
	45 °C	59.2		69.7		66.8
	65 °C	83.4		80.0		63.0
$[r_{Ca}]^{\circ}$	25 °C	8.1	10.0	12.0	11.3	10.1
	45 °C	10.0		12.0		8.1
	65 °C	13.5		11.6		8.2
$[r_{Mg}]^{\circ}$	25 °C	0.5	1.0	2.9	0.9	1.9
	45 °C	1.7		3.2		2.7
	65 °C	4.1		3.5		2.6

(a): cation exchange capacity, expressed in mequiv.g^{-1}, assuming that all Al sites correspond to cation exchange sites.

At a given ion-exchange temperature such as ambient temperature, the total ion removal depends strongly on the Si/Al ratio, and thus, on the CEC of the zeolite used, resulting in the following sequence of effectiveness:

$$Na(m)X_{1.0} \approx NaA_{1.0} > NaX_{1.2} \approx Na(m)Y_{1.3} > NaY_{2.4}$$

Therefore, the present results provide further experimental evidence that all the Al species in the modified zeolites have the tetrahedral configuration and thus generate effective cation-exchange sites, as discussed earlier.

For those zeolites with similar Si/Al ratio, the initial rate of Mg^{2+} removal depends strongly on the micropore size of the zeolite investigated at a given temperature. In general, it increases with the micropore size, and results in the following sequence:

NaA(4.2Å) < Na(m)Y(6.8Å) < Na(m)X(7.2Å) < NaY(7.4Å) < NaX(7.4Å)

For example, Na(m)X had almost the same Si/Al ratio as NaA, however a much higher initial rate for Mg^{2+} removal. Also, both the modified X and Y zeolites exhibit lower initial rates of Mg^{2+} removal than their parent X and Y zeolites. This is due to the slight pore narrowing of the X and Y zeolites upon treatment with the base solution (Figure 3.6 and Table 3.5).

In conclusion, the above results have shown that: (i) at ambient temperature, the total ion removal increases with decreasing Si/Al ratio of the zeolite; (ii) the rate of Mg ion removal of the NaA zeolite which is low at

ambient temperature because of diffusion problems within the narrow pores, improves substantially at higher temperature; this indicates that the NaA zeolite is effective for water softening only under warm conditions of washing; (iii) base-treatment of NaX and NaY zeolites significantly enhances the overall ion-exchange properties, mostly for Ca ion removal. Particularly interesting is the case of Na(m)X which appears to be more effective, at lower temperature, than the NaA zeolite, the preferred phosphate substitute in powder detergents [100-101].

3.3.3 Thermal Stability of La-containing Zeolites

Thermal instability of zeolites used as cracking catalysts is a serious problem encountered mostly during catalyst activation in the regeneration zone where a higher temperature is employed than in the reaction zone. Thus, various dealumination techniques have been developed to increase the Si/Al ratio of zeolites. Here, we deal with desilicated zeolites having a lower Si/Al ratio than their parent zeolites. The sodium forms of these lower Si/Al ratio zeolites exhibit a fairly high thermal stability as shown previously. But, this is not the case for the ammonium or proton forms of such materials.

Figure 3.7 shows the XRD patterns of NH_4X and $NH_4(m)Y_{2.0}$ zeolites

before and after the activation. It is worth noting that this activation was carried out in air at 573 K which is the lowest temperature used to convert a zeolite from the ammonium form to the proton form for catalytic uses. However, it is seen that both zeolite structures collapse upon activation. Therefore, it is necessary to find a way to stabilize these protonic zeolites before making the final catalysts.

It is known that the presence of rare earth metals in the faujasite zeolites increases their stability and catalytic activity[72]. The objectives of my work in this section was to study the influence of ion-exchanging La^{3+} ions on the thermal stability and catalytic activity of these faujasite zeolites, namely the NaY, Na(m)Y and NaX and their H-forms.

Tables 3.6 and 3.7 report the chemical and textural/adsorptive properties of all the zeolites before and after ion-exchange of La^{3+} ions. Figures 3.8 to 3.11 show the X-ray powder diffraction patterns while Figures 3.12 to 3.15 show the TGA/DTA profiles of the zeolites investigated.

These results lead to the following interpretations:

i) The sodium forms of all the zeolites studied are stable, even at an activation temperature higher than 623 K.

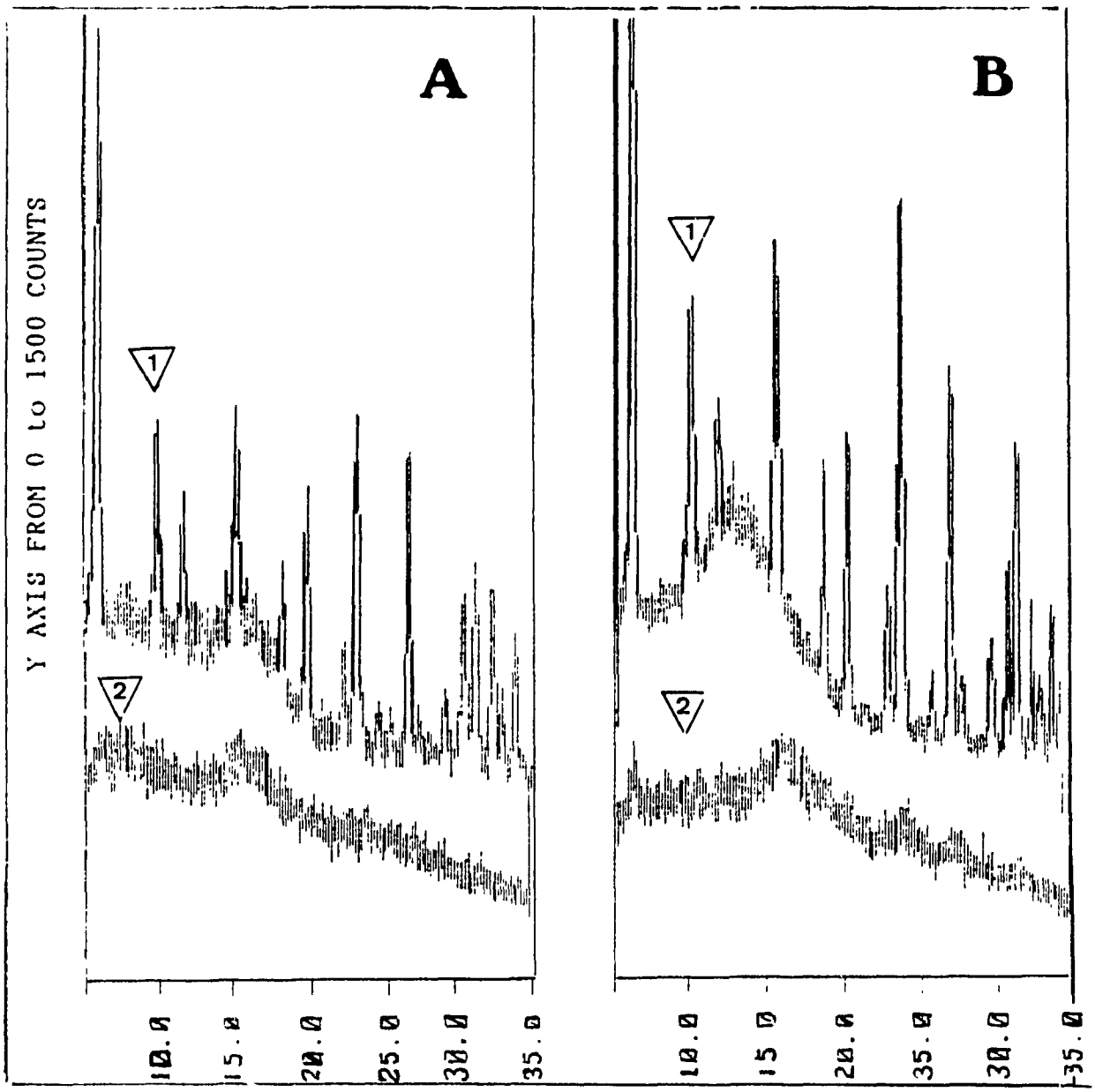

Figure 3.7 XRD patterns of NH_4X (A) and NH_4(m)Y(B) sample before(1) and after calcination(2) at 573 K

Table 3.6 Chemical properties of some zeolites

Sample	Si/Al[a]	Al_2O_3[b]	Na_2O[b]	La_2O_3[b]	La_{ex}[c]
NaY	2.7	20.6	13.8	0	0
Na(m)Y	2.0	22.5	15.0	0	0
NaX	1.2	31.4	19.0	0	0
LaNaY	2.5	20.4	3.7	16.2	70
LaNa(m)Y	2.2	21.4	1.7	18.3	90
LaNaX	1.3	27.2	1.4	31.6	91
HY	2.9	22.1	1.2	0	0
H(m)Y	2.2	27.6	0.5	0	0
HX	1.4	35.5	3.5	0	0
LaHY	2.5	20.1	0.7	20.4	79
LaH(m)Y	2.0	22.9	0.4	19.3	78
LaHX	1.3	28.4	0.9	27.3	80

(a): atomic ratio; (b): weight %; (c): extent of La^{3+} ion exchange.

Table 3.7 Textural and adsorptive properties of some zeolites

Sample	Surface area [a]		Vol.of adsorption[b]		Pore size[c]	
	Total	Micro-p	Total	Micro-p	BJH	HK
NaY	742	699	0.357	0.326	4.6	0.74
Na(m)Y	680	645	0.336	0.300	8.0	0.73
NaX	633	596	0.311	0.278	5.3	0.73
LaNaY	626	571	0.307	0.267	4.2	0.77
LaNa(m)Y	618	574	0.309	0.267	7.0	0.75
LaNaX	560	518	0.277	0.240	5.3	na
HY	410	213	0.349	0.088	9.1	0.76
H(m)Y	71	56	0.062	0.026	19.4	0.73
HX	281	280	0.159	0.096	3.8	na
LaHY	637	595	0.307	0.277	4.6	0.77
LaH(m)	624	584	0.324	0.273	9.5	0.76
LaHX	492	404	0.284	0.187	4.3	na

(a) BET surface area, in m^2g^{-1}; (b) volume of adsorbed nitrogen, in cm^3g^{-1}; Micro-p = Micropores; (c) mesopores, BJH method; and micropores, HK method. na = not available.

Table 3.8 The dependence of textural properties of sample NH_4X and $LaNH_4X$ on outgassing temperature

Outgas Temperature (°C) 1*Pa, 12 hr	150	250	300	350	400
NH_4X					
BET Surface Area(m^2g^{-1})	371	327	305	281	271
Langm. Surface Area(m^2g^{-1})	490	433	404	373	359
Micropore Area(m^2g^{-1})	281	252	230	289	197
Total Volume (cm^3g^{-1})	0.210	0.186	0.172	0.159	0.154
Micropore Volume(cm^3g^{-1})	0.130	0.112	0.107	0.096	0.063
BJH Des. Diameter-4V/A(Å)	38.5	39.2	36.4	37.7	37.3
Peak from dV/dlog(D) (Å)	34.5	34.4	34.3	35.1	35.2
$LaNH_4X$					
BET Surface Area(m^2g^{-1})	474	488	491	492	491
Langm. Surface Area(m^2g^{-1})	625	643	647	648	647
Micropore Area(m^2g^{-1})	388	400	383	404	404
Total Volume (cm^3g^{-1})	0.274	0.283	0.288	0.286	0.286
Micropore Volume(cm^3g^{-1})	0.180	0.186	0.187	0.187	0.187
BJH Des. Diameter-4V/A(Å)	42.1	42.9	42.5	43.0	43.9
Peak from dV/dlog(D) (Å)	43.1	38.7	37.2	39.4	39.1

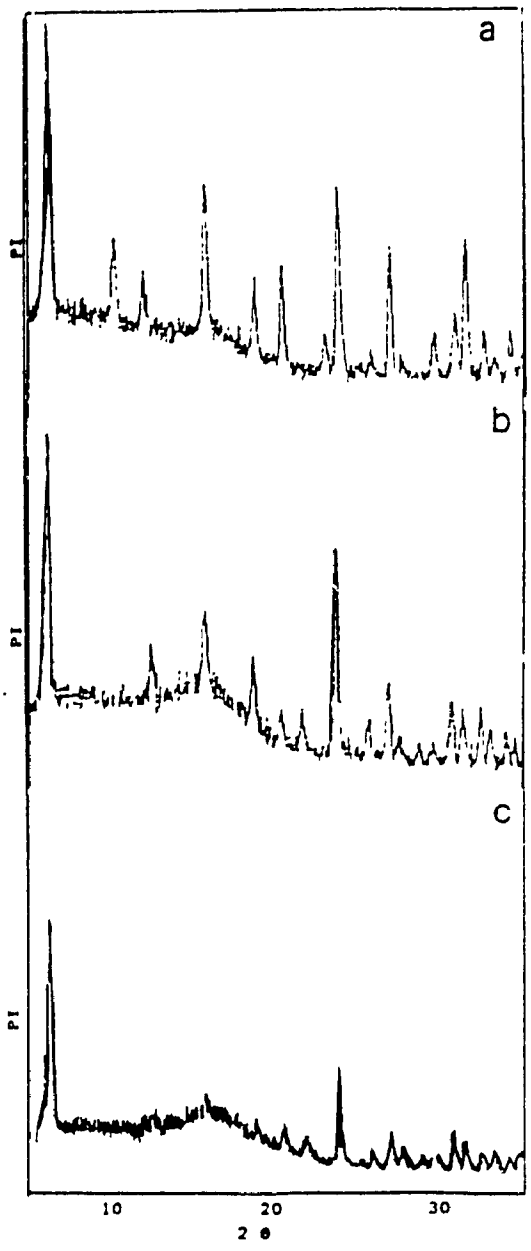

Figure 3.8 XRD patterns of
(a) NaY, PI = 1,000 cts;
(b) LaNaY, PI = 737 cts;
(c) LaHY, PI = 1,000 cts;

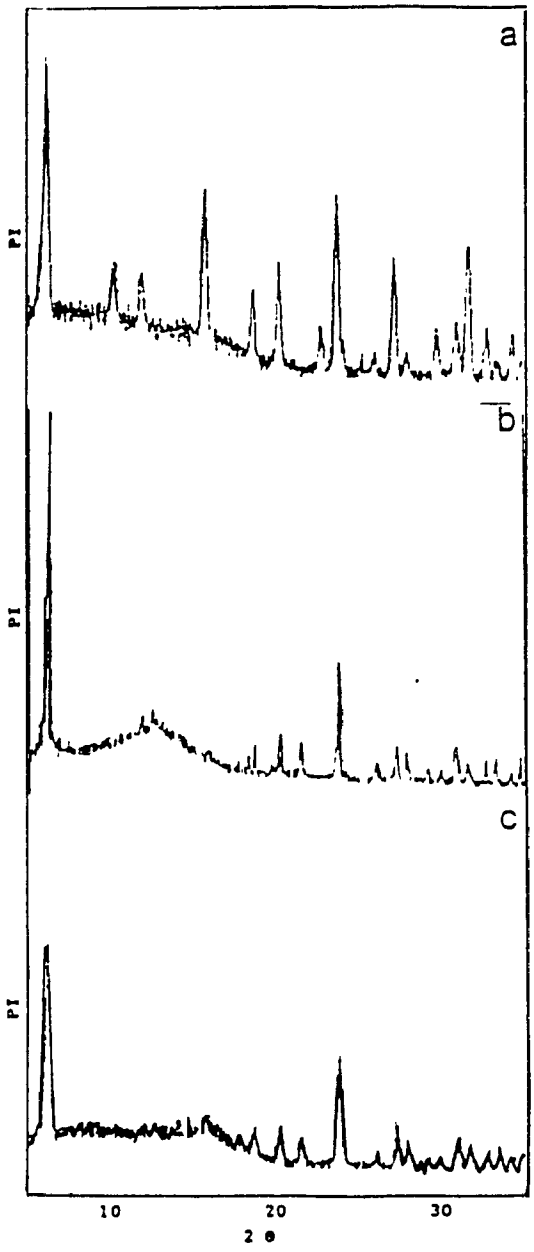

Figure 3.9 XRD patterns of
(a) Na(m)Y, PI = 1,000 cts
(b) LaNa(m)Y, PI = 1,200cts
(c) LaH(m)Y, PI = 1,000 cts

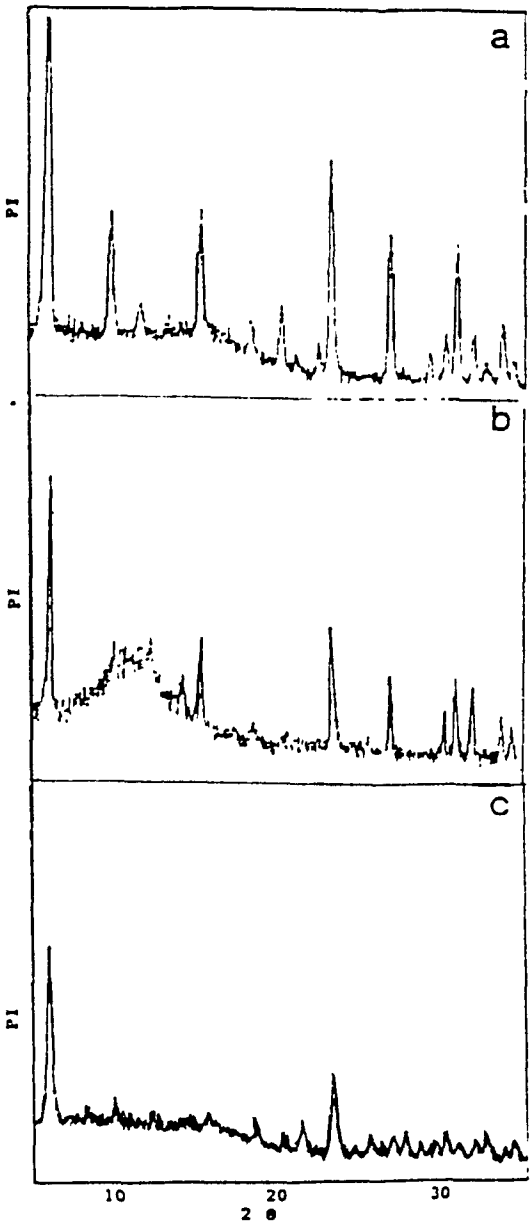

Figure 3.10 XRD pattern of
(a)NaX, PI = 1,000 cts
(b)LaNaX, PI = 500 cts
(c)LaHX, PI = 1,200 cts

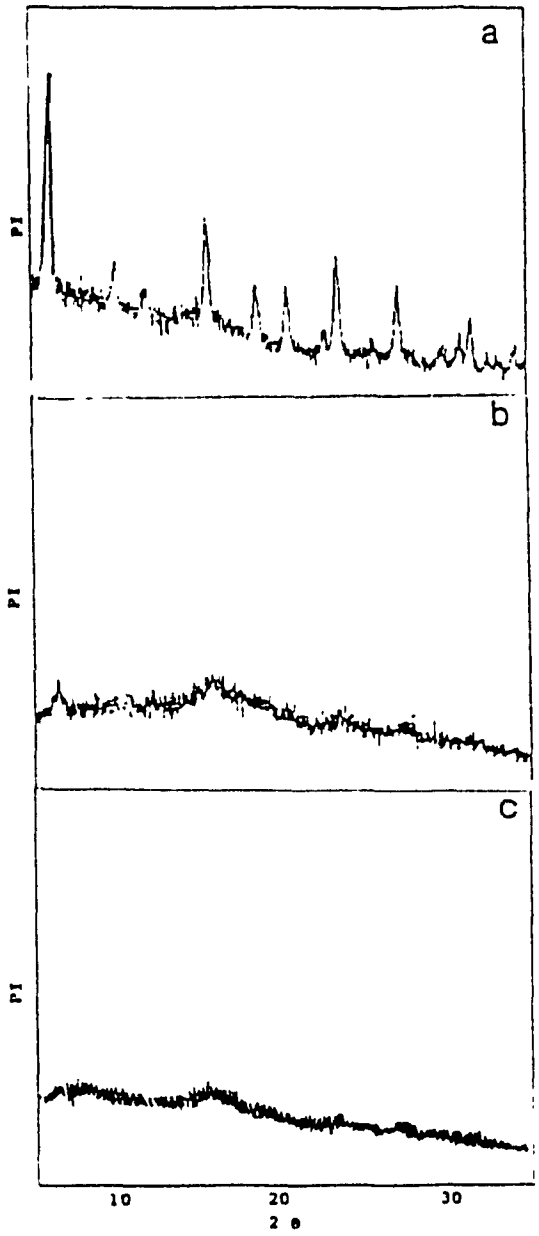

Figure 3.11 XRD pattern of
(a)HY, PI = 1,000 cts
(b)H(m)Y, PI = 1,000 cts
(c)HX, PI = 1,200 cts

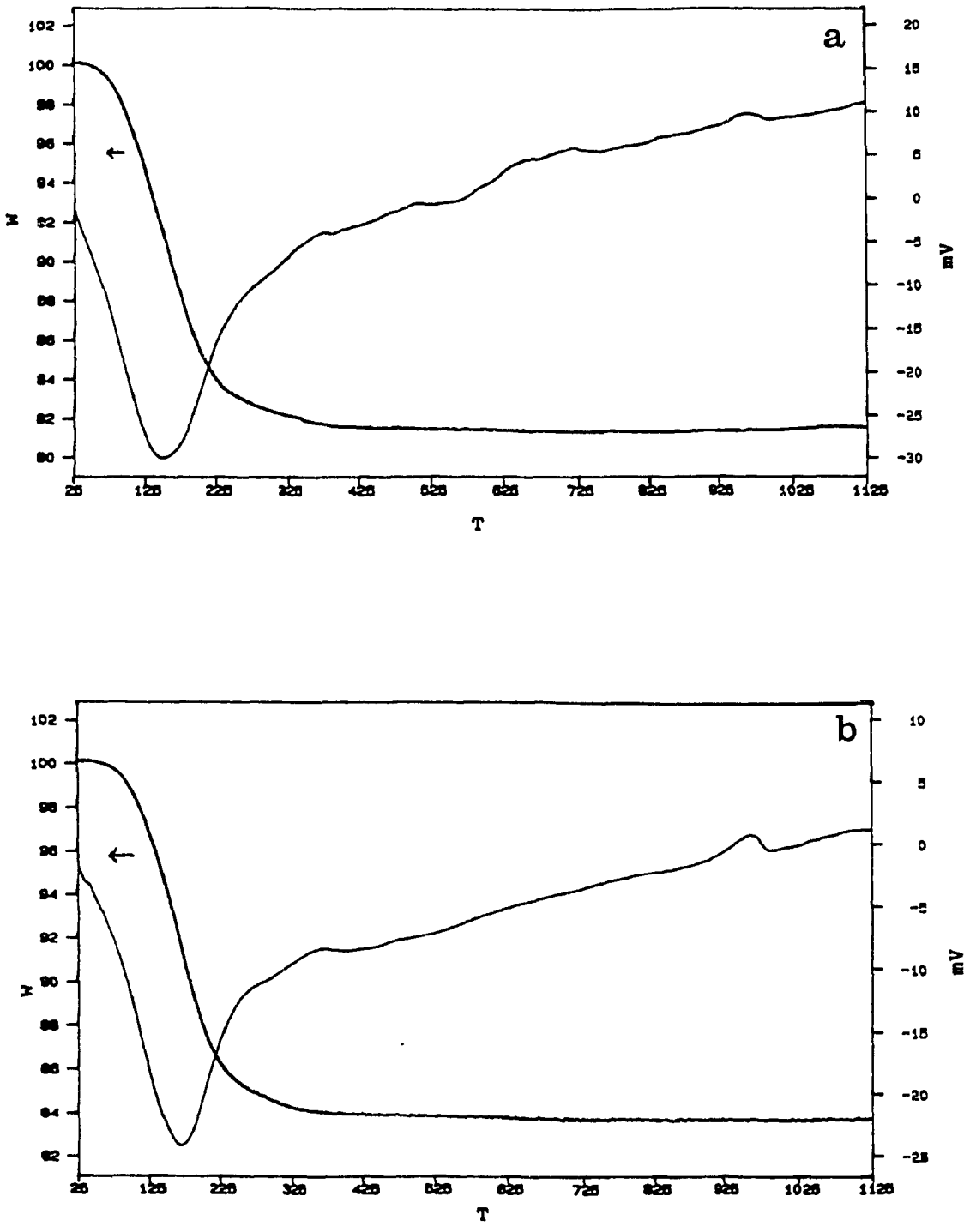

Figure 3.12 DTA/TGA curves of NaY(a) and Na(m)Y
T = temperature in °C, W = weight%, mV = millivolts

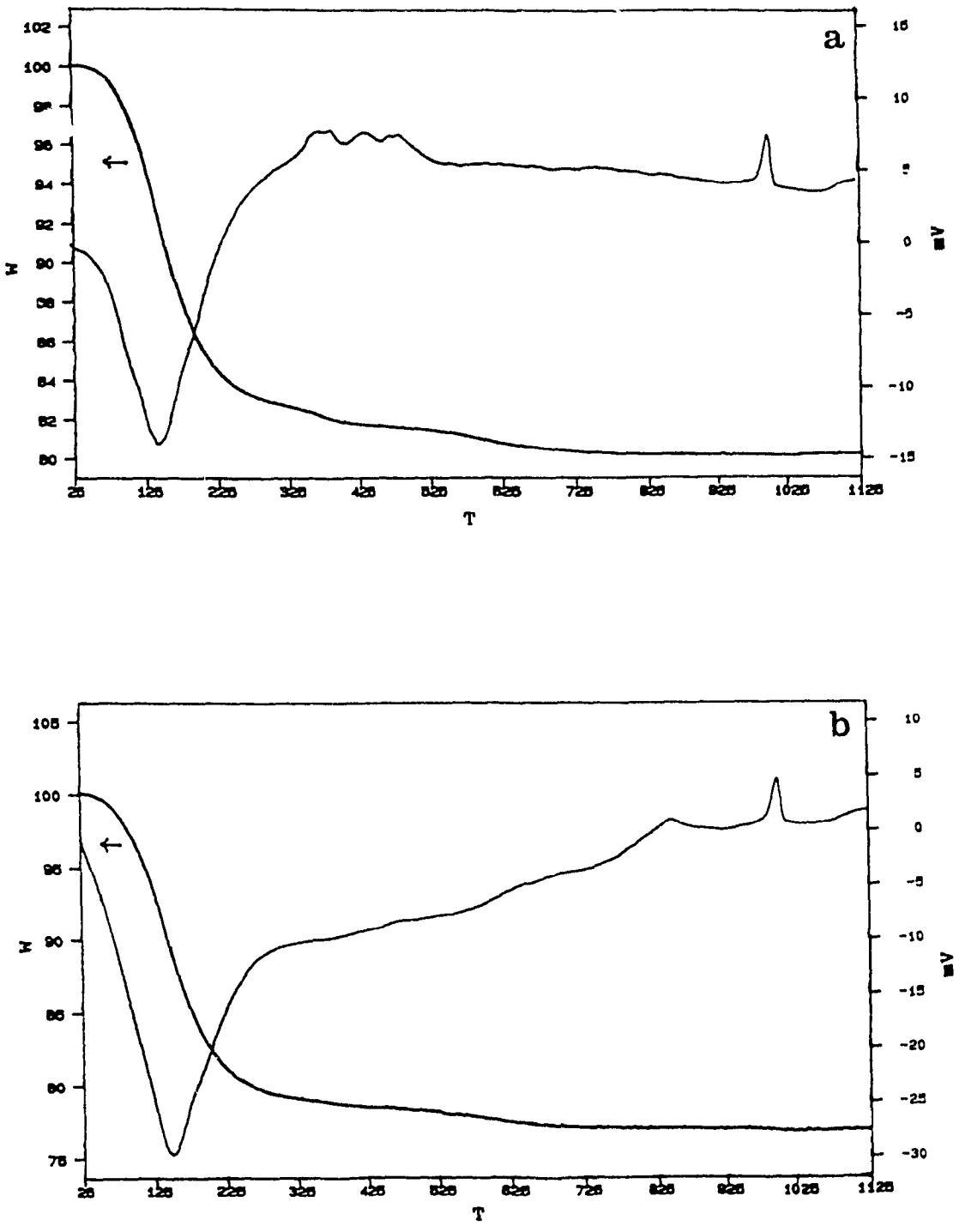

Figure 3.13 DTA/TGA curves of LaNaY(a) and LaNa(m)Y(b)

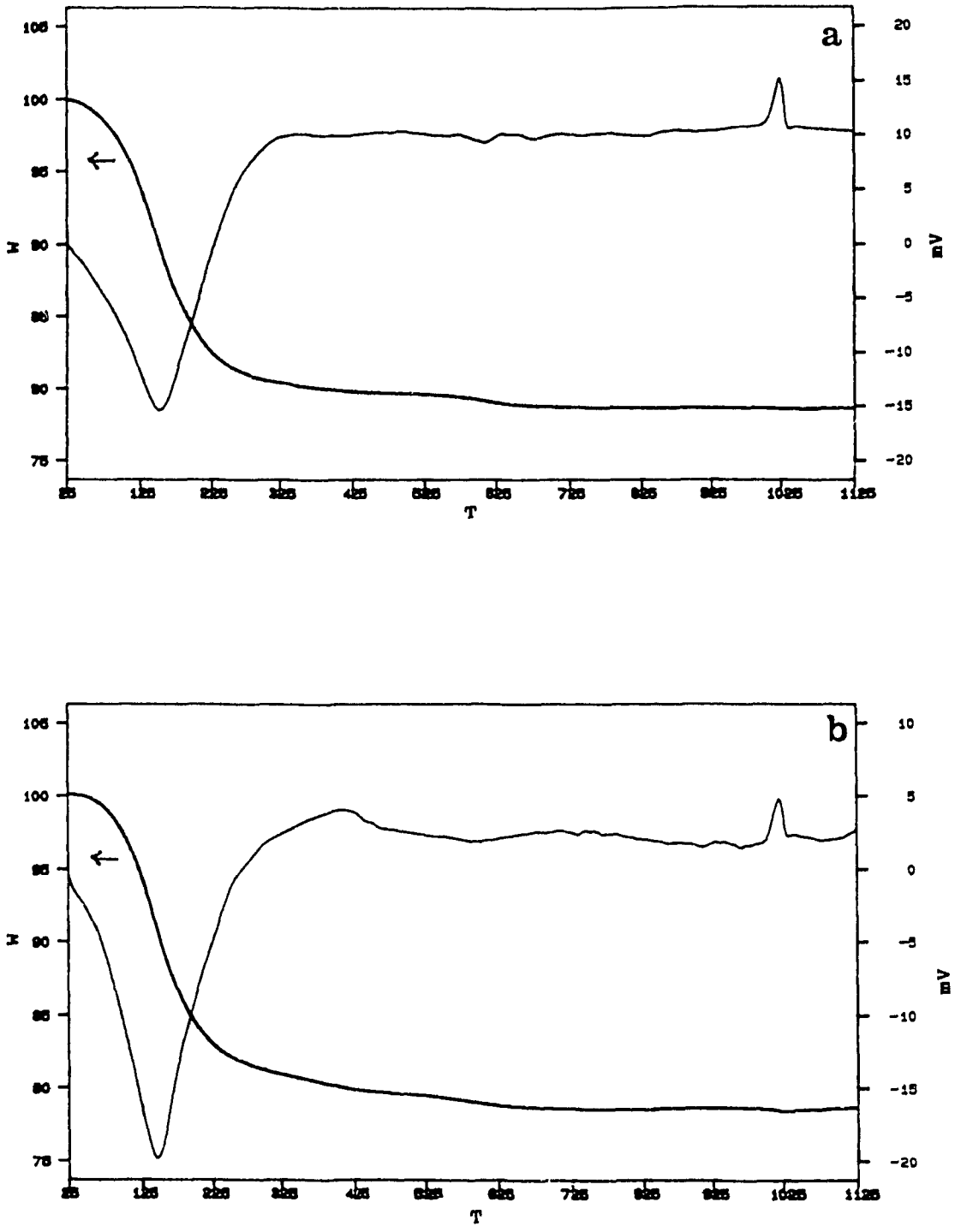

Figure 3.14 DTA/TGA curves of $LaNH_4Y$(a) and $LaNH_4$(m)Y(b)

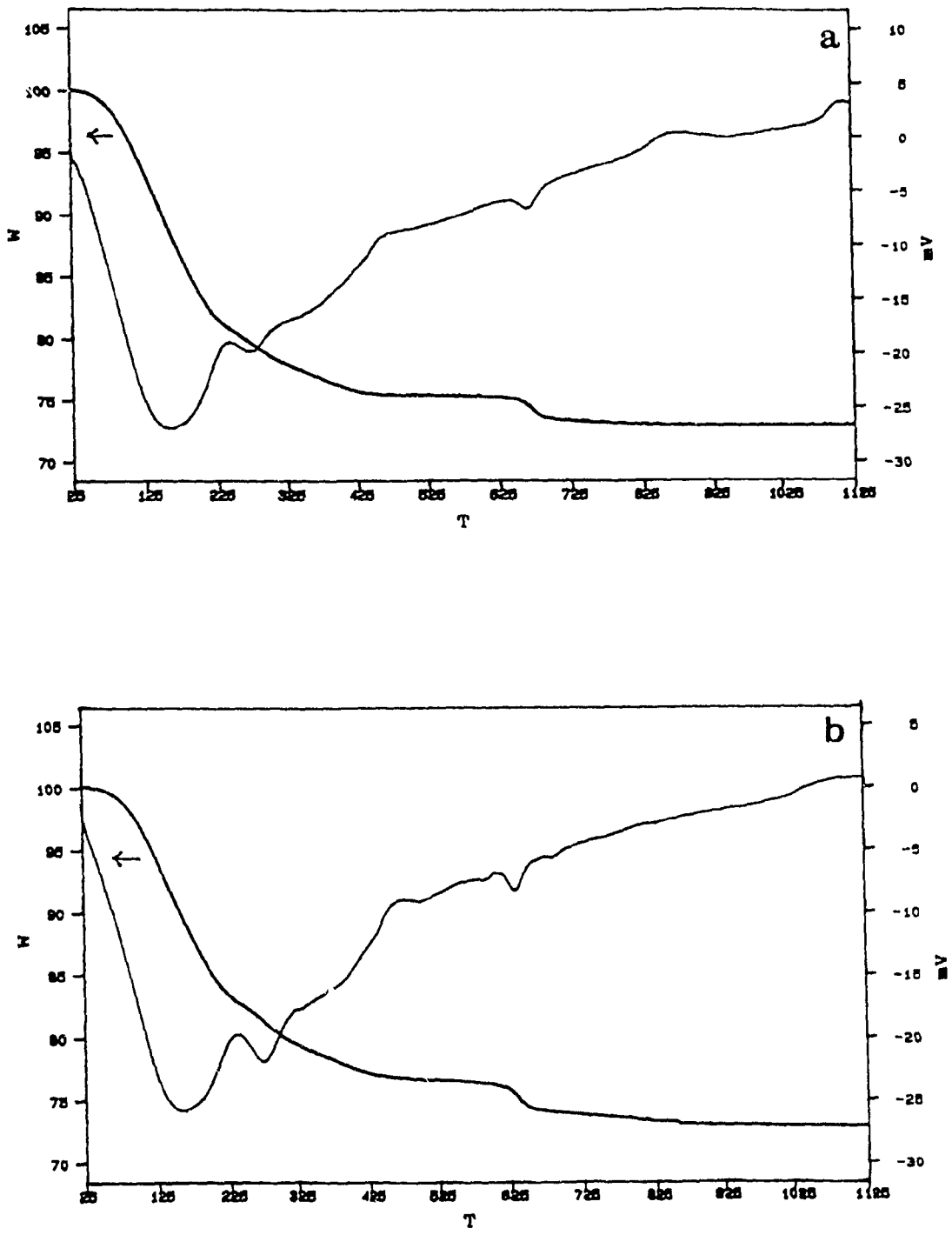

Figure 3.15 DTA/TGA curves of NH_4Y(a) and NH_4(m)Y(b)

ii) The transformation of the sodium forms of the faujasite zeolites into the acid forms result in some structural collapse. The extent of this collapse depend mainly on the Si/Al ratio of the zeolite and its preparation method. The X zeolite in the H-form is less stable than the H-form of the Y zeolite, owing to the lower Si/Al ratio of the former zeolite. The H(m)Y sample although having a Si/Al ratio higher than that of the HX zeolite, is less stable than the HX, probably, because the structure of the former has been loosened during the desilication process. Such a weakened framework of the desilicated zeolite would favour some dealumination at the position of healed Al sites [102] during the heating of the ammonium form to obtain the acid form.

iii) The incorporation of a fairly high amount of lanthanum by ion exchange into all the Na zeolites enhances their acidic properties(Figure 3.16 to Figure 3.18). It is well known that framework hydroxyl groups in lanthanum exchanged zeolites can be formed by hydrolysis of the cation and dissociation of the water molecule due to the electrostatic field created by the cation. The mechanism results in the formation of four hydroxyl groups for every six initial cation exchanged sites as shown in Scheme VI.[72,103]. These hydroxyl groups have been related to catalytic activity and are similar to the hydroxyl groups observed in the ammoniated zeolites.

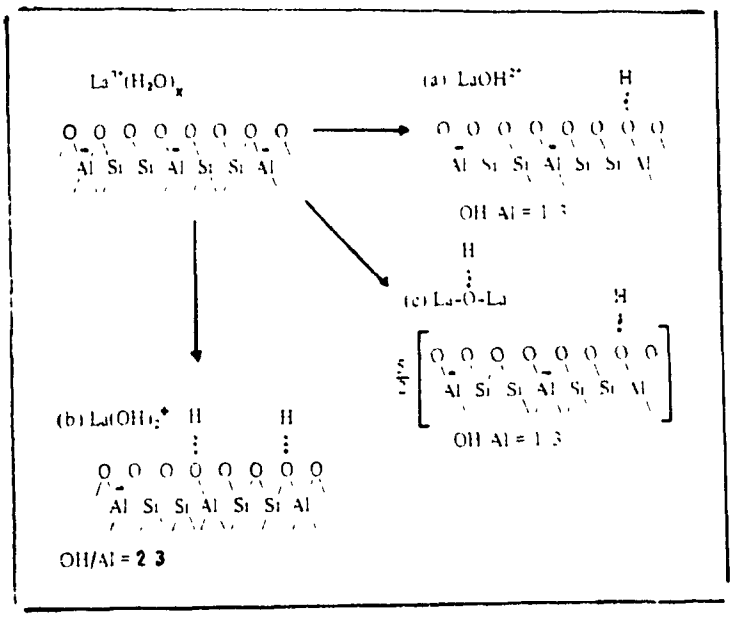

Scheme VI Lanthanum ion hydrolysis and dehydration forms a hydroxyl cation

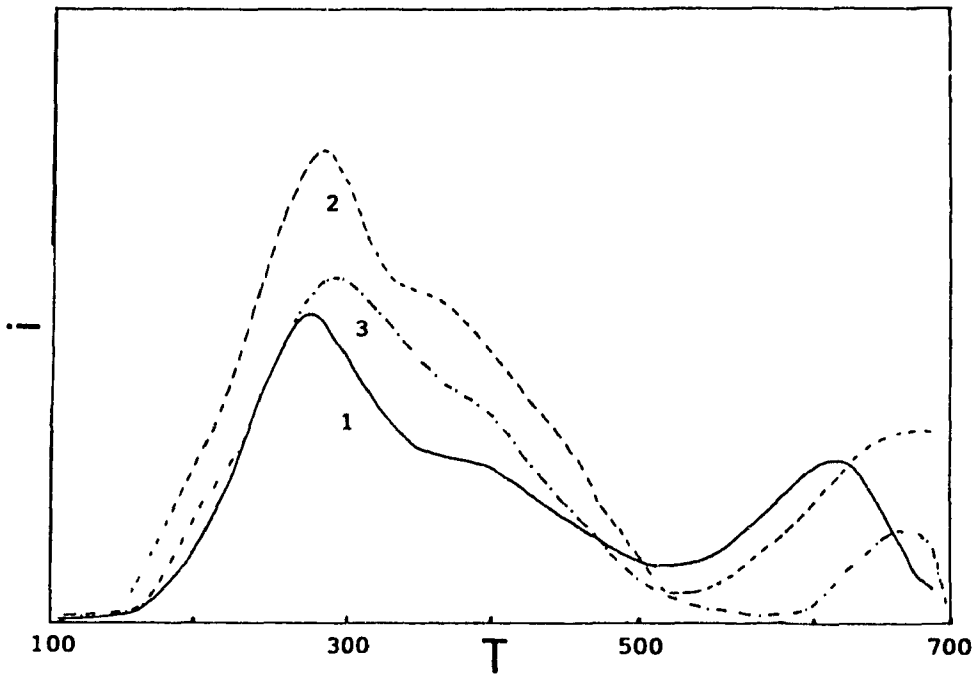

Figure 3.16 NH_3-TPD profiles of 1) HY, 2)LaNaY and 3) LaHY

I = response of the GC-TCD in arbitrary units and T = temperature in °C

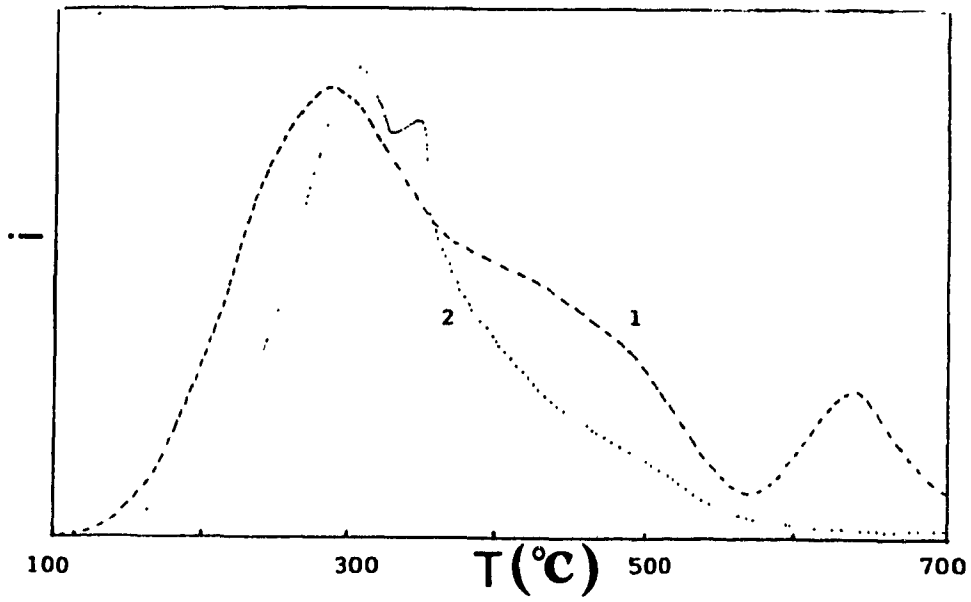

Figure 3.17 NH_3-TPD Profiles of 1)LaNa(m)Y and 2)LaH(m)Y

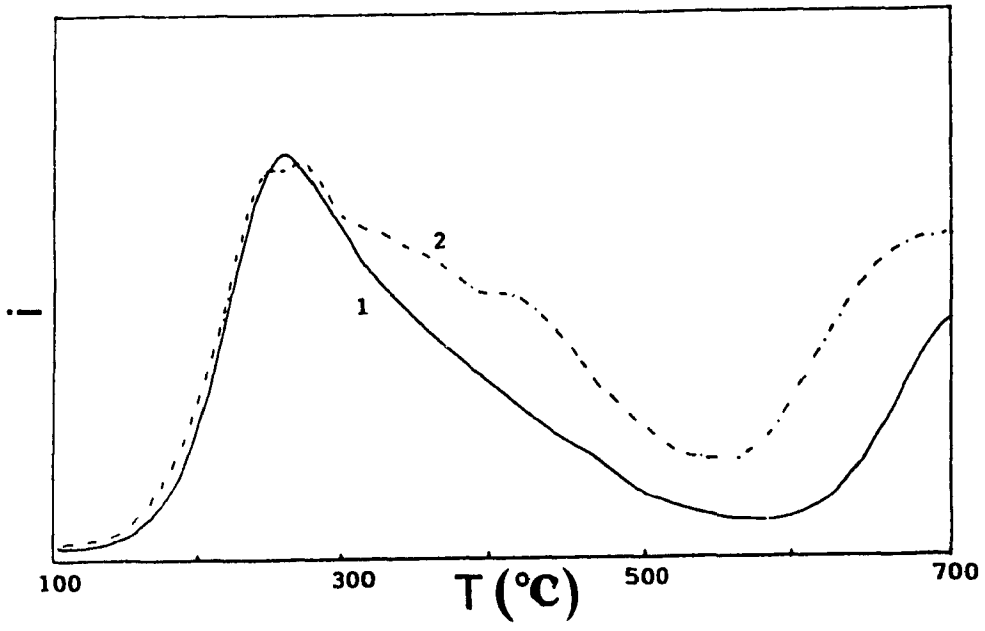

Figure 3.18 NH_3-TPD profiles of 1)LaNaX and 2)LaHX

iv) The incorporation of lanthanum by ion exchange into ammonium forms of zeolites, which were subsequently activated at 623 K to provide the acid forms, significantly enhances the thermal stability of all the samples. The main structural and textural properties of the modified Y sample, whose acid form before La^{3+} ions were loaded collapses upon heating at high temperature, are almost preserved during the activation processes after La^{3+} ions are loaded. Also, the (BET and Langmuir) surface area and micropore volume increase slightly at first and then are preserved with rising outgas temperature for the La^{3+} ion-exchanged NH_4X zeolite, but continuously decrease for the NH_4X zeolite (Table 3.8). The reason may be found in the results of Li et al[104] who reported that La^{3+} ions could stabilize the Si(3Al) and Si(2Al) units of the framework of LaH-faujasite zeolites. As it has been demonstrated previously that the environment of Si atoms of zeolites was significantly enriched in Al upon desilication, our results imply that La^{3+} ions can also exert a stabilizing action on desilicated Y zeolite.

Thus, the incorporation of La^{3+} ions into the Al-enriched faujasite zeolites not only introduces acidity, but also stabilizes the structure of these zeolites, and therefore makes it possible for these Al-enriched zeolites to be used as acidic catalysts.

3.3.4 Catalytic Activity of La-containing Zeolites

Table 3.9 and Table 3.10 report the catalytic performance for the hydrocracking of n-octane obtained with the LaNa forms and with LaH forms of the Y, (m)Y and X zeolites, respectively. The NaY catalyst exhibits almost zero activity due to its lack of acidity. The HY catalyst shows a lower activity than La-containing catalysts although it has a comparable acidity(Table 3.11), which is probably due to some extent to a structural collapse and a partial pore blockage upon heating at high temperature. A very high conversion of n-octane to (mainly) isobutane has been obtained over all La-containing catalysts. Thus, it is remarkable that the acid sites of the LaNa zeolites, presumably of the Bronsted nature, which are generated by the partial hydrolysis of La^{3+} ions[72, 103] are capable of catalyzing the hydrocracking of n-octane without resulting in serious "proton attack" on the framework[105]. This is also the reason why LaX zeolites are claimed to be active in the hydroisomerization/ hydrocracking of C_5-C_{12} normal paraffins[106].

The results of this work have very important implications also for the use of desilicated zeolites as acid catalysts in reactions requiring relatively high temperatures. As shown earlier, although the Na form of the desilicated zeolite was thermally stable, this was not the case of the acid form of such a zeolite. Thus, there are presently two ways to prepare stable acid catalysts with these

Al-enriched zeolites such as desilicated Y and X materials. One is to directly ion-exchange the Na form with La ions. Another is to ion-exchange the Na form with ammonium ions, then to re-ion-exchange with La^{3+} ions before activation at high temperature to decompose the ammonium ions. For the latter method, there should be a balance between La^{3+} ions and ammonium ions for the best performance of the final catalyst towards a given reaction. Therefore, it would be very interesting to determine the minimum extent of La ion-exchange in LaH(m)Y or LaHX to meet the thermal stability requirements of various catalytic reactions.

In summary, the incorporation of La^{3+} ions by ion-exchange into the sodium and ammonium forms(precursors of the acid forms) of the Y, desilicated Y and X zeolites results in thermally stable materials which also exhibit interesting activity and selectivity in the hydrocracking of n-octane for the production of isobutane. For this reaction, the LaNa and LaH based forms of these zeolite catalysts show equally high performance.

Table 3.9 Catalytic results obtained with LaNa-form zeolites

Catalyst	Pt/NaY	Pt/LaNaY	Pt/LaNa(m)Y	Pt/LaNaX
Total Conversion	0.1	93.5	87.7	94.1
C_1+C_2	100	0	0	0
C_3	0	13	13	11
n-Butane	0	12	12	10
iso-Butane	0	53	54	49
n-C_5 + n-C_6	0	1	1	2
iso-C_5 + iso-CC_6	0	13	13	10
mono-branched-C_8	0	3	3	11
multi-branched-C_8	0	5	4	6

Table 3.10 Catalytic results obtained with LaH-form zeolites

Catalyst	Pt/HY	Pt/LaHY	Pt/LaH(m)Y	Pt/LaHX
Total Conversion	30.6	96.3	92.6	90.8
C_1+C_2	0	0	0	0
C_3	13	14	14	13
n-Butane	11	13	13	12
iso-Butane	48	56	56	54
n-C_5 + n-C_6	2	2	2	2
iso-C_5 + iso-CC_6	11	13	13	13
mono-branched-C_8	8	1	1	4
multi-branched-C_8	7	1	1	2

Table 3.11 Acid densities of the zeolites investigated*

Zeolites	BET surface area (m^2g^{-1})	$\mu mol.g^{-1}$	$\mu mol.m^2$
NaY	742	0	0
LaNaY	626	986	1.6
LaHY	637	933	1.5
HY	410	909	2.3
LaNa(m)Y	618	789	1.3
La(m)Y	624	892	1.4
NaX	633	0	0
LaNaX	560	1067	1.9
LaHX	492	878	1.8

*: weight based on dried sample

3.4 Conclusions

The technique of selective removal of silicon from frameworks of various zeolites has been developed by precisely controlling the base-treatment conditions, particularly the initial pH of the base solution. The original structure, surface area and size of the micropores are essentially preserved upon this desilication process even though a slight micropore narrowing is observed. Moreover, all the aluminum atoms remain in the tetrahedral configuration in these Al-enriched zeolites.

As a tetrahedral Al site corresponds to a cationic site, the cation-exchange capacity (CEC) of zeolites has been significantly enhanced upon desilication. This is of particular interest in removing Ca^{2+} and Mg^{2+} ions from hard water.

The ammonium forms of Al-enriched zeolites are not as thermally stable as the sodium forms, but their stability can be improved by incorporating La^{3+} ions. The incorporation of lanthanum ions into these zeolites also introduced acidic properties. Both sodium and ammonium forms of the La-containing zeolites exhibit interesting activities and selectivities in the hydrocracking of n-octane for the production of isobutane.

CHAPTER IV

SULFATE-PROMOTED ZIRCONIA HYBRID CATALYST

4.1 Introduction

Liquid acids and bases have been used as catalysts in diverse chemical reactions and processes for several hundred years. A major disadvantage is that they are difficult to separate from products. Large amounts of catalyst are usually required. Furthermore, liquid acids are corrosive to the reaction vessels, and their liquid waste becomes an environmental concern. In this century, particularly since 1950, many new types of solid acids have been developed and applied as heterogenous catalysts which circumvent many of the problems associated with liquid acids. Of these, solid superacids are those whose acid strengths are stronger than that of 100% sulfuric acid(Hammett acidity function, H_o =-11.9) [107-108]. With such strong acid strengths, they are capable of lowering reaction temperatures and forming reaction intermediates unattainable with conventional acid catalysts. A lower reaction temperature not only represents an energy saving, but also is thermodynamically favorable for the production of the desired products.

One promising type of solid superacid is sulfate-promoted zirconium oxide(zirconia) which was first reported in 1979 by Hino et al.[109]. One method for the preparation of sulfate-promoted zirconia is to immerse zirconium hydroxide in dilute sulfuric acid. Other methods, such as impregnating zirconium hydroxide with a solution of ammonium sulfate or with H_2S or SO_2,

have also been used.

The acid strength of sulfate-promoted zirconia has been determined by visual observation of indicator colours to be $H_o < -16.04$[108], which is 10000 times as strong as that of 100% sulfuric acid. The type of acidity present on sulfate-promoted zirconia has been studied using pyridine adsorption. Although reports were initially conflicting about whether Lewis or Brønsted acidity was generated, the formation of Brønsted acidity is said to be presently favoured [120].

Researchers are not as yet prepared to agree on specific structures for zirconia or for sulfate-promoted zirconia. Many studies have been attempted to determine the structure of the sulfate species on the surface of zirconia in order to understand how sulfate promotion generates superacidity [110-119]. It is generally believed that superacidity is associated with the S=O double bond, with two different classes of structures having been proposed. One is the chelating bidentate structure proposed by Tanabe and co-workers [116-117], which is very similar to inorganic sulfate complexes in the hydrated form and to an organic sulfate in the dehydrated form, as presented in Figures 4.1(a) and (b), respectively. Another class of structure was proposed by Lavalley and co-workers[118-119], which has only a single S=O double bond with the sulfur atom anchored to the oxide surface through three S-O-Zr linkages at low sulfate

coverage as presented in Figure 4.1(c) . At a higher sulfate loading, a polysulfate structure like S_2O_7 (Figure 4.1(d)) is formed. For the hydrated form, a more ionic sulfate structure attached to only two metal atoms (Figure 4.1(e)) was postulated.

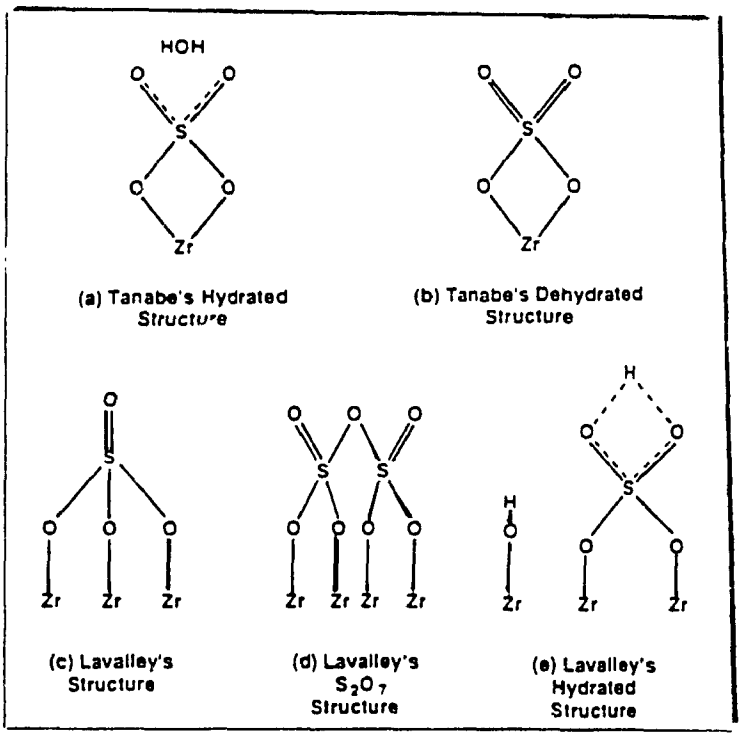

Figure 4.1 Proposed structures for the sulfate ion on sulfate-zirconia

Other than the generation of superacid sites, sulfate promotion has been found to inhibit the sintering and surface area decrease of zirconia upon heat treatment[111-115]. It has been shown to be active for a number of reactions including isomerization[109], cracking, alkylation and esterification[110].

Despite the fact that the relations between preparation and structure and between structure and acidity/activity have been extensively studied, little information about the textural properties, especially the relationship between pore size distribution and catalytic selectivity, is available in the literature. Moreover, no studies have yet been reported on hybridizing this superacid solid with another solid acid such as a zeolite with a regular pore system. This hybridization seems promising since it may combine the activity of the sulfate-promoted zirconia with the shape selectivity of a zeolite.

In this part of the thesis, I report preliminary results obtained with hybrid catalysts which are basically intimate mechanical mixtures of the Y zeolite and sulfate-promoted zirconia. The objective of this study was to show the synergistic effect of these two catalytic components and to decide on the best way to hybridize these two components in order to achieve the maximum catalytic performance.

4.2 Experimental

4.2.1 Sample Preparation

1) Raw materials and samples.

LZY-82(HY) zeolite powder was purchased from U.O.P., and activated in air at 673 K for 12 h. Silica-Alumina(SA) was purchased from Aldrich, and Quartz (Qz) was obtained by crushing the pure quartz glass. Zirconium hydroxide ($Zr(OH)_x$) was prepared by hydrolysis of zirconyl nitrate (Zirconyl Nitrate Hydrate, Aldrich) with aqueous ammonium hydroxide (28 wt.%, Anachemia) at room temperature. The solid was filtered and thoroughly washed with distilled water in order to remove all the nitrate ions, and dried in air at 393 K for 24 hours, to obtain the $Zr(OH)_x$ form. Calcining of $Zr(OH)_x$ in air at 873 K for 2.5 h resulted in the ZrO_2.

2) Sulfated-promoted zirconia (SZr).

SZr was prepared by immersing 9 g of $Zr(OH)_x$ into 100 mL of a 0.5 $mol.dm^{-3}$ solution of sulfuric acid. After 1 h of stirring at ambient temperature, the solid was filtered and dried at 393 K for 24 h, then calcined in air at 873 K for 2.5 h.

3) Pt-loading.

Some of the Pt-containing HY and SZr samples were prepared by the wet impregnation method as described in Chaper II. They are called Pt-HY and Pt-

SZr, respectively. Reference catalysts Pt/HY and Pt/SZr and Pt/SA were prepared by the dry impregnation method as described in Chapter II, but with 10 wt% (otherwise as specified) of bentonite clay. Pt content in all these catalysts was 0.5% by weight.

4) Hybrid catalyst.

4a). One series of the hybrid catalysts which were prepared by a procedure similar to that of the wet impregnation method were used to study the influence of the co-catalyst component. Bentonite clay was added (10 wt.%) to the Pt-HY(Pt-zeolite main component, 50 wt %) as binder, and either quartz(Qz), sulfate-promoted zirconia(SZr), Pt-containing sulfate-promoted zirconia (Pt-SZr), silica-alumina(SA), or pure zeolite(HY) was added as co-catalyst (40 wt %). Water was then added dropwise until a malleable paste was obtained. The hybrid catalyst was obtained by extrusion of this paste. The resulting extrudates were dried at 393 K for 12 h and activated in air at 673 K for another 12 h. The hybrid catalysts thus prepared were: PtHY/Qz, PtHY/SZr, PtHY/SA, PtHY/PtSZr and PtHY/Y. The same procedure was also used to make the hybrid catalyst, PtSZr/Y, in which Pt-SZr(40 wt.%), HY(50 wt.%) and Bentonite (10 wt.%) were used, respectively.

4b). Another series of hybrid catalysts were prepared by a procedure similar to that of the dry impregnation method for studying the effect of the

weight ratio(Rw) between zeolite and sulfate-promoted zirconia. For example, the $Pt/(Y\text{-}SZr)_{64}$ catalyst was obtained by extrusion of the solid mixture of HY zeolite(50 wt %) and sulfate-promoted zirconia(SZr, 40 wt %) with bentonite (10 wt %) using a solution containing tetraammine platinum (II) chloride in lieu of pure distilled water. The weight ratio(Rw) between Y zeolite and sulfate-promoted zirconia was varied as such, the hybrid catalysts $Pt/(Y\text{-}SZr)_{64}$, $Pt/(Y\text{-}SZr)_{63}$, $Pt/(Y\text{-}SZr)_{72}$, and $Pt/(Y\text{-}SZr)_{81}$ have values for Rw of 5/4, 6/3, 7/2, and 8/1 respectively.

For comparison purposes, a series of Pt/Y_n catalysts with values of n from 5 to 9 were prepared according to the above dry impregnation method, but using bentonite clay instead of the SZr material.

4.2.2 Characterization

Sulphur content in sulfate-promoted zirconia was directly determined by a sulphur analyzer to be 5 % by weight.

Atomic absorption, X-ray powder diffraction, nitrogen and argon adsorption/desorption, FT-IR, ammonia adsorption /temperature programmed desorption, TGA/DTA techniques were used to determine, respectively, the chemical composition, the structure and degree of crystallinity, the textural

properties including the surface area and the micropore and mesopore size distribution, the surface acidity (density and strength) and the thermal stability of all materials investigated. These techniques are identical to those described in chapters II and III.

A scanning electron microscope was used to study the particle size and the surface topography of samples. Dry powder samples were mounted on the sticky surface of aluminium stubs and coated with about 10 nm of gold in a sputter coater (Palason E 5100). Specimens were examined and photographed using a Hitachi-520 scanning electron microscopy operating at an accelerating voltage of 15 kV, with 200 μm diameter illuminating at a working distance of 15 mm.

The reaction studied was the hydrocracking of n-octane. The reaction parameters, the method for calculation of the conversion of n-octane and the product selectivity were identical to those in Chapter III. To determine the extent of n-octane hydrocracking, the sum of the yields of the β-scission products (iso-butane, iso-pentane and propane) is defined as:

$Y_{Hy} = \Sigma Y_{\beta_i}$ with $Y_{\beta_i} = 1/100\ (\ S_{\beta i} * C_t\ )$.

4.3 Results and Discussion

4.3.1 Physical Structure of Sulfate-promoted Zirconia

1) Crystalline structure from XRD

Figure 4.2 presents the XRD patterns for zirconia and sulfate-promoted zirconia after calcination at different temperatures. It reveals that both samples exhibit x-ray amorphism when calcined at lower temperatures and become tetragonal when calcined at higher temperatures. The temperatures at which this occurs are different for each sample. The zirconia changes to the tetragonal phase at a calcination temperature of ca. 670 K, while the sulfate-promoted zirconia requires a calcination temperature above 770 K for the formation of tetragonal crystallites. It seems that the presence of the SO_4^{2-} ion retards the tetragonal crystallization. This phase transition for sulfated zirconia according to the calcination temperature agrees well with the results of Mukaida[121] and other authors[113,122]. However, different structures have been reported for the pure zirconia upon calcination. Mukaida and co-workers[121] found that the crystalline structure for zirconia prepared from zirconyl chloride was amorphous when calcined at 473K and simply monoclinic after calcination at 798 K. Parera[113] reported that calcining $ZrO_2 \bullet nH_2O$ at 673 K resulted in a mixture of tetragonal and monoclinic phases of ZrO_2 and that increasing the calcination temperature increased the amount in the monoclinic phase. Both our results and that of Ward[123] show that pure zirconia crystallized into the tetragonal phase upon heat treatment, although

different temperatures were observed for obtainning this crystallization. Thus, it can be seen that the crystalline structure of zirconia is subject to its preparation. However, the sulfated-promoted zirconia changes to the simply tetragonal phase upon heating, no matter how it is prepared.

2) Sulfur state from FTIR

Not only does the zirconia crystalline structure of sulfate-promoted zirconia change upon heating, but also the sulfate species is found to undergo changes with increasing temperatures. Figure 4.3 shows the sulfate region of the FTIR spectra of different samples after heating treatment.

Interestingly, an opposite change with increasing temperature is observed when the sulfate-promoted zirconia is compared to zirconium sulfate hydrate. Specifically, for zirconium sulfate hydrate, the peaks become more distinguishable with an increase of temperature; while for sulfate-promoted zirconia, four poorly separated peaks are observed in the region of 900-1400 cm^{-1} when heated to ca. 393 K, but they overlap with each other when heated to over 620 K. Additionally, a slight shift of the peak maxima to higher wavenumbers with increasing temperatures is observed for the sulfate-promoted zirconia, but not for zirconium sulfate hydrate. All these results imply that the configuration of the sulfate on zirconia is similar to that of an organic sulfate proposed by Tanabe et al[116,117].

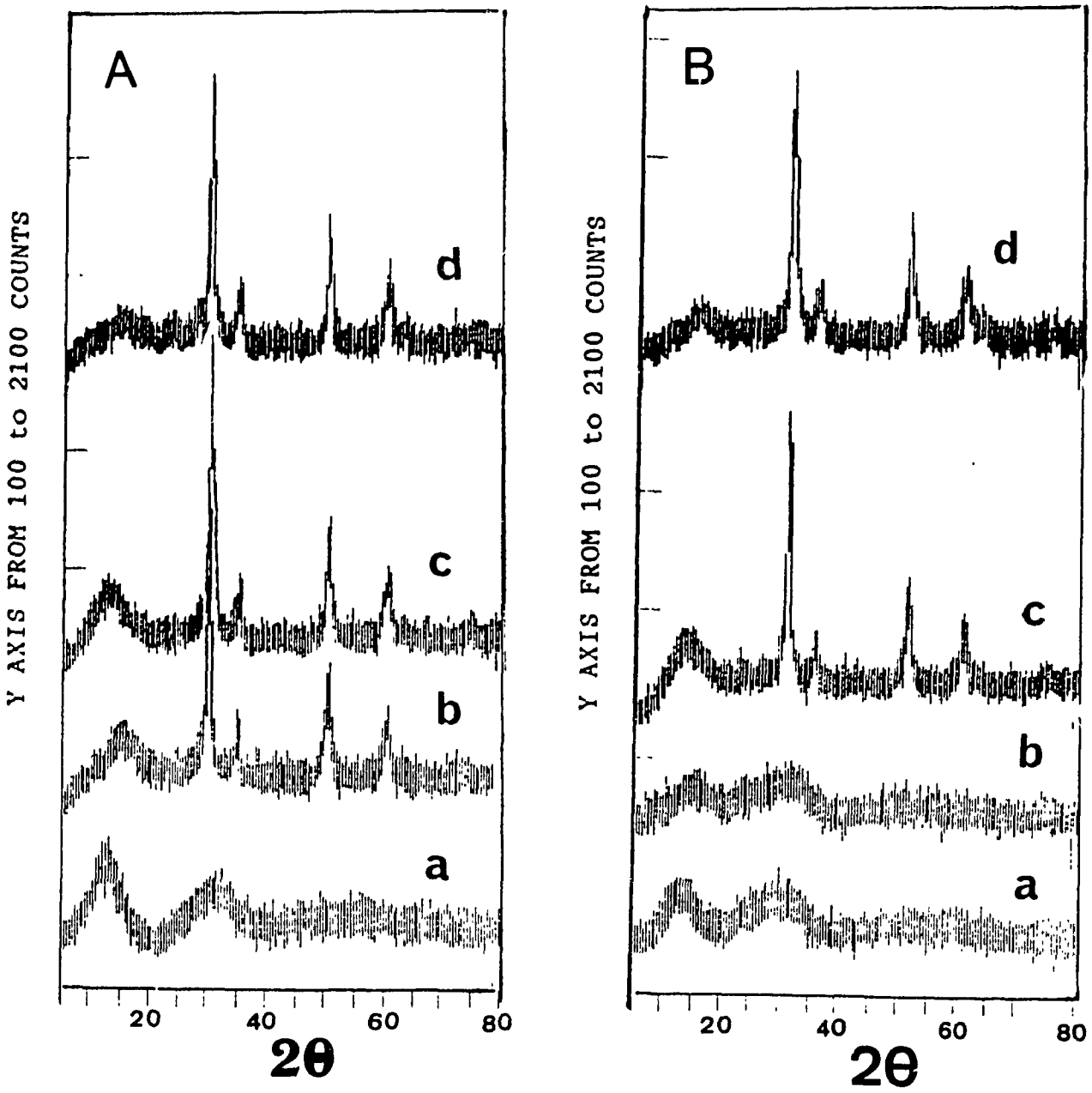

Figure 4.2 XRD patterns of zirconia(A) and sulfate-promoted zirconia(B) at different calacination temperatures(°C). a = 350, b = 450, c = 550, d = 650.

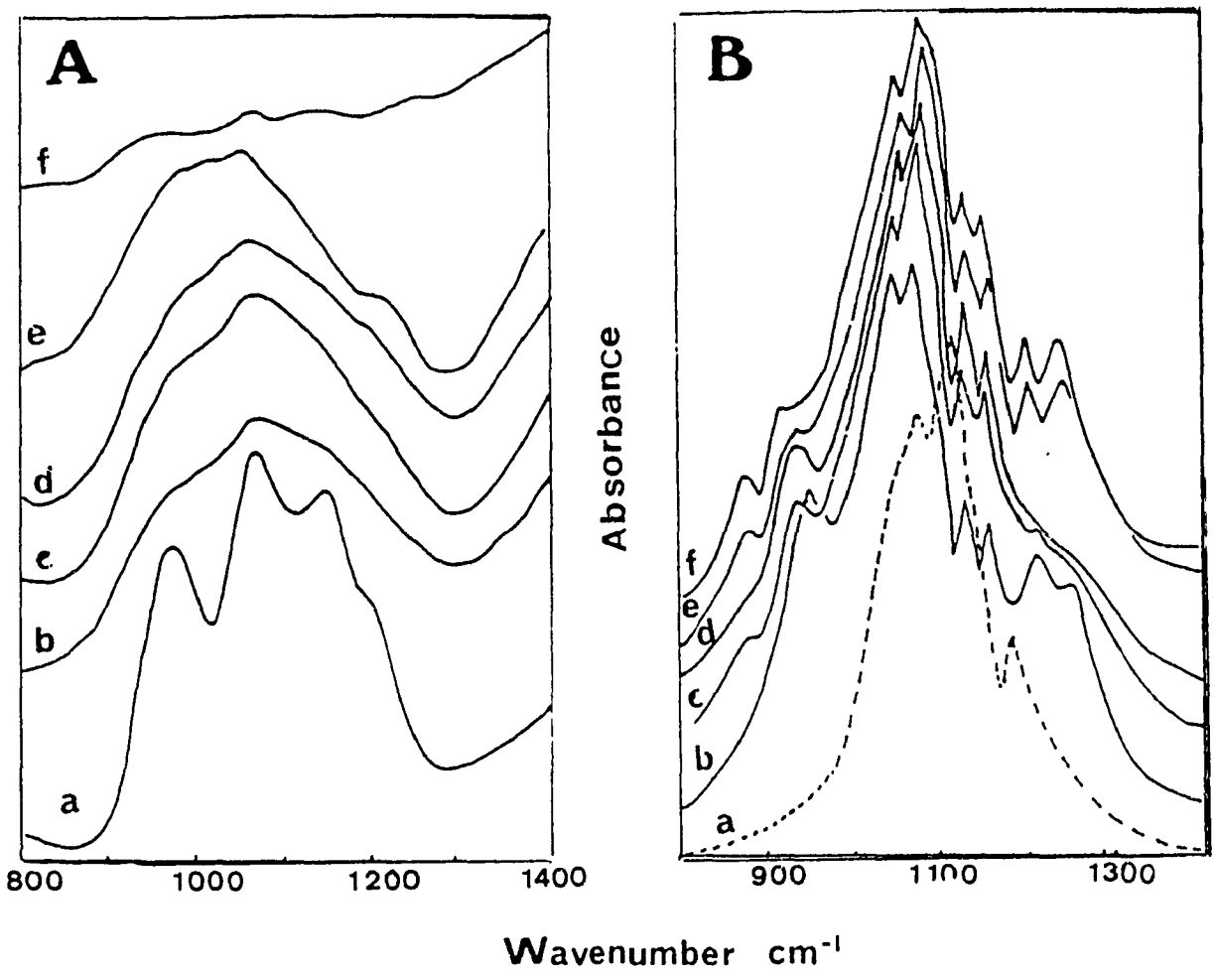

Figure 4.3 FTIR spectra for sulfate-promoted zirconia(A) and zirconium sulfate(B) after calcination at different temperatures: a: 120 °C; b: 350 °C; c: 450 °C; d: 550 °C; e: 600 °C; f: 650 °C.

3) Stability of sulfur from FTIR and TGA/DTA observations

From the FTIR spectra, it can also be seen that sulfate-promoted zirconia rapidly loses its sulfate groups when heated to temperatures higher than 920 K. Figure 4.4 is a plot of the difference in absorbance (1173 cm^{-1}) versus

calcination temperature between the sulfate-promoted zirconia and the pure zirconia. It is seen that the loss of the sulfate groups begins at about 873K, and remarkably increases when the temperature approaches 900 K. The results of FTIR and XRD imply that there is a temperature window from 770 K to 870 K for sulfate-promoted zirconia where it exists in a tetragonal crystallite phase and keeps its sulfate groups. It was such a temperature window which was preferred by many authors when activating this material as reported in most of the published papers[123].

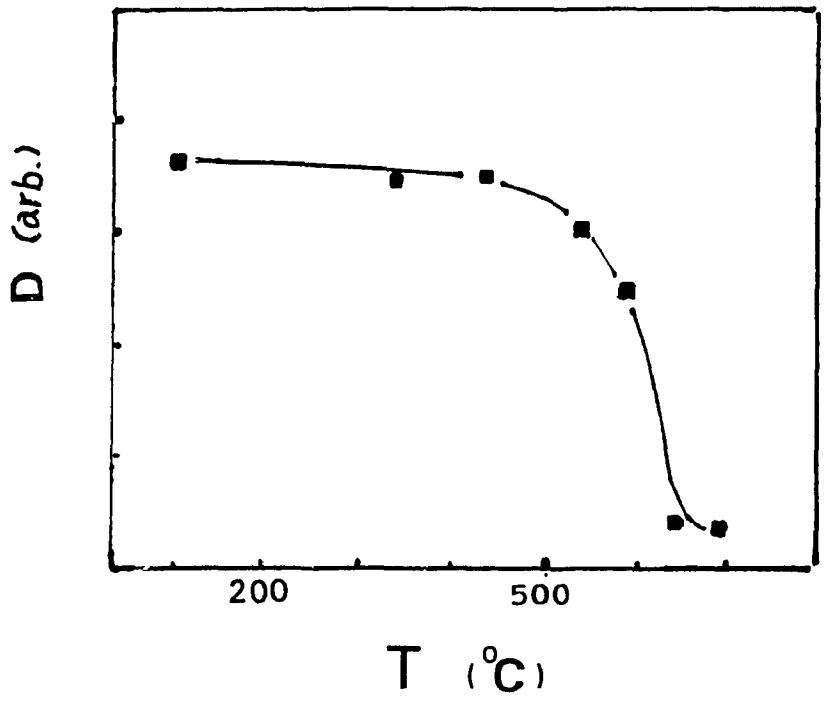

Figure 4.4 Differences in FTIR absorbance between sulfated-promoted zirconia and zirconia versus the calcination temperatures

TGA/DTA studies (Figure 4.5 and Figure 4.6) further confirm the presence of this temperature window for the phase change of zirconia and its loss of sulfate groups. In Figure 4.5, it is seen that zirconium hydroxide undergoes water loss twice at 380 K and 445 K and then undergoes a phase change at 740 K. The water losses are endothermal according to the DTA curve and are associated with weight losses as expressed in the TGA curve. The phase change, however, is exothermal and is without any observable weight loss in the TGA curve. This agrees well with our results obtained from XRD spectra. In Figure 4.6, it is seen that the loss of sulfate groups occurs at ca 970 K which is consistent with that observed from FTIR spectra. Associated with the weight loss expressed in the TGA curve, is an exothermal peak. Additionally, since the $Pt/HS/ZrO_2$ sample exhibits a similar percent weight loss in the same temperature region as HS/ZrO_2, this indicates that the platinum loading does not change the content nor the state of sulfate on zirconia. Comparing the percent weight loss as seen with the TGA curve with the sulfur content as analyzed by a sulfur analyzer shows that the sulfate groups on both HS/ZrO_2 and $Pt/HS/ZrO_2$ are lost in the form SO_3, which implies that the sulfur species existing before their loss were in the form SO_4^{2-}. Such a sulfur loss is expressed in the following equation:

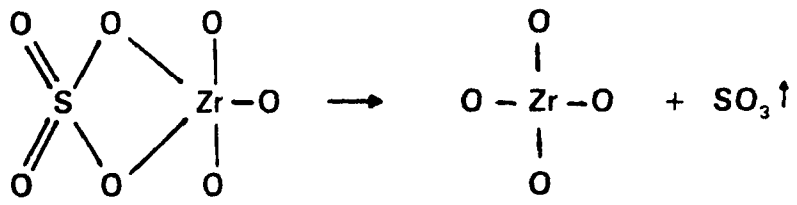

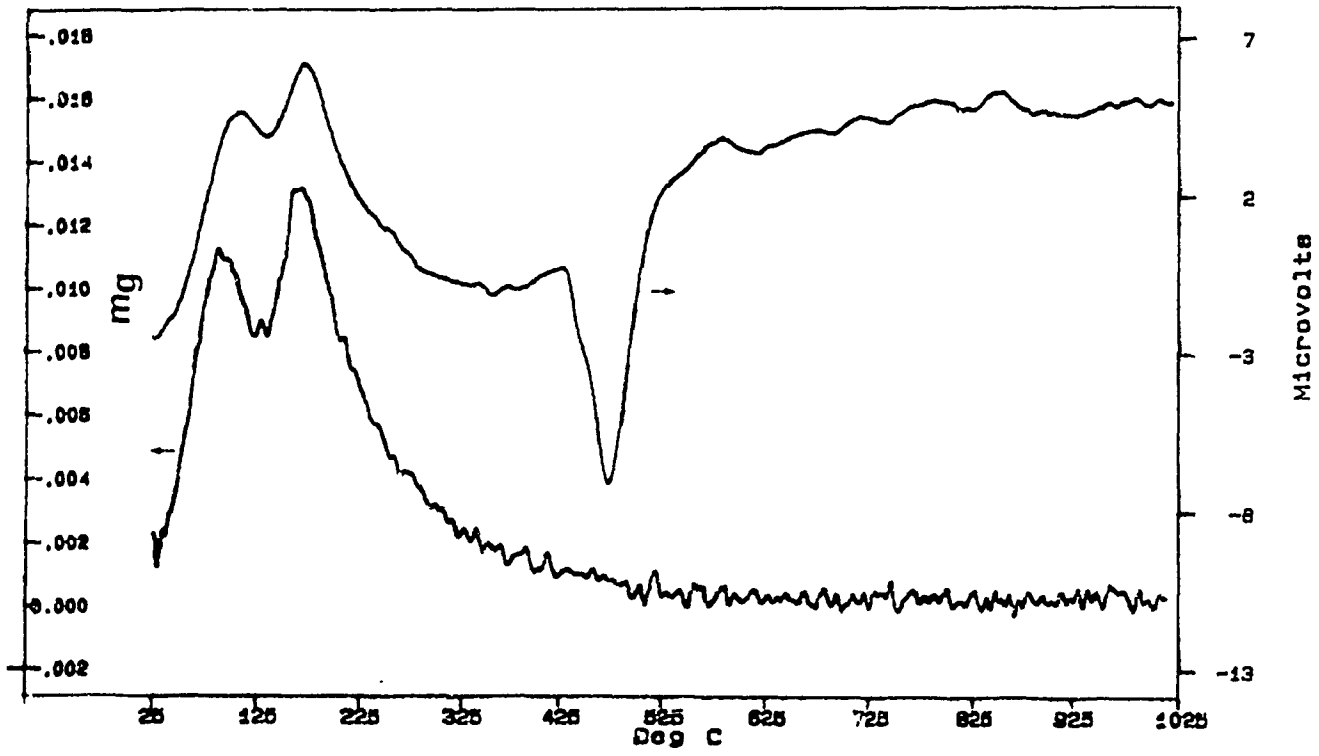

Figure 4.5 DTA and the first derivate of TGA curves of $Zr(OH)_x$

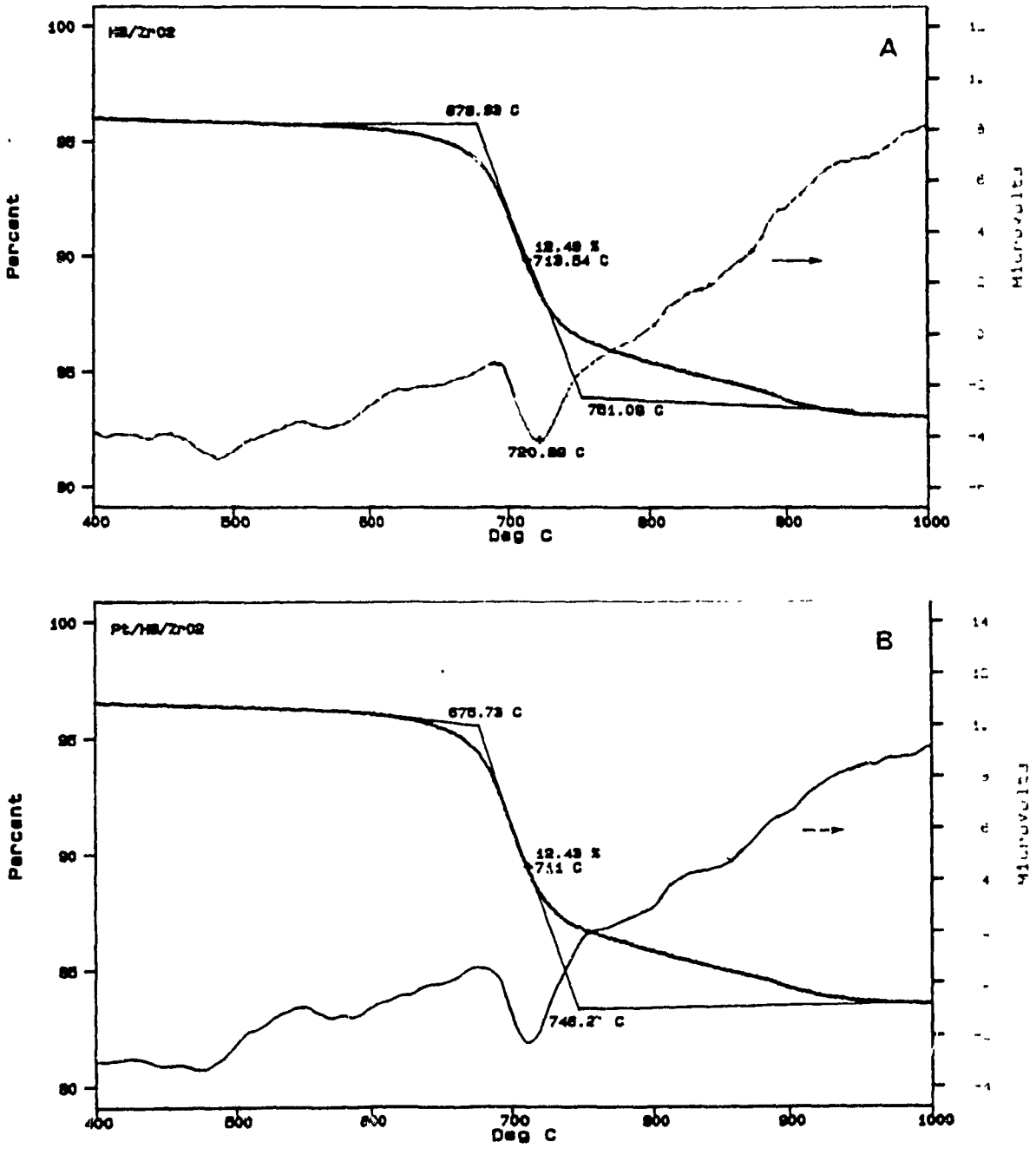

Figure 4.6 DTA/TGA curves of SZr(A) and Pt/SZr(B)

4.3.2 Textural Properties

Table 4.1 lists texture properties for these samples. Figures 4.7 and 4.8 present pore size distributions. SEM photographs Figures 4.9 and 4.10 are of a typical sample. It can be seen that the specific surface area is remarkably enhanced after zirconia is promoted by sulfate. This enhancement is also experienced by the pore volumes.

Table 4.1 Textural properties of the varoius catalyst components studied

Sample	BET(m^2g^{-1})		Volume (mm^3g^{-1})		BJH Pore	Particle
	Total	MP[a]	Total	MP	size(nm)	size(μm)
Qz	1.9	0.2	3	0.0	18.5	150
ZrO_2	66	2.9	113	1.0	5.6	200
SZr	116	9.2	154	3.0	4.8	60
SA	641	47	837	14.0	4.6	80
Y	610	505	393	234	5.9	250

(a): MP = micropores

(b) Particle size was obtained from SEM observations.

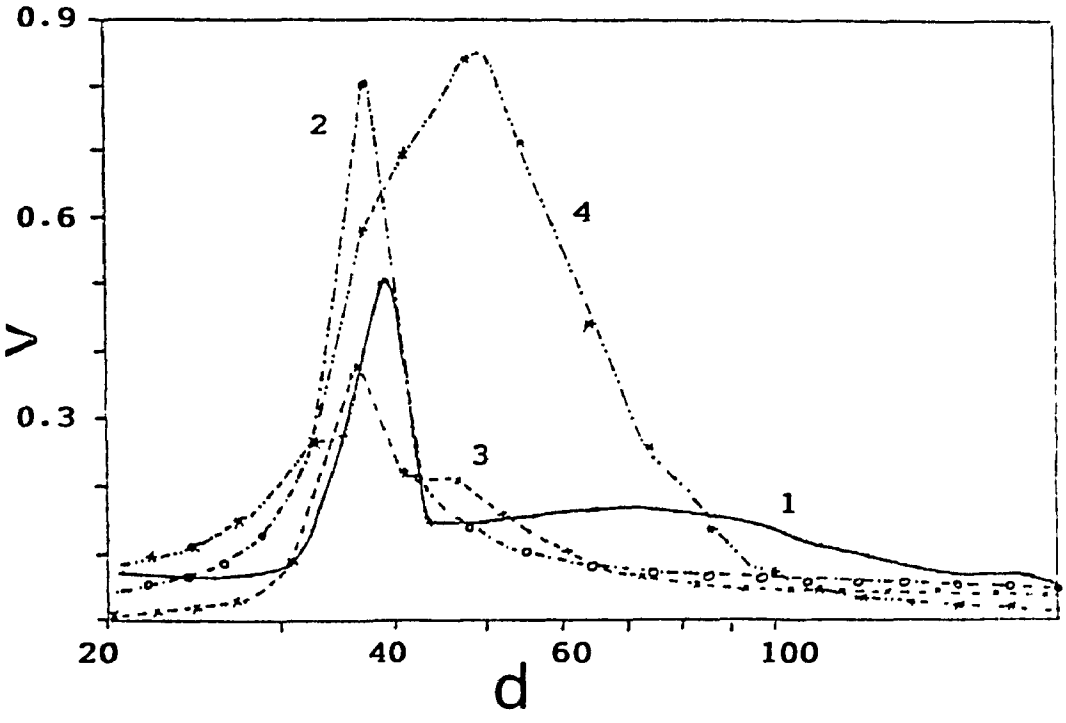

Figure 4.7 Mesopore size distribution of: (1) HY zeolite; (2) sulfate-promoted zirconia; (3) zirconium hydroxide and (4) silica-alumina(V/3). V = volume of argon adsorbed in cm^3g^{-1}; d = mesopore size in 10^{-10} m.

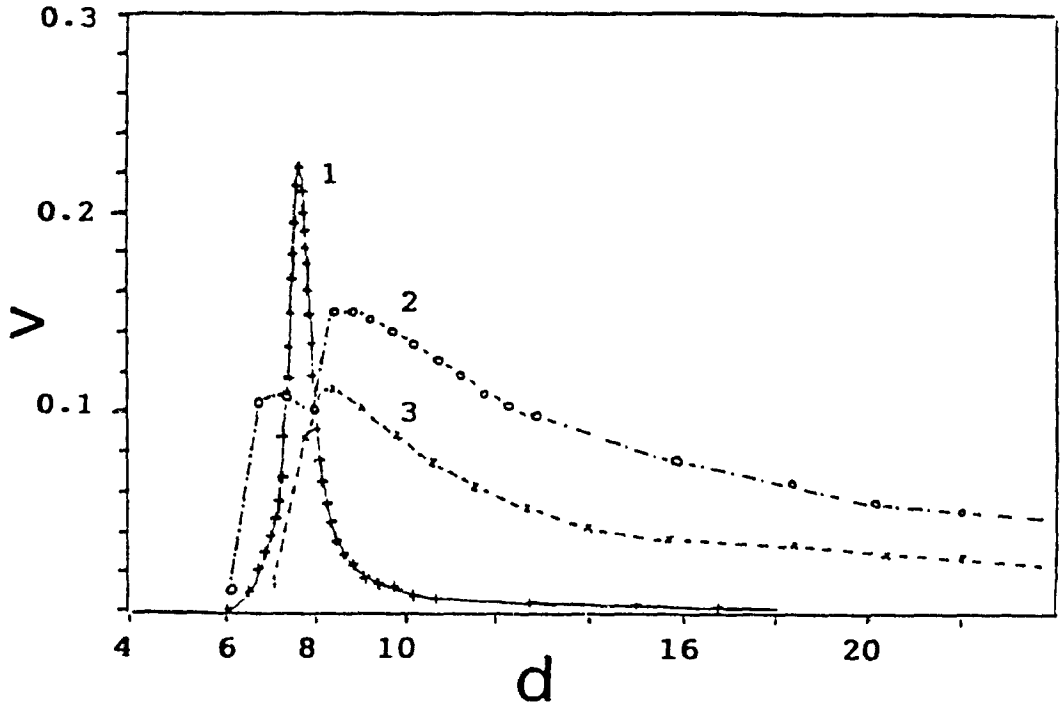

Figure 4.8 Micropore size distribution of: (1) Y zeolite; (2) sulfate-promoted zirconia(V*50) and (3) zirconium hydroxide (V*50). V = volume of argon adsorbed in cm^3g^{-1}; d = micropore size in 10^{-10} m.

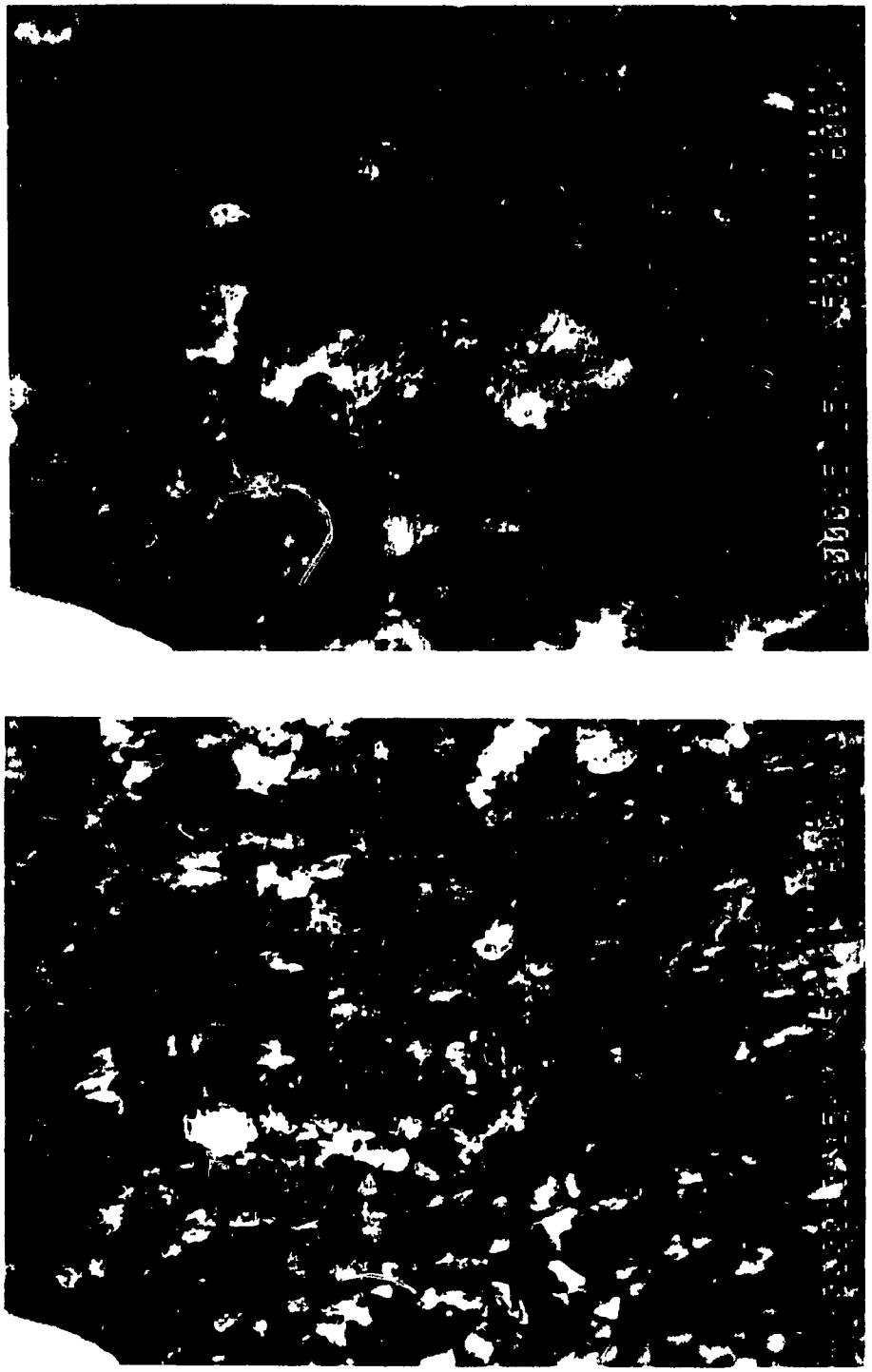

Figure 4.9 Scanning electron micrographs showing distribution of particles, ZrO_2(the top one) and SZr(the bottom one) in a sample (* 50).

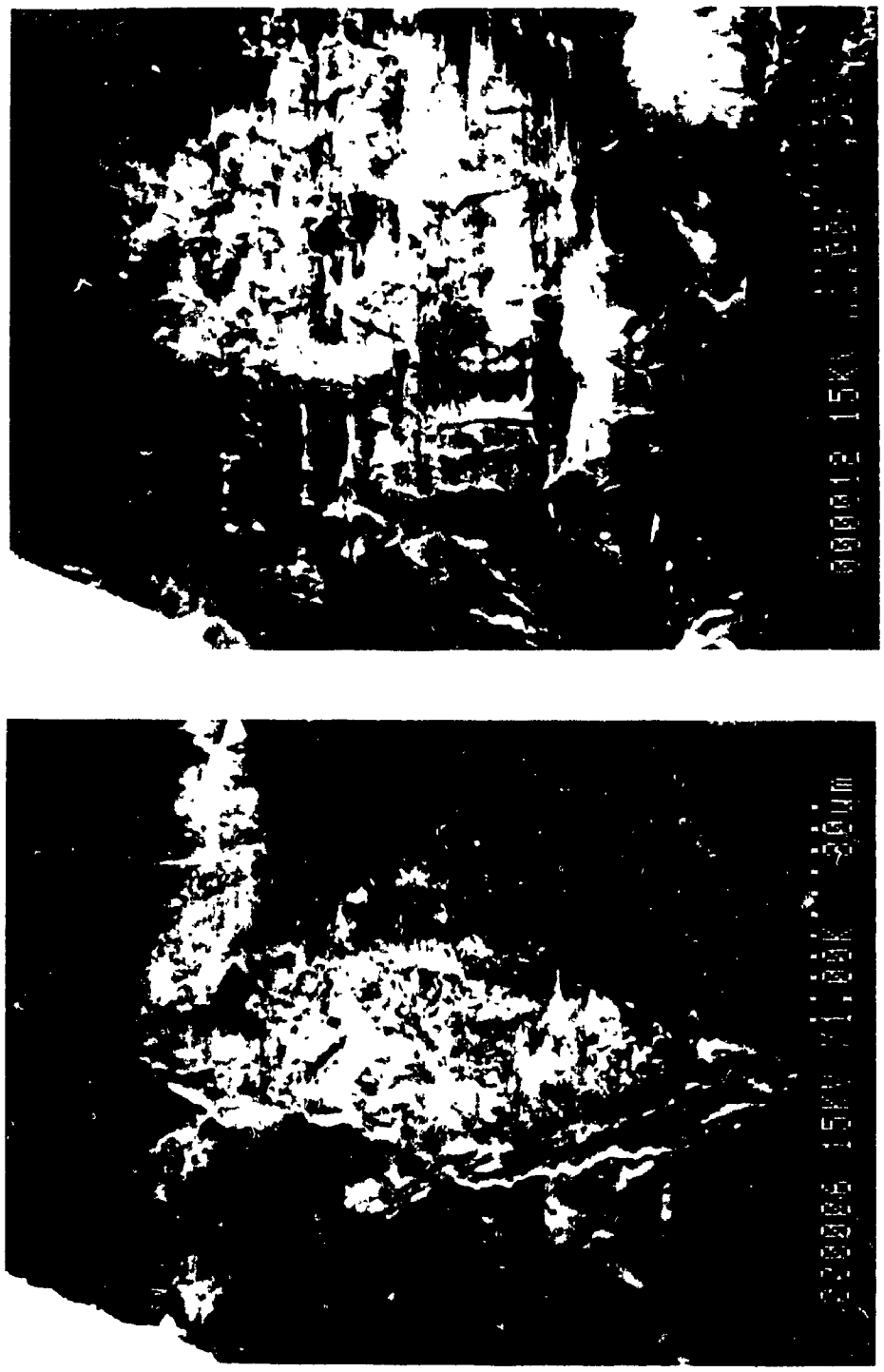

Figure 4.10 Scanning electron micrographs showing topography of ZrO_2 (the top one) and SZr(the bottom one) particles in a sample (* 1000)

This increase in specific surface area upon sulfate-promotion probably has two causes: 1) formation of surface sulfate species which results in mainly new mesoporosity (Figures 4.7 and 4.8) and retards the aggregation of the zirconia phase[124] during heating (Figure 4.9), and 2) leaching action of sulfuric acid which occurs when zirconium hydroxide is immersed into the aqueous sulfuric acid solution. The latter action can be seen from the pore volume increase (Figure 4.7, Figure 4.8, and Table 4.1) and the surface topographies (Figure 4.10).

4.3.3 Acidity

Figure 4.11 presents NH_3-TPD profiles of the samples. The profile for amorphous silica-alumina shows two desorption peaks at temperatures of 500 K and 600 K, corresponding to the weak and medium strong acidic sites, respectively. Besides these two overlapping peaks, another at 750 K, is observed for zeolite HY, which corresponds to the strong acidic sites. Of particular interest is a well separated ammonia desorption peak starting at 810 K, only observed with sulfate-promoted zirconia. The SZr sample, when heated similarly from 373 K to over 973 K, eliminates any doubts in the assignment of the decomposition peak for the sulfate species. Corma et al [124] have also observed this high temperature TPD peak and assigned it to ammonia desorbing from the superacid sites of the sulfate-promoted zirconia.

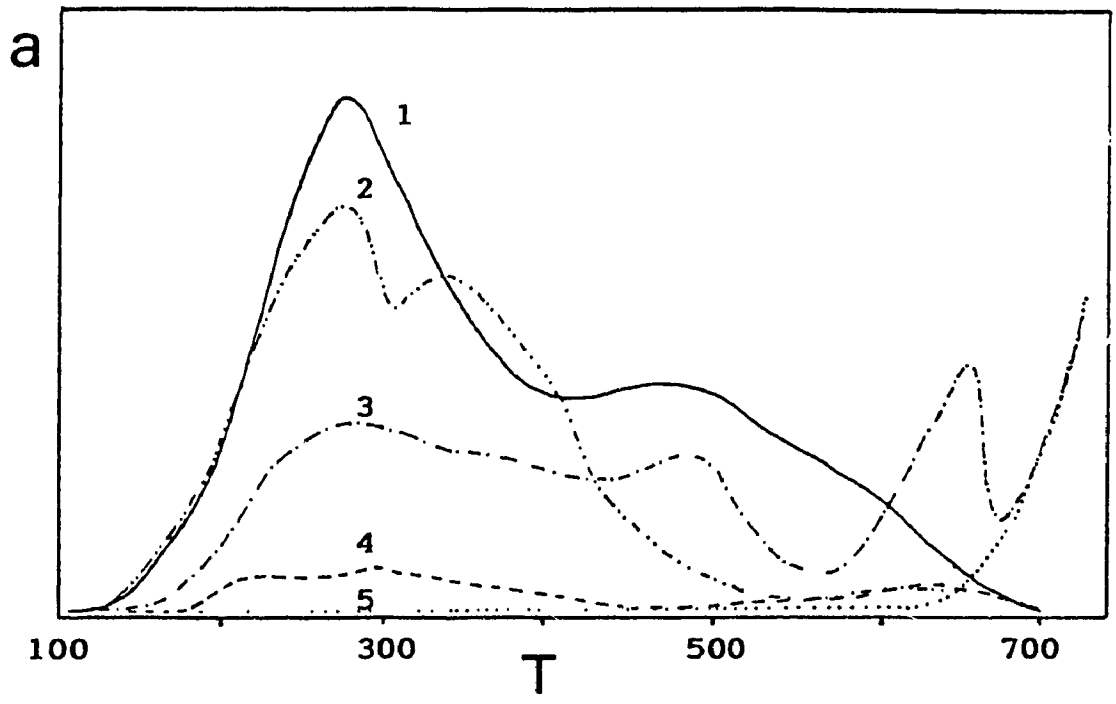

Figure 4.11 NH_3-TPD curves for (1):Y; (2):SA(*2); (3): SZr(*2); (4): ZrO_2(*2) and (5): SZr(*2, blank test without prior adsorption of ammonia at 373 K)

a = response of the TCD (arbitrary units); T = temperature in °C

Table 4.2 lists the total acidities obtained from the NH_3-TPD tests. In terms of total acid density per unit weight, the HY zeolite, when compared with the sulfate-promoted zirconia, exhibits a higher acid density. However, if the acid density per surface area unit is considered, the sulfate-promoted zirconia exhibits a significantly higher value. Moreover, if the entire diagram for ammonia desorption (Fighure 4.11) is considered, the percentage of ammonia desorbed at higher temperatures in the case of the sulfate-promoted zirconia is much higher than that of the HY zeolite, in particular, the peak due to the superacidic sites of the sulfate-promoted zirconia at ca. 800 K, which is different from the peak for decomposition of sulfate species at ca. 900 K. In conclusion, sulfate-promoted zirconia, when compared with the HY zeolite and other materials used in this work, exhibits the highest acid density per surface unit area and the highest acid strength.

Table 4.2 Acidity measurements by NH_3-TPD

Sample	BET surface area (m^2g^{-1})	Density of acidity	
		μmol g^{-1}	μmol m^2
Qz	2	0	0
ZrO_2	66	63	1.0
SZr	116	208	1.8
Y	610	848	1.4
SA	641	322	0.5

4.3.4 Catalytic Activity

1) Effect of hydrogen on sulfate-promoted zirconia.

Table 4.3 lists conversions for n-octane and product selectivities over Pt-ZrO_2 and Pt-SZr catalysts under different reaction atmospheres. It is demonstrated that, in either N_2 or mixed H_2/N_2 atmospheres, there is essentially no conversion of n-octane over Pt/ZrO_2. Only a very low conversion of n-octane (< 3%) is observed over Pt/SZr under a N_2 atmosphere, with no branched cracking products. This indicates that no β-scission occured under these conditions. As β-scission is catalyzed by Brønsted acid sites as shown elsewhere of this thesis(Chapter 2, 3 and 5), the acidity on the surface of sulfate-promoted zirconia must be Lewis in nature under an inert atmosphere. When the reaction atmosphere is switched to a mixture of hydrogen and nitrogen, a much higher conversion (48%), with a product distribution similar to that of HY, is obtained with the sulfate-promoted zirconia catalyst. This indicates that β-scission does occur, and that there are indeed protonic acid sites under these conditions. This generation and elimination of the protonic acid sites in relation to the presence or absence of molecular gaseous hydrogen agrees well with the observations of Ebitani et al[125]. They found that by heating Pt/SO_4^{2}-ZrO_2 in the presence of molecular hydrogen, the protonic acid sites were generated and the Lewis acid sites were weakened; by removal of molecular hydrogen, the surface acidic properties returned to their original

states. They also indicated that the generation of the Brønsted acid sites involved dissociative adsorption of the hydrogen molecule on Pt, spillover of the H atom onto the sulfate-promoted zirconia surface, and electron transfer from the H atom to Lewis acid sites leaving H^+ on the surface. It is also worth mentioning that the Pt species on the surface of sulfate-promoted zirconia may be much easier to reduce than those on the surface of zeolites. The auto-reduction of these Pt species on the surface of SO_4^{2-}-ZrO_2 in air upon heating has even been shown by using XPS, XRD and TPR[126,127]. In this respect, it appears un-necessary for the Pt-containing sulfate-promoted zirconia to be reduced in situ with hydrogen before its use as a catalyst since these Pt species may have already turned to metallic particles during the activation step.

2) Effect of reaction temperature on catalytic activity of Pt/SZr

Table 4.4 reports the variation of the conversion and product selectivity for hydrocracking of n-octane over the sulfate-promoted zirconia catalyst with reaction temperature. The conversion increases rapidly until the reaction temperature approaches 220 °C, and much more slowly thereafter. This behavior is different from that of the Pt/HY catalyst for which a linear increase of conversion with temperature over the whole temperature range investigated had been found. Such a variation of conversion with temperature for Pt/SZr may be due to the loss of sulfate species in the reducing atmosphere (hydrogen) at relatively high temperatures as discussed in Tanabe 's report[128].

Table 4.3 Conversion of n-octane over Pt-ZrO2 and Pt-SZr under different reaction atmospheres*

Catalyst	$Pt\text{-}ZrO_2$		Pt-SZr	
Carrier gas(H_2/N_2)	0 / 28	12 / 16	0 /28	12 /16
Conversion	0.0	0.0	2.8	47.8
Methane	0.0	0.0	0.3	0.0
Ethane	0.0	0.0	0.0	0.0
Propane	0.0	0.0	1.2	11.4
n-Butane	0.0	0.0	7.3	11.5
iso-Butane	0.0	0.0	31.9	58.9
Butenes	0.0	0.0	1.0	0.0
n-Pentane	0.0	0.0	0.0	3.7
iso-Pentane	0.0	0.0	3.8	8.0
mono-branched-C_8	0.0	0.0	54.7	3.5
multi-branched-C_8	0.0	0.0	0.0	3.0

* (a): Catalysts were prepared by the wet impregnation method.
(b): Without reduction before reaction.
(c): Reaction temperature = 493 K; WHSV = 0.1 h^{-1}.
(d): Data in the table were the average for time on stream of 4 h.

Table 4.4 Hydrocracking of n-Octane over Pt-SZr at different temperatures*

Reaction (°C) Temperature	160	190	220	230	250	270	290
CONVERSION	2.3	26.6	47.8	47.2	53.8	59.5	59.6
Carbon-1	0.0	0.0	0.0	0.0	0.0	0.0	0.1
Ethane	0.0	0.0	0.0	0.0	0.0	0.1	0.1
Propane	3.7	9.3	11.4	12.9	14.1	15.2	15.3
Carbon-4	29.0	62.5	70.4	72.4	70.6	69.1	68.2
n-C_4	2.7	8.0	11.5	16.3	20.8	24.8	28.0
iso-C_4	26.3	54.5	58.9	56.1	49.8	44.2	39.9
un-C_4	0.0	0.0	0.0	0.0	0.0	0.0	0.3
Carbon-5	2.1	9.3	11.7	13.4	14.2	14.9	15.5
n-C_5	0.0	1.7	3.7	5.6	6.3	6.8	7.2
iso-C_5	2.1	7.6	8.0	7.8	7.9	8.1	8.2
mult-B-C_8	0.0	9.2	3.0	0.0	0.0	0.0	0.0
mono-B-C_8	65.3	9.7	3.5	1.4	1.1	0.8	1.0

(*): N_2/H_2 = 16/12 (ml/min), WHSV = 0.1 h^{-1}, other parameters as Table 4.3.

3) Hybrid effect

Table 4.5 reports the catalytic results obtained with "one-component, 90% " catalysts. Although the sulfate-promoted zirconia (SZr) is much more acidic but with much less surface area than the Y zeolite as discussed above (Table 4.2), the Pt/SZr sample exhibits a lower conversion. On the other hand, although the silica-alumina(SA) has a larger surface area but a lower surface acidity than the Y zeolite (Table 4.2), the Pt/SA is much less productive than the Pt/Y sample. This means that both surface acidity and surface area are critical factors for n-octane cracking. The presence of less cracking products (β-scission products of n-octane: propane, iso-butane and iso-pentane), as shown by much lower values of S_{Hy}, and of more mono-branched and multi-branched C_8 hydrocarbons (isomerisation products) in the product spectra of the Pt/SZr and Pt/SA (when compared to the Pt/Y, Table 4.5), may be ascribed at first glance to the lower conversions obtained with these two samples. However, when comparing selectivity data (Pt/SZr in Table 4.5) with reactions exhibiting comparable conversion (C_t) levels obtained with the Y zeolite containing hybrid catalysts (HY/PtSZr in Table 4.6), the latter tends to promote more complete hydrocracking (higher values of S_{Hy}) than non-zeolitic catalysts. This further demonstrates that the product distribution depends not only on the conversions as expected from classical mechanisms[6], but also on the structure of the catalyst used. By complete hydrocracking, it is meant that the β-scission step[8] leading to the products isobutane, isopentane and propane

is much more effective with the Y zeolite containing catalysts.

Table 4.6 shows that when the sulfate-promoted zirconia is used in lieu of the low-surface-area and non-acidic-surface quartz in the (PtHY/Qz) hybrid catalyst, the conversion of the resulting hybrid catalyst (PtHY/SZr) is dramatically enhanced. Moreover, the fact that the PtHY/Qz hybrid catalyst exhibits a performance almost identical to that of the catalyst obtained by extruding PtHY directly with bentonite (50 % by weight) indicates that there is no contribution from quartz towards this reaction. In addition, the PtHY/Y sample obtained by incorporating PtHY component with HY zeolite which has a higher surface area and a more acidic surface than quartz, demonstrates improved catalytic properties but not to the same extent as with sulfated-promoted zirconia (Table 4.6). On the other hand, when Pt is absent in the zeolite component and present in the sulfate-promoted zirconia co-catalyst (case of the hybrid catalyst Y/PtSZr), the improvement is much smaller. Since previous results in Chapter II showed that Pt is required for stabilizing the on-stream conversion of n-octane hydrocracking over zeolite catalysts, the results here indicate that the SZr component (or another cocatalyst such as SA) is not the main reaction locus for the overall n-octane hydrocracking over the hybrid catalysts. Further evidence is given by the reference Pt/SZr and Pt/SA catalysts themselves which exhibit lower β-scission properties than the Pt/Y sample (S_{Hy}, Table 4.5).

Table 4.5 n-octane hydrocracking over the reference catalysts

Catalyst	Pt/HY	Pt/SZr	Pt/SA
Conversion(C_t)	97.1	54.4	22.2
Product selectivities(S_i)			
$C_1 + C_2$	0.0	0.0	0.0
C_3	15.5	10.9	1.3
n-C_4	12.8	10.7	0.9
iso-C_4	52.4	49.4	1.9
n-C_5	2.6	2.8	0.0
iso-C_5	13.3	8.7	1.1
n-C_6	0.0	0.0	0.0
iso-C_6	0.1	0.0	0.0
mono-br-C_8	3.4	14.2	91.0
multi-br-C_8	0.0	3.4	3.8
S_{HY}	81.2	69.0	4.3
Y_{HY}	78.8	37.5	1.0

Table 4.6 n-octane hydrocracking over the hybrid catalysts

Catalyst	PtHY/ Qz	PtHY /HY	PtHY /SZr	HY/ PtSZr	PtHY/ PtSZr	PtHY /SA
Conversion (C_t)	40.8	65.7	77.6	54.6	80.4	80.9
Product selectivities (S_i)						
$C_1 + C_2$	0.2	0.1	0.1	0.0	0.0	0.0
C_3	15.1	14.8	15.1	15.4	16.0	14.2
n-C_4	11.9	10.9	12.2	12.3	13.3	12.0
iso-$_4$	55.4	58.0	56.0	56.2	53.6	49.1
n-C_5	1.4	1.3	2.8	2.5	4.0	3.4
iso-C_5	13.6	12.9	12.3	11.9	12.1	11.6
n-C_6	0.1	0.2	0.3	0.3	0.3	0.1
iso-C_6	1.1	1.5	0.9	1.2	0.7	0.2
mono-br-C_8	0.8	0.3	0.2	0.0	0.1	6.2
multi-br-C_8	0.3	0.1	0.1	0.1	0.1	2.8
S_{HY}	84.1	85.7	83.4	83.5	81.7	74.9
Y_{HY}	34.3	56.3	64.7	45.6	65.7	60.6

In conclusion, the activity and the on-stream stability of the hybrid catalysts in the selective hydrocracking of n-octane are determined by the following factors:

i) the zeolite pore system is the main location for the entire reaction;

ii) there is a synergy between the zeolite and the co-catalyst (sulfate-promoted zirconia or SA);

iii) the Pt species which is known to have a "cleaning" role for the reaction, is more effective if it is also present on the sulfate-promoted zirconia surface (case of the Pt-Y/Pt-SZr sample, Table 4.6).

Thus, I conclude that the ideal situation may be found in a hybrid catalyst where the Pt species are associated with all of the catalyst's components, including the binder (bentonite). The technique of "dry impregnation" ensures a homogeneous distribution of Pt species within the hybrid catalyst. The resulting catalyst, the $Pt/(Y\text{-}SZr)_{54}$ (Table4.7), indeed shows a higher catalytic performance than the PtY/PtSZr (Table 4.6).

A further insight derived from this work was achieved when studying the influence of the R_w ratio as defined previously. When R_w increases from 5/4 to 8/1, the total conversion of n-octane increases from 88.4 % to 99.4 % (Table 4.7). Results for the corresponding Pt/HY_n containing identical amounts of HY zeolite but without any sulfate-promoted zirconia (Table 4.8), show that there

must be some synergistic effect between the two components to provide such enhanced catalytic performances for the hybrid catalysts. In fact, the mechanical admixing of the SZr particles to those of the Y zeolite significantly increases the production of hydrocracked hydrocarbons (isobutane, isopentane and propane) at the expense of the isomers of n-octane (Tables 4.7 and 4.8). The selectivity towards the latter products would normally increase if there were no transfer from the SZr surface to that of the Y zeolite, as expected from the results of Table 4.5. Moreover, the Pt/(Y-SZr) hybrid catalyst with a R_w ratio of 8/1 appears to be extremely productive (Table 4.7), even when compared to the reference HY zeolite catalyst, Pt/HY (Table 4.5). It is worth mentioning that the R_w ratio corresponding to the maximum activity depends on the co-catalyst used.

Finally, it is interesting to consider in more detail the textural and acidic properties of sulfate-promoted zirconia used as the co-catalyst, and its role in the catalytic reaction studied:

i) Although possessing acid sites stronger than those of the HY zeolite, sulfate-promoted zirconia has a surface area per weight unit more than five times smaller than that of the HY zeolite (Table 4.2). However, if we refer the acid density to the surface area unit, sulfate-promoted zirconia has the highest density among the co-catalysts studied in this work (Table4.2).

ii) Alone, sulfate-promoted zirconia is far less active and selective than the HY

zeolite (Table 4.5). However, combined with HY zeolite, this material contributes to a significant improvement in the catalytic performance (PtHY/PtSZr, Table 4.6). Similarly, the Pt/SA exhibits extremely low activity and selectivity to deep hydrocracking products (Table 4.5). However, when combined with the HY zeolite, the SA co-catalyst provides a fairly high catalytic performance (Table 4.6).

The explanation I can propose is that sulfate-promoted zirconia and silica-alumina are capable of transferring to the zeolite surface some of the incomplete hydrocracking intermediates (mono/di-branched isomers of n-octane) which undergo further isomerization and cracking on the zeolite acid sites. The more acidic and more open structure of the SZr sample when compared to that of the HY zeolite makes the former material a better co-catalyst because of its higher adsorption rate for n-octane accompanied by less diffusion problems. The same situation is found with the (PtHY/SA) hybrid catalyst (Table 4.6). Although the SA component has a surface acidity lower than those of the sulfate-promoted zirconia and the HY zeolite (Table 4.2), it has a surface area higher than those of the co-catalysts studied and a fairly open porous structure (Table 4.2 and Figure 4.8).

The effects of acidic and textural properties of the catalyst capable of efficiently promoting the catalytic performance of the hybrid catalyst are

summarized by:

--Acidity [density per surface unit area (Table 4.2) and strength (qualitative consideration, Figure 4.8)]: Qz << SA < HY < SZr;

--Surface area: Qz << SZr << HY < SA (Table 4.2);

--Openness of the pore structure: HY < SA < SZr < Qz (Figures 4.7 and 4.8);

--Observed total catalytic conversion for hybrid catalyst: Qz << HY < SZr < SA (Table 4.6);

--Observed β-scission selectivity and extent of n-octane hydrocracking (S_{Hy} and Y_{Hy}) of hybrid catalysts: Qz << HY < SA < SZr (Table 4.6).

These results suggest that the co-catalyst properties which influence the catalytic performance of the hybrid catalyst in the hydrocracking of n-octane are dependent on, and according to decreasing importance by:
surface acidity > surface area > openness of the pore system.

It is my intention to carefully measure the kinetic parameters of the reactions over these two non-conventional hybrid catalyst systems (Pt/(Y-SZr) and Pt/(Y-SA) in order to confirm the suggested transfer phenomena and to determine their influence on the overall reactions.

Table 4.7 Catalytic results obtained with the hybrid catalysts having various R_w (zeolite/sulfate-promoted zirconia) ratios

Catalyst R_w	Pt/Y-SZr 5/4	Pt/Y-SZr 6/3	Pt/Y-SZr 7/2	Pt/Y-SZr 8/1
Conversion (C_t)	88.4	91.9	93.3	99.4
	Product selectivities (S_i)			
$C_1 + C_2$	0.0	0.0	0.0	0.0
C_3	16.0	13.8	15.0	16.2
n-C_4	13.0	11.7	12.5	13.4
iso-C_4	54.1	50.2	51.9	53.0
n-C_5	3.9	2.0	4.0	2.7
iso-C_5	12.1	12.2	11.6	13.0
n-C_6	0.3	0.0	0.0	0.0
iso-C_6	0.5	0.0	0.2	0.3
mono-br-C_8	0.1	7.4	4.8	0.4
multi-br-C_8	0.1	2.7	0.0	0.0
S_{HY}	82.2	76.2	78.5	82.2
Y_{HY}	72.7	70.0	73.2	81.7

Table 4.8 Catalytic results obtained with the Pt//Y catalysts with various zeolite contents

Catalyst	Pt/Y_5	Pt/Y_6	Pt/Y_7	Pt/Y_8
Conversion(C_t)	78.8	81.4	87.1	92.5
	Product selectivities (S_i)			
$C_1 + C_2$	0.0	0.0	0.0	0.0
C_3	13.5	14.5	15.0	15.1
n-C_4	11.6	12.2	12.3	12.6
iso-C_4	48.6	50.7	52.1	50.8
n-C_5	2.4	3.3	3.4	3.8
iso-C_5	11.7	11.7	11.4	11.7
n-C_6	0.2	0.1	0.3	0.1
iso-C_6	0.2	0.4	0.8	0.3
mono-br-C_8	8.4	5.9	4.6	4.9
multi-br-C_8	2.6	1.4	0.2	0.7
S_{HY}	73.8	76.9	78.5	77.6
Y_{HY}	58.2	62.6	68.4	71.8

4.4 Conclusions

It was confirmed from XRD and FTIR studies that there exists a temperature window from 770 K to 870 K for the optimum activation of sulfate-promoted zirconia to obtain a tetragonal crystalline structure for zirconia, without loss of sulfate groups and with subsequent good catalytic performance. The presence of sulfate groups on zirconia retarded this phase transition and also its aggregation upon heating.

Superacidic properties of the sulfate-promoted zirconia were observed with the NH_3-TPD profile, which corresponded with a NH_3 desorption peak beginning at 800 K. The acid density on the surface of sulfate-promoted zirconia was lower per unit weight, but higher per surface unit area when compared with that of the HY zeolites.

It has also been shown that there is a synergistic effect between the different components of the hybrid catalysts. This is likely due to the transfer of reaction intermediates from the sulfate-promoted zirconia (or the silica-alumina) surface to the zeolite pore system. Such a transfer is favored by the following characteristics of the co-catalyst: surface acidity, surface area, and openness of the pore system. Hybrid catalysts prepared by dry impregnation of Pt show the best catalytic performances.

CHAPTER V

HYDROCRACKING OF N-PARAFFINS OVER DIFFERENT ZEOLITES

Reaction Mechanism Considerations

5.1 Introduction

Catalytic hydrocracking can be considered as catalytic cracking with hydro/dehydrogenation superimposed. The suppressed coke formation, due to the hydrogen atmosphere, allows the cracking components of the catalyst to function near maximum activity for a longer period of time. The hydrocracking process proceeds at lower temperatures than does catalytic cracking. Due to the high acidity of zeolites, their introduction into hydrocracking catalysts allows this reaction to occur at even lower temperatures[51].

A large quantity of research has been done with the intention to rationalize the product distribution from reaction mechanisms [7-14]. It is generally believed that the hydrocracking reaction is an acid-catalyzed process and involves carbenium ion intermediates. But which type of acid site, Brønsted or Lewis and particularly the function of Lewis sites, is still unclear. Additionally, although it has been shown that the product distribution is mainly a function of the level of conversion and the chain length of the n-paraffin feed[6], the relationship between this distribution and the structure of the zeolites used has not been thoroughly investigated as yet.

The mechanistic considerations presented in this chapter have the objectives to clarify the function of each type of acid site, and to investigate

the influence of catalyst structure on each step of the reaction pathway. This has been approached by subjecting a series of n-paraffins of varying chain lengths over different types zeolites having different pore sizes and structures to the hydrocracking process.

5.2 Experimental

5.2.1 Sample Preparation

1. Silica-alumina and Y zeolites

Silica-alumina(SA) and Y(NaY: LZY-52, HY: LZY-82, both in powder form) zeolites employed in this section are the same as those used in previous chapters.

2. Mordenite zeolite

Mordenite zeolite powder (assigned as HM, hereafter) was purchased from Chemie Uetikon AG (Zeocat FM-8/25 H). Activation was done by calcination in air at 673 K overnight.

3. ZSM-5 zeolite

ZSM-5 zeolite was synthesized by the hydrothermal method[39]. Silica gel was added to an aqueous solution of sodium hydroxide and tetrapropyl-

ammonium bromide at 353 K. The gel mixture was then stirred vigorously for one hour at this temperature An aqueous solution of sodium aluminate was added to the above mixture, and stirred for another 15 minutes. Then, the whole gel mixture was poured into a Hastelloy container which was then placed in an autoclave. The crystallization process took 10 days at 443 K under autogenous pressure, after which, the crystallized product was filtered, washed thoroughly with deionized water, dried at 393 K, and finally calcined in air at 823 K for 12 h. This zeolite is in sodium form, and is called NaZSM-5 hereafter.

The acidic form of the ZSM-5 zeolite, HZSM-5, was obtained by ion-exchange of the sodium form with ammonium chloride, which was subsequently calcined to the hydrogen form. The procedure is the following. The sodium form of ZSM-5 zeolite powder was added to an aqueous solution of 5 wt% NH_4Cl (10 ml of solution per gram of solid), and stirred at 353 K for 2 h. This ion-exchange step was repeated another five times. Between successive exchange steps, the solution was replaced with a fresh one. After the sixth ion-exchange, the solid was filtered, thoroughly washed with deionized water until free of Cl as indicated by $AgNO_3$ spot test, and dried at 393 K for 24 h. At this stage the zeolite is still in the ammonium form and is called NH_4ZSM-5. Calcination of NH_4ZSM-5 in air at 823 K for 12 h resulted in the protonic form of the zeolite which is called HZSM-5 (or HZ) hereafter.

4. β-zeolite

The β-zeolite was prepared according to a procedure similar to that for the HZSM-5 zeolite, where Ludox silica gel (AS-40) and tetraethyl-ammoniumhydroxide (Aldrich 35wt.-% solution in water) replace the silica gel and tetrapropylammonium bromide used as silicon source and template, respectively. The crystallization was carried out in an autoclave at a temperature of 423 K.

NH_4-β and H-β were prepared according to the same procedures as those mentioned earlier for the NH_4ZSM-5 and HZSM-5 zeolites.

5.2.2 Pt-loading and Catalyst Preparation

The dry impregnation method was used to make the final catalyst. Bentonite(20 wt.%) clay was used as binder. Pt content in all the final catalysts was 0.5 wt %.

5.2.3 Characterization

All the techniques used to characterize the different zeolites, including XRD, nitrogen and argon adsorption, FTIR and NH_3-TPD, are identical to these introduced in earlier chapters. Y zeolites were prepared for AA analysis by the

acid-leaching method whereas other zeolites were prepared by the fusion melting method as described in Chapter II.

Catalytic testing was similar to tests described in previous chapters, with reaction parameters as follows: reaction temperature = 495 K; WHSV (of hydrocarbon reactant) = 0.1 h^{-1}; H_2/N_2 = 12/16 (cm^3min^{-1}). The feed was varied as later specified.

Poison testing was performed using pyridine and 2,6-lutidine. The poison, 10 μL of either pyridine or 2,6-lutidine was injected into the reaction system at intervals of 1 h. Conversions and the product selectivities were determined after each input of poison.

5.3 Results and Discussion

5.3.1 Identification of Zeolites

Table 5.1 lists the chemical composition for the zeolites investigated as obtained by AA analysis. The Si/Al ratios for these zeolites are all in agreement with values expected from their typical chemical composition. The x-ray diffraction patterns in Figures 5.1 to 5.4 identify their crystalline structures. The x-ray diffraction patterns are for the H-forms of these zeolites, which may

introduce some differences when compared to the standard x-ray diffraction patterns which were obtained from the corresponding Na-forms of these zeolites[129]. Of these, the x-ray diffraction patterns of either Y, ZSM-5 or Mordenite zeolites are characterized by sharp peaks, which indicates that they are all good crystallites. However, the x-ray powder diffraction pattern of the synthesized β zeolite is characterized by a combination of sharp and broad reflections, which suggests that structural disorder pervades the framework although some amorphous materials or microcrystallites can not be excluded. In fact, this is generally observed with the β-zeolite, and has been reported by other researchers[130]. Higgins and Lapierre[129] interpreted the disorder of the tetrahedral framework structure of β-zeolite to be along [001] planes, whereas a disordered beta framework and three simple ordered polytypes were related through layer displacements on [001] planes. Three mutually perpendicular 12-ring channel systems are claimed to be characteristic of the three ordered polytypes and the disordered beta structure (Figure 5.5).

Table 5.2 lists the textural properties of the zeolites investigated, which further supports their structural identifications. The specific surface areas are high with major surface areas attributable to micropores, whose size distributions as obtained from the argon adsorption isotherms are quite sharp. There is one type of pore with a diameter of 0.74 nm for the Y zeolite, whereas there are two types of pores with different diameters observed for either ZSM-

5, Mordenite or β-zeolite. These pore diameters are all in agreement with those expected from their characteristic structures (Figures 5.5 to 5.8)[131]. As both ZSM-5 zeolite and β-zeolites were synthesized for this work, these results substantiate our confidence in the success of my synthetic methods.

Table 5.1 Chemical Composition of samples investigated*

Sample	Al_2O_3	Na_2O	SiO_2	Si/Al	Na/Al
SA	9.8	0.1	81.5	7.1	0.02
Y82(or HY)	24.9	0.2	74.9	2.6	0.02
Y82b	34.9	0.1	60.7	1.5	0.01
M(or HM)	9.2	1.1	89.4	8.2	0.19
HZSM-5(or HZ)	3.2	0.3	96.5	25.6	0.15
Hβ	5.9	1.0	92.9	13.6	0.29

* : in weight percent, based on the dried sample.

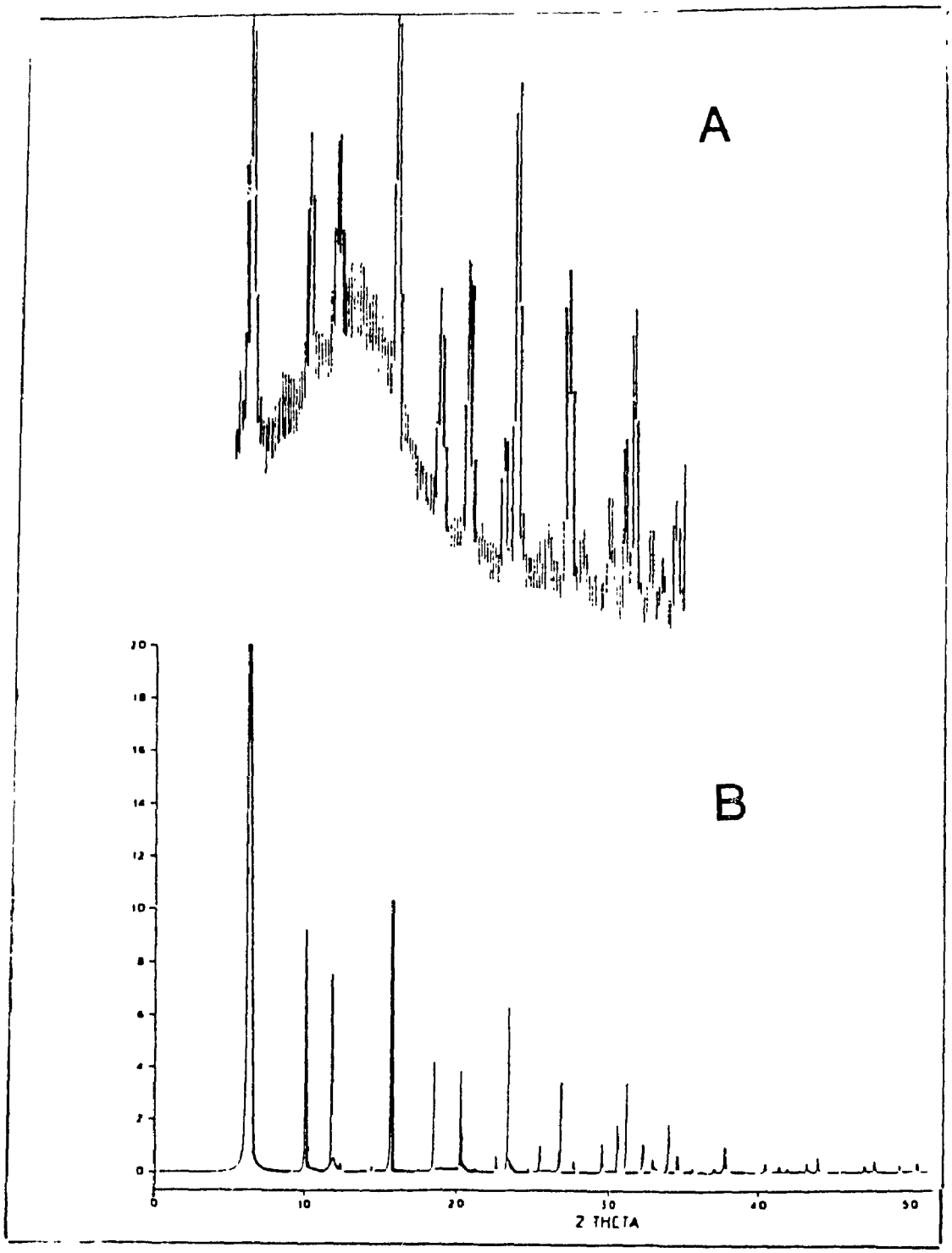

Figure 5.1 XRD patterns of Y zeolites: (A) HY (LZY82) used in this work; (B) NaY(Faujasite) zeolite adapted from ref[130]

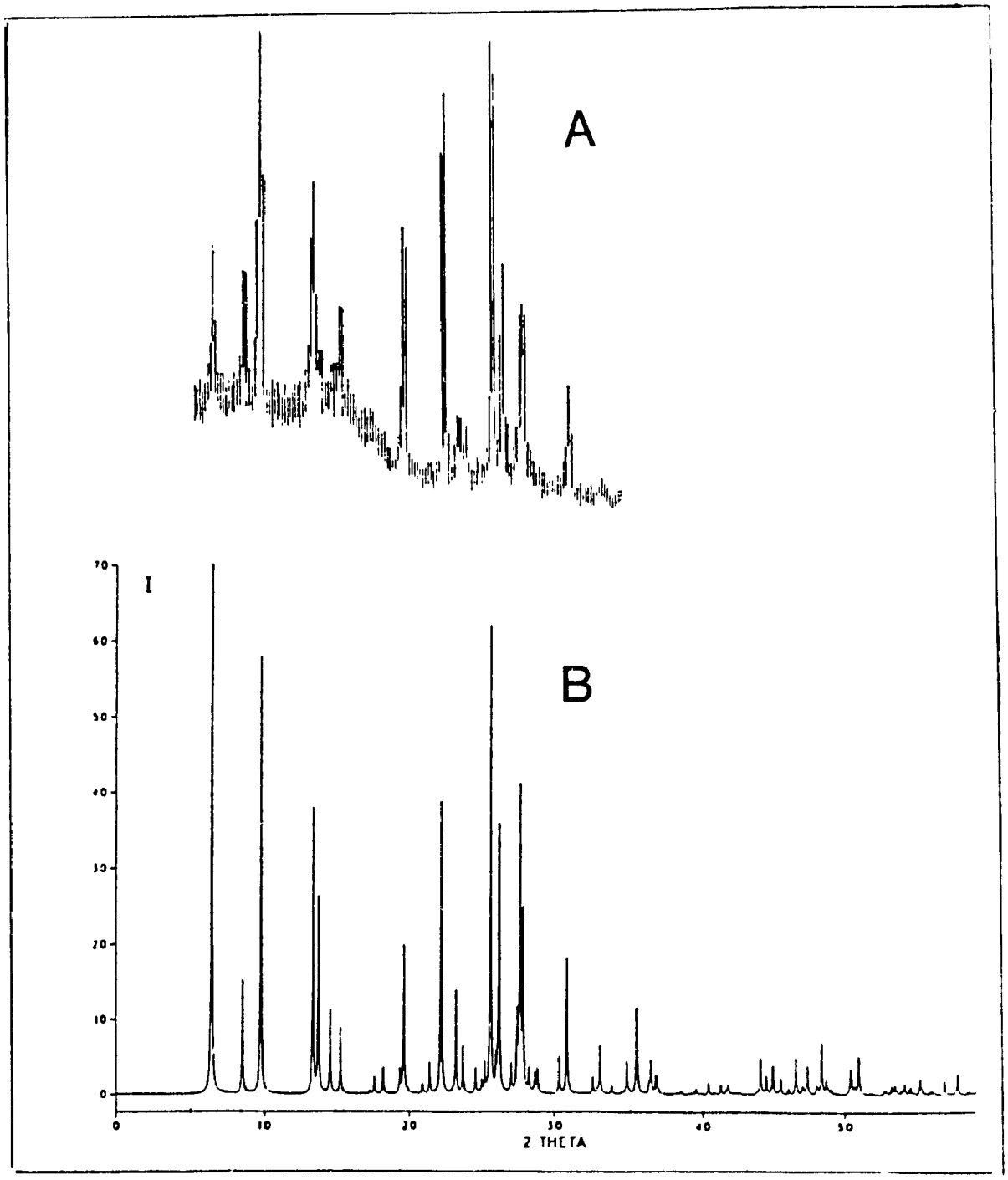

Figure 5.2 XRD patterns of Mordenite zeolites: (A)HM used in this work; (B) Na-Mordenite adapted from ref[129]

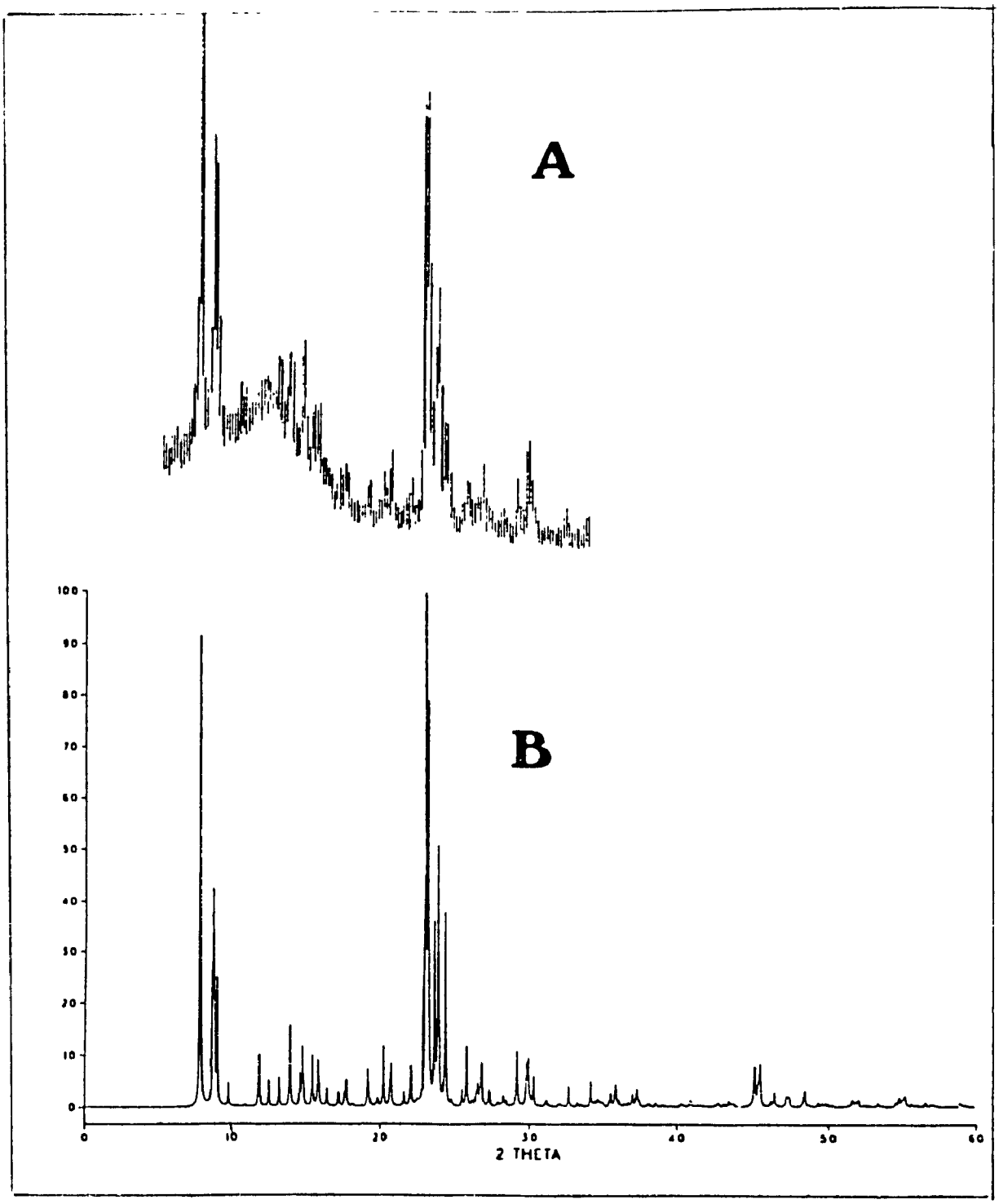

Figure 5.3 XRD patterns of ZSM-5 zeolites: (A)HZSM-5 zeolite synthesized in this work; (B)NaZSM-5 zeolite adapted from ref[129]

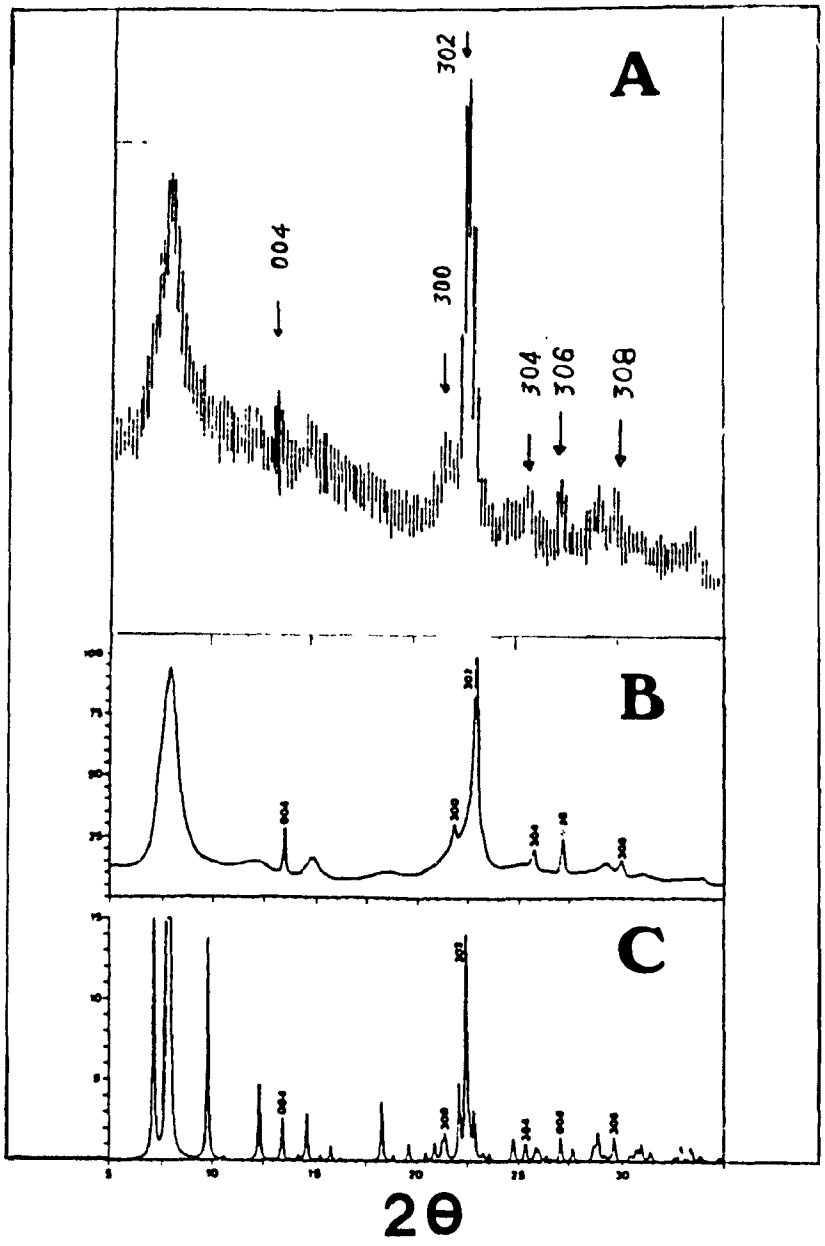

Figure 5.4 XRD patterns of β-Zeolites: (A)Hβ synthesized in this work; (B)Na-β zeolite reported by J.B. Higgins et al.[130]; (C)the calculated pattern for the ordered tetragonal A polytype. Six sharp reflections on the β pattern are indexed on the tetragonal unit cell.

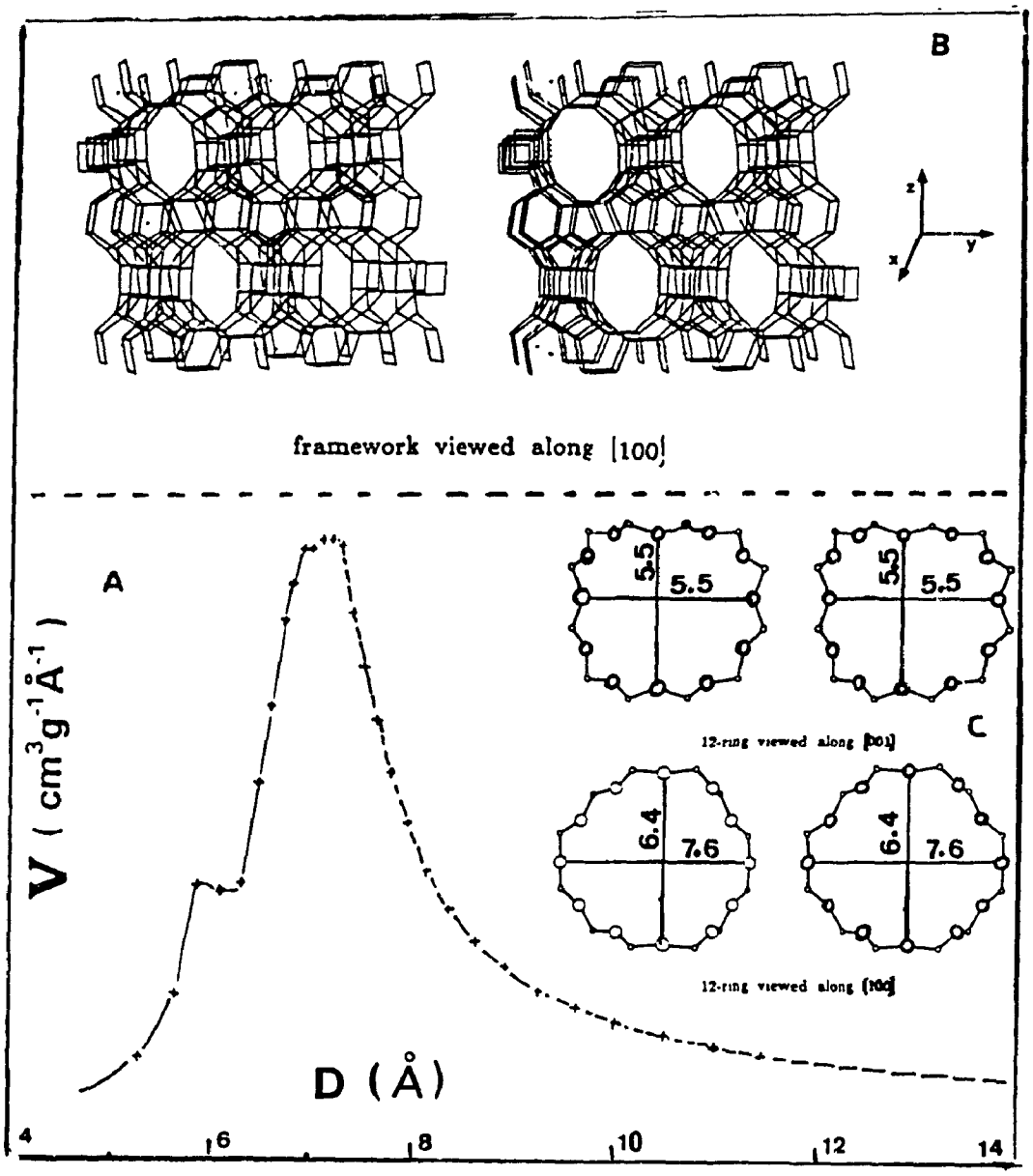

Figure 5.5 Micropore size distribution(A) of β zeolite and its theoretical structure(B) and pore system(C)

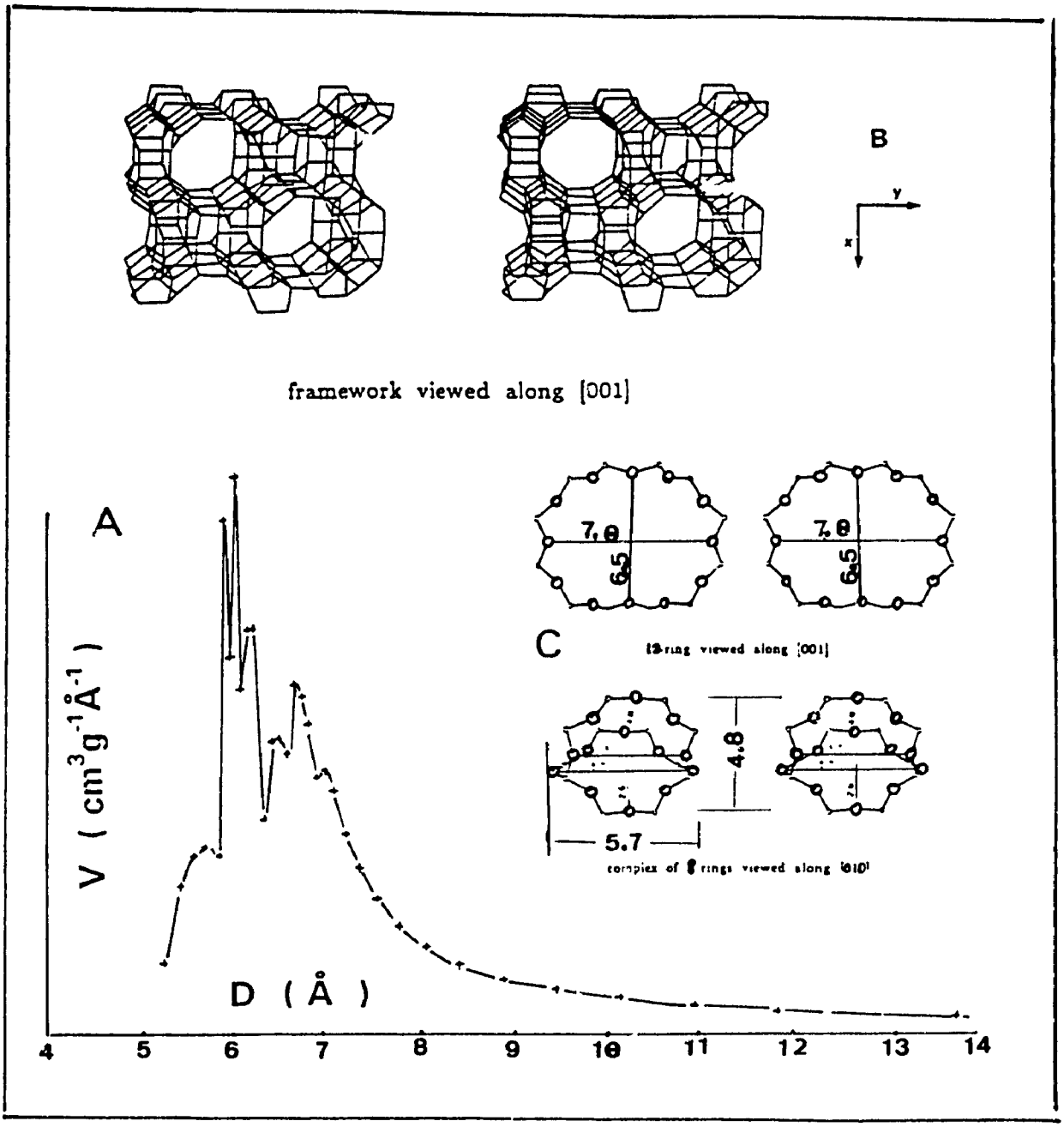

Figure 5.6 Micropore size distribution(A) of Mordenite zeolite and its theoretical structure(B) and pore system(C)

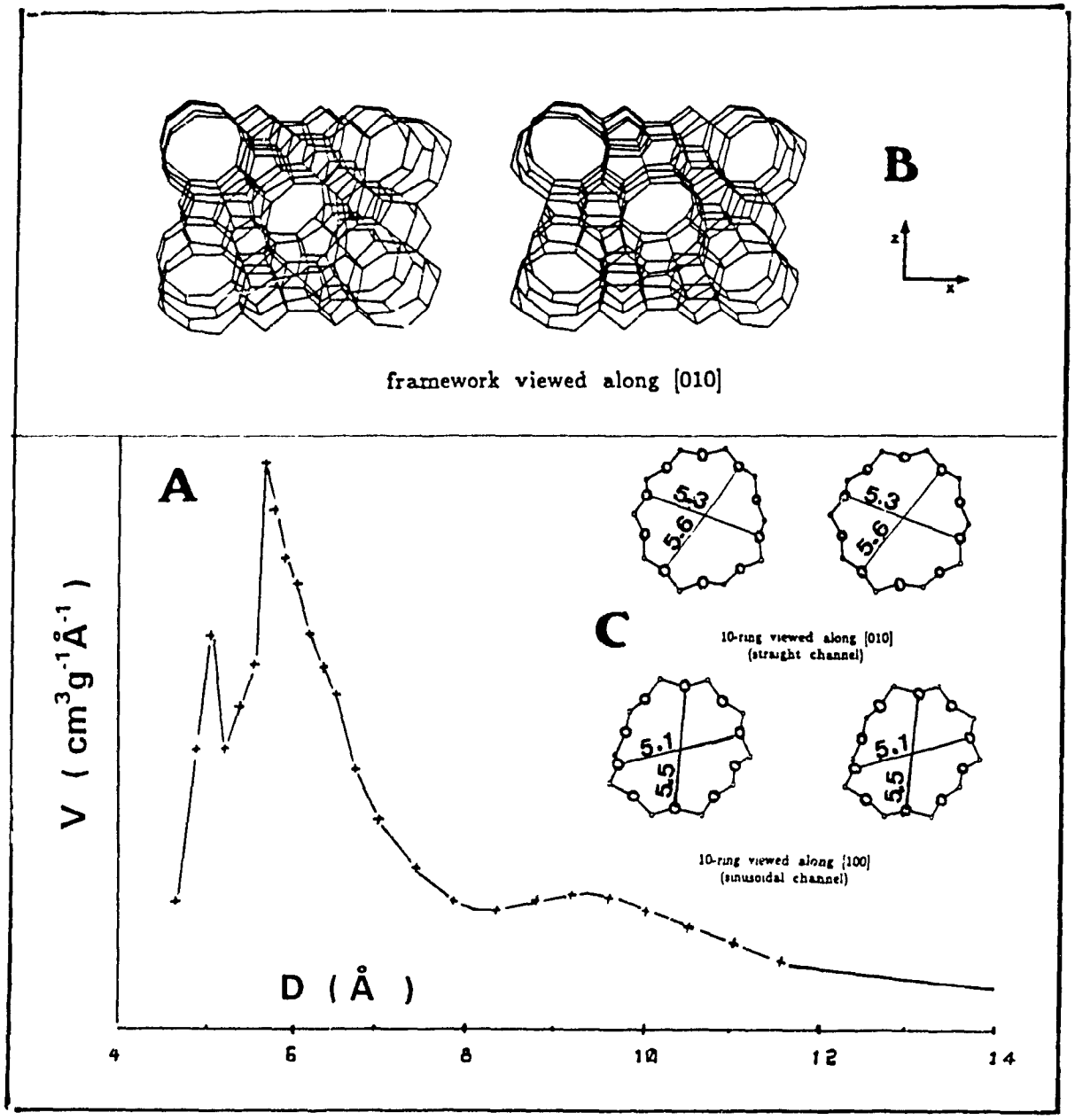

Figure 5.7 Micropore size distribution(A) of ZSM-5 zeolite and its theoretical structure(B) and pore system(C)

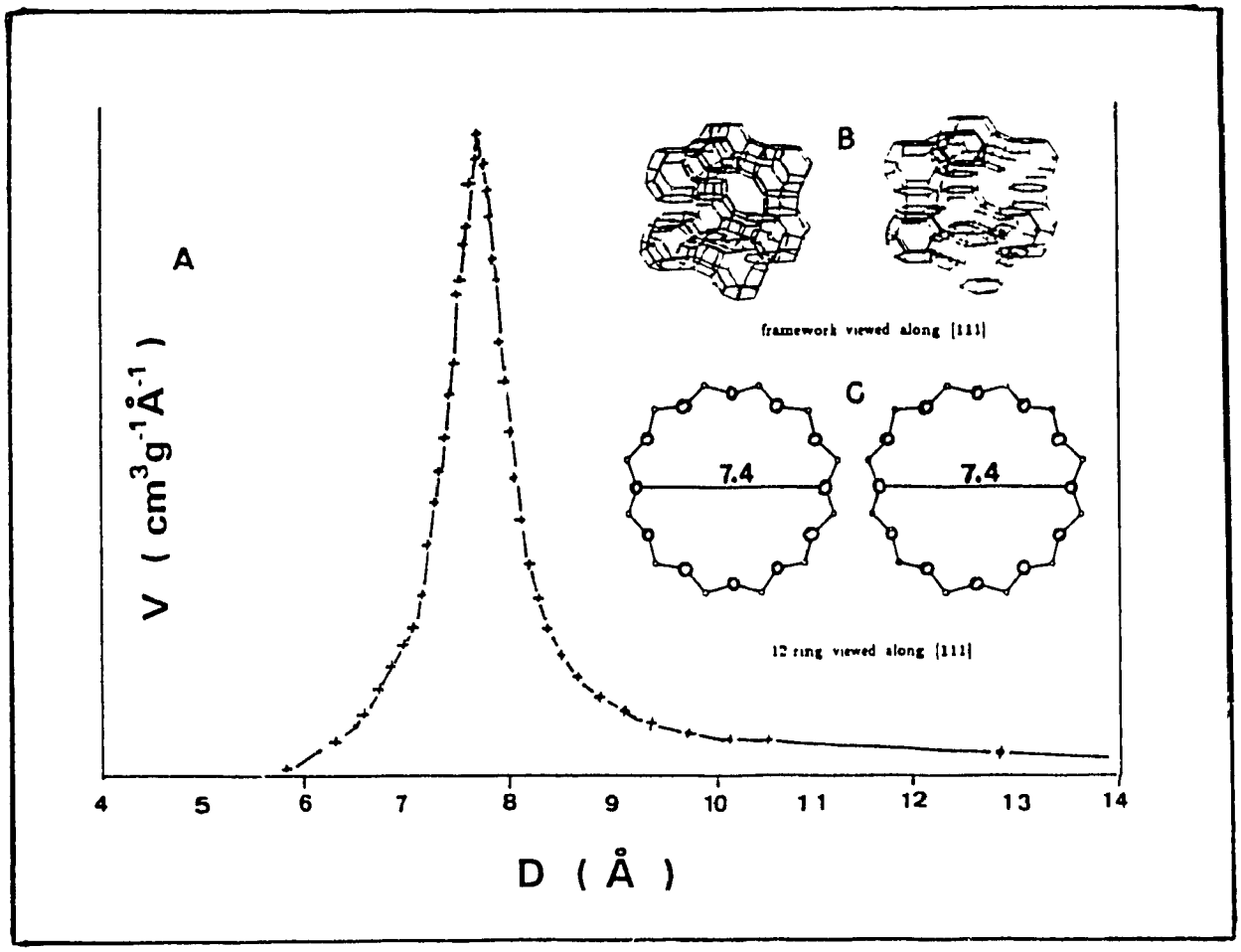

Figure 5.8 Micropore size distribution(A) of Y zeolite and its theoretical structure(B) and pore system(C)

Table 5.2 Textural Properties of Zeolites investigated

Sample	SA	HY	HM	HZ	Hβ
BET Area(m^2g^{-1})					
total	593	610	475	405	533
micropore	39	505	427	182	421
MP/Total *100%	7%	83%	90%	45%	79%
Volume(mm^3g^{-1})					
total	736	393	243	254	381
micropore	11	234	198	84	209
MP/Total *100%	1%	60%	81%	33%	55%
Pore Size(nm)					
BJH(4V/A)	4.54	5.86	5.78	3.55	4.12

5.3.2 Active Sites for Hydrocracking

There are three observations in this work that support my conclusion about the hydrocracking reactions that are catalyzed by acid sites, and in particular the Brønsted acid sites:

i) The sodium form of the zeolite Y(NaY) has no catalytic activity under the given reaction conditions due to its lack of acidity (Tables 3.9 and 5.3). But, both its hydrogen and lanthanum forms are acidic and thus exhibit catalytic activity. The generation of Brønsted acid sites with rare earth (such as La) substituted zeolites proceeds according to the equation:

$$La^{3+} + H_2O = (LaOH)^{2+} + H^+$$

and has long been accepted and associated with catalytic activity.

ii) Sulfate-promoted zirconia has a very low catalytic activity (Table 4.3) without a co-feed of hydrogen. This is probably because the acidity of this material is mainly Lewis in nature in an inert atmosphere even though it shows a considerable acid density (Table 4.2) with a superacidic character (Figure 4.11). Such Lewis acid sites can be transformed to Brønsted acid site in the presence of hydrogen[125]. Thus, a relatively high catalytic activity was obtained when the carrier gas was switched from pure nitrogen to a mixture of nitrogen and hydrogen as shown in Table 4.3.

iii) Figure 5.9 depicts the conversion of n-octane according to the accumulated amount of the poison injected, which may be considered as indirect evidence for this reaction being catalyzed by the Brønsted acid sites. It is worth mentioning that the conversion of n-octane and the product distribution over Pt/HY under the testing conditions is relative stable with time on stream without injection of poison. This implies that the variations in both conversion and selectivity when poison is added is a result of the poison itself. The conversion of n-octane decreased with increasing accumulated amount of poison injected, either pyridine or 2,6-lutidine. Finally, the conversion of n-octane to any product is totally inhibited when all the acid sites have been

neutralized by either pyridine or 2,6-lutidine, which clearly demonstrates that both poisons can completely subdue this reaction. Since 2,6-lutidine is specific to the Brønsted acid sites[132] and leaves Lewis acid sites unaffected, the total inhibition of activity by this base implies that the remaining Lewis acid sites following saturation of 2,6-lutidine onto this catalyst have no catalytic activity towards this reaction. The catalytic activity of this catalyst is therefore only contributed from the Brønsted acid sites. If one molecule of poison just neutralizes one acid site, the density of Brønsted acid sites can be estimated from the minimum amount of poison required to completely stop any conversion of n-octane. From Figure 5.9, it can be seen that the density of acid sites is about 800 μmol.g^{-1} for catalyst Pt/HY. This value is close to that obtained from the NH_3-TPD test(Table 5.4) result of 984 μmol.g^{-1} for sample HY, corresponding to 787 μmol.g^{-1} for catalyst Pt/HY when the 20 wt-% of the non-acidic bentonite clay is discounted.

These results also indicate that the acids present in hydrogen-form Y zeolite are mainly Brønsted in nature, as expected. The silica-alumina showed a comparable acidity from the NH_3-TPD tests, but its much lower activity than the HY zeolite indicates that a certain number of acid sites in the silica-alumina are Lewis in nature which do not possess any catalytic activity towards the given reaction. Since the NH_3-TPD test measures both Brønsted and Lewis acid sites having pKa values greater than that of ammonia, whereas the catalytic

activity is only controlled by the Brønsted acid, it is not surprising that an apparent relationship between the acidity obtained from NH_3-TPD testing and conversion of n-octane is not observed. Although there is continuing debate about the catalytic role of Lewis acid sites, our results, consistent with increasing evidence[133], indicate that Lewis acid sites are not active in catalyzing the desirable n-octane conversion[134].

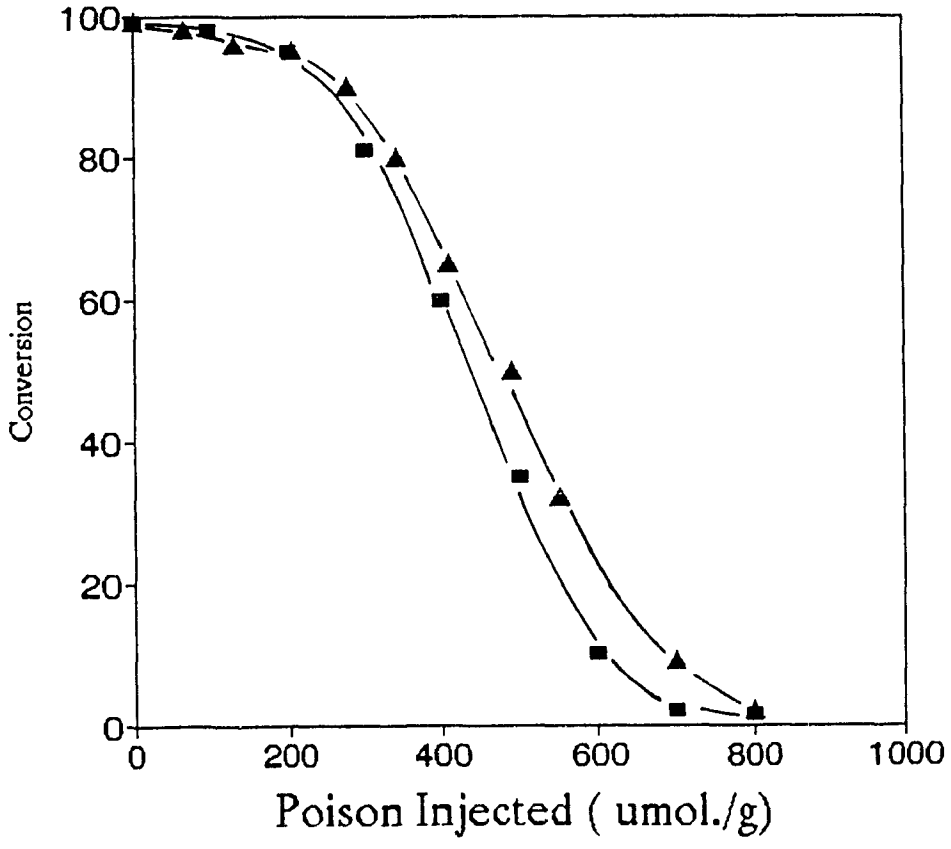

Figure 5.9 Conversion of n-octane over Pt/HY versus the accumulated amount of injected poison: Pyridine(■) and Lutidine (▲).

Table 5.3 Acidic properties of the various zeolites

Sample	Surface area m^2g^{-1}	Acid density $\mu mol.g^{-1}$	$\mu mol.m^{-2}$
NaY	780	0	0
HY	610	984	1.61
HZSM-5	405	525	1.30
HM	475	838	1.76
Hβ	533	932	1.75
Silica-alumina	593	428	0.72

5.3.3 Zeolite Structure and Catalytic Performance

Tables 5.4 and 5.5 present the comparisons of catalytic performances for the hydrocracking of n-octane with the different zeolite-based catalysts under identical reaction conditions. It can be seen that:

i). The amorphous silica-alumina has no essentially catalytic activity

towards the production of isobutane although it has a high surface area (Table 5.2) and a moderate acidity with respect to acid strength and density (Table 5.3).

ii), The conversion of n-octane on HM zeolite is much lower than that on other zeolites such as HY, Hβ and HZ.

iii). HZSM-5 zeolite shows a remarkably different product distribution compared to those obtained with either HM, Hβ or HY zeolites. In particular, the selectivities to propane and n-pentane over HZSM-5 is much higher; the iso/normal ratios for both C_4 and C_5 over HZSM-5 are much lower than those observed with the other zeolites.

iv). Hβ zeolite seems a good catalyst with respect to high conversion and high selectivity to isobutane but only at a longer catalyst contact time (i.e. a low weight hourly space velocity of reactant). The conversion rapidly drops with increasing weight hourly space velocity of n-octane or a shorter catalytic contact time.

v). Both relatively high conversion and high isobutane selectivity are obtained with the HY zeolite. Also, its catalytic activity is the most stable with respect to altering the catalyst contact time amongst all the zeolites investigated as it still provides the highest isobutane yield even at a short contact time (Table 5.5).

Table 5.4 Conversion of n-octane over different zeolite-based catalysts

Catalyst	Pt/Hβ	Pt/HY	Pt/HM	Pt/HZ	Pt/SA
Methane	0.0	0.0	0.1	0.0	0.0
Ethane	0.0	0.0	0.2	0.0	0.0
Propane	13.4	15.2	20.5	26.5	1.3
n-Butane	11.1	13.0	13.9	17.3	0.9
iso-Butane	59.6	54.6	45.9	24.8	1.9
n-Pentane	3.2	1.1	3.9	16.7	0.0
iso-Pentane	9.2	14.8	12.1	11.4	1.1
n-Hexane	0.9	0.0	0.8	0.1	0.0
iso-hexane	1.9	0.0	2.3	0.0	0.0
n-Heptane	0.0	0.0	0.0	0.0	0.0
iso-Heptane	0.0	0.0	0.1	0.0	0.0
multi-branched-C_8	0.0	0.2	0.1	0.2	3.8
mono-branched-C_8	0.5	0.5	0.1	3.0	91.0
Conversion of n-C_8	99.8	97.7	67.6	98.6	22.2
Isobutane yield	59.5	53.3	31.0	24.4	0.4
iso/n(C_4)	5.4	4.2	3.3	1.4	2.1
iso/n(C_5)	2.9	13.5	3.1	0.7	∞

T = 495 K, WHSV = 0.1 h^{-1}

Table 5.5 Conversion of n-octane over different zeolite-based catalysts

Catalyst	Pt/HY	Pt/Hβ	Pt/HZ	Pt/HM	Pt/SA
Methane	0.0	0.0	0.0	0.0	0.2
Ethane	0.0	0.2	0.0	0.0	0.0
Propene	0.0	1.2	0.0	0.0	0.0
Propane	13.8	8.6	25.8	19.7	2.4
n-Butane	11.5	7.5	15.9	14.5	1.8
iso-Butane	48.0	53.1	23.0	39.7	5.1
Butenes	0.0	2.3	0.0	0.0	0.0
n-Pentane	1.1	2.0	16.5	4.1	0.0
iso-Pentane	13.5	11.0	11.0	11.4	2.1
n-Hexane	0.0	0.4	0.0	0.0	0.0
iso-hexane	0.0	3.4	0.0	0.0	0.0
n-Heptane	0.0	0.3	0.0	0.0	0.0
iso-Heptane	0.0	1.1	0.0	0.3	0.0
multi-branched-C_8	6.1	1.3	0.0	2.0	0.0
mono-branched-C_8	5.5	7.7	7.9	8.1	88.4
Conversion of n-C_8	71.7	28.9	46.1	6.5	1.9
Isobutane yield	34.2	15.3	10.6	2.6	0.1
iso/n(C_4)	4.2	7.1	1.4	2.7	2.8
iso/n(C_6)	12.0	5.5	0.7	2.8	∞

T = 495 K, WHSV = 1.0 h^{-1}

An interpretation of the above observations can be that these different catalytic behaviours are due to different pore structures. Amorphous silica-alumina has a high surface area and total volume, but its micropore volume only represents about 1 % of the total pore volume(Table 5.2). Its extremely low activity is probably related to its weaker acid sites, or implies that the conversion of n-octane is associated with the acid sites inside the micropores instead of on the outside surfaces.

All the zeolites investigated are microporous, possessing different pore shapes and diameters for different structures (Figures 5.5 to 5.8). ZSM-5 zeolite has micropores no larger than 0.7 nm in diameter. Mordenite zeolite has a two-dimensional network. These zeolites exhibit lower selectivities towards the production of isobutane than the β and Y zeolites which have intersecting and three-dimensional micropores with diameter larger than 0.7 nm. These facts probably indicate that the reaction pathway towards isobutane is favoured by the structures of the latter zeolites. Additionally, the remarkably higher isobutane yield at short reaction contact time for HY zeolite than for Hβ zeolite suggests that not only the pore size but also the supercages in faujasite zeolites influence this reaction. Therefore, a "cage effect" concept is tentatively used to explain the formation of isobutane from hydrocracking of n-octane.

5.3.4 Different n-Paraffins as Reactants

Table 5.6 reports the conversions (C_t) and the product selectivities (S_i) obtained with various n-paraffin feeds. Figure 5.10 shows the yields of the cracking-derived branched paraffins (bP) and the ratio (R) of the selectivity of cracking-derived branched paraffins to that of their linear homologs as functions of the molecular length (ML) of the feed n-paraffins. It can be seen that:

i) the highest yields of cracking-derived branched paraffins (bP) are obtained with n-nonane and n-decane as feeds. The R ratio displays a maximum for n-nonane.

ii) the highest yield of isobutane is obtained with n-octane as feed.

iii) there is a significant decrease in the yield of bP products and the R ratio when the feed is changed from n-undecane to n-dodecane. Also, n-tetradecane exhibits the same low bP yield and R ratio as n-dodecane.

To explain point i) of the above observations, the conventional mechanistic scheme for hydrocracking is used. As described in Figure 1.4, the reaction pathways start with an acid-catalyzed skeletal isomerization leading to a di- or tribranched carbenium ion, which subsequently undergoes beta-scission leading to various products. In particular, the highest branching probability for the final products is given by the A-cracking mode (Figure 1.3) which requires the (α,γ,γ) tribranched carbenium ions as intermediates. B1 and B2 modes, which are based on (γ,γ) and (α,γ) dibranched ion intermediates respectively, provide equimolar amounts of branched and linear products. The C mode,

which is based on a (γ) monobranched intermediate, results in only linear products. Therefore, if the R ratio is higher than 1, this indicates that the A-mode is predominant over other beta-scission modes. However, for long n-paraffins, there are several possible reaction pathways for A, B1/B2 or C beta-scission modes, according to the location of the positive charge on the carbon chain of the carbenium ion. Thus, different products with the same degree of branching for the carbenium ions can be obtained from the same beta-scission mode but via different pathways. Table 5.7 reports the reaction products predicted for each n-paraffin according to the above mechanistic scheme. Thus, our experimental results allow us to determine which beta-scission pathway is predominant for a given paraffin feed.

a). With n-heptane(C_7), the relatively short length of this n-paraffin excludes any possibility of A-mode beta-scission, such that the B1/B2 pathways, which produce isobutane and propane in almost equal amounts, are predominant. Thus, high selectivity to isobutane and propane was obtained. Moreover, the very low production of n-butane almost precludes the C-mode beta-scission.

b). With n-octane(C_8), there are two possible pathways of A-mode beta-scission. The result that isobutane is by far the main product indicates that the pathway of A-mode beta-scission which is capable of producing two moles of

isobutane at the same time is predominant. On the other hand, the relatively low yield of isopentane rules out any important contribution from the pathway of A-mode beta-scission which could generate this product. Moreover, the role of the B1/B2 beta-scission for the production of isobutane and n-butane appears to be of minor importance because of the low yield of n-butane.

c). With n-nonane(C_9), the pathway of A-mode beta-scission yielding isobutane nd isopentane is predominant since these two products exhibit the highest selectivities.

d). With n-dodecane, there are two predominant pathways of A-mode beta-scission which produce isobutane/isohexane and isopentane/isopentane, respectively. Higher selectivities of both isobutane and isohexane than that of isopentane indicates the former pathway is much more important.

e). With n-undecane(C_{11}), the pathway of A-mode beta-scission producing isobutane again predominates. However, the co-product of such a beta-scission pathway, e.g: isoheptane, does not exhibit the same high selectivity as isobutane. This is probably due to the secondary cracking of relatively long chain primary products. Some C_1 and C_2 products appear in small amounts in the outstream, suggesting that beta-scission is not the only cracking possibility with such a long paraffin.

Table 5.6 Selective hydrocracking of naphtha-type n-paraffins

Feed	C_7	C_8	C_9	C_{10}	C_{11}	C_{12}	C_{14}*
Conversion C_t	92.6	99.0	99.8	100	100	100	100
$C_1 + C_2$	0.0	0.0	0.2	0.1	1.0	26.5	16.6
Propane	31.2	15.7	7.7	7.2	13.7	19.6	16.5
n-Butane	0.7	12.6	9.1	5.2	4.9	6.5	7.2
iso-Butane	43.6	53.8	38.6	30.1	33.8	23.5	27.4
n-Pentane	0.0	1.9	7.9	6.0	3.9	1.6	3.2
iso-Pentane	0.8	13.2	28.3	21.0	14.6	10.0	13.2
n-Hexane	0.1	0.0	1.3	5.9	4.2	1.3	2.7
iso-Hexanes	0.6	0.5	7.6	22.7	16.6	8.0	10.0
n-Heptane	7.4	0.1	0.0	0.6	1.2	1.4	0.2
mono-bra. C_7	10.0	0.3	0.0	0.7	2.7	0.6	1.0
multi-bra. C_7	12.4	0.4	0.0	0.6	1.2	0.2	0.0
n-Octane		-	0.0	0.0	0.0	0.7	1.6
mono-bra. C_8		-	0.0	0.0	0.0	0.0	0.0
multi-bra. C_8		-	0.0	0.0	2.3	0.1	0.0
C_9			-	0.0	0.1	0.2	0.5
C_{10}				-	0.1	0.0	0.0

Catalyst: Pt/HY

* T = 538 K (since boiling point of tetradecane: 527 K)

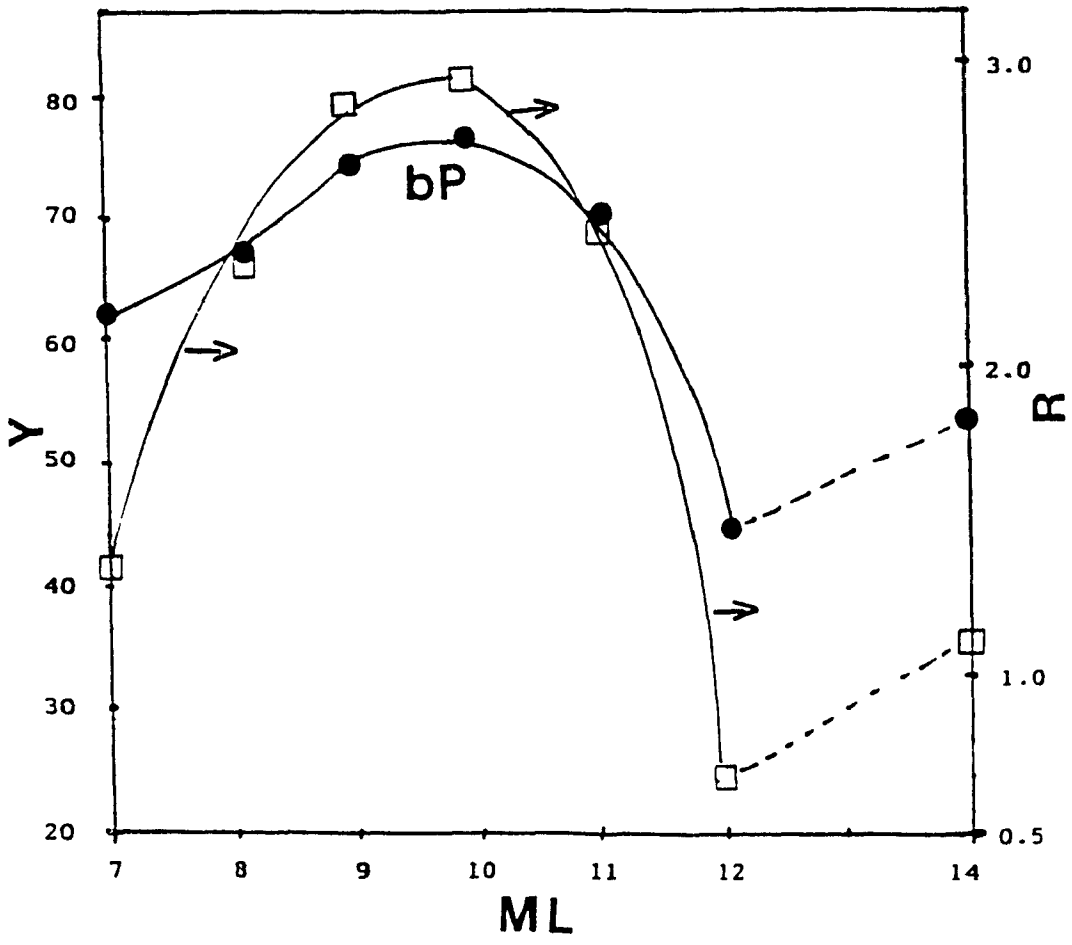

Figure 5.10 Yield of the cracking-derived branched paraffins(bP) and the ratio(R) of the selectivity of cracking derived branched paraffins to that of their linear homologs versus the molecular length(ML) of the feed n-paraffins.

Table 5.7 Predicted products of beta-scission according to the classical carbenium mechanism and experimental results.

FEED	PATHWAY INVOLVED[1]	PRODUCTS OF BETA SCISSION
n-heptane C_7	B1 + B2 C Exp.results[2]	isobutane + propane n-butane + propane isobutane > propane > > others
n-octane C_8	A A B1 + B2 B1 + B2 Exp. results	isobutane + isobutane isopentane + propane isopentane + propane isobutane + n-butane isobutane > > propane > isopentane > n-butane
n-nonane C_9	A A B1 + B2 B1 + B2 B1 + B2 B1 + B2 Exp. results	isobutane + isopentane isohexane + propane isobutane + n-pentane isopentane + n-butane isohexane + propane propane + n-hexane isobutane > isopentane > > n-butane > n-pentane > propane > isohexane
n-decane C_{10}	A A A B1 + B2 B1 + B2 B1 + B2 B1 + B2 B1 + B2 Exp. results	isobutane + isohexane isopentane + isopentane isoheptane + propane isobutane + n-hexane isohexane + n-butane isoheptane + propane propane + n-heptane isobutane > isohexane > isopentane > > propane > n-pentane > n-hexane > n-butane

	A	isobutane + isoheptane[3]
	A	isopentane + isohexane
	A	propane + isooctane[4]
	B1 + B2	isobutane + n-heptane[3]
n-undecane	B1 + B2	isoheptane + n-butane
	B1 + B2	isopentane + n-hexane
	B1 + B2	isohexane + n-pentane
C_{11}	B1 + B2	isooctane[4] + propane
	B1 + B2	propane + n-octane[4]
	RAC[3]	as for n-heptane
	RAC[4]	as for n-octane
	Exp. results	isobutane > > isohexane > isopentane > propane
	A	isobutane + isooctane[4]
	A	isopentane + isoheptane[3]
	A	isohexane + isohexane
	A	isononane[5] + propane
	B1 + B2	isobutane + n-octane[4]
n-dodecane	B1 + B2	isooctane[4] + n-butane
	B1 + B2	isopentane + n-heptane[3]
	B1 + B2	isoheptane[3] + n-pentane
C_{12}	B1 + B2	isohexane + n-hexane
	B1 + B2	isononane[5] + propane
	B1 + B2	propane + n-nonane[5]
	RAC[3]	as for n-heptane
	RAC[4]	as for n-octane
	RAC[5]	as for n-nonane
	OMC[6]	methane, ethane, ●●●
	Exp. results	isobutane > ethane > propane > isopentane > isohexane > n-butane > methane

(1): see ref[9]; (2): see Table 5.6; RAC(3), (4), (5): readsorption + cracking; OMC(6): other modes of cracking

Table 5.8 Selective hydrocracking of n-dodecane and n-octane

Feed	n-Dodecane		n-Octane	
WHSV (h^{-1})	0.24	0.12	0.24	0.12
Conversion, C_t	100	100	82.3	98
BP[a]	64.0	42.4	50.2	67.4
R[b]	1.8	0.7	2.3	2.2
$C_1 + C_2$	5.5	26.5	0.0	0.0
Propane	14.5	19.6	13.6	15.5
n-Butane	6.9	6.5	11.0	12.6
iso-Butane	32.1	23.5	48.0	54.8
n-Pentane	3.2	1.6	1.4	1.9
iso-Pentane	13.9	10.0	12.1	13.1
n-Hexane	3.0	1.3	0.0	0.0
iso-Hexanes	12.2	8.0	0.4	0.0
n-Heptane	2.1	1.3	0.0	0.4
mono-branched C_7	2.6	0.6	0.0	0.3
multi-branched C_7	2.9	0.2	0.0	0.1
n-Octane	0.9	0.7	-	-
mono-branched C_8	0.2	0.0	8.5	1.8
multi-branched C_8	0.1	0.1	5.5	0.6
C_9	0.3	0.2	0.0	0.0

Catalyst: Pt/HY

(a): Yield of cracking-derived branched paraffins; (b): ratio(selectivity) of cracking-derived branched paraffins to linear ones.

f). With n-dodecane(C_{12}), although isobutane is still the main reaction product, its selectivity is much lower than with n-undecane or shorter n-paraffin feeds. The non-beta-scission activity becomes more important as a significant amount of C_1-C_2 products are produced. Furthermore, the R ratio decreases sharply and even exhibits a value much lower than 1. This means that under such conditions, the A-mode beta scission is no longer effective with n-dodecane, in strong contrast to n-octane(Table 5.8). All these results indicate that n-dodecane behaves very differently from the other shorter n-paraffins, and there is a turning point in product distribution when the carbon chain of the n-paraffin feed goes from "carbon 11" to "carbon 12".

g). n-tetradecane (C_{14}) displays the same type of behaviour as n-dodecane over Pt/HY zeolite catalysts, indicating further that there is actually some reactivity barrier between n-undecane and n-dodecane. As a general rule for all n-paraffins no longer than C_{11} and non shorter than C_8, the A-mode beta scission prevails over all other modes. This is probably due to the faster cracking rate for the tribranched intermediate, which is also observed with superacids [8,9].

To explain point ii) of my results, I must know why the pathway of A-mode beta-scission leading to isobutane is predominant over other pathways of A-mode beta-scission producing branched paraffins other than isobutane.

This, however, can hardly be associated with their slightly different rates for the various pathways of the same mode(A) beta-scission, because the relatively long residence times used in this work precludes any effect due to such small kinetic differences. This cannot be explained by a simple mid-molecular cracking, either, since, a) n-octane is capable of producing two isobutane molecules by an A-mode beta-scission of the middle molecule; but, b) n-decane does not show the same efficiency in such a mid-molecule cracking mode which would otherwise produce much more isopentane than isobutane; and, c) the main reaction product for all the n-paraffins conversion over Pt/HY zeolite catalysts is iso-butane. Therefore, the reaction scheme cannot by itself provide a satisfactory explanation for these observations. The reaction environment, i.e. the structure of catalyst, must be recognized as having some influence. Observations previously obtained by variation of zeolite structures indicate that there must be a certain reaction locus inside the Y zeolite matrices which favours a particular kind of pathway of the A-mode beta-scission that leads to the product isobutane regardless of the length of the feed n-paraffin. Such a conclusion can be drawn from the speculation that, regardless of the length of the feed n-paraffin, during the chemisorption stage on the zeolite acid sites, the linear hydrocarbon is adsorbed at only one end. With this adsorption end, the dominant reaction pathway is that which leads to isobutane. Figure 5.11 is a picture used to show this type of adsorption. N-octane, with a chain length just matching the diameter of the supercage (Table 5.9), is not

restricted to this type of adsorption. With linear paraffins possessing longer chain lengths greater than the diameter of the supercage, one end is adsorbed onto the wall of the supercage where it can function as a reaction active site, while the other end is stretched out of the supercage due to chain strain. There must be some allowance for restriction allowing them to fit inside the supercage at one end. The longer the chain length, the less allowance exists for one end to fit properly at the correct location in the supercage. Obviously, this is that kind of "cage effect" observed by Chen and co-workers[135, 136] studying the diffusion coefficient in erionite and the closely related zeolite KT (Figure 2.11), an effect that determines the extent of adsorption of the reactant here. This "cage effect" not only provides a satisfactory explanation to our result ii), but also explains why low isobutane yields and low conversions are obtained with an ethyl-cyclohexane feed although this reactant has the same carbon number as n-octane has (Table 5.10). Furthermore, such a "cage effect" should be less important when the reactions occur at much higher temperatures due to the "breathing effect" of either cages or pores (windows to cages). Indeed, this implication was observed in our previous results when the effect of reaction temperature was studied (Chapter II).

Table 5.9 Chain lengths of n-paraffins investigated

n-Paraffin	Length (in nm)	Diffusion coefficient (in $*10^{-13}$ cm^2s^{-1})
C_7	1.16	1.5
C_8	1.28	1
C_9	1.41	3
C_{10}	1.53	9
C_{11}	1.66	85
C_{12}	1.79	105

(Adapted from ref [70])

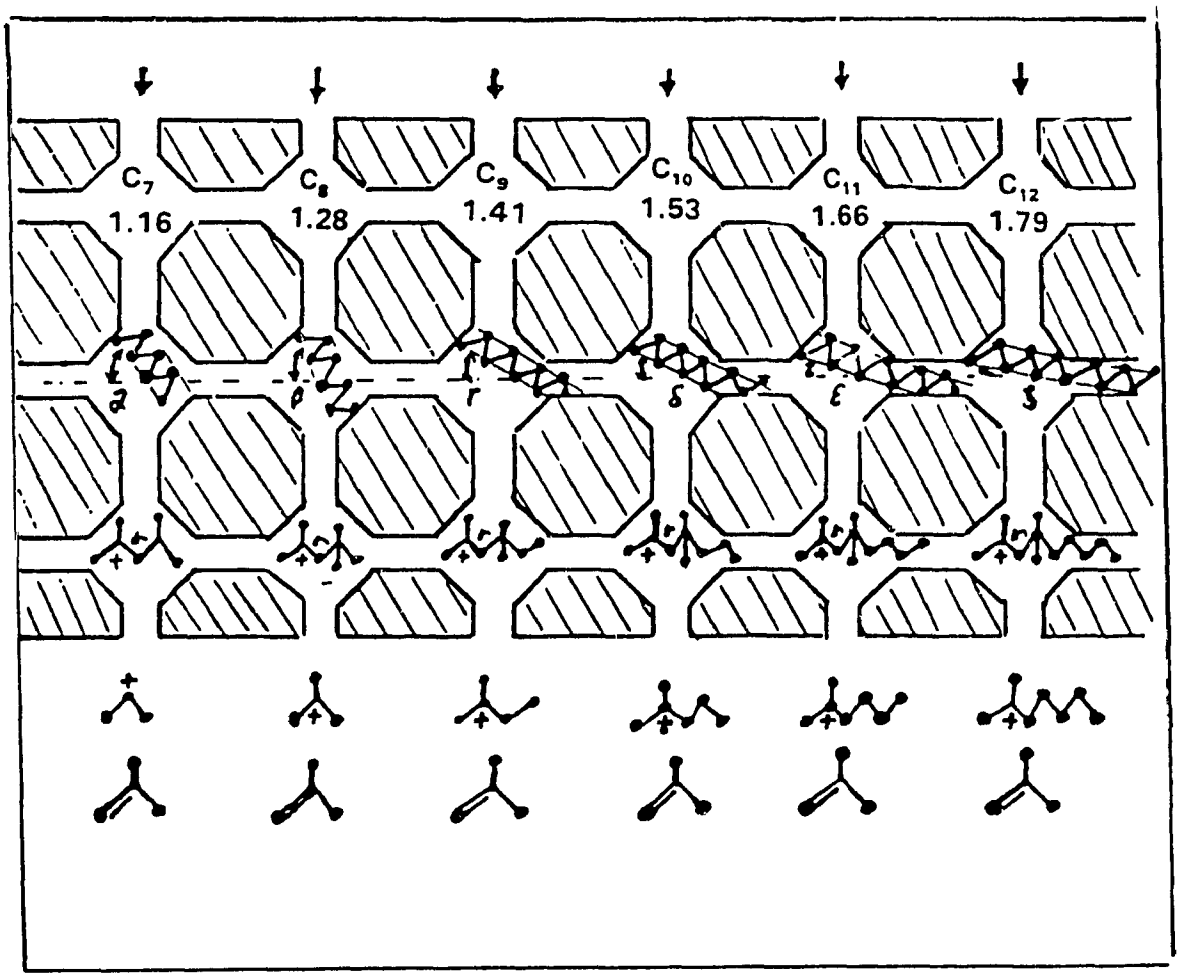

Figure 5.11 Pictorial representation of n-paraffins adsorbed inside supercages of Y zeolite

Table 5.10 Hydrocracking of ethyl-cyclohexane over Pt/HY zeolites

Temperature	495	545
Conversion	88.6	86.7
Methane	0.0	0.1
Ethane	0.1	1.3
Propane	1.7	3.9
n-Butane	1.1	1.7
iso-Butane	7.3	5.6
n-Pentane	0.2	0.3
iso-Pentane	2.7	1.7
n-Hexane	0.0	0.0
iso-Hexane	1.3	0.3
Cyclohexane	0.5	0.3
methyl-Cyclopentane	1.9	1.4
n-Heptane	1.8	0.0
iso-Heptane	0.6	0.0
methyl-Cyclohexane	7.4	1.9
n-Octane	31.1	4.9
branched-Octanes	13.3	0.0
di-methyl-Cyclohexanes	14.6	1.9
Benzene	0.0	7.3
Toluene	9.9	28.8
Xylenes	4.0	38.8
$C9^+$	0.3	0.2

To explain point iii) of my results for the remarkable difference in the yield of the cracking-derived branched paraffins (bP) between n-undecane and n-dodecane as feed, the reaction intermediates have to be considered. As previously mentioned, with n-octane and higher n-paraffins, the A-mode beta-scission predominates over Pt/HY zeolite catalysts as it has a much faster reaction rate than other modes of beta-scission. Such a mode of beta-scission requires a specific branching configuration for the involved acyclic carbenium ion, i.e. a tribranching with three branches in α, γ, and γ positions to the positively charged carbon atom of this acyclic carbenium ion intermediate (Figure 1.3). Only the A-mode of beta-scission provides more branching paraffin products (bP) than linear ones, and has a product distribution with an R greater than 1. Therefore, if these kinds of tribranching carbenium ion intermediates are easily formed inside the zeolite matrices, the resulting products should have higher R values. Inversely, if these tribranching carbenium ions are formed with difficult, the resulting products should have lower R values. Thus, the sizes of such ions and the catalyst structures both have an important influence on the subsequent step of the reaction, the formation of such trimethyl carbenium intermediates, once the reactants are adsorbed at the right place. Y zeolite has the largest cage, i.e. supercage, among the zeolites investigated here, and had the highest yield of isobutane even with shorter contact times. Heptane, with seven carbon atoms in its chain, is too short to show A-mode beta-scission, and thus can't provide high yields of isobutane. Octane has the shortest carbon

chain sufficient for A-mode beta-scission, and as such both its adsorption inside the supercage and the formation of the specific (α, γ, γ) tribranching carbenium ion suffer the least restriction from the surroundings and thus has the highest isobutane yield. The longer the chain length of the n-paraffin feed, the greater is the restriction against the formation of the desired tribranching carbenium ions, and lesser is the contribution from A-mode beta-scission. Such a trend would change abruptly when the size of the resulting tribranching carbenium ions becomes greater than that of the supercage of the Y zeolite. This did indeed occur when the feed was changed from n-undecane to dodecane(Figure 5.12). The trimethyl carbenium ion intermediate generated by the n-undecane has a backbone of similar configuration and size of that of n-octane, whereas that formed by n-dodecane has a backbone similar to that of n-nonane. The lengths of n-octane and n-nonane are 1.28 nm and 1.41 nm respectively (Table 5.9). Since the diameter of the supercage of the Y zeolite is ca 1.3 nm, it is possible to have a complete accommodation of the tribranched intermediate of n-undecane within the zeolite supercage whereas the (larger) size of the tribranched intermediate of the n-dodecane inhibits its complete inclusion into the same supercage. Thus, for the n-dodecane, the possibility of incomplete inclusion of the tribranched intermediates presumably results in blockage of the isomerization process after its adsorption. This leads to a lower production of cracking-derived branched paraffins(bP) and a lower R ratio(Figure 5.10 and Table 5.6). The limit imposed by the formation of branched

carbenium ions in the cage of zeolites also leads to an increase of the non-beta-scission cracking activity, mostly at the outer surface of zeolite. These results constitute evidence of the well-known transition state selectivity. Interestingly, this transition state is controlled again by the cage of the Y zeolite, more specifically the size and shape of the supercage. Obviously, this is another kind of "cage effect". Therefore, the cage effect brought forward in this thesis not only influences the reactant adsorption state, but also the formation of the reaction transition state. The latter function may be more important than the former with respect to the production of isobutane.

Besides such theoretical considerations concerning the variation of n-paraffin feeds, there is a practical significance in the choice of feed for a desired product. In the petroleum industry, there is a distinction between short naphthas(C_7-C_9 or 100 °C - 150 °C as boiling range), and long naphthas (up to C_{12} or 216 °C) as used in steam cracking[135]. To simulate these naphathas, we prepared two mixtures which had the following compositions:

A(wt- %) = C_7(20) + C_8(50) + C_9(30)

B(wt- %) = C_7(14) + C_8(35) + C_9(21) + C_{10}(15) + C_{11}(10) + C_{12}(5)

The on-stream stability of the Pt/HY catalyst was excellent with these "naphthas" under the specific conditions of reaction. Averaged data are reported in Table 5.11. It can be seen that the mixture A (short naphtha) gave

more isobutane than did the mixture B (long naphtha). This is in agreement with that expected with the pure n-paraffins as feed.

5.4. Conclusions

Hydrocracking of n-paraffins is catalyzed by Brønsted acid sites. Lewis acid sites have no essential catalytic activity towards this reaction.

Hydrocracking of n-paraffins for the production of iso-butane involves carbenium ion intermediates and, is a sequential step reaction. The cage of the zeolite has an effect on both the adsorption of n-paraffins onto the active sites which are located inside the micropores, and the formation of the specific branched carbenium intermediate configurations. Since iso-butane is mainly produced from A-mode β-scission of a α,γ,γ-tribranched carbenium ion, Y zeolites with supercages and C_8-C_{11} paraffins which allow for the appearance of the tribranched carbenium ions with sizes not greater than the diameter of the supercage are the restrictions concerning the choice of catalyst and feed for optimizing productivity.

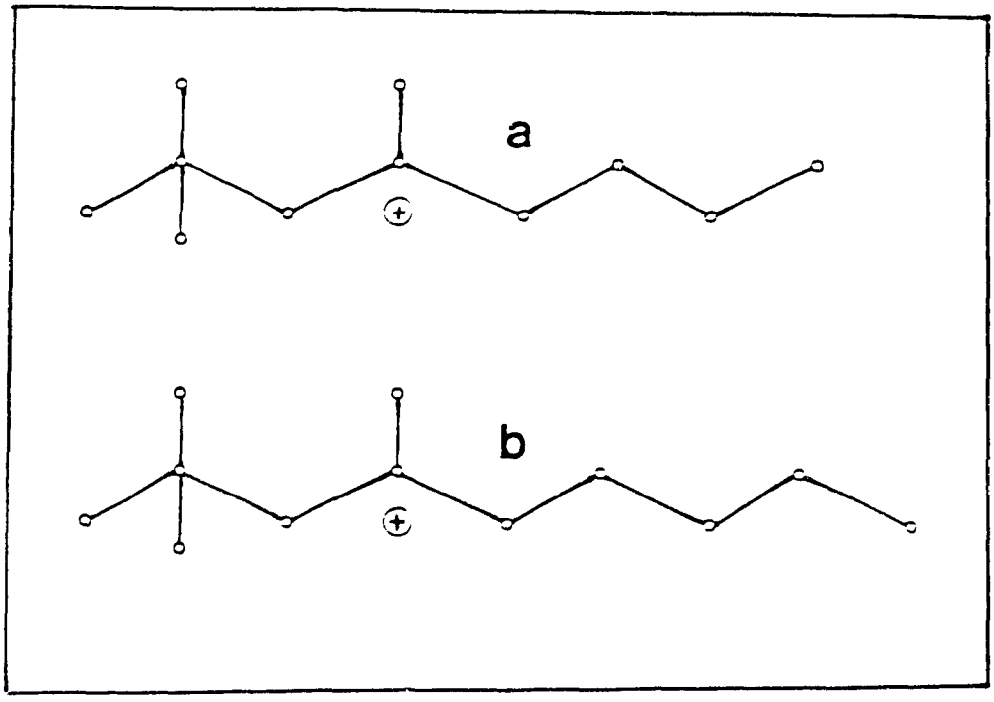

Figure 5.12 Chain bone of α,γ,γ-trimethyl-branched carbenium ions derived from nonane(a) and dodecane(b), respectively.

Table 5.11 Hydrocracking of two different naphthas on Pt/HY catalyst.

Feed	Mixture (A)	Mixture (B)
Conversion	98.5	98.9
$C_1 + C_2$	0.1	0.6
Propane	16.5	15.6
n-Butane	9.4	8.5
iso-Butane	49.1	44.1
n-Pentane	3.3	3.7
iso-Pentane	15.5	15.9
n-Hexane	0.4	1.7
iso-Hexane	2.3	6.6
n-Heptane	1.3	0.9
mono-branched C_7	1.9	1.7
multi-branched C_7	1.3	1.4
n-Octane	0.2	0.2
branched-Octanes	0.2	0.4

Catalyst: Pt/HY

Reaction conditions: T = 495 K, WHSV(naphthas) = 0.1 h^{-1}.

Average data of 6 hours on stream.

CHAPTER VI

KINETIC STUDIES OF THE CONVERSION OF N-OCTANE OVER ZEOLITE CATALYSTS

6.1 Introduction

Zeolite catalysts are extensively used in several acid-catalysed reactions, including hydrocracking and hydroisomerization of long-chain hydrocarbons, due to their high activity, selectivity, and resistance to poisons[33,55, 137-140]. A considerable effort has been invested in the understanding of the reaction networks that lead to the formation of isomers, as well as cracked products, from normal and branched paraffins[141-143]. Hydroisomerization and hydrocracking of n-alkanes have been shown to proceed in consecutive steps[141,142]. Two reactions have been proposed to have approximately the same values of activation energy [6,8,9]. However, there is no direct evidence reported as yet supporting this speculation. Indeed, such a speculation is poorly supported by a thermodynamic view, since a cracking reaction must involve scission of a C-C bond, whereas isomerization may not involve this C-C bond cleavage. Additionally, the competition between these two reactions is affected by the nature of the catalyst used and the reaction conditions, and as such may exhibit different values of apparent activation energies with different catalysts.

The objectives of the kinetic studies in this work include: i) the determination of the initial rates of the isomerization cracking reactions within the conversion process of n-octane, and the study of the delay between the initial contact

times and the initial rates (ie the induction period) for these two reactions as a function of temperature; ii) the calculation of the apparent activation energies and the pre-exponential factors for each catalyst investigated following the Arrhenius equation, and; iii) the comparison of tne kinetic data for different types of catalysts, ultimately aiming at drawing some useful information regarding the n-octane hydrocracking-hydroisomerization reaction which is of great industrial interest. These results can be considered as a novel and non-conventional set of "microkinetic analyses" which can be useful for "catalytic reaction synthesis" [144].

6.2 Experimental

6.2.1 Catalyst Preparations

Three catalysts were used in the kinetic studies: Pt/HY, Pt/LaNaY, Pt/Y-SZr, all prepared by the "dry impregnation" method, which exhibit interesting performance for the hydrocracking of C_7-C_{16} n-paraffins as shown in Chapters II, III, and IV respectively. For the hybrid catalyst(Pt/Y-SZr) prepared according to the method developed previously[145], a mechanical mixture of zeolite (HY) (65 parts) and sulfate-promoted zirconia (SZr) (15 parts) powders were used.

6.2.2 Catalytic testing

The experimental set-up for the catalytic testing was identical to that described in Chapter II, except 0.625 g of catalyst was used for each run. The procedure for catalyst testing and that for product analysis were also similar to those described in the previous chapters and in reference[146].

The reaction parameters were as follows: WHSV (weight hourly space velocity or g of n-octane injected per hour and per g of catalyst) = 1.41 to 7.65 h^{-1}, except = 0.29 to 7.65 h^{-1} for the Pt/LaNaY at 172 °C; temperature = 172 to 272 °C (445 to 545 K); ratio of flow-rate of nitrogen (used as carrier gas) to flow-rate of hydrogen = 4/3; molar ratio of n-octane to hydrogen = 1/30. The reaction contact time τ, being the reciprocal of the WHSV, was varied from 0.13 to 0.71 h, and to 3.5 h^{-1} for the Pt/LaNaY at 172 °C. The partial pressure of n-octane(P = 0.02 atm) was identical in all the runs.

A new indicator of catalytic performance, the conversion to cracking products C_{cr}, is introduced and defined as follow:

$$C_{cr} = 100 \times (NC)_{cr} / (NC)_t \qquad (6.1)$$

where $(NC)_{cr}$ and $(NC)_t$ are, respectively, the number of carbon atoms of hydrocarbon products having less than 8 in their molecules and the total hydrocarbons in the reactor outstream.

6.2.3 Kinetic data processing

As usual, external diffusion problems have to be ruled out prior to any catalytic study. Thus, preliminary tests were carried out by varying both the catalyst weight and the reactant flow-rate, keeping the WHSV and temperature constant. Table 6.1 compares two sets of data obtained with different catalyst weights and different n-octane flow-rates, which show no significant variation in terms of conversion and selectivity.

As shown in the NH_3-TPD profiles of Figures 3.16 to 3.18, zeolite catalysts are not homogenous materials with respect to their distributions of acid site strength, and the actual number of active sites (or the number of reaction loci) actually affecting a particular reaction is difficult to determine. The use of turnover frequency (TOF) in kinetic considerations as used with homogeneous catalysis and photocatalysis systems is not applicable with such a heterogenous catalytic system as we are studying here. The modelling of the multi-component reaction networks found in hydrotreating has evolved from a pseudo-first-order kinetic approach to rate expressions accounting for competitive adsorption on the active sites[10]. Physical adsorption of the hydrocarbons in the pores of zeolite catalysts had been included in these considerations[143]. The contribution from adsorption of the reactant or readsorption of products obviously depends on the partial pressures of the species involved. Therefore, an empirical kinetic approach based mainly on the initial reaction rates is used without any assumptions.

Table 6.1 The effect of catalyst weight on the hydrocracking of n-octane*

Catalyst Weight(g)	0.625	1.30	Variation
n-Octane Feed(g/h)	0.88	1.83	
WHSV(h^{-1})	1.41	1.41	(%)
N_2(ml/min)	120	240	
H_2(ml/min)	90	180	Δ
Conversion	51.0	48.4	1.6
Methane	0.1	0.0	0.1
Ethane	0.0	0.0	0.0
Propane	11.6	11.6	0.0
Carbon-4	49.5	49.3	0.2
n-C_4	9.6	9.6	0.0
iso-C_4	39.9	39.7	0.2
Carbon-5	11.9	11.6	0.3
n-C_5	0.4	0.6	0.2
iso-C_5	11.5	11.0	0.5
Carbon-6	0.0	1.0	1.0
n-C_6	0.0	0.0	0.0
iso-C_6	0.0	1.0	1.0
n-C_7	0.0	0.0	0.0
iso-C_7	0.0	0.0	0.0
multi-B-C_8	14.9	12.9	1.5
mono-B-C_8	12.1	14.0	1.9

*: Catalyst: Pt/HY , Reduction :N_2/H_2 = 16/12 (ml/min) 300 °C 2h. Reaction T= 222 °C, WHSV = 1.41 h^{-1}.

For each catalyst at each reaction temperature, the experimental data for total conversion were fit to a function, $f(\tau)$, based on the contact time, τ, using a nonlinear regression simplex algorithm(Figures 6.1-6.3). A third-order polynomial function, $f(\tau)$, was found to have a good correlation factor, and is expressed by:

$$C_t = a\tau + b\tau^2 + c\tau^3 \qquad (6.2)$$

The general form for the rate equation used is:

$$r = k P^n \qquad (6.3)$$

where k, P and n are the rate constant, the partial pressure of n-octane and the order of the reaction, respectively. Since P (for all runs) and n (for each catalyst) are constant, we have:

$$r = P^n \times k = dC_t/d\tau \qquad (6.4a)$$

$$\text{or} \quad k = P^{-n} \times r = P^{-n} \times dC_t/d\tau \qquad (6.4b)$$

$$\text{Thus,} \quad k = \text{constant} \times r = \text{constant} \times dC_t/d\tau \qquad (6.5)$$

The temperature dependence of the rate constant can be expressed by the Arrhenius equation:

$$k = Ae^{-E/RT} \qquad (6.6)$$

where A is the pre-exponential factor, E is the apparent activation energy and R is the molar gas constant. Therefore, knowing r at different temperatures allows us to determine E and A.

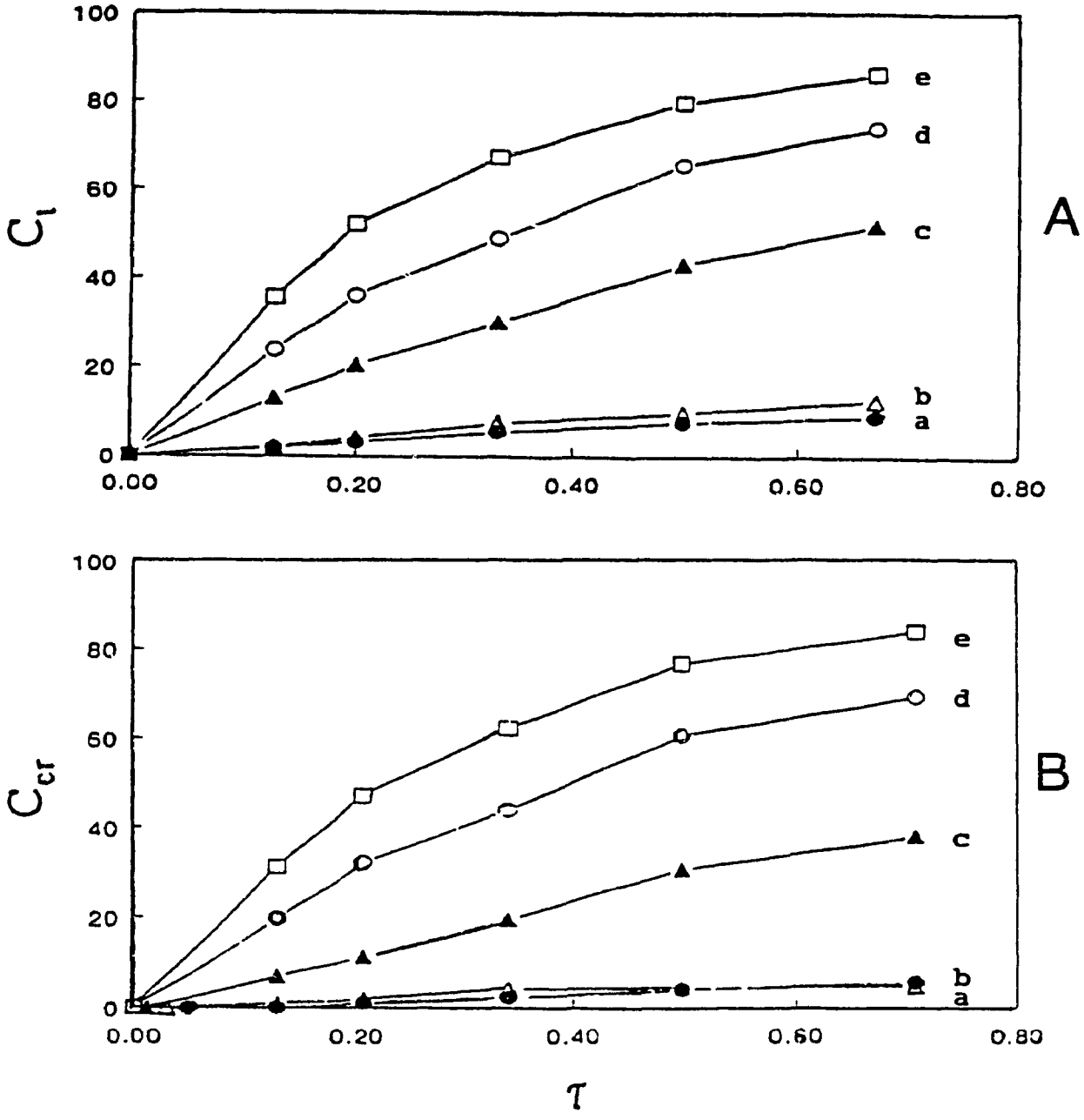

Figure 6.1 Total conversion, C_t(A), and conversion to cracked products, C_{cr}(B), obtained with the Pt/HY catalyst, versus contact time at different reaction temperatures (in °C): a) 172, b) 197, c) 222, d) 247 and e) 272.

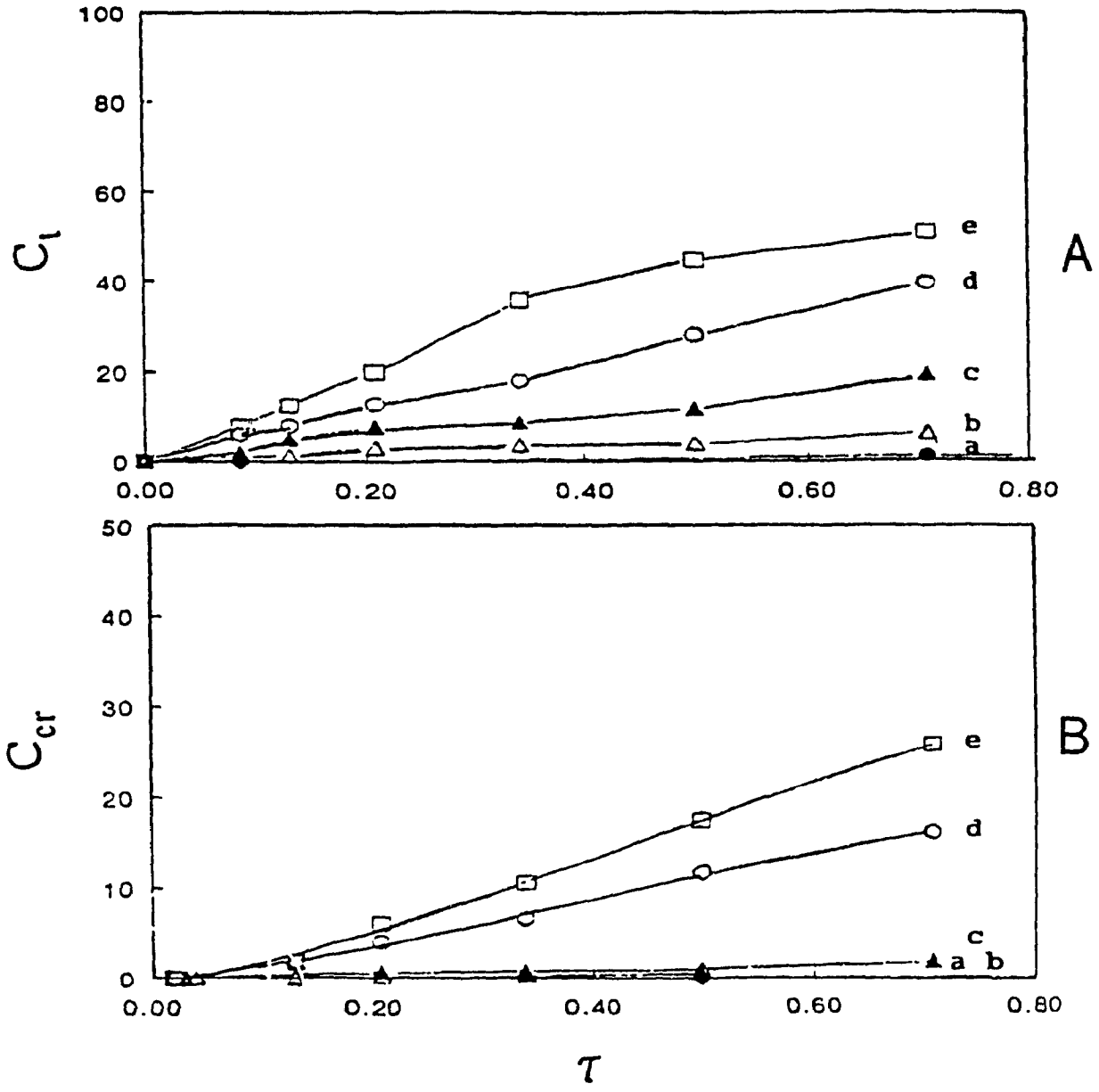

Figure 6.2 Total conversion, C_t(A), and conversion to cracked products, C_{cr}(B), obtained with the Pt/LaNaY catalyst, versus contact time at different reaction temperatures (in °C): a) 172, b) 197, c) 222, d) 247 and e) 272.

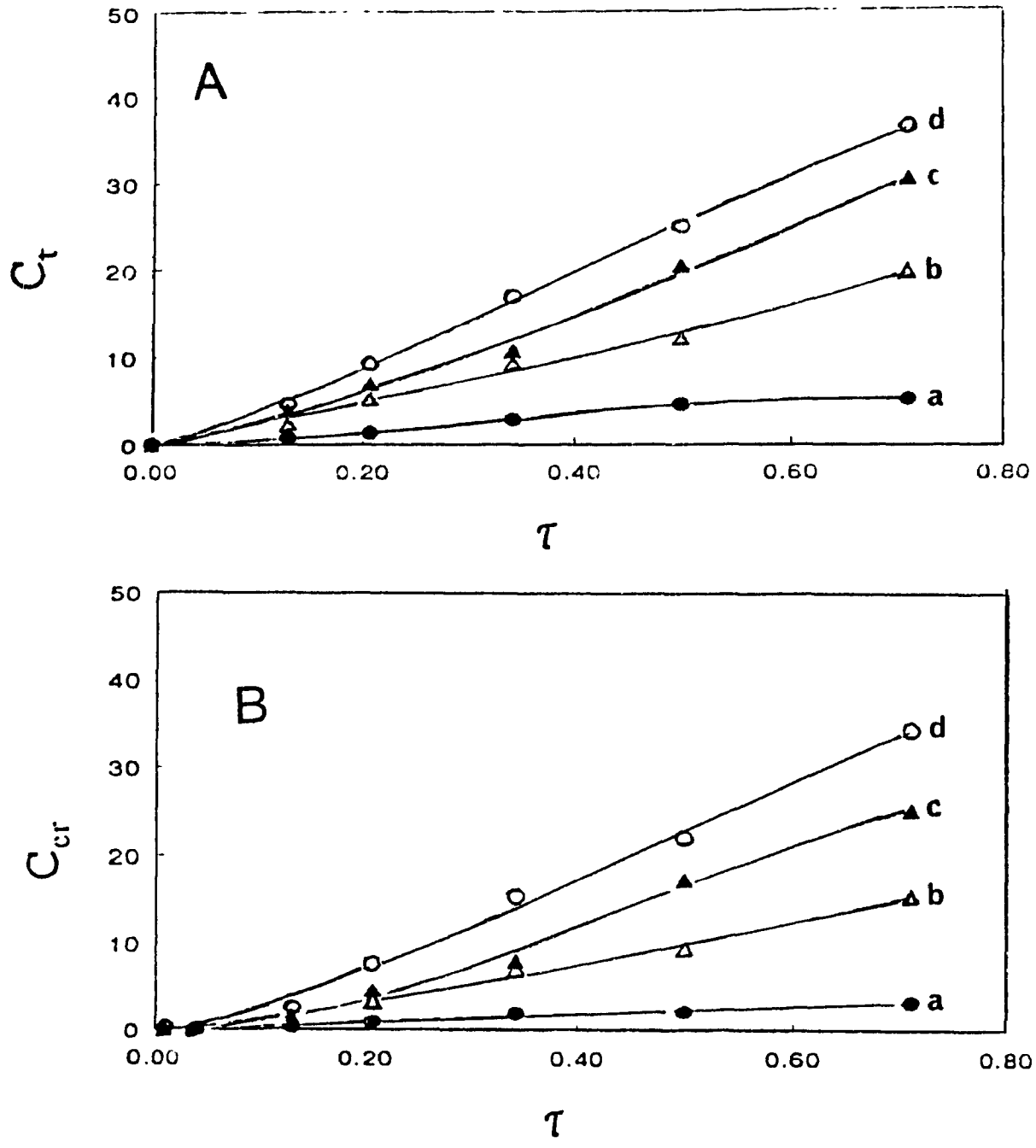

Figure 6.3 Total conversion, C_t(A), and conversion to cracked products, C_{cr}(B), obtained with the Pt/Y-SZr catalyst, versus contact time at different reaction temperatures (in °C): a) 172, b) 197, c) 222, and d) 247.

Considering the overall reaction mechanism for the hydrocracking of n-paraffins, it is generally accepted [6,50], and has also been shown in the previous chapters of this work, that the conversion of n-paraffins over bifunctional catalysts proceeds in two consecutive steps, represented by:

n-octane --(I)---> isomers ---(II)---> cracked products

As seen in previous chapters, during conversion of n-octane over HY zeolite-containing catalyst, all the cracked products are produced by the β-scission of the isomeric intermediates and not by hydrogenolysis (e.g. almost no C_1-C_2 products). This sequential reaction mechanism allows us to equate the initial rate of total conversion to the initial rate of isomerization, (e.g. at $\tau = 0 + \xi$ (infinitesimal value), where the rate is that of the primary isomerization of n-octane, in other words: $r_o = \lim dC_t/d\tau\ (\tau \rightarrow 0) = (r_{iso})_o$). This enables us to determine the kinetic data for the isomerization.

Furthermore, such a sequential mechanism implies that significant cracking (β-scission) occurs only after a contact time τ_o which is most likely not zero at the relatively low reaction temperatures used as illustrated in Figures 6.1-6.3. As well, Figure 6.4, which describes the total conversion, the conversion to cracking products and the conversion to isomerization products changing with the variation of contact time for these three catalysts at 172 °C, clearly indicates a delay in the onset the cracking reaction. Thus, to obtain kinetic data for the cracking reaction, we can use the following basic equation:

$$C_{cr} = f_{cr}(\tau-\tau_o) = a'(\tau - \tau_o) + b' (\tau -\tau_o)^2 + \ldots \quad (6.7)$$

in which $C_{cr} = 0$ when $\tau = \tau_o$. Since for a catalyst τ_o is a constant at constant temperature, this then becomes:

$$C_{cr} = f_{cr}(\tau) = a'' + b''\tau + c''\tau^2 + \ldots \quad (6.8)$$

Limiting this to the second degree of the polynomial, we obtain:

$$C_{cr} \text{ (at } \tau = \tau_o) = a'' + b''\tau_o + c''(\tau_o)^2 = 0 \quad (6.9)$$

and τ_o can easily be calculated. I can now calculate the initial rate of cracking (at τ_o) by using the equation(6.7) mentioned earlier. This means that at a contact time of $\tau = \tau_o$, β-scission begins with an initial rate equal to r_{cr}. The τ_o, which measures the delay between the two reaction steps (primary isomerization and cracking), is believed to depend on the catalyst and the reaction temperature, and τ_o is hereafter called the contact time delay.

In summary, the use of these equations allows me to obtain the values for the initial rates, the apparent activation energies, and the pre-exponential factors for both the isomerization and the cracking reactions involved in the conversion of n-octane.

6.3 Results and Discussion

6.3.1 Theoretical Considerations

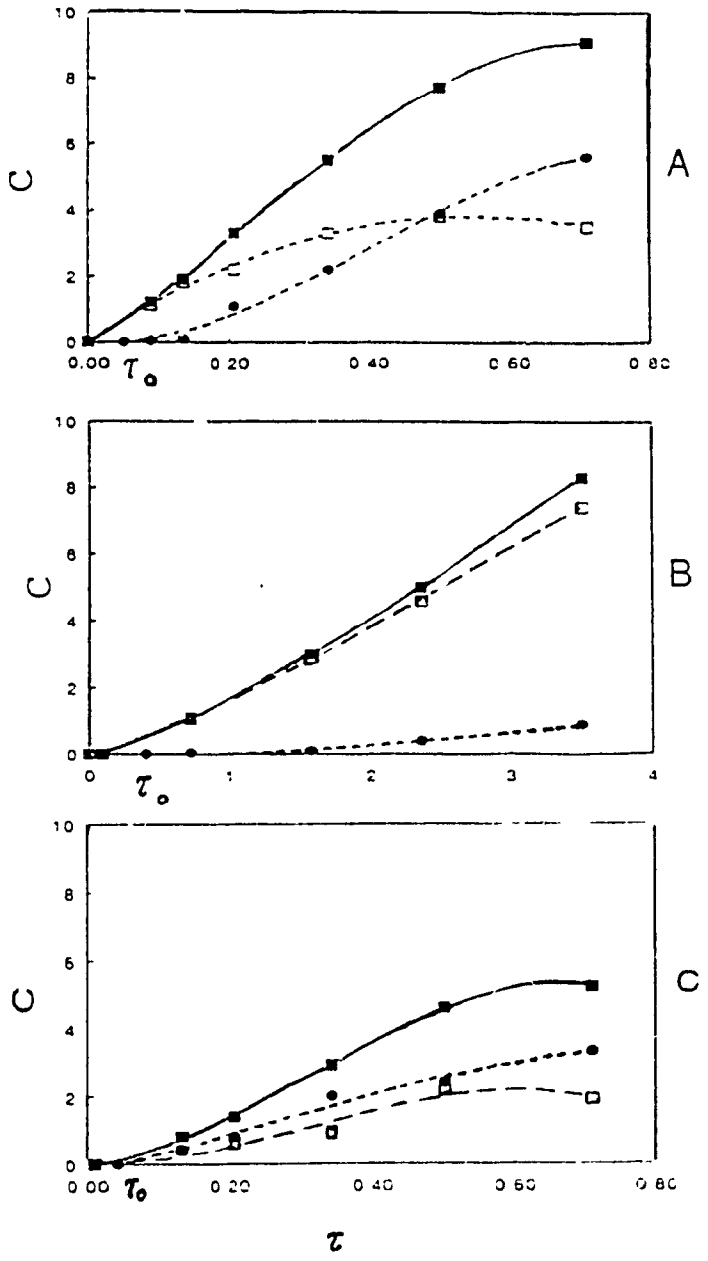

Figure 6.4 Contact time delay, τ_o, at 172 °C, for A) Pt/HY, B) Pt/LaNaY and C)Pt/Y-SZr. (■) = total conversion; (●) = conversion to cracked products and (□) = conversion to isomerization products(n-octane isomers).

In order to compare the kinetic behaviour of the three catalysts investigated, I reconsider some of the physico-chemical properties of the catalysts' components which were presented in Chapters III and VI. Of particular interest are the acidity data obtained from the ammonia TPD profiles (Figures 3.16 and 4.11, Table 4.2). Although the density of acid sites per gram is similar for the HY and LaNaY samples (Table 3.10), a comparison of their ammonia desorption profiles indicates that the LaNaY sample has many more weak acid sites than does the HY zeolite (Figure 3.16). On the other hand, sulfate-promoted zirconia exhibits a stronger acid strength but a lower acid site density (by weight unit, Table 4.2) than both the HY and the LaNaY samples.

Figures 6.1 - 6.3 show the conversion to cracked products versus the reaction contact time at various temperatures, as obtained with the three catalysts studied. For the hybrid catalyst Pt/(HY-SZr), conversion data obtained at 272 °C are not presented because the SZr used as co-catalyst risks loss of its sulfate species at temperatures above 240 °C under a reducing atmosphere (hydrogen) as discussed previously in Chapter iV.

Figures 6.5 - 6.7 present the Arrhenius plots used for the calculation of the apparent activation energies and the pre-exponential factors for both reaction steps (isomerization and β-scission or cracking), for Pt/HY, Pt/LaNaY and the Pt/Y-SZr. Linear regressions of Ln(r) vs. 1/T among the isothermal sets yielded

correlation coefficients greater than 0.96 for both reaction steps with all three catalysts. Since the plots of $Ln(1-C_t)$ against contact time, τ, are nearly linear (Figures 6.8) with correlation coefficients greater than 0.99 for all three catalysts in the temperature range studied, the following equation is satisfied:

$$-Ln(1-C_t) = \text{constant} * \tau \qquad (6.10)$$

and it can be simplified by the fact that the reactions on all three catalysts are pseudo-first-order[136]. Moreover, it is necessary to incorporate the fractional surface coverage, θ, into the Arrhenius equation as proposed by Dumesic, et al[144]. We can immediately assume that, at the early stage of the n-octane conversion (isomerization), θ is equal to 1 because the reaction system is always saturated with n-octane vapour. Therefore, we have:

$$k_{iso} = p^{-1} * \theta^{-1} * dC_t/d\tau \text{ (when } \tau \text{ tends to 0)}$$

$$= P^{-1} * \theta^{-1} * A_{iso}' \, e^{-\Delta E/RT} = A \, e^{-\Delta E/RT} \text{ , with} \qquad (6.11a)$$

$$A_{iso} = P^{-1} * \theta^{-1} * A_{iso}' = A_{iso}'/[\, 0.02 * 1.013 * 10^{5} \text{ (Pa)} * 1] \qquad (6.11b)$$

In any event, this only approximates values for the pre-exponential factors A_{iso} (Table 6.2). On the other hand, for the cracking reaction, the rate constant is determined at $\tau = \tau_o$ also according to ref. 144 as follows:

$$K_{cr} = \theta^{*-1} * dC_{cr}/d\tau, \text{ so that } A_{cr} = A'/\theta^{*}. \qquad (6.12)$$

where θ^{*} is the fractional surface coverage which corresponds to the occupancy of (active) acid sites by the reaction intermediates undergoing the β-scission. θ^{*}, assumed to be equal to $r_{cr}/(r_{cr} + r_{iso})$ at $\tau_o = 0$, shows the percentage of sites covered by the reaction intermediates which originate the

cracked products. Therefore, the values of θ^* are estimated from data of $r_{cr}/(r_{cr} + r_{iso})$ at $\tau = 0$ (Table 6.3). Finally, the values of the pre-exponential factors for cracking, A_{cr}, are determined (Table 6.4).

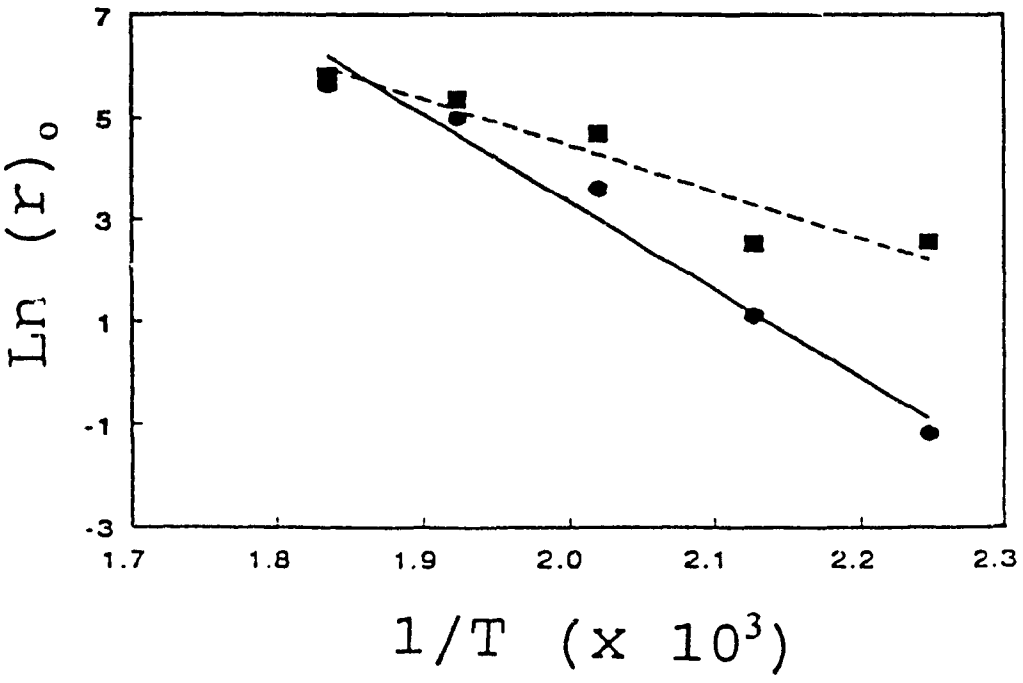

Figure 6.5 Arrhenius plots for the Pt/HY in terms of: (■) isomerization and (●) cracking.

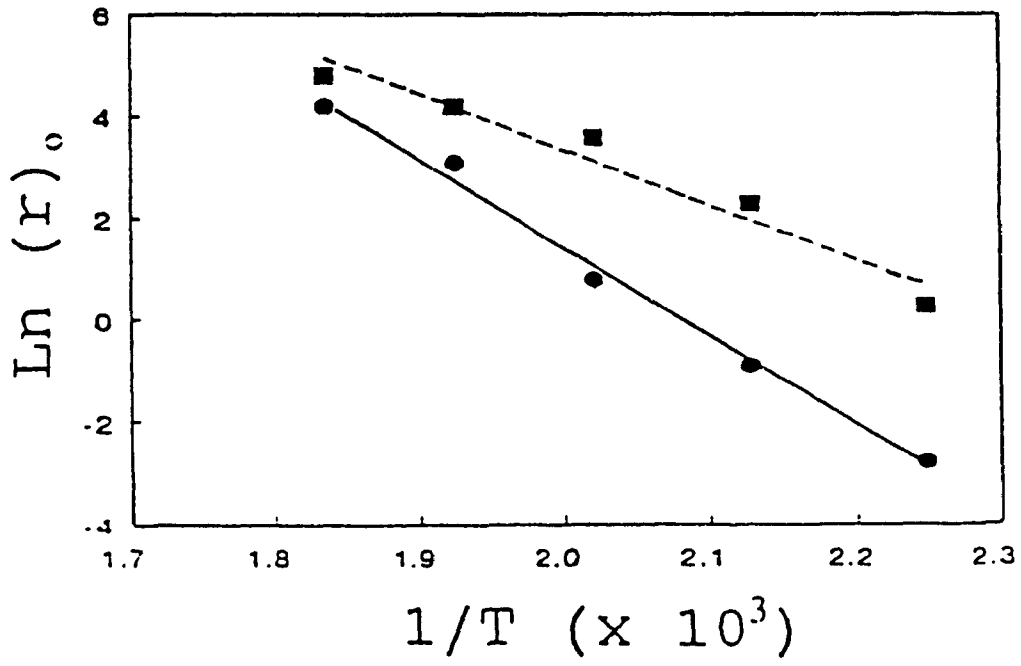

Figure 6.6 Arrhenius plots for the Pt/LaNaY in terms of: (■) isomerization and (●) cracking.

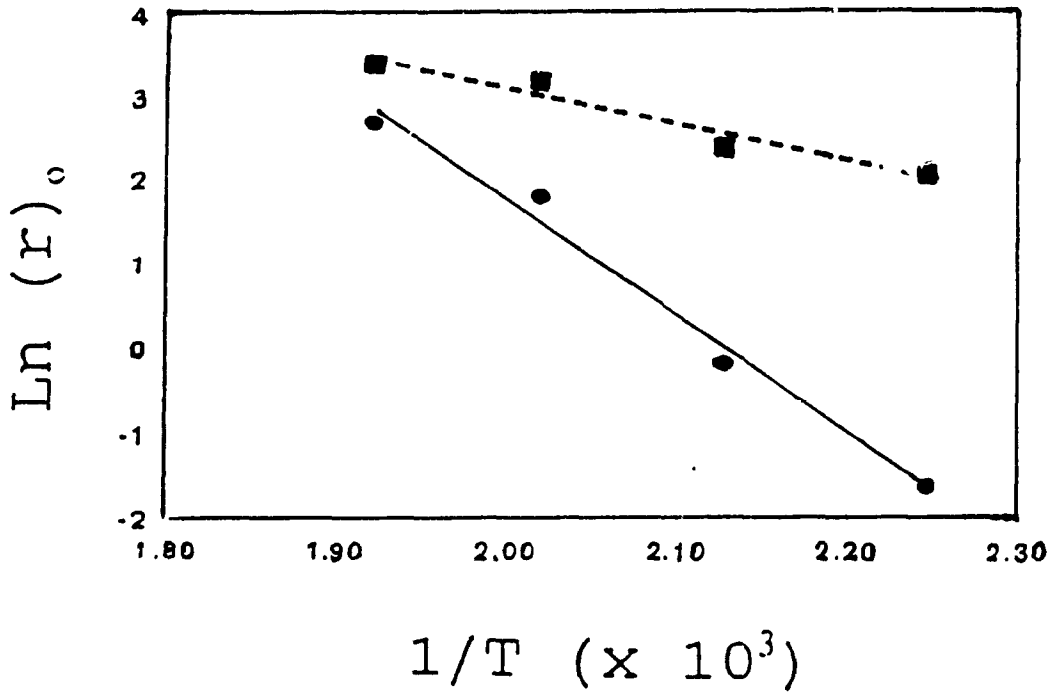

Figure 6.7 Arrhenius plots for the Pt/Y-SZr in terms of: (■) isomerization and (●) cracking.

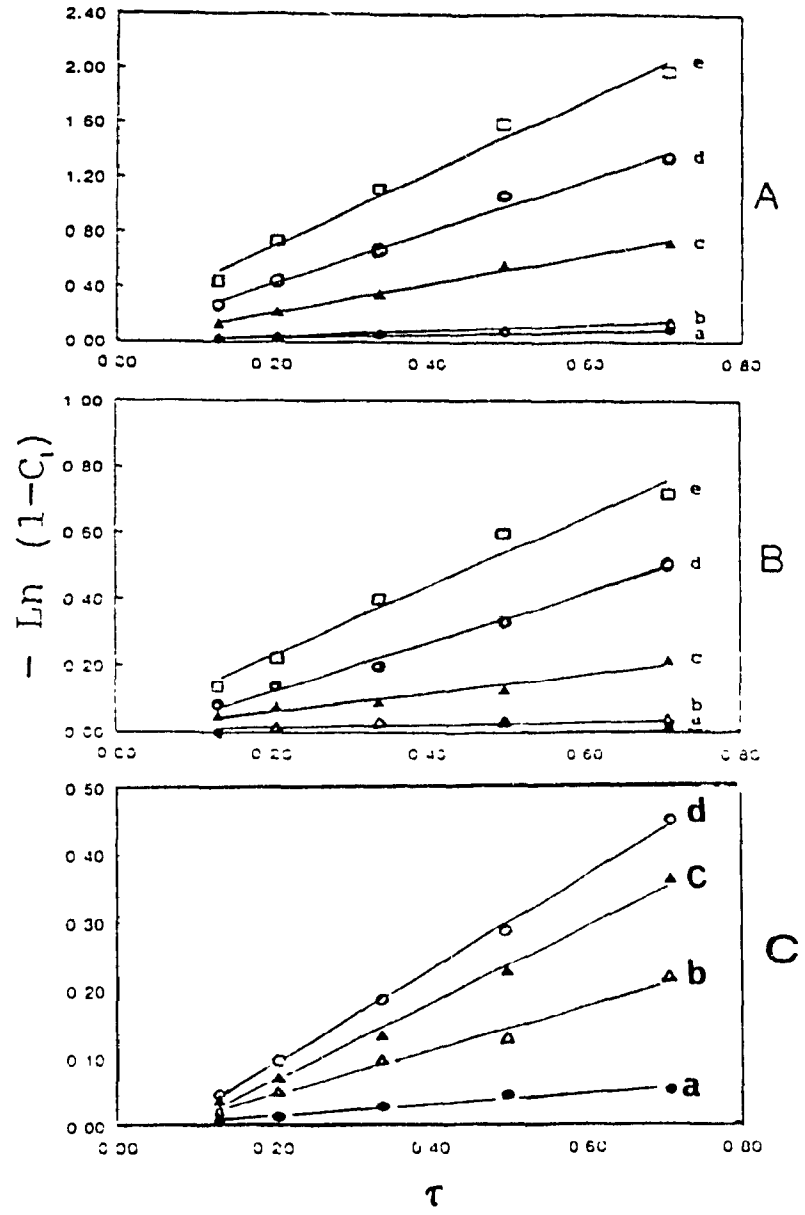

Figure 6.8 Plot of -Ln(1-C_t) against contact time, τ, for A) Pt/HY, B) Pt/LaNaY and C) Pt/Y-SZr, at different reaction temperatures(in °C): a) = 172, b) = 197, c) = 222, d) = 247 and e) = 272.

Table 6.2 Kinetic data for the isomerization reaction

Catalyst	T °C (K)	$(r_{iso})_o$ (h^{-1})	ΔE°_{iso} (kJ/mol)	A_{iso} ($Pa^{-1}s^{-1}$)
	172 (445)	12.8		
	197 (470)	12.5		
Pt/HY	222 (495)	108.6	75.9	$1.0*10^{3}$
	247 (520)	213.5		
	272 (545)	340.6		
	172 (445)	1.3		
	197 (470)	10.5		
Pt/LaNaY	222 (495)	38.3	89.7	$9.7*10^{3}$
	247 (520)	63.7		
	272 (545)	117.0		
	172 (445)	8.5		
Pt/Y-SZr	197 (470)	10.7	36.3	$2.5*10^{-2}$
	222 (475)	27.4		
	247 (520)	29.5		

Table 6.3 Contact time delay, τ_o and fractional surface coverage for cracking, θ^*.

Catalyst	T (°C)	τ_o (s)	$r_{cr}/(r_{cr}+r_{iso})$	θ^*
	172	173	0.023	
	197	108	0.193	
Pt/HY	222	47	0.302	0.44
	247	0	0.438	
	272	0	0.455	
	172	1440	0.034	
	197	144	0.037	
Pt/LaNaY	222	108	0.057	0.38
	247	72	0.267	
	272	68	0.371	
	172	108	0.023	
Pt/Y-SZr	197	43	0.070	0.34
	222	36	0.182	
	247	36	0.333	

Table 6.4 Kinetic data for the cracking (β-scission) reaction

Catalyst	T °C (K)	τ_o (h)	$(r_{cr})_o$ (h^{-1})	ΔE°_{cr} (kJ/mol)	A_{cr} (s^{-1})
	172 (445)	0.048	0.3		
	197 (470)	0.030	3.0		
Pt/HY	222 (495)	0.013	46.9	144.7	$2.6*10^{13}$
	247 (520)	0.000	166.4		
	272 (545)	0.000	284.5		
	172 (445)	0.400	0.1		
	197 (470)	0.045	0.4		
Pt/LaNaY	222 (495)	0.031	2.3	145.3	$4.5*10^{13}$
	247 (520)	0.019	23.2		
	272 (545)	0.020	69.0		
	172 (445)	0.030	0.2		
Pt/Y-SZr	197 (470)	0.012	0.8	114.7	$8.2*10^{9}$
	222 (475)	0.010	6.1		
	247 (520)	0.010	14.7		

As expected, the initial rates of isomerization and cracking(β-scission) increase with increasing reaction temperature for all catalysts studied(Tables 6.2 and 6.4). However, the rate of increase depends on the particular catalyst studied:

i) In the case of the Pt/HY catalyst, the initial rates of isomerization and cracking increase steadily with temperature (Tables 6.2 and 6.4). In particular, cracking starts with a much lower rate alue at 172 °C and with a noticeable value for the contact time delay (τ_o) (Figure 6.4 and Table 6.3). However, the initial rate of cracking recovers rapidly over that of isomerization, such that from 247 to 272 °C, the delay (τ_o) is essentially zero, and the initial rates of cracking and isomerization are almost equal. In terms of product distribution, similar results to those obtained by Vansina et al [10] who studied the n-octane conversion over ultrastable Y zeolite containing 0.5 wt % Pt were observed. Also, according to these authors, within the temperature range investigated (180-240 °C), the product distribution from hydroisomerization and hydrocracking was a unique function of the total conversion. In my case, by using extremely low contact times which resulted in extremely low conversions, I was able to determine the contact time delay τ_o (e.g. large differences in product selectivities, isomerization and cracking) although its value was very small even at 172 °C and tending towards zero at 247 °C (Table 6.3). However, in terms of the apparent activation energy, the value obtained

for the isomerization was half that of cracking (Tables 6.2 and 6.4, $\Delta E_{iso}/\Delta E_{cr}$ = 0.5). This is obviously different from that estimated by Baltanas et al [55], who proposed the same activation energy (136. 8 kJ/mol) for these two reaction steps in the modelling of the rate equations. It is worth mentioning that the values calculated in this work were derived from the initial rates. The extremely low partial pressure of n-octane and the resulting low conversion such that only isomerization products are formed at that moment allow us to isolate any contribution of cracking reactions from the consideration of the kinetic behaviours of the isomerization step. As the cracking step predominates with an increase in conversion, which can be seen by the fact that the cracking step has pre-exponential factors about 10^{10} times greater than that of isomerization step(Tables 6.2 and 6.4,), the cracking rate approaches the overall rate of conversion of n-octane(Figures 6.1 and 6.4). Thus, Bultanas et al's estimation, which was derived from the overall rate of conversion, and not at such very low conversion levels, probably only reflected the cracking step, and their estimation for the isomerization step becomes questionable. The similarities in the values for the activation energy of the cracking step between my results and those in ref[55] indicate that the cracking step comes after the isomerization step and with a greater energy demand, but much faster(as seen from the much greater pre-exponential values) as long as the intermediates formed from the isomerization step have internal energies greater than the energy barrier (activation energy).

ii) For the Pt/LaNaY catalyst prepared from the LaNaY zeolite having much weaker acid sites than the HY zeolite, the initial rate of isomerization at 172°C was significantly lower than that of the Pt/HY catalyst (Tables 6.2). The corresponding initial rates of cracking for both catalysts were essentially zero at such a low reaction temperature. However, at this temperature, the contact time delay, τ_o, for the Pt/LaNaY was several times greater than that of the Pt/HY sample. Similar to that of Pt/HY, τ_o, for Pt/LaNaY decreased with increasing temperature. However, the τ_o of the LaNaY catalyst did not go to zero even at 272 °C, in contrast to the Pt/HY catalyst. Therefore, what differentiates the Pt/LaNaY from the Pt/HY is that the former catalyst exhibits longer contact time delays, which probably favours the desorption of multi-branched octanes (various methylheptanes and trimethyl-pentanes) from the reaction sites, before the β-scission phenomenon can "destroy" the corresponding intermediates.

iii) At low reaction temperatures, the values of the initial rates for the hybrid catalyst, Pt/(Y-SZr), are close to those of the Pt/HY catalyst (Tables 6.2 and 6.4). This is why such hybrid catalysts are found to be as active and selective as the HY zeolite based catalysts at lower temperatures [128]. However, above 230 °C, the values of the initial rates with such a hybrid catalyst are much smaller than those found with the Pt/HY catalyst. This is probably due to the some loss of sulfur species[128]. As well, the apparent activation energies and

the pre-exponential factors calculated for the hybrid catalyst are much smaller, and the contact time delay, τ_o, is essentially constant within the range of temperatures studied. This behaviour of the hybrid catalyst, tested within the temperature range where the sulfate-promoted zirconia is stable, which is very different from that of the two other non-hybrid catalysts, can be attributed to the synergistic effects between the two components (zeolite and sulfate-promoted zirconia) as observed in the previous chapter. In fact, it was seen that, at 200 to 230 °C, sulfate-promoted zirconia, having some superacid character, showed relatively high n-octane conversion (Table 4.4). Combined with the HY zeolite in an intimate particle mixture, there was a general enhancement in the n-octane conversion with a product distribution similar to that of the Pt/HY zeolite catalyst. This suggests that some isomerization products are transferred from the surface of the sulfate-promoted zirconia (co-catalyst) to the surface of the HY zeolite where further conversion take places. The lower values for the apparent activation energies compared to those of the "pure" Pt/HY catalyst, and in particular the constancy of the contact time delay τ_o, are indicative of such a (physical) transfer between the different components of the hybrid catalyst.

In relation to their acidic properties and with respect to their kinetic behaviours, it can be concluded that there exists: (i) a decreasing acid strength: Pt/Y-SZr > > Pt/HY > Pt/LaNaY, and an increasing apparent activation energy (particularly for the cracking step): Pt/Y-SZr < < Pt/HY = < Pt/LaNaY; (ii) an

increasing acid site density (per gram): Pt/Y-SZr << Pt/LaNaY < Pt/HY, and an increasing pre-exponential factor: Pt/Y-SZr << Pt/LaNaY < Pt/HY. In conclusion, the apparent activation energy is primarily dependent on the strength of the acid sites, while the pre-exponential factor is basically controlled by the density of acid sites present on the catalyst, although the relationship between the activation energy and the pre-exponential factor can not be ignored.

Indeed, the values of the pre-exponential factor are said to be indicative of the involvement of mobile and immobile species in surface reactions by using the transition-state theory estimates of pre-exponential factors as presented in Table 6.5 [144]. Thus, with zeolite catalysts, Pt/HY and Pt/LaNaY, the order of magnitude of $10^3(Pa^{-1}.s^{-1})$ obtained for the pre-exponential factor of isomerization, A_{iso}, corresponds to the "molecular adsorption with mobile transition state"[144], while the order of magnitude of $10^{12\,13}(s^{-1})$ obtained for the pre-exponential factor of cracking, A_{cr}, suggests some specific problems during desorption (and readsorption) of "cracked" products (specifically, "molecular desorption with similar freedom for adsorbed and transition states" [144]). These results appear to be in agreement with the kinetic models of Baltanas et al[55] in which "physical adsorption of both octanes and cracked products determining the concentrations at the active sites were accounted for".

Table 6.5 Transition-state theory estimates of pre-exponential factor[144]

Reaction and conditions	*Estimates*
Molecular Adsorption	
$A + {}^{\bullet} \rightarrow A^{\bullet}$	$r = A[\exp-(E_a/k_BT)]P_A\theta^{\bullet}$
Mobile transition state	$A = 10^3$/Pa s
Immobile transition state	$A = 10^1$/Pa s
Dissociative Adsorption	
$A_2 + 2^{\bullet} \rightarrow 2A^{\bullet}$	$r = A[\exp-(E_a/k_BT)]P_{A2}(\theta^{\bullet})^2$
Mobile transition state	$A = 10^3$/Pa s
Immobile transition state	$A = 10^1$/Pa s
Lagmuir-Hinshelwood Reaction	
$A^{\bullet} + B^{\bullet} \rightarrow C^{\bullet} + D^{\bullet}$	$r = A[\exp-(E_a/k_BT)]\theta_A\theta_B$
Mobile surface species with rotation	$A = 10^8$/s
Mobile surface species without rotation	$A = 10^{11}$/s
Immobile surface species without rotation	$A = 10^{13}$/s
Eley-Rideal Reaction	
$A + B^{\bullet} \rightarrow AB^{\bullet}$	$r = A[\exp-(E_a/k_BT)]P_A\theta_B$
Mobile transition state	$A = 10^3$/Pa s
Immobile transition state	$A = 10^1$/Pa s
Molecular Desorption	
$A^{\bullet} \rightarrow A + {}^{\bullet}$	$r = A[\exp-(E_a/k_BT)]\theta_A$
	$A = 10^{13}$/s
Similar freedom for adsorbed and transition state	
More rotation and transition freedom for transition state	$A = 10^{16}$/s
Associative Desorption	
$2A^{\bullet} \rightarrow A_2 + 2^{\bullet}$	$r = A[\exp-(E_a/k_BT)](\theta_A)^2$
Mobile adsorbed and transition states with full rotation freedom	$A = 10^{3}$/s
Mobile adsorbed and transition states without rotation	$A = 10^{11}$/s
Immobile adsorbed and transition state	$A = 10^{13}$/s
Immobile species with more rotational and transition freedom for transition state	$A = 10^{16}$/s

The extremely low values of both the apparent activation energies and the pre-exponential factors for both the isomerization and cracking reaction with the hybrid catalyst, Pt/Y-SZr, probably indicates the existence of the transfer between two phases of this catalyst. As the sulfate-promoted zirconia phase has the superacidic sites and can easily activate the octane molecules into carbenium ion intermediates, a low value of activation energy for isomerization was observed. The resulting carbenium ion intermediates have two paths to follow. One is desorption (of course, combining with protons first) from the surface of sulfate-promoted zirconia, producing octane and its isomers. The other path involves transfer to another active site (here, the active site on the surface of HY zeolite) to undergo further reactions such as cracking reactions, although they can also undergo cracking without transfer (not as efficiently as on the surface of the zeolite as shown in Chapter 4). Furthermore, the desorption of a species from an active site usually has a higher enthalpy than does its transfer from one active site to another, ie. spillover. The intermediate transfer may be predominant in such a situation. However, this transfer process requires the cooperation of two active sites which are located in different phases. Statistically, the possibility of such a transfer process is small even though it is easier. As a final result, an extremely low value of the pre-exponential factor was found with this hybrid catalyst. On the other hand, the order of magnitude of $10^9(s^{-1})$ obtained for the pre-exponential factor of cracking, A_{cr}, with this hybrid catalyst, further demonstrates the occurrence of

cracking reactions on the surface of the zeolite and the problems of desorption of "cracked" products from there.

6.3.2 Practical interests of kinetic studies

The practical interest of such kinetic studies is their use as a guide towards catalyst design and reaction condition optimization in order to favour a desirable product distribution. For example, the hydroisomerization of n-paraffins with more than 6 carbons is a process of industrial interest owing to the possibility of obtaining high octane rated branched paraffins. Isomerization of, for instance, n-octane to isooctane (mono-branched), can be achieved over superacidic catalysts such as sulfate-promoted zirconia at relatively low temperature, but, if multi-branched liquid paraffins are also desired in order to obtain high octane fuels, the problem cannot easily be resolved because multi-branched isomers, once formed, undergo very rapid β-scission resulting in less desirable cracking products.

There are several approaches towards achieving the objective of producing higher yields of high octane liquid fuels:

a) the use of solid superacidic catalysts at low temperatures;

b) the use of hydrogen donating substances (for instance, adamantane) to desorb the isomeric intermediates, and

c) the use of solid acidic catalysts of moderate acidity but under well-defined reaction conditions to keep the "isomerization/cracking" competition optimized towards a favourable outcome.

At the present time, approach a) seems to be achievable but requires the use of fairly harsh conditions such as a high hydrogen pressure [147]. Meanwhile approach b) does not seem to be very viable in practice[138]. Approach c) is promising since moderately acidic SAPO-11 has recently been shown to provide better results than do other zeolites, although here too, high hydrogen pressures are necessary[148].

I intend to support approach c) as being very promising. For this, consider the index R as follows[149]:

R = (selectivity to multi-branched/selectivity to mono-branched octanes) * (conversion to isomers of octane).

This index R and the conversion to liquid hydrocarbons can be considered an index of quality and quantity of liquid hydrocarbons produced. As shown in Table 6.6, the Pt/HY catalyst has an index R that increases with increasing contact time, and decreases with increasing temperature. With the Pt/LaNaY, high values for the index R are achieved even at 272 °C, (e.g., at τ of 0.34 h, an R of 19 was obtained with total conversion of 41.4 %, and conversion to liquid products of 32.7 %). In the case of the Pt/(Y-SZr) hybrid catalyst, the R

index exhibits low values(not reported because of low values of conversion to liquid hydrocarbons) over the whole temperature range. Considering this, the kinetic results obtained with the moderately acidic Pt/LaNaY catalyst when compared to the HY zeolite can be interpreted follows: i) lower initial rates of isomerization and cracking increase slowly with increasing reaction temperature; ii) a longer contact time delay τ_o which does not disappear at higher temperatures; and iii) a high resulting $\Delta E_{iso}/\Delta E_{cr}$ ratio. These characteristics, which can be ascribed to the moderate acidity of the Pt/LaNaY when compared to the reference catalyst(Pt/HY), allow for the desorption of more isomerization products, including the multi-branched isomers, which therefore escape from the devastating effects of the β-scission.

6.4 Conclusions

It has been shown that the initial rates of isomerization and cracking in the conversion of n-octane over zeolite acidic catalysts can be calculated from conversion and selectivity data obtained when varying the contact time. The contact time delay, which shows how "separated" are these two sequential reaction steps, can also be calculated. These results clearly demonstrate that the hydrocracking of n-octane proceeds in consecutive steps. Different values of the activation energy have been determined for these two reaction steps, the isomerization and cracking reactions. This does not agree with Baltanas, et al's

speculation.

Kinetic results obtained with the moderately acidic zeolite LaNaY, when compared to the more acidic HY zeolite, allow the identification of the most advantageous reaction conditions for the production of multi-branched octanes while still providing useful conversions to liquid hydrocarbons. Kinetic data obtained with the hybrid catalyst that is a mechanical mixture of two solid components (HY zeolite and sulfate-promoted zirconia as co-catalyst), suggest the existence of a transfer process of the reaction intermediates between the surfaces of these two catalyst components.

Table 6.6 Conversion to liquid hydrocarbons and values of the R index

Contact time	Pt/HY						Pt/LaNaY		
	T = 222 °C			T = 247 °C			T = 272 °C		
(t, in h)	C_t	C_{liq}*	R	C_t	C_{liq}	R	C_t	C_{liq}	R
0.13	13.1	7.3	6	23.9	7.7	4	12.6	11.0	1
0.21	20.6	11.3	9	36.3	9.4	3	34.5	28.4	16
0.34	30.1	13.9	11	49.1	13.0	3	41.4	32.7	19
0.50	43.2	17.6	14	65.7	15.9	5	40.0	25.7	4
0.71	51.9	20.2	17	74.0	17.3	6	51.2	29.9	4

* : liquid hydrocarbons C_5-C_8 excluding unconverted n-octane

CHAPTER VII

CONCLUSIONS

Isobutane is used to produced MTBE and high octane rating gasoline by "isobutane/olefin" type alkylation. The increasing need for addition of oxygenates to reformulated gasoline requires higher industrial production levels of isobutane, but, the traditional petroleum sources of isobutane are no longer sufficient. A new technique with a flexible product distribution tailored to the market demand has been developed in this work. Two novel classes of solid acid microporous materials based on the Y zeolite structure have been developed: lanthanum Y zeolites including desilicated Y zeolites, and hybrid catalysts. Their catalytic performances regarding the conversion of n-paraffins have been evaluated in relation to their physico-chemical properties as obtained by various characterization techniques.

Selective removal of framework silicon from various zeolites has been achieved by precisely controlling the base-treatment conditions, particularly the initial pH of the suspension. The original structure and surface area are essentially preserved upon desilication, but a slight micropore narrowing is observed. As all the aluminum atoms remain in the tetrahedral configuration in the desilicated zeolites, this treatment provides a novel technique for improvement of the cation-exchange capacity and modification of acidic properties. The incorporation of lanthanum ions into zeolites not only introduces acid sites into the zeolite framework, but also enhances the thermal stability of the ammonium forms of aluminum-enriched zeolites such as X type and

desilicated Y zeolites.

The presence of sulfate groups on the zirconia surface retards the phase transition of zirconia from the amorphous form to the tetragonal form. There is a temperature window from 770 K to 870 K for optimum activation of the sulfate-promoted zirconia for obtaining a tetragonal crystalline structure for zirconia, without loss of sulfate groups. Superacidic properties of sulfate-promoted zirconia were observed in the ammonia-TPD profile, which corresponded to an ammonia desorption peak beginning at 800 K. Although sulfate-promoted zirconia alone exhibited a certain catalytic activity towards the hydrocracking of n-octane, this material is not as efficient as HY zeolite. When sulfate-promoted zirconia was hybridized with HY zeolite, there is a synergistic effect between the two components, mostly due to a transfer of reaction intermediates from the surface of the former to the surface of the latter.

Hydrocracking of n-paraffins is catalyzed at Brønsted acid sites and involves carbenium ion intermediates. Pt may help hydrogenation of the primary cracked products and the desorption of the final products, thus stabilizing the catalytic activity. The cage of the zeolite, particularly the supercage of the faujasite type zeolites, has an effect on both the adsorption of n-paraffins and the formation of the specific branched carbenium intermediate configuration. Isobutane is mainly produced through A-mode β-scission of a α,γ,γ-tribranched

carbenium ion, thus the Y zeolite, which has accommodating supercages, and the use of C_8-C_{11} paraffins which form suitable tribranched carbenium ions in such a supercage without any space restriction, constitutes a good choice for the catalytic production of isobutane.

From my kinetic method and the accepted reaction mechanism, the initial rates of isomerization and cracking for the conversion of *n*-octane have been calculated. The contact time delay, which shows how "separated" these two sequential reaction steps are, has also been estimated. These results further demonstrate that the hydrocracking of n-paraffins over zeolite acidic catalysts is a consecutive process. Two reaction steps have different values of the apparent activation energy, and in particular, the cracking reaction exhibits a higher apparent activation energy than does isomerization, and it occurs second. The values for the pre-exponential factor, in light of the estimates based on the transition state theory, suggest some problems at the level of molecular adsorption of n-octane during the isomerization step and at the level of desorption of cracked products during the cracking step. The kinetic results obtained with sulfate-promoted zirconia hybridized HY zeolite further proved the existence of an intermediate transfer from the surface of zirconia to that of the zeolite.

The final product distribution depends on the reaction conditions and the

structure of the catalyst. The moderately acidic zeolite LaNaY allows the identification of the most advantageous reaction conditions for the production of multi-branched octanes while still providing significant conversions to liquid hydrocarbons. The superacidic sulfate-promoted zirconia hybridized catalyst may allow the reaction to occur at lower temperatures while still yielding high selectivity towards isobutane.

Future studies should concentrate on the most interesting class of catalysts, hybrid catalysts, since the proven synergistic effects between the main component and the co-catalyst[150-151] may provide not only a superior yield but also a greater flexibility in product distributions. The co-catalyst component could be either sulfate-promoted zirconia or the high surface area silica-alumina while the main component should be the HY zeolite. The promoting function of the co-catalysts should be further investigated with regard to surface area, acidity and porosity. It would also be interesting to study the contact phenomena between the two co-catalyst components and the transfer of intermediates from one site to another by observing the effect of changing the particle sizes.

CHAPTER VIII

REFERENCES

1. J.G. Speight, *The Chemistry and Technology of Petroleum*, March Dekker, Inc., New York, 1980

2. J.E. Johnson and F.M. Peterson, *Chemtech*, 1991, May, 296.

3. H.H. Schobert, *The Chemistry of Hydrocarbon Fuels*, Butterworths, London, 1990,

4. D. Decroocq, *Catalytic Cracking of Heavy Petroleum Fractions*, Editions Techniq, Paris, 1984,

5. H.H.Voge in *Heterogeneous Catalysis, Selected American Histories, ACS Symposium Series 222*, Eds., B.H. Davis and W.P. Hettinger, Washington, 1983, p.235.

6. J.A. Martens and P.A. Jacobs, in *Theretical Aspects of Heterogenous Catalysis*, Ed. by J.B. Moffat, VNR Publishers, New York, 1990, p52

7. P. Vogel, *Carbocation Chemistry*, Amsterdam, Elsevier, 1985, p62

8. J.A. Martens, P.A. Jacobs and J. Weitkamp, *Appl. Catal.*, 1986, 20, 239

9. J.A. Martens, P.A Jacobs and J. Weitkamp, *Appl. Catal.*, 1986, 20, 283

10. H. Vansina, M.A. Baltanas and G. Froment, *Ind. Eng. Chem. Prod. Res. Dev.*, 1983, 22, 526

11. S. Tiong Sie, *Ind. Eng. Chem. Res.*, 1992, 31, 1881

12. S. Tiong Sie, *Ind. Eng. Chem. Res.*, 1993, 32, 397

13. S. Tiong Sie, *Ind. Eng. Chem. Res.*, 1993, 32, 403

14. Julius Scherzer, *Octane-Enhancing Zeolitic FCC Catalysts: Scientific and Technical Aspects*, Marcel Dekker Inc., New York, 1990, p3.

15. J.M. Thomas, *Angew. Chem. Int. Ed. Engl.*, 1994, 33, 913.

16 D.W. Breck, *Zeolite Molecular Sieves. Structure, Chemistry, and Use*, John Wiley & Sons, Inc., New York, 1974, p.5.

17. E.M. Flanigen, B.M. Lok, P.L. Patton and S.T. Wilson, *Stud. Surf. Sci. Catal.*, 1986, 28, 103

18. M.A. Uguina, G. Ovejero, R. Van Grieken, D.P. Serrano and M. Camacho, *J. Chem. Soc., Chem. Comm.*, 1994, 9, 27.

19. D. Venkataraman, S. Lee, J. Zhang and J.S. Moore, *Nature*, 1994, 371, 591.

20. J. Yu, K. Tu and R. Xu, *Stud. Surf. Sci. Catal.*, 1994, 84, 315

21. G. Alberti, F. Marmottini, S. Murcia-Mascaros and R. Vivani, *Angew. Chem. Int. Ed. Engl.*, 1994, 33, 1594

22. M.E. Davis, *Ind. Eng. Chem. Res.* 1991, 30, 1675.

23. J. Chen, R.H. Jones, S.Natarajam, M.B. Hursthos and J.M. Thomas, *Angew. Chem. Int. Ed. Engl.*, 1994, 33, 639.

24. R. Le Van Mao, N.T.C. Vo, B. Sjiariel, L. Lee and G. Denes, *J. Mater. Chem.*, 1992, 2, 595

25. I.E. Maxwell, J.E. Naber and K.P. de Jong, *Appl. Catal.*, 1994, 113, 153

26. J.H. Lichtblau, *Hydrocarbon Processing*, 1993, 72(11), 148J-W.

27. B.C. Gates, J.R. Katzer and G.C.A. Schuit, *Chemistry of Catalytic Processes*, McGraw-Hill, New York, 1979, p.464.

28. H.L. Hoffman, *Hydrocarbon Processing*, 1987, February, 41

29. *Chemical Week*, 1987, June 24, 20.

30. R. Le Van Mao, J. Yao and R. Carli, *Appl. Catal.A*, 1992, 86, 127

31. R. Le Van Mao, J. Yao and B. Sjiariel, *Catal. Lett.*, 1990, 6, 23.

32. P.C. Doolan and P.R. Pujado, *Hydrocarbon Processing*, 1989, 68(9), 72.

33. R.J. Schmidt, P.L. Bogdan and N.L. Gilsdorf, *Chemtech*, 1993, February, 41.

34. Marcia Roberson, *Hydrocarbon Processing*, 1994, 73(9), 27.

35. R. Le Van Mao, H. Ahlafi and T.S. Le, in *Selectivity in Catalysis*, Eds., M.E. Davis and S.L. Suib, ACS 517, New York, 1991, p.233.

36. D. Biswas and L.E. Maxwell, *Appl. Catal.*, 1976, 63, 197

37. J.N. Armor, *Appl. Catal.*, 1991, 78, 141

38. Gabriele Centi and Giorgio Golineli, *J. Catal.*, 1989, 115, 452

39. R. Le Van Mao and L. Dufresne, *Appl. Catal.*, 1989, 17, 141

40. M. Guisnet and N.S. Gnep, *Appl. catal.A*, 1992, 89, 1

41. Y. Ono, *Catal. Rev.-Sci.Eng.*, 1992, 34, 179

42. J. Yao, R. Le Van Mao and L. Dufresne, *Appl. Catal.*, 1990, 65, 175

43. R. Le Van Mao, *US Patent 4692424*, 1987.

44. L.M. Tam and B.H. Davis, *Appl. Catal.*, 1989, 53, 263

45. R.A. Flinn, O.A. Larson and Harold Beuther, *Ind. Eng. Chem.*, 1960, 52(2), 153.

46. R.C. Archibald, B.S.Greensfelder, G. Holzman and D.H. Rowe, *Ind. Eng. Chem.*, 1960, 52(9), 745

47. H.L. Coonradt, F.G. Ciapetta, W.E. Garwood, W.K Leaman and J.N. Miale, *Ind. Eng. Chem.*, 1961, 53(9), 727

48. H. Clough, *Ind. Eng. Chem.*, 1957, 49, 672

49. D.H. Sterenson and H. Heinemann, *Ind. Eng Chem.*, 1957, 49, 664

50. H.L. Coonradt and W.E. Garwood, *I&EC. Process Design and Development*, 1964, 3(1), 38

51. H.F. Schulz and J.H. Weitkamp, *Ind. Eng. Chem., Prod. Res. Develop.*, 1972 11(1), 46

52. A.P. Bolton and M.A. Lanewala, *J. Catal.*, 1970, 18, 1

53. J.A. Rabo, P.E. Pickert and R.L. Mays, *Ind. Eng. Chem.*, 1961, 53, 733

54. P.H. Lewis, *J. Catal.*, 1968, 11, 162

55. M.A. Baltanas, H. Vansina and G. Froment, *Ind. Eng. Chem. Prod. Res. Dev.*, 1983, 22, 531

56. H.W. Kouwenhoven and W.C. Vanzijll, *Chem. Eng. Prog.*, 1971, 67, 65

57. R. Le Van Mao, P. Levesque and B. Sjiariel, *Can. J. Chem. Eng.*, 1986, 54, 514

58. R. Le Van Mao, *US Patent*, 4692424, 1987

59. R. Le Van Mao and G.P. McLaughlim, *J. Energy & Fuels*, 1989, 3, 62064.

60. B.C. Gates, "*Catalytic Chemistry*" John Wiley and Sons, New York, 1992, p276

61. B.S. Greensfelder, H.H. Voge and G.M. Good, *Ind. Eng. Chem.*, 1949, 41, 2573

62. E.A. Lombardo and W.K. Hall, *J. Catal.*, 1988, 112, 565

63. J. Planelles, J. Sanchez-Marin, F. Tomas and A Corma, *J. Molec. catal.*, 1985, 32, 365

64. A. Corma and B.W. Wojciechowski, *Catal. Rev. Sci. Eng.*, 1982, 24, 1

65. W.A. Groten and B.W. Wojciechowski, *J. Catal.*, 1993, 140, 262

66. Stanislas Jean Teichner, *Appl. Catal.*, 1990, 62, 1

67. Jean Bandiera and Younes Ben Taarit, *Appl. Catal.*, 1991, 76, 199

68. J.H. Sinfelt and J.C. Rohrer, *J. Phys. Chem.*, 1961, 65, 2272

69. J.H. Sinfelt and J.C. Rohrer, *J. Phys. Chem.*, 1962, 56, 1559

70. R.L. Gorring, *J. Catal.*, 1973, 31, 13

71. J.A. Rabo, *Zeolite Chemistry and Catalysis*, ACS Monograph 171, Washington, D.C., 1976, p306

72. J. Scherzer, *Catal. Rev.-Sci. Eng.*, 1986, 31(3), 215

73. D.W. Breck and E.M. Flanigen, *Molecular Sieves*, Society of Chemical Industry, London, 1968, p47

74. E.J.P. Feijen, J.A. Martens and P.A. Jacobs, *Stud. Surf. Sci.Catal.*, 1994, 84, 3

75. C.V. McDaniel and P.K. Maher, *US. Patent*, 3 292 196(1966)

76. H.K. Beyer and I. Belenzkaza, *Catalysis by Zeolites*, Ed. by B. Imelik, Elsevier, Amsterdam, 1980, p203

77. R. Le Van Mao, J. A. Lavigne, B. Sjiariel and C.H. Langford, *J. Mater. Chem.*, 1993, 3(6), 679

78. G.T. Kerr, J. Phys. Chem., *1968*, 72, 2594 and 1969, 73, 2780

79. J. Dwyer, J. Dewing, K.Karim, S. Holmes, A.F. Ojo, A.A. Garforth and D.J. Rawlence, *Stud. Surf. Sci. Catal.*, 1991, 69, 1

80. R.M. Dessau and G.T. Kerr, *Zeolites*, 1984, 4, 315

81. C.D. Chang, C.T.W. Chu, J.N. Miale, R.F. Bridger and R.B. Calvert, *J. Am. Chem. Soc.*, 1984, 106, 8143

82. J.N. Miale and C.N. Chang, *US. Patent*, 4,427,788(1984)

83. A. Cizmek, L. Komunjer and B. Subotic, *9th International Zeolite Conference*, Ed. by J.B. Higgins, R. von Ballmoos and M.M. Treacy, Publ. by Butterworth-Heinemann, Stoneham, MAY(1992), RP247

84. R.M. Dessau, E.W. Valyocsik and N.H. Goeke, *9th International Zeolite Conference*, Ed. by J.B. Higgins, R. von Ballmoos and M.M. Treacy, Publ. by Butterworth-Heinemann, Stoneham, MAY(1992), RP96

85. R.M. Dessau, E.W. Valyocsik and N.H. Goeke, *Zeolites*, 1992, 12, 776

86. R. Le Van Mao, S. Xiao, A. Ramsaran and J. Yao, *J. Mater. Chem.*, 1994, 4, 605

87. R. Le Van Mao, N.T. Vu, S. Xiao and A. Ramsaran, *J. Mater.Chem.*, 1994, 4, 1143

88. R. Le Van Mao, A. Ramsaran, S. Xiao, J. Yao and V. Semmer, *J. Mater. Chem.*, 1995, 5, in press

89. S. Xiao, R. Le Van Mao and G. Denes, *J. Mater. Chem.*, 1995, in press.

90. R. von Ballmoos, " *Collection of Simulated XRD Powder Pattern for Zeolites*" Butterworth Scientific Limited, Guildford, 1984, Faujasite: p34, Mordenite: p76, and ZSM-5: p74.

91. K.S.W. Sing, D.H. Everett, R.A.W. Haul, L. Moscou, R.A. Pierrotti, J. Rouquerol and T. Siemienewska, *Pure Appl. Chem.*, 1985, 57, 603

92. S. Bruuauer, P.H. Emmett and E. Teller, *J. Am. Chem. Soc.*, 1938, 60, 309

93. I. Langmuir, *J. Am. Chem. Soc.*, 1918, 40, 1361

94. E. P. Barrett, L.G. Joyner and P.P. Halenda, *J. Am. Chem. Soc.*, 1951, 73, 373

95. G. Horvath and K. Kawazoe, *J. Chem. Eng. Japan*, 1983, 16(6), 470

96. E. Oldfield and R.J. Kirkpatrick, *Science*, 1985, 227, 1537

97. C.A. Fyfe and R.E. Wasylislen, *Soild State Chemistry Techniques*, Ed. by A.K. Cheetham and P. Day, Oxford Sci.Publ. 1988, p190

98. E.M. Flanigen and H. Khatami, *Adv. Chem. Ser.*, 1971, 101, 201

99. G.H. Kuhl and H.S. Sherry, *Proc. V Intern. Zeolite Conf.* Naples, 1988, p813

100. S.J. Ainsworth, *Chem. Eng. News*, 1994, June 24, 34

101. J.D. Sherman, A.F. Derny and A.J. Gioffre, *Soap/Cosmetics/Chemical Specialties*, 1978, Dec., 33

102. R. Le Van Mao, A. Ramsaran, C. Doremieux-Morin, P. Batamack, L. Heeribout, V. Semmer, G. Denes and J.Fraissard, *Catal. Lett.*, submitted.

103. D.W. Breck, *Zeolite Molecular Sieves*, J. Wiley and Sons, New York, 1974, p464-470

104. Q. Li, L. Dai, L. Zhu and Z. Xue, *Zeolites*, 1994, 14, 367.

105. J.A. Rabo and G.J. Gajda, *Catal. Rev.-Sci.Eng.*, 1989, 31(4), 385

106. S.E. Shamshoum, A.K. Ghosh and T.R. Schuler, *Can. Pat. Appl.* Sept. 27, 1993 (mentioned in CA 120:222199g(1994))

107. T Yamaguchi, *Appl. Catal.*, 1990, 6, 1

108. M.Hino and K.Arata, *J.C.S. Chem. Comm.*, 1980, 851

109. M. Hino, S. Kobayashi and K. Arata, *J. Am. Chem. Soc.*, 1979, 101, 6439

110. K. Arata, *Adv. Catal.*, 1990, 37, 165

111. J.R. Sohn, and H.W. Kim, *J. Mol. Catal.*, 1989, 52, 361

112. M.S. Scurrell, *Appl. Catal.*, 1987, 34, 481

113. J.M. Parera, *Catal. Today*, 1992, 15, 481

114. F.R. Chen, G. Coudurier, J.F. Joly and J.C. Vedrine, *J. Catal.*, 1993, 143, 616

115. R. Srinivasan, D. Taulbee and B.H. Davis, *Catal. Lett.*, 1991, 9, 1

116. T. Jin, T. Yamaguchi and K. Tanabe, *J. Phys. Chem.*, 1986, 90, 4794

117. T. Yamaguchi, T. Jin and K. Tanabe, *J. Phys. Chem.*, 1986, 90, 3148

118. M. Bensitel, O. saur, J.C. Lavalley and B.A. Morrow, *Mater. Chem. Phys.*, 1988, 19, 147

119. M. Waqif, J. Bachelier, O. Saur and J.C. Lavalley, *J.Mol.Catal.*, 1992, 72, 127

120. P. Nascimento, C. Akratopoulou, M. Oszagyan, G.Coudurier, C. Travers, J.F. Joly and J.C. Vedrine, *Stud. Surf.Sci. Catal* , 1993, 75, 1185

121. K. Mukaida, T. Miyoshi and T. Saton, in *Acid-Base Catalysis*, ed. by K. Tanabe, H. Hatton, T. Yamaguchi and T. Tanaka, VCH Publisher, Kodanshi (Japan), 1989, p363

122. T. Yamaguchi, K. Tanabe and Y.C. Kung, *Mater. Chem. Phys.*, 1986, 16, 67

123. D.A. Ward and E.I. Ko, *J. Catal.*, 1994, 150, 18

124. A. Corma, M.I. Juan-Rajadell, J.M. Lopez-Nieto, A. Martinez and C. Martinez, *Appl. Catal.*, 1994, 111, 175

125. K. Ebitani, J. Tsuji, H. Hattori and H. Kita, *J. Catal.*, 1992, 135 , 609

126. A. Sayari and A. Dicko, *J. Catal.*, 1994, 145, 561

127. A. Dicko, X. Song, A. Adnot and A. Sayari, *J. Catal*, 1994, 150, 254

128. K. Tanabe, *Appl. Catal., A: General*, 1994, 113, 147 and discussion

129. J.B. Higgins, R.B. Lapierre, J.L. Schlenker, A.G. Rohrman, J.D. Wood, G.T. Kerr and W.J. Rohrbaugh, *Zeolites*, 1981, 8, 466

130. W.M. Meier and D.H. Olson, "*Atlas of Zeolite Structure Types*" Butterworth-Heinemann, London, 3rd Edition, 1992,

131. S. Jolly, J. Saussey, J.C. Lavalley, N. Zanier, E. Benazzi and J.F. Joly, *J.Phys.Chem.*, 1993, 97, 313

132. H.G.Karge, V. Mavrodinova, Z. Zheng and H.K. Beyer, *Appl.Catal.* 1991, 75, 343.

133. W.O.Hagg, *Stud.Surf.Sci.Catal.*, 1994, 84, 1375

134. N.Y. Chen, W.E. Garwood, *Advan.Chem.Ser.*, 1993, 121, 575

135. N.Y. Chen, S.J. Lucki, E.B. Mower, *J.Catal.*, 1969, 13, 329

136. A. Chauvel and G. Lefebvre, in *Petrochemical Processes*, Ed. technip (Paris), 1989, p130

137. J. Weitkamp, *Ind. Eng. Chem. Prod. Res. Dev.* 1982, 21, 550.

138. E. Iglesia, S.L. Soled and G.M. Kramer, *J. Catal.* 1993, 144, 238.

139. J.W. Ward, R.C. Hansford, A.D. Reichle and J.Shaviski, *Oil Gas J.* 1973, 5, 69

140. A.P. Bolton , *ACS. Monogr.* 1976, 171, 714

141. M.Steijns, *Ind. Eng. Chem. Prod. Res. Dev.*, 1981, 20, 654

142. J. Weitkamp, H. Faray, *Acta, Phys. Chem.*, 1978, 24, 327

143. M. Steijns, G.F. Froment, *Ind.Eng.Chem.Pro.Res.Dev.* 1981, 20, 660

144. J.A. Dumesic, D.F. Rudd, L.M. Aparicio, J.E. Rekoske and A.A. Trevino, in "*The Microkinetics of Heterogeneous Catalysis*", ACS Prof. Ref. Book, ACS, Washington, DC, 1993, pp 1- 21.

145. S.Xiao and R. Le Van Mao, *J. Microporous Mater.*, 1995, in press.

146. R. Le Van Mao and L. Dufresne, *Appl. Catal.*,1989, 52, 1.

147. M. Y. Wen, I. Wender and J.W. Tierney, *Energy & Fuels*, 1990, 4, 372.

148. R.J. Taylor and R.H. Petty, *Appl. Catal. A: General,* 1994, 119, 121

149. R. Le Van Mao and S. Xiao, *Appl. Catal.*, 1995, submitted.

150. J.M. Grau and J.M. Parera, *Appl. Catal. A: General,* 1993, 106, 27

151. R. Le Van Mao, S. Xiao and J.A. Lavigne, *45th Can. Chem. Eng. Conf.*, Quebec City, October, 15-18, 1995